UNIVERSITÀ DEGLI STUDI DI MILANO
FACOLTÀ DI SCIENZE E TECNOLOGIE

DIPARTIMENTO DI CHIMICA

Doctorate School of Chemical Science and Tecnologies

Doctorate in Chemical Science
XXVII Cycle
CHIM/06

# METHODOLOGIES FOR THE SYNTHESIS OF THIAHELICENE-BASED PHOSPHORUS DERIVATIVES AND THEIR APPLICATIONS IN ASYMMETRIC CATALYSIS

Davide DOVA
Matr.R09645

Tutor: Prof. Emanuela LICANDRO
Co-Tutor: Dr. Silvia CAUTERUCCIO

Coordinator: Prof. Emanuela LICANDRO

A.A. 2013-2014

# Table of Contents

# Abstract

Helicenes are *ortho*-annulated polycyclic aromatic or heteroaromatic compounds endowed with inherent chirality due to the helical shape of their π-conjugated system, whose unique structural features and physicochemical properties have stimulated countless studies in several fields, including nanosciences, chemosensing, materials science, biomolecular recognition, and asymmetric catalysis.[1] In fact, asymmetric syntheses are the indispensable source of a large number of chiral compounds that have become essential for human society, and the phosphorus-based molecules play a prominent role as catalyst ligands in some of the most important asymmetric processes, in which the choice of the chiral ligand is critical both for catalytic activity and for achieving a high level of chiral induction. However, whilst axial, central and planar chirality have been largely exploited to build chiral phosphorus ligands and organocatalysts, helical chirality has been rather neglected so far in this field. Several carbohelicenes and heterohelicenes with appended phosphorus functions have been prepared in either racemic or enantiomerically pure form, but catalytic screenings are limited mainly to Rh- or Ir-catalyzed olefin hydrogenations. Moreover, from literature overview it results that only a few structural variations have been made so far on phosphane containing helicenes. In particular, only $PPh_2$ function has been considered for catalytic purposes, and in almost all of the cases the phosphorus functions are located at the 2-position of the carbohelicene scaffolds. It is easily understood that more extensive investigations and structural variations are needed to fully establish the potential and usefulness of these compounds in both catalysis and other fields.

For several years in our laboratories we have been interested in the study and functionalization of tetrathia[7]helicene (7-TH) derivatives for applications in optoelectronics, and more recently also in catalysis. At the onset of this study, we synthesized 7-TH based mono and diphosphanes, and their corresponding Rh(I)[2] and Au(I)[3] complexes (Figure 1), exploiting the reactivity of the alpha positions of the terminal thiophene rings to introduce $PPh_2$ moieties.

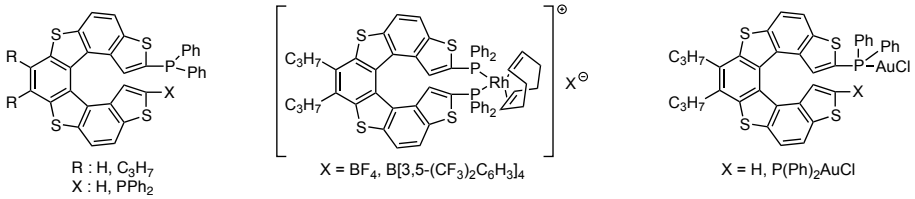


Figure 1

In preliminary studies on their catalytic activity, both Rh(I) and Au(I) complexes were found to be very efficient catalysts in hydrogenation reactions and cycloisomerizations of unsaturated substrates, respectively, albeit the asymmetric version of these reactions gave moderate *e.e.* (up to 40%).

On the basis of these preliminary results, the work of this PhD thesis has focused on the following main goals:

1. **Study of a new class of 7-TH-based alkyl phosphanes**
2. **Study of 7-TH aryl and alkyl phosphine oxides as chiral Lewis bases in polyhalosilane-mediated reactions**
3. **Study of Au(I) complexes based on chiral phospha-thiahelicenes**

In the course of this thesis, other three sub-topics in the field of the 7-TH derivatives have been developed:

4. **Set up of a new non-photochemical synthesis of functionalized benzo[1,2-*b*:4,3-*b*']dithiophenes (BdTs)**
5. **Synthesis of nanoconstruct based on PLGA nanoparticles loaded with a 7-TH derivative conjugated to a fluorescent probe**
6. **Synthesis of a new 7-TH based push-pull system and its preliminary application in DSSCs**

**1. Study of a new class of 7-TH-based alkyl phosphanes**

Based on our previous experience with the preparation of 7-TH diphenylphosphine-borane adducts, whose corresponding free phosphanes were found to be very air-sensitive, we have prepared a set of new 7-TH dialkyl phosphanes as air-stable borane adducts, starting from the tetrathiahelicene scaffold **1** according to the one-pot procedure reported in Scheme 1.

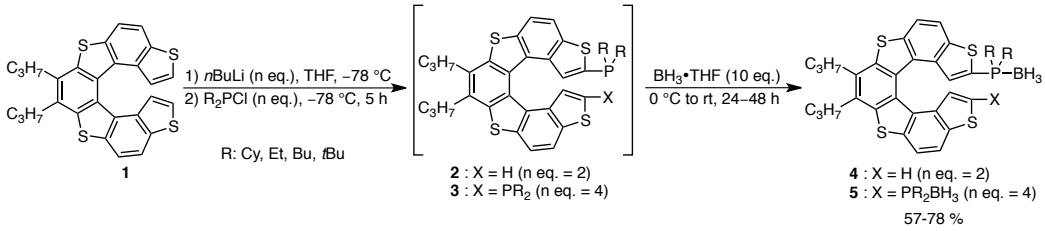


Scheme 1.

Thanks to their air-stability, the adducts **4** and **5** were fully characterized by standard analytical and spectroscopic techniques, and the tridimensional structure of two of them were fully elucidated by X-ray analysis, demonstrating the peculiar flexibility of the helix in the presence of different substituents. Next, the resolution of a diborane complex **5** (R = *n*Bu) by HPLC on chiral stationary phase gave the corresponding enantiopure antipodes, whose X-ray structures confirmed the right-handed helix, the (*P*) configuration, for the (+)-enantiomer, and *viceversa*. The chiroptical properties of these antipodes were investigated by experimental and theoretical CD spectra. This latter study was accomplished by a depth computational study using RI-CC2/cc-pVDZ method that has been used for the first time on 7-TH derivatives, obtaining a good agreement between experimental and theoretical data.[4]

Moreover, borane adducts **4** and **5** could be easily and completely converted into the corresponding free phosphanes **2** and **3**, respectively. The electronic properties of these 7-TH alkyl and aryl phosphanes have been studied by two complementary approaches: *i)* the determination of the first order Se-P coupling constants, $^{1}J_{Se\text{-}P}$, of the corresponding phosphine selenides, *ii)* electrochemical studies by means of cyclic voltammetry.

Thus, the electron-donating ability of these phosphanes has been investigated by the coupling constant $^{1}J_{Se\text{-}P}$ of the corresponding 7-TH phosphine selenides, and we found that 7-TH alkyl phosphanes showed lower coupling constants than those of the 7-TH aryl ones. As expected, alkyl 7-TH phosphanes resulted more electron-rich than the aryl ones.

Next, the first systematic study on electrochemical properties of 7-TH phosphanes **2** and **3** have been performed in terms of localization and features of the redox centers, and compared with

those of the corresponding borane adducts and phosphine oxides. In this study, we have found that the electrochemical properties of each phosphane are the results of the combination of electronic and steric factors showed by the substituents on the phosphorus atoms.

Some of mono 7-TH phosphanes have been used as organocatalysts, for the first time, in two typical phosphine-catalyzed [3+2]-annulations. Noteworthy, while the 7-TH diphenyl phosphane provide no cyclized product, 7-TH dicyclohexyl phosphane gave the corresponding products in high conversion (up to 82%), demonstrating how the combination of electronic and steric nature of the substituents on the phosphorus atoms strongly influences the efficiency of these phosphanes as organocatalysts.[5]

## 2. Study of 7-TH aryl and alkyl phosphine oxides as chiral Lewis bases in polyhalosilane-mediated reactions

The first studies on the catalytic activity of 7-TH-based tertiary diphosphine oxides **6a**–**c** as innovative chiral Lewis base organocatalysts in some $SiCl_4$-aldol-type reactions were carried out. For this study, three different tertiary diphosphine oxides, characterized

by substituents on the phosphorus atoms featuring different electronic and steric properties, have been synthetized (Scheme 2).

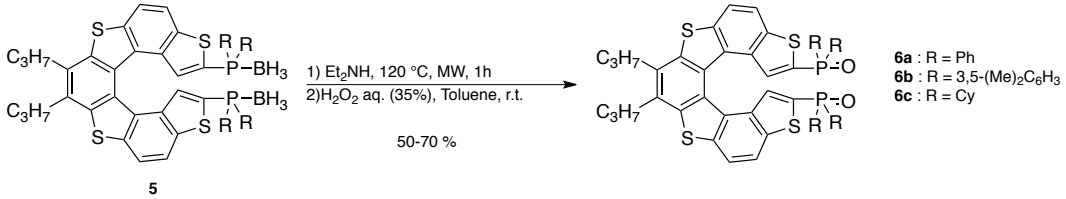


Scheme 2.

It was found the 7-TH aryl phosphine oxides **6a**–**b** showed to be chemically active organocatalysts in $SiCl_4$- or $HSiCl_3$-mediated aldol-type reactions and ketoimines reduction, affording the products with good chemical yield (up to 80%), and in some cases excellent diastereoselectivity (up to 93%), despite the reaction products were obtained in modest enantioselectivity (up to 23%).[6]

## 3. Study of chiral Au(I) complexes based on phospha-thiahelicenes

On the basis of these results, which demonstrate the good activity but the very low enantioselectivity of these systems, and in collaboration with Dr. Marinetti group, we designed a new enantiopure thiahelical phosphorus ligand **12**, in which a trivalent phosphorus function is embedded in the helical structure itself as a phosphole unit. This new ligand was prepared exploiting the highly regioselective and complete diastereoselective three-step procedure reported in Scheme 3.

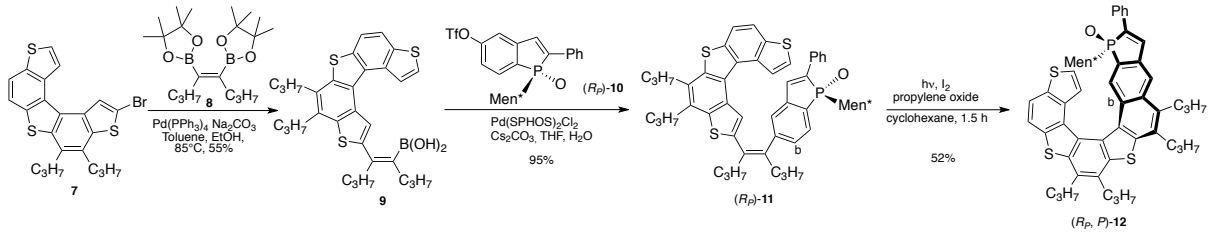


Scheme 3.

Next, ($R_P$,*P*)-**12** was converted into the corresponding Au(I) complex ($S_P$,*P*)-**13** as a single diastereoisomer, according to the diastereoselective one-pot procedure reported in Scheme 4.

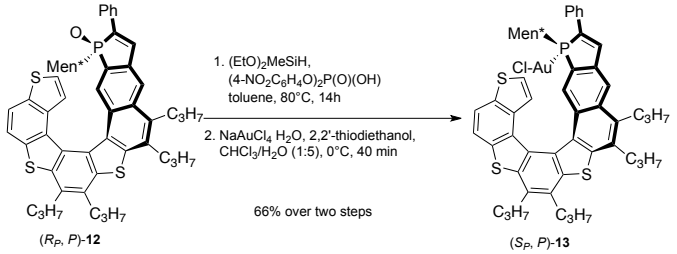


Scheme 4.

We then tested the catalytic activity of ($S_P$,*P*)-**13** in the cycloisomerization of different classes of enynes.

At first, depending on the nature of R, the cycloisomerization of dienynes **14** affords either the tricyclic derivative **15** (for R = Ph) or the bicyclo **16** (for R = H) in excellent *ee* (96% and 89% respectively) using Au (I) complex ($S_P$,*P*)-**13** activated with the proper silver (I) salt (Scheme 5). These represent the highest enantiomeric excesses attained so far in these cycloisomerizations.

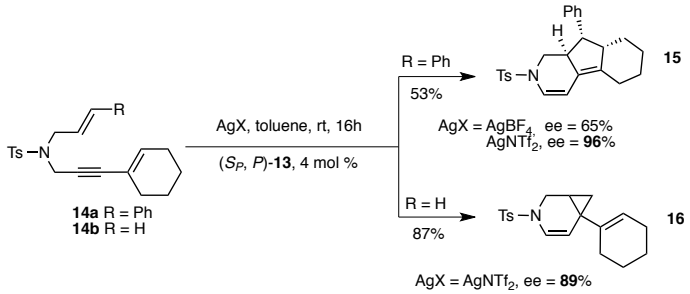


Scheme 5.

Again, the same catalyst ($S_P$,*P*)-**13** used in the cycloisomerization of enyne **17** provided the expected tricyclic derivative **18** as a single diastereomer, with very high enantiomeric excesses (93%, Scheme 6).

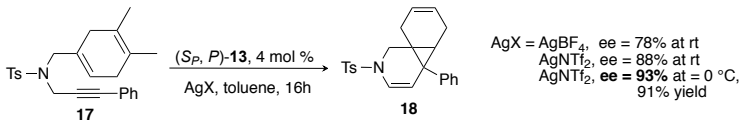


Scheme 6.

As far as we know, this is the first Au(I)-catalyzed asymmetric version of this reaction.[7]

These very promising enantioselectivity levels encouraged us to perform more extended catalytic screening so as to assess the potential of these helical ligands in enantioselective gold catalysis.[8]

## 4. Set up of a new non-photochemical synthesis of functionalized benzo[1,2-*b*:4,3-*b*']dithiophenes (BdTs)

To develop a general and scalable synthesis of benzo[1,2-*b*:4,3-*b*']dithiophenes (BdTs) **19**, that represent key intermediates for the preparation of 7-TH derivatives, a non-photochemical route involving $FeCl_3$-mediated oxidative intramolecular cyclization of $\alpha,\alpha'$-disubstituted dithienyl ethenes (*Z*)-**20** was developed. After a screening to optimize the experimental reaction conditions, some functionalized BdTs **19** have been obtained in moderate to good yields (Scheme 7).[9]

A similar procedure has been successfully used for the non-photochemical synthesis of 7-TH scaffolds.

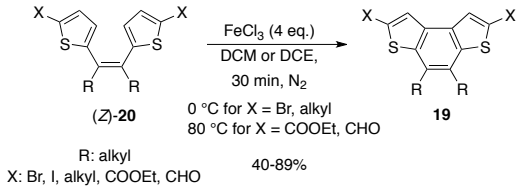


Scheme 7.

**5. Synthesis of a nanoconstruct based on PLGA nanoparticles loaded with a 7-TH derivative conjugated to a fluorescent probe**

In the second sub-topic, the synthesis, the characterization, and preliminary release, cytotoxicity and cell uptake studies were performed on a novel nanoconstruct obtained by nanoprecipitation of PLGA in the presence of 7-TH derivative conjugated to a fluorescent probe. These studies reveal interesting behaviors: (i) the particle size distribution was very narrow and no statistically significant difference was observed in the average size between blank nanoparticles (NPs) and nanoconstruct; (ii) the *in vitro* release of luminescent 7-TH derivative from NPs was time controlled, and did not display an initial burst step; (iii) the *in vitro* toxicity resulted to be significantly lower with respect to the free 7-TH derivative; (iv) the preliminary cell uptake study suggests a macropinocytosis pathway of entry into cells. The outcomes of these studies suggest the suitability of the developed nanosystem to act as a vector for the intracellular delivery of hydrophobic small molecules, such as helicenes, thus contributing to their possible future exploitation as novel cytotoxic compounds.[10]

**6. Synthesis of a new 7-TH based push-pull system and its preliminary application in DSSCs**

In the third and last sub-topic, the potential application of a 7-TH-based push-pull system, in which the thiahelical skeleton represents the π-conjugated-bridge spacer, was synthesized and preliminary used for the construction of a Dye Sensitizer Solar Cell (DSSC).

The optical characterization of this 7-TH-based dye was carried out by UV-vis absorption spectroscopy, and its electron transfer properties were studied by cyclic voltammetry, which has confirmed that this 7-TH-based dye satisfies the fundamental requisites for its use in DSSCs. So, a preliminary study on the photovoltaic performances of a DSSC based on 7-TH dye has been performed, obtaining a cell efficiency of 2.4%, that represents the highest value so far achieved with a helical skeleton as π-spacer in a push-pull systems.

***References***

1. a) Shen, Y.; Chen, C.- F. *Chem. Rev.* **2012**, *112*, 1463-1535; b) Aillard, P.; Voituriez, A.; Marinetti, A. *Dalton Trans.*, **2014**, *43*, 15263.

2. Monteforte, M.; Cauteruccio, S.; Maiorana, S.; Benincori, T.; Forni, A.; Raimondi, L.; Graiff, C.; Tiripicchio, A.; Stephenson, G.R.; Licandro, E. *Eur. J. Org. Chem.* **2011**, 5649.

3. Cauteruccio, S.; Loos, A.; Bossi, A.; Jaimes, M. C. B.; Dova, D.; Licandro, E.; Hashmi, A.E. *Inorg. Chem*. **2013**, *52*, 7995.

4. Dova, D.; Cauteruccio, S.; Dreuw, A.; Graiff, C.; Licandro, E. Manuscript *in preparation*.

5. Dova, D.; Cauteruccio, S.; Dreuw, A.; Mussini, P. R.; Licandro, E. Manuscript *in preparation*.

6. Cauteruccio, S.; Dova, D.; Benaglia, M.; Genoni, A.; Orlandi, M.; Licandro, E. *Eur. J. Org. Chem*., **2014**, 2694

7. Aillard, P.; Voituriez, A.; Dova, D.; Cauteruccio, S.; Licandro E.; Marinetti, A. *Chem. Eur. J.*, **2014**, *20*, 12373.

8. Aillard, P.; Voituriez, A.; Dova, D.; Cauteruccio, S.; Licandro E.; Marinetti, A. Manuscript *in preparation*.

9. Cauteruccio, S.; Dova, D.; Graiff, C.; Carrara, C.; Doulcet, J.; Stephenson, G. R.; Licandro E. *New J. Chem*. **2014**, *38*, 2241.

10. Cauteruccio, S.; Bartoli, C.; Carrara, C.; Dova, D.; Errico, C.; Ciampi, G.; Dinucci, D.; Licandro, E.; Chiellini, F.; *submitted*

# Introduction

## 1. Helicenes: an elegant and intriguing class of polyaromatic compounds

Helicenes are polycyclic aromatic compounds with non planar screw-shaped skeletons formed by *ortho*-fused benzene or other aromatic rings, which adopt a helical configuration, due to geometrical constraints and overlapping of the terminal rings (Figure 1). [1]

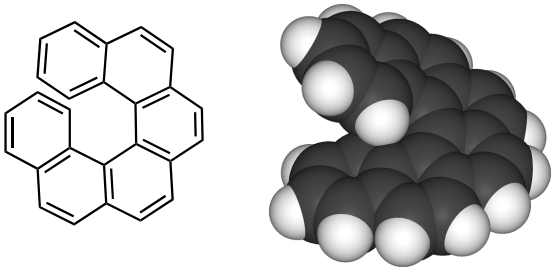

Figure 1.

In order to simplify the IUPAC nomenclature, Newman and Lednicer first introduced the name hexahelicene for phenanthro[3,4-*c*]phenanthrene in 1956. Adding a Greek prefix or using a number, *n*, in brackets [*n*] before the helicene name was also adopted: thus, pentahelicene = [5]helicene. The prefix or number denotes the number of aromatic rings in the helical backbone. Provided all these rings are benzenes, such compounds are called carbohelicenes. If one (or more) benzene unit is formally replaced by a heterocycle, such a skeletal modification leads to heterohelicenes. When the heteroaromatic rings are thiophenes, pyrroles or pyridines, and furans, they are named thia[*n*]helicenes, aza[*n*]helicenes, and oxa[*n*]helicenes, respectively (Figure 2). In some cases, they are named [*n*]heterohelicenes, hetero[*n*]helicenes, or [*n*]helicenes for simplicity and clarity.

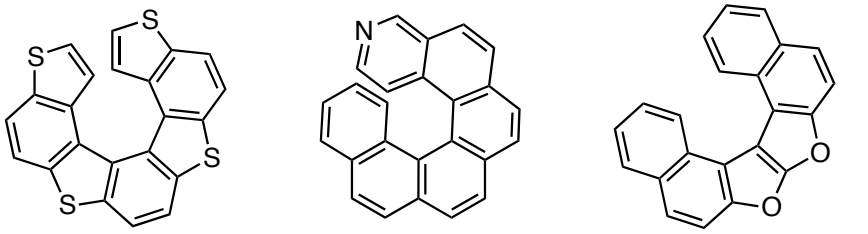


Tetrathia[7]helicene 3-Aza[6]helicene 7,8-Dioxa[6]helicene

Figure 2.

Note, however, that helicene must be fully aromatic. If some cycles are not aromatic, the correct nomenclature of these helical molecules is "*pseudo*-helicenes" or helicene-like compounds, and represent the third family of helicenes.

The defining property of a helicene is its helical structure. Because of the steric hindrance of the terminal rings, helicenes can wind in opposite directions, and have a $C_2$-symmetric axis, which is perpendicular to the helical axis (Figure 3a). This renders them chiral even though they have no stereogenic centers. On the basis of the helicity rule proposed by Cahn, Ingold, and Prelog in 1966, a left-handed helix is designated **"***minus***"** and denoted by *M*, whereas a right-handed one is designated **"***plus***"** and denoted by *P* (Figure 3b).

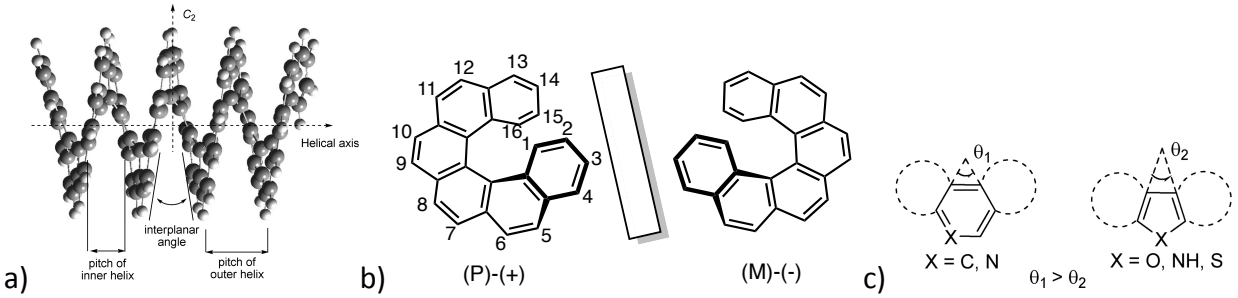


Figure 3.

Furthermore, according to the results of ORD and CD spectroscopy, as a general trend in a homochiral series, the *P* series of helicenes has a (+) dextrorotatory specific rotation and the *M* series has a (−) levorotatory specific rotation. As the number of fused rings increases, the helicene spirals up along the helical axis to form a cylindrical structure with a constant pitch (in both the inner and the outer helixes). For helicenes composed of six membered aromatic rings, it takes nearly six rings to cover a complete 360 °C rotation of a screw, while four thiophene and three benzene units are required for thiahelicenes, because of the smaller in-plane turn (θ) that the thiophene units contribute to the helical structure (Figure 3c). If other five-membered aromatic rings are incorporated into the skeleton, one complete 360 °C rotation also requires more rings.

**1.1 Structural properties**

The nonplanar structure arises because the connections between the rings are twisted. The interplanar angles (or the dihedral angles) of the two terminal rings depend on the lengths of the helicenes and the substituents present. As reported in Figure 4, the interplanar angles of carbohelicenes increase as the helicenes are elongated from [4]helicene (26.7°) to [6]helicene (58.5°), but decrease with further elongation (*e.g.* for [11]helicene the angle between the rings A and H is only 4.0°).

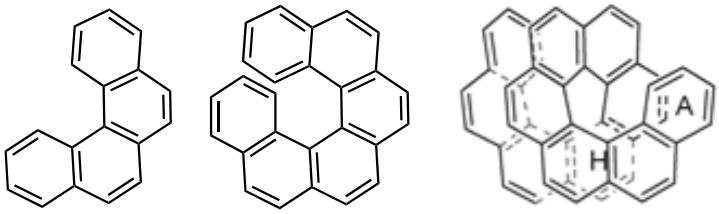


| | [4]helicene | [6]helicene | [11]helicene |
|---|---|---|---|
| interplanar angle (°) | 26.7 | 58.5 | 15.2 |

Figure 4.

Moreover, the pitch of the helix can be also modulated by the number and the nature of substituents on the helical skeleton (Figure 5).

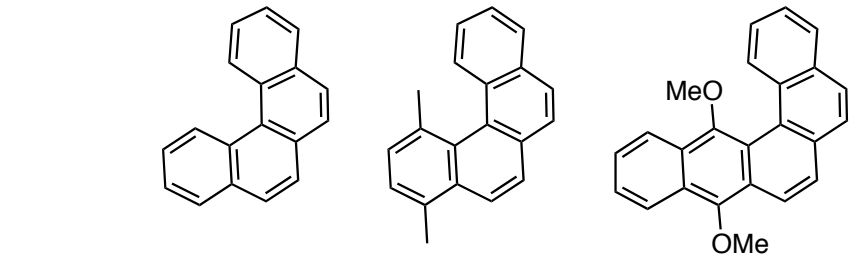


Figure 5.

In addition, overlap of the rings as well as the van der Waals interactions between nearby groups have been demonstrated by observing shielding and deshielding effects in the $^1$H NMR spectra of these helicenes. As a result of torsional strain, the bond lengths in the skeleton are different, with different C−C bonds having features of a single bond or a double bond. In comparison with the bond length of benzene (1.393 Å), the average bond length of the C−C bonds in the inner helix is lengthened to about 1.430 Å, while the average length of the ones on the periphery is shortened to about 1.360 Å. Surprisingly, numerous studies of the crystallographic structures of helicenes have always shown that there is a lack of C2 symmetry, not only because of the bond lengths but also because of the torsional angles between the inner carbon atoms, although the atoms on the same ring are approximately coplanar.

### 1.2 Racemization barrier of helicenes[1]

The racemization of helicenes is another intriguing property. In an attempt to understand the racemization process, two transition states (TS) of pentahelicene have been proposed as shown in Figure 6

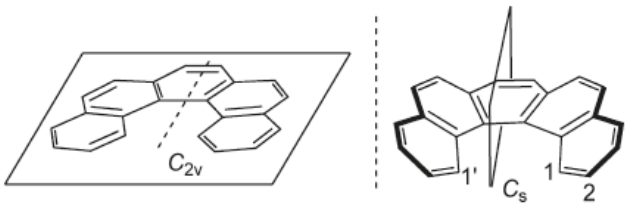


Figure 6.

In one TS, with $C_{2v}$ symmetry, the rings stretch outward but all the atoms are coplanar, while the other TS has $C_s$ symmetry with the terminal rings bending to the same side. The TS with $C_s$ symmetry has been adopted in most of the reported theoretical calculations. These suggest that the structure of an unsubstituted pentahelicene in the ground state (GS) first twists into the nonchiral $C_s$−TS, and the subsequent transformation to (*P*)- or (*M*)-configuration with equal probability releases the torsional strain and the repulsion and results in racemization. This suggests that fixing one or both of the terminal rings or introducing bulky substituents on the terminal rings are two practical methods of hindering the racemization by increasing the racemization barrier (even longer helicenes, like [9]helicene, $t_{1/2}$ = 123 min at 293.5 °C, undergo racemization via a more complicated process in which more than one TS might be involved). For example, the former can be achieved by forming metallocenes or by introducing two methyl groups at the 1,1'-positions of hexahelicene, in which case the half-life of racemization ($t_{1/2}$) is

increased from 13.4 min at 221.7 °C to 444 min at 270 °C. In contrast, substitution at the 2,2'-positions of helicenes does not have a significant effect on the racemization. However, if an aryl group is incorporated into the 1- or 1'-position, another method of racemization is feasible. In comparison with 1-methyltetrahelicene, the rotation around the single bond between the two aryl units of 1-phenyl-tetrahelicene accelerated the racemization process. Sometimes even the electronic effects of different substituents on the backbones may affect the racemization barrier.
In this regard, it is particularly interesting to understand the flexibility of a polyaromatic π-system as a dynamic conformational process during a helical racemization. In a general manner, a substituent effect in the 1st position of the helicene (in the bay area) causes an increase in the energy barrier of racemization. If two substituents are present in the bay area, such steric effects are even higher.

### 1.3 Tetrathia[7]helicenes: an emerging class of heterohelicenes

Although the domain has been dominated by carbohelicenes, an emerging trend is the fusion of thiophenes into the helical skeleton of the helicene, giving birth to various thiaheterohelicenes.[1] Among them, tetrathia[7]helicenes (7-TH, Figure 7), in which thiophene rings are fused to alternating arene rings, have an extended conjugated π system, and a configurationally stable helix with intrinsic asymmetry, which can be separated into *M* and *P* enantiomers.

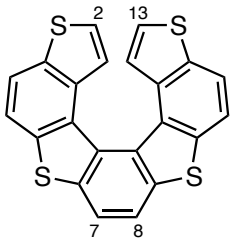


**7-TH**

Figure 7.

Thank to the possibility of combining the electronic properties of oligothiophenes with the unique chiroptical properties of helical shaped molecules, these systems have found manifold applications, especially in the field of materials with nonlinear optical properties.[2]
Furthermore, we have established that the 7-TH system can be easily functionalized at the alpha positions of the two terminal thiophene rings, allowing the modulation of the chemical and physical properties by varying the substituents.[3] In addition, the presence of substituents with different steric demands can tune the distance between the two terminal thiophene rings, resulting in remarkable variations in the dihedral angle of the molecule, which can accommodate a variety of bulky groups at C2 and C13 positions.
Concerning the synthesis of the 7-TH scaffold, two different approaches have been reported in literature, involving the formation of C-C bond between the β positions of the thiophene rings (*Route 1*, Figure 8), or by the construction of the double C=C bond between the alpha positions of the thiophene rings (*Route 2*, Figure 8).

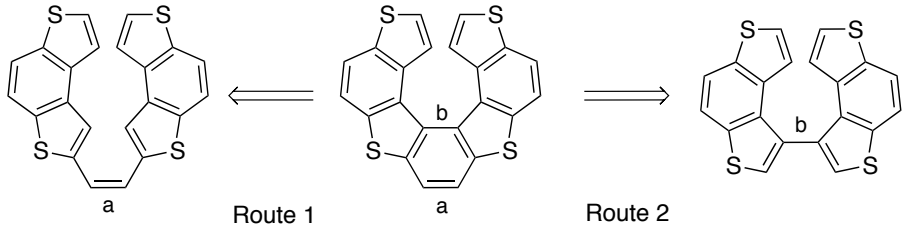


Figure 8.

Concerning the *Route 1*, this represents the classic method for the carbo and heterohelicene synthesis, involving a photocyclization of the corresponding stilbene-like precursors as key step. Despite the fact that this chemistry was developed over 30 years ago, it remains the most popular method for the preparation also of 7-TH systems. In particular, the synthesis of the 7-TH skeleton can be performed through the proper functionalization of the benzodi[1,2-*b*:4,3-*b*']thiophene scaffold (BDT) to selectively obtained the (*Z*)-alkenes **A**, which can be converted into the corresponding 7-TH systems by a photocyclization reaction using a medium-pressure Hg lamp in diluted toluene solutions (Scheme 1).[2]

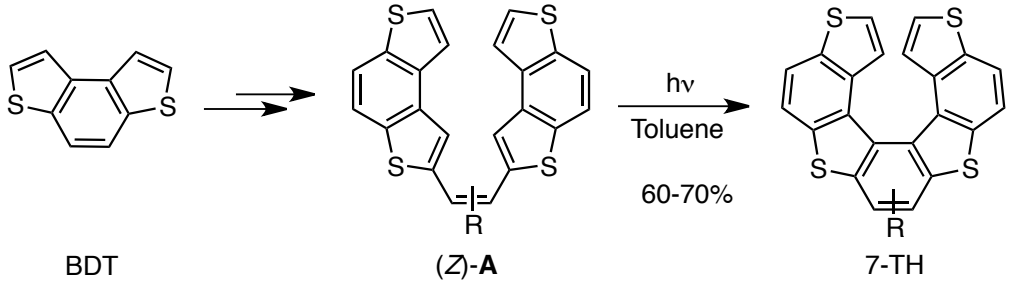


Scheme 1.

The photocyclization step usually provides isolated yields of the 7-TH ranging from 60-70%, albeit the efficiency of this reaction is strongly influenced by the concentration of the reaction solution, and then by the solubility of the (*Z*)-**A** precursors. As this regard, the configuration (*Z*)- or (*E*)-of the stilbenoid precursors **A** plays a crucial role in the efficiency of the photocyclization, since (*Z*)-isomers are often more soluble in organic solvents than the corresponding (*E*)-isomers, which also took place longer reaction times. For these reasons, two alternative procedures have been developed by Licandro's group to selectively obtained (*Z*)-alkenes (Scheme 2).[3]

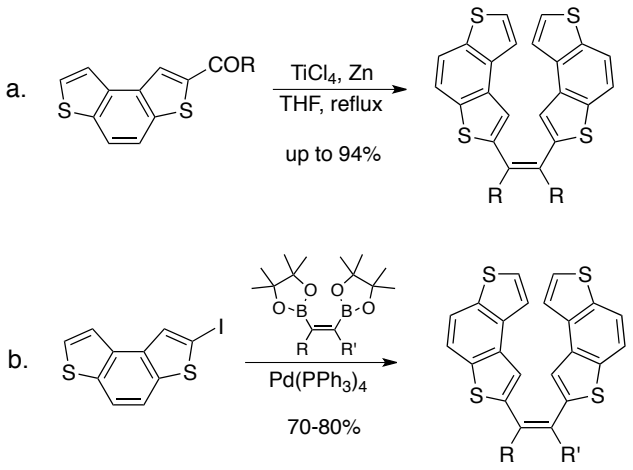


Scheme 2.

The first procedure involves the synthesis of an alkyl ketone of the corresponding BDT, followed by a stereoselective McMurry coupling in the presence of $TiCl_4$ and Zn in THF (Scheme 2a).
In the second procedure, BDT scaffold is converted into the corresponding 2-iodo derivative which undergo a subsequent palladium-catalyzed Suzuki coupling with symmetrical or unsymmetrical bis-boronates (Scheme 2b). In this case, unsymmetrical 7-TH scaffolds could be obtained.

Concerning the *Route 2*, Tanaka and co-workers[4] reported an alternative diastereoselective synthesis of the 7-TH skeleton, which didn't involve a photochemical step (Scheme 3).

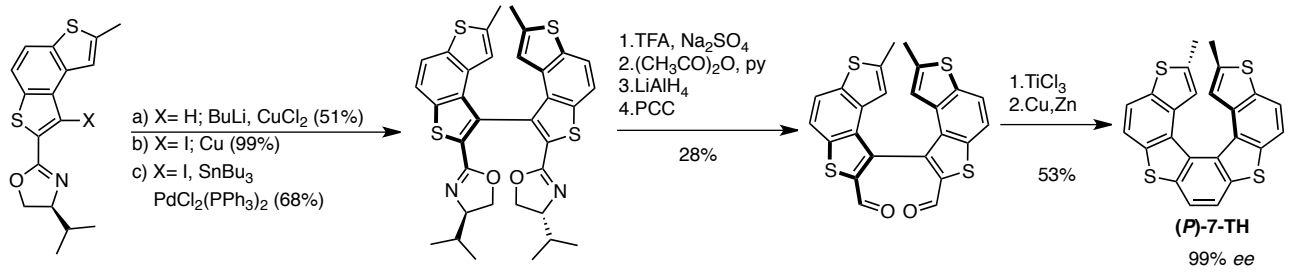


Scheme 3.

In particular, the asymmetric Ullmann or Stille coupling of the starting BDT precursor having a chiral moiety in the alpha position, followed by an intramolecular McMurry coupling gave the tetrathia[7]helicene scaffold in 99% *ee*. It should be noted that the sterogenic centre was successfully transformed into a stereogenic axis, and then in a helical stereogenic element. The chiral oxazoline substituent plays a key role, not only in the enantioselectivity, but also in providing an atropisomeric biaryl system with stable $C_2$ symmetry, which subsequently is converted into a dialdehyde for the further coupling reaction.

**1.4 Helicenes: general features and applications**

In summary, the chirality and the helical pitch of the helix are mainly due to a conformational distortion of the π-system imposed by an intramolecular steric repulsion and sometimes to a lesser extent, from an electronic contribution. The helical topology of carbohelicenes provides a high optical rotation, high circular dichroism values, and several enhanced physical-organic properties. Another peculiarity is their polarizability, which provides a propensity for making π-complexes. These interests in carbohelicenes were further sustained by some theoretical investigations for testing the limits of aromaticity, for testing chiral charge-transfer complexations and to further understand helical chirality in some polyaromatic compounds with distorted π-systems. Because of all the above-mentioned features, helicenes were an intriguing class of molecules that have been some synthetic targets of historical importance. However, the interest toward the helicenes chemistry increased dramatically during the last years as demonstrated by the diagrams on the number of articles and related citations on helicenes, obtained by "*Web of Science* " (Charts 1).

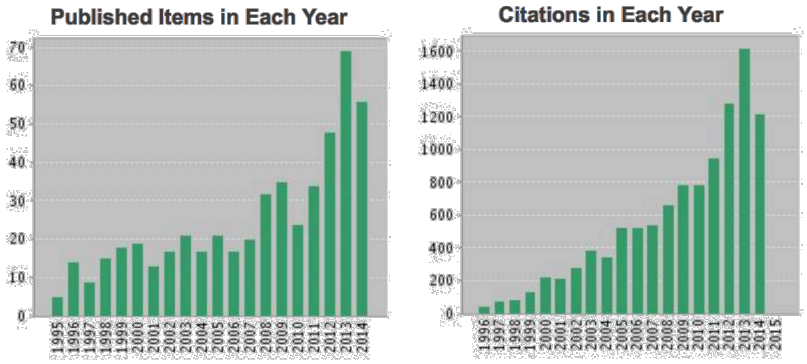


Chart 1.

Historically, many efforts have been devoted to the synthesis of carbohelicenes and a plethora of helicene molecules have been produced over 100 years. They were often generated from the oxidative photocyclodehydrogenation methodology. More recently, numerous non-photochemical methods have been investigated. Since the first reports on the resolution and asymmetric synthesis of helicenes, the discovery of their exceptional chiroptical and physicochemical properties has encouraged their uses in many fields.

Due their chiral properties, helicenes were applied to asymmetric synthesis, indeed different phosphine ligands carrying a helicene moiety have been prepared. Such compounds were, for instance, used for asymmetric hydrogenation or helicenes carrying a nitrile group have been used for asymmetric epoxidations. Helicenes were also applied to asymmetric organocatalysis. Optically enriched helicene samples added to the reaction mixture of an asymmetric autocatalytic Soai reaction, are able to induce very efficiently chirality. Due to high chiral amplification in this reaction, the chiral information is only needed in low amounts. In the present case, this means that efficient chiral induction is possible with helicene samples possessing low enantiomeric excess. Again, a helicene moiety can also be incorporated in a crown-ether. Such compounds may be applied to chiral recognition. Helicene structures could be found in chemosensors, and some foldamer structures with helicene moieties have been synthesized. They are also incorporated into supramolecular structures; and they have been used to induce chirality in liquid crystals by twisting a nematic phase. Applications in material science have also been reported. Thus, capto/dative substituted helicenes have been tested in OLEDs. In biological field, helicene interaction with DNA or enzymes, such as telomerase or topoisomerase I, may be used for medicinal purposes. It must be pointed out that although the number of application fields is high, many applications are only superficially or occasionally investigated. In such cases, more profound studies are necessary in order to develop the whole potential of helicenes in the corresponding application domains.

For the purposes of this thesis, herein the following applications of the helicenes will be discussed in more detail: *i)* the most important results on the chiral recognition of helicenes; *ii)* the use of helical molecules in asymmetric organocatalysis; *iii)* the synthesis of the helicene phosphorus derivatives, and their use in asymmetric organometallic catalysis.

## 2. Helicenes in chiral recognition

The peculiar chirality of the helical systems has been used in the enantioselective phenomena of the chiral recognition discrimination. To start with, it is worth mentioning that the high efficiency of helical compounds in stereocontrol phenomena related to chiral induction, has been demonstrated by Martin et al.[5] These authors demonstrated, for instance, that the racemic 2-hydroxy-[7]helicene derived pivalate **1** undergoes addition of Grignard reagents with total diastereoselectivity (Scheme 4).[6]

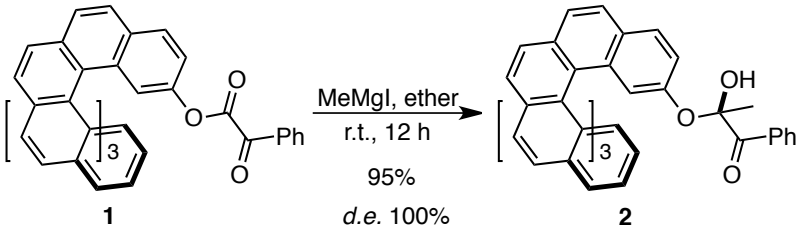


Scheme 4.

The same authors[7] also reported the first example of the use of an enantioenriched carbohelicene in organic synthesis to induce asymmetry (Scheme 5).

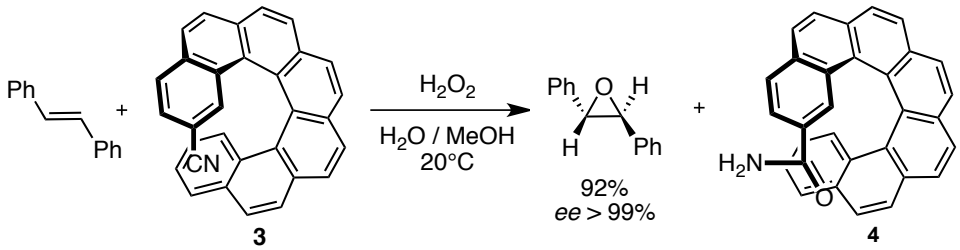


Scheme 5.

In particular, using a stoichiometric amount of enantioenriched 2-cyano[7]helicene **3** in the oxidation reaction of the *E*-stilbene by $H_2O_2$, it was possible to obtain the corresponding enantiopure epoxide in excellent *ee*, along with the helical derivatives **4**.

Similarly, helicene **3** afforded excellent results in the oxidation of the α-methylstyrene (yield: 84%, *ee*: 98%). This work was a nice demonstration of an excellent diastereotopic face discrimination of a non-functionalized alkene. More importantly, it emphasized the utility of a large chiral template from a helicene skeleton, as an effective chiral stereodiscriminating element in asymmetric synthesis. However, although these results are very promising, no other application has been reported because of the need to use a stoichiometric amount of the chiral inductor. In fact, similar catalytic asymmetric epoxidations of non-functionalized alkenes with other chiral iminium salts from a hetero[5]helicene were reported, but with a less stereoselective efficiency.

In 2000, Reetz[8] and co-workers reported the use of the (−)-**HELIXOL**, the 2,15-dihydroxy-[6]helicene, as fluorescent sensor for chiral aminoalcohol and amines (Figure 9).

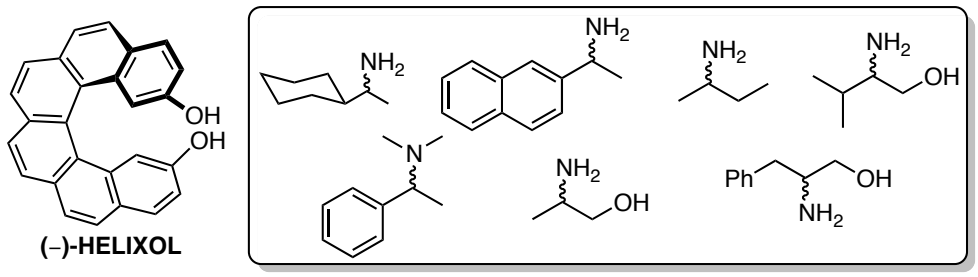


Figure 9

In particular, when (−)-**HELIXOL** was treated with pairs of (*R*)- and (*S*)-enantiomers, different quenching rates were obtained, indicating chiral recognition between (−)-**HELIXOL** and the quenchers (the amine derivatives). Thus, optically pure [6]**HELIXOL** might be a useful enantioselective sensor by virtue of its high fluorescent intensity and high degree of chiral recognition.

## 3. Helicenes in asymmetric catalysis

Although many different kinds of chiral ligands and chiral catalysts have been developed so far, it is surprising that no ligands bearing helical chirality were used in asymmetric catalysis until 1997. In fact, the use of helicenes as catalytic scaffolds had long been considered an impractical choice, presumably due to the difficulties in the preparation of appreciable amounts. However, thanks to the development of new methodologies for the enantioselective or diastereoselective synthesis of helicenes, along with the possibility to separate significant amounts of racemic helicenes by chiral HPLC, their use in catalysis is growing significantly. Several features would position them favorably with a large chiral polyaromatic template, which could favor some efficient and long range chiral inductions and some secondary binding interactions to the substrate by π-stacking. Additionally, reactions at higher temperatures might be possible without racemizing the helicene ligand. It would be an advantage compared to a lower-energy thermal racemization of many binaphthyl ligands (*e.g.* BINAP and DIOP ligands).

In particular, different types of helical structures have been reported to use in catalysis, including helicene derivatives as chiral additives, azahelicenes as chiral organocatalysts, and helicene containing phosphorous atoms as chiral ligands in organometallic catalysis.

### 3.1 Helicenes as chiral additives in asymmetric catalysis

Since the configurational stability of some [4]helicenes at 20 °C comes from the steric hindrance of inner methyl groups, in 1998 Yamaguchi and co-workers[9] reported the use of [4]helicenes as chiral ligands or chiral building blocks. In particular, a (*P*,*P*) macrocyclic polyamide **5**, incorporating two [4]helicene units, promoted a catalytic asymmetric reaction as a chiral additive, for generating many enantioenriched aromatic alcohols with modest enantioselectivities (Scheme 6).

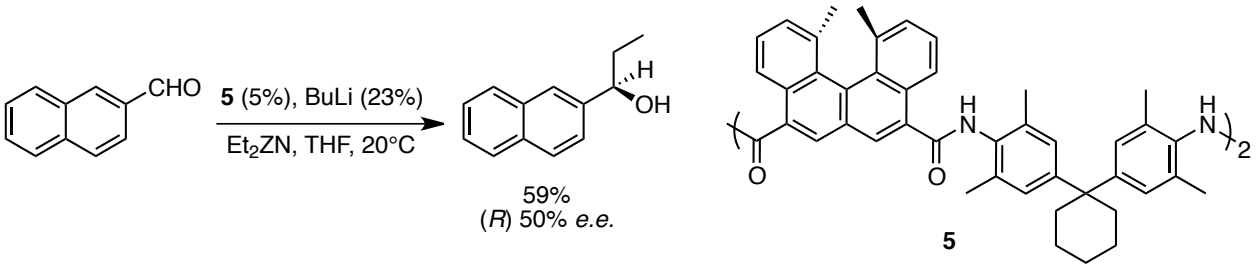


Scheme 6.

Again, Katz[10] reported the use of the ligand (*P*,*P*,*S*)-[5]HELOL **6**, bearing a chiral pocket topology with inner hydroxyls, in the addition of diethyl zinc to benzaldehyde to form the corresponding alcohol with 81% *ee* (Scheme 7).

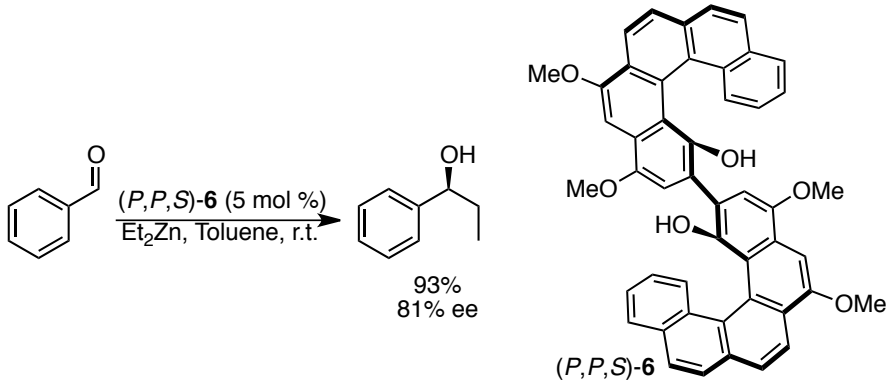


Scheme 7.

Katz postulated that this reaction proceeds through an intermediate in which the zinc, covalently bound to **6**, coordinates the benzaldehyde. One side of the aldehyde is then locked forcing $Et_2Zn$ attack from the opposite side.

Finally, Soai and co-workers[11] found that hexahelicene **7** and tetrathiahelicene **8** could be used as asymmetric triggers for the autocatalytic reaction between dialkylzinc and a pyrimidyl aldehyde (Scheme 8).

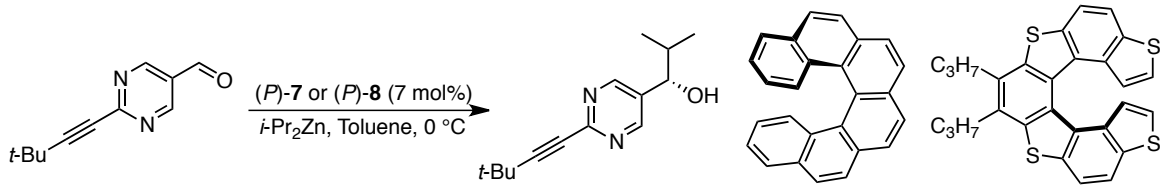


Scheme 8.

In these reactions, all (*P*)-helicenes induced formation of the (*S*)-alcohol in high *ee*. Even if helicenes with very low *ee* were used, for example (*P*)-**7** in nearly 0.13% *ee* and (*P*)-**8** in 2% *ee*, the reactions still gave products with 56% and 83% *ee*, respectively.

### 3.2 Heterohelicenes as organocatalysts in asymmetric reactions

The use of helicene derivatives in organocatalysis has been highly neglected in carbohelicene chemistry. However, a few examples were reported by using a series of 1-aza-helicene *N*-oxides as chiral organocatalysts in heterohelicene chemistry. In particular, it is only until 2008 that

Takenaka[12] reported the first example on the use of a helical pyridine *N*-oxide **9** as organocatalyst in reactions of epoxides desymmetrisation in the presence of $SiCl_4$ (Scheme 9).

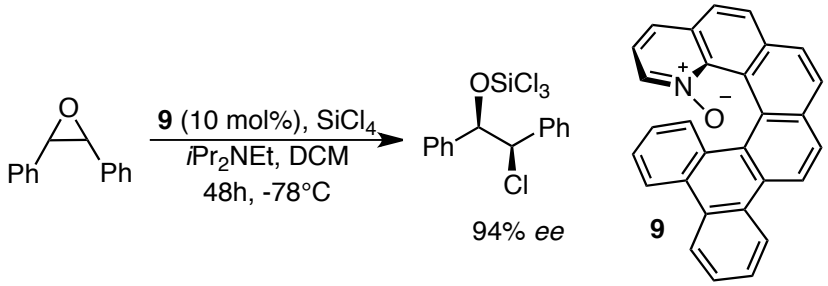


Scheme 9.

In this case, the catalyst **9** provides good yields and high enantiomeric excesses up to 94%. Furthermore, modification of the helical pyridine *N*-oxides can increase both the substrate scope and the enantioselectivity, as demonstrated by the use of the helically pyridine *N*-oxide **10** to catalyze the reactions between aldehydes and the allene trichlorosilane (Scheme 10).[13]

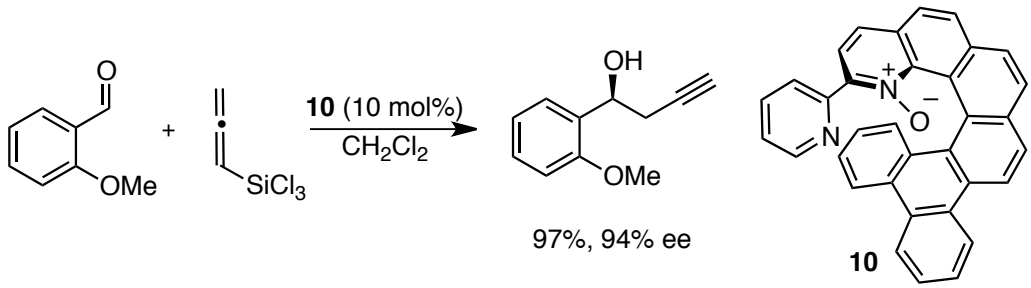


Scheme 10.

Next, in 2009 Starý e Stará[14] utilized (*P*)-1-aza- and (*M*)-2-aza[6]helicene as organocatalysts in the asymmetric acyl transfer reactions of (±)-1-phenylethanol (Scheme 11).

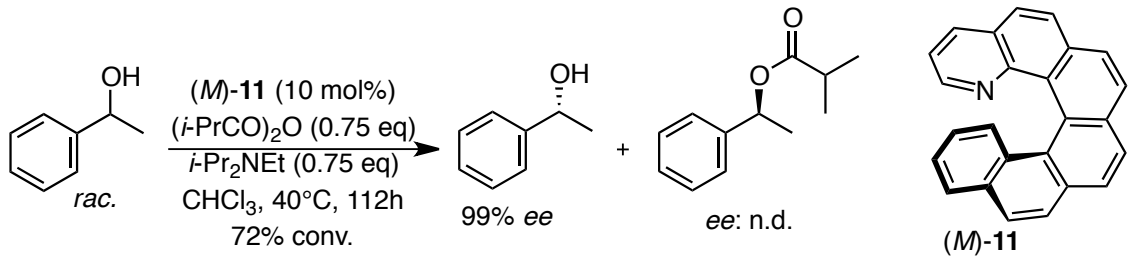


Scheme 11.

The authors found that (*P*)-1-aza[6]helicene had low activity (<5% conversion), which might be a result of the limited accessibility because the N atom is at the most sterically hindered position. However, 2-aza[6]helicene **11**, with high proton affinity and a pKa (in $H_2O$) of 5.28 showed good catalytic efficiency, affording (*R*)-alcohol in 99% *ee* with up to 72% conversion when the reaction was carried out using (*i*-PrCO)$_2$O as the anhydride and *i*-$Pr_2$NEt as the base.

Recently, the kinetic resolution of secondary alcohols was re-examined by Carbery and co-workers (Scheme 12).[15]

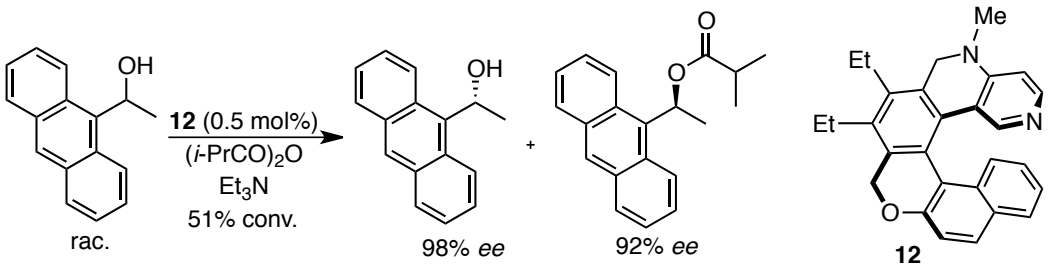


Scheme 12.

They designed a helicenoidal DMAP analogue **12** bearing a dialkylaminopyridine unit and helical scaffold as a Lewis base catalyst, which afforded the secondary alcohol, the (*R*) configuration, in 98% *ee* and the ester, with (*S*)-configuration, in 92% *ee*. This organocatalyst showed high levels of selectivity (selectivity factor s up to 116) and excellent reactivity.

In 2010, a new kind of helicene **13**, bearing a 2-aminopyridinium terminal ring was prepared and shown to be an efficient dual-hydrogen-bond donor catalyst for the addition reactions of dihydroindole with a nitroalkene at low temperature (Scheme 13).[16]

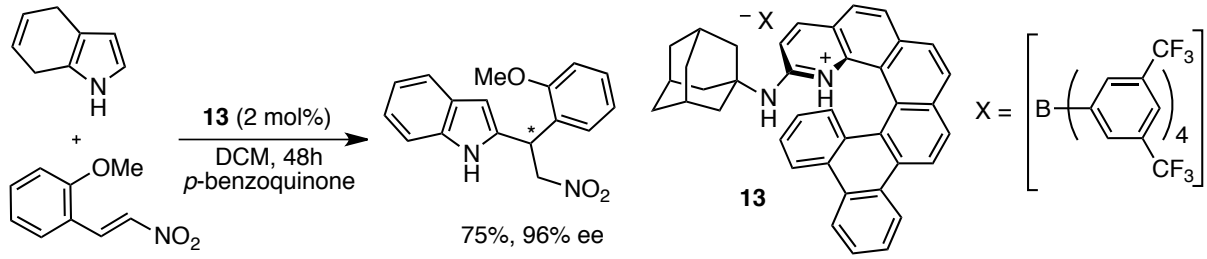


Scheme 13.

Again, very good enantiomeric excesses of up to 96% are obtained using the helical catalyst **13**. To note the excellent catalyst activity of this organocatalyst that requires only 2 mol% of catalyst charge.

In summary, almost all of azahelicenes applications in this field refer to helicenes where the heteroatom is incorporated into the helical structure. For example, the nitrogen atom on helicene **13**, used successfully by Takenaka in the organocatalyzed addition of nitroalkenes to indoles, is part of the helical structure, and is located at the end of the helical skeleton. The effectiveness of this catalyst could be explained by this particular positioning of the nitrogen function.

### 3.3 Helicene phosphorus derivatives in asymmetric organometallic catalysis

Whilst axial, central and planar chirality have been largely exploited to build chiral phosphorus ligands and organocatalysts, helical chirality has been rather neglected so far in this field. Several carbohelicenes and heterohelicenes with appended phosphorus functions have been prepared in either racemic or enantiomerically pure form, but catalytic screenings are limited mainly to a few benchmark reactions, such as olefin hydrogenations or palladium promoted allylic substitutions. The most representative examples of helicene phosphine molecules, reported by Reetz,[8,17] Katz,[18] Yamaguchi,[19] Starý,[20] Licandro[21] and Marinetti,[22] are reported in Figure 10.

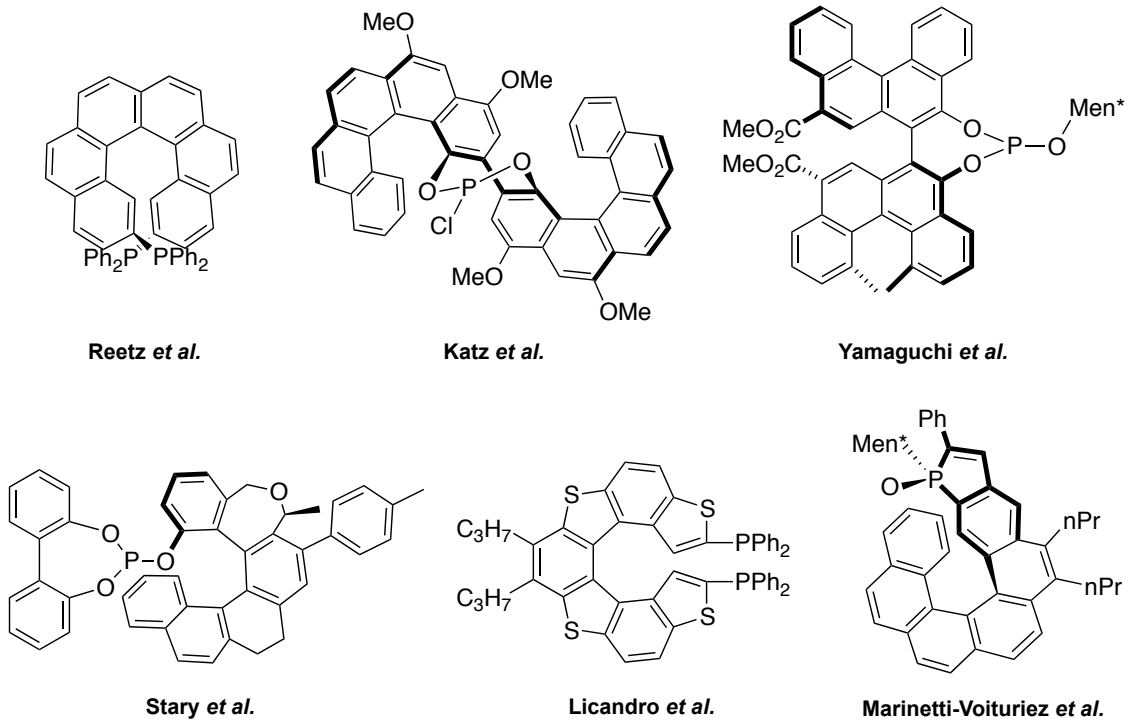


Figure 10.

### *3.3.1 Helicenes with appended phosphorus functions*

The largest class of helicenes with appended phosphorus functions is made of helical derivatives displaying $P(X)Ph_2$ substituents (X = O, $BH_3$, lone pair). The most common access to these helicenes involves introduction of the phosphorus function from a suitably functionalized helical precursor, at a late step of the synthetic sequence. Thus, one of the first known methods is the reaction of bromohelicenes with $ClPPh_2$ or $ClP(O)Ph_2$ via halide-lithium exchange, typified in Scheme 14.

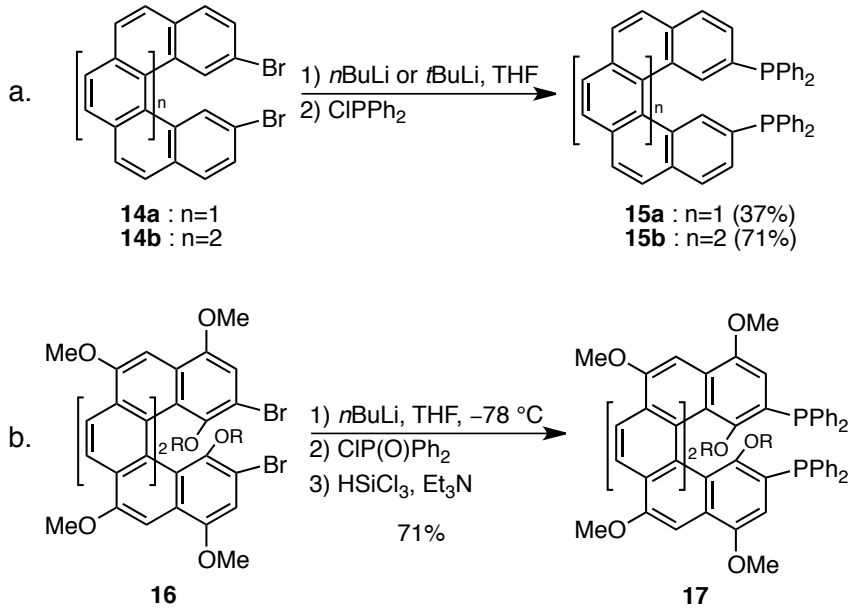


Scheme 14.

In 1997, the first syntheses of helical phosphanes in racemic form, namely phosphines **15a**-**b**, were reported by Brunner and Reetz's groups in two independent works (Scheme 14a).[23,17a]

In particular, Reetz's group also reported the tridimensional structure of (±)-**15b** by X-ray analysis, in which the twisted helical form of the carbon backbone was geometrically quite similar to the structure of hexahelicene itself, and the phosphorus-phosphorous atoms distance of 6.481(1) Å, [P1---P2], was much longer than the 4.6 Å, predicted on the theoretical calculations (Figure 11).

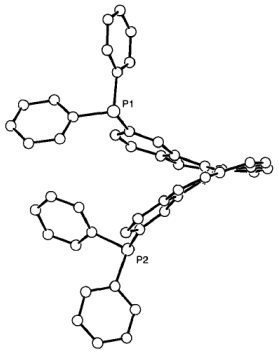


Figure 11.

In 2003, Katz and co-workers[24] reported the synthesis of funcionalized [6]- and [7]-helicene-based diphosphanes **17** (Scheme 14b). Optically pure phosphines **15b** and **17** have been obtained by either resolution of the starting bromide **14b** and phosphine oxides, respectively, by HPLC on chiral stationary phase.

Finally, Starý's group[20a] reported the synthesis of [6]-carbohelicene-based monophosphine **18**, in which the $PPh_2$ moiety is the 3-position of the helical skeleton (Figure 12).

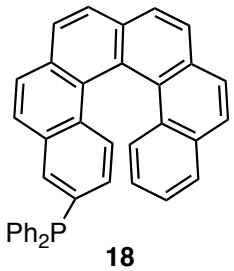


**18**

Figure 12.

In all these cases, the phosphorus functions were added by bromide/litium exchange reactions on the pre-formed carbohelicene scaffolds.

Alternatively, phosphorus functions can be introduced on helical scaffolds by palladium promoted couplings between $Ph_2PH$[25] or $Ph_2P(O)H$[20a] and helicenes **19** and **21** bearing suitable leaving groups (Scheme 15).

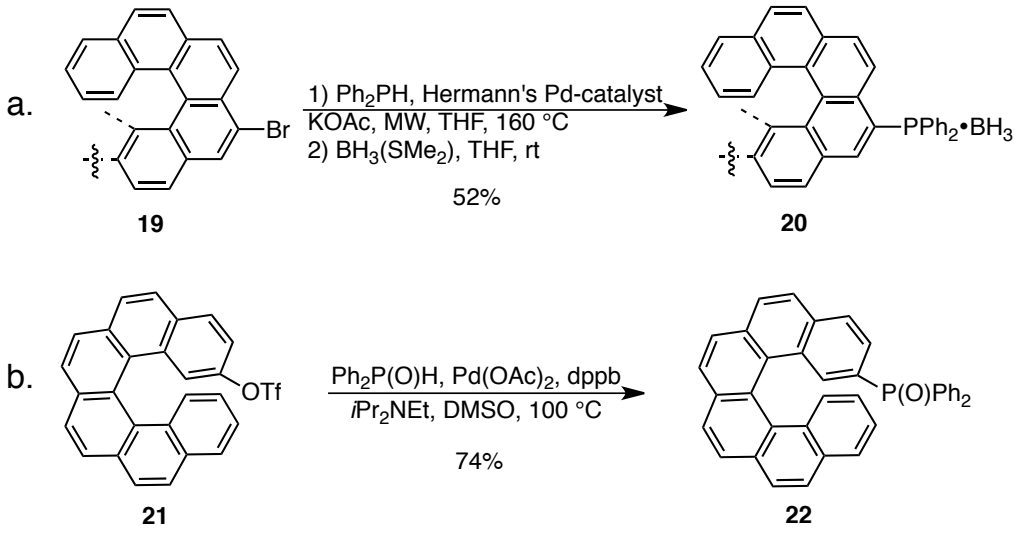


Scheme 15.

Both helical bromide **19** and triflate **21** are suitable substrates for these catalytic reactions.

A totally different approach to helical phosphines involves building of the helical scaffold from non-helical precursors, which bear the phosphorus function. Thus, Marinetti and co-workers[22a] reported the oxidative photocyclization of the dienic phosphine oxide **23** to give the 2-diphenylphosphinoyl[7]helicene **24** in 57% yield (Scheme 16).

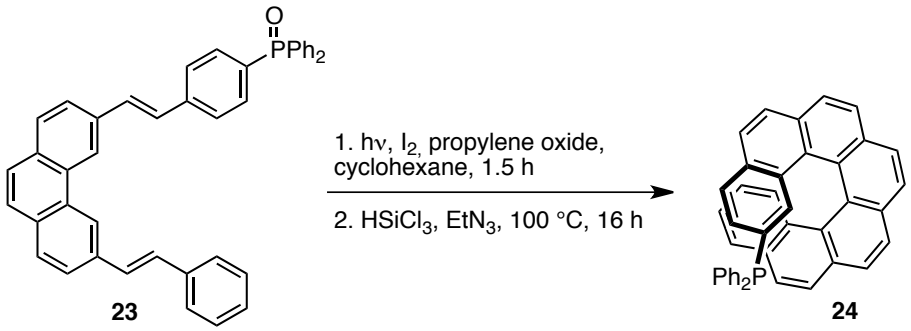


Schema 16.

Moreover, the resolution of the trivalent helical phosphine **24** has been carried out through formation of diastereomeric palladium complexes.

Again, in the same year Marinetti's group [26] reported the synthesis of an unsymmetrical disubstituted hexacarbohelical mono phosphane **25** (Figure 13).

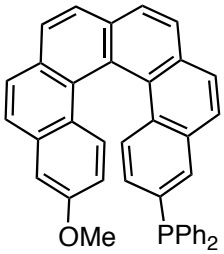


Figure 13.

Concerning the study of helical phosphorus derivatives characterized by a heterohelicene scaffold, only in 2011 Licandro's group[21a] reported the synthesis of tetrathiahelicene-based mono and diphosphanes as air-stable phosphane-borane complexes **26** and **27**, by a one-pot protocol that

involved the treatment of the starting thiahelicene **8** with the proper amount of *n*BuLi and the $ClPPh_2$, followed by the addition of a large molar excess of $BH_3$THF complex (Scheme 17).

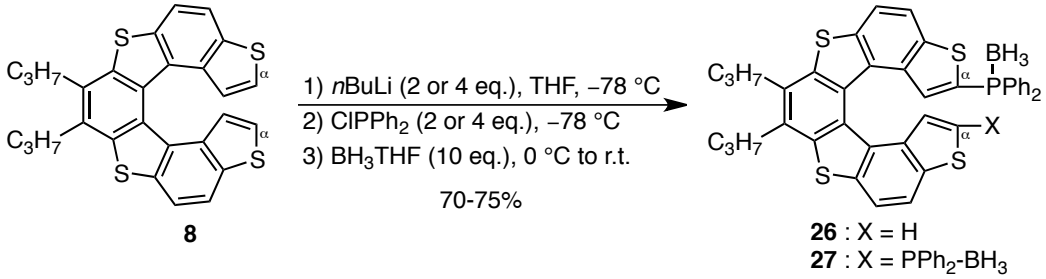


Scheme 17.

The synthesis of the 7-TH phosphanes as stable borane adducts allowed to an easier manipulation and storage of the corresponding very air-sensitive free phosphanes **28** and **29**, which could smoothly obtained treating adducts **26** and **27**, respectively, with a refluxing mixture of MeOH and THF under an inert atmosphere (Scheme 18).

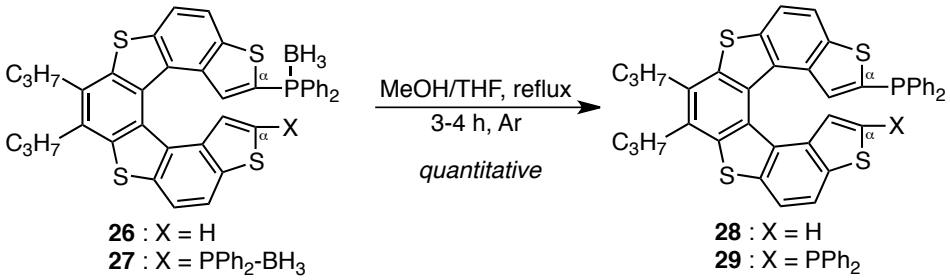


Scheme 18.

The presence of the two terminal thiophene rings on helicene **8** allowed the direct lithiation of the thiophene rings at their 2-positions to introduce $PPh_2$ groups, without previous functionalization of the helical scaffold. By this method, $P(O)(OEt)_2$ function was also introduced on the thiahelicene scaffold **30** to afford the phosphonate **31** in 77% yield[21a] (Scheme 19).

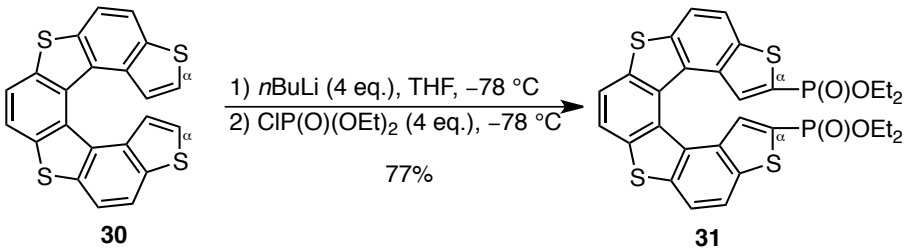


Scheme 19.

Successively, Hassine's group[27] reported the synthesis of two other thiahelicene-based mono phosphanes **32** and **33**, characterized by an internal and a terminal thiophene ring, respectively, on the helical skeleton (Figure 14).

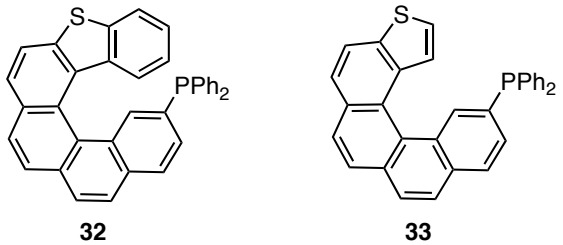


Figure 14.

These are the most important examples of helical phosphines reported in literature, and in particular only 3 examples of heterohelicene-based phosphanes, especially thiahelicenes, have been reported to date.

### *3.3.2 Helical phosphites*

In addition to phosphane derivatives, the literature reports a few examples of helical phosphites. These compounds are available from the corresponding helical diols or alcohols with chloro- or dichlorophosphites, under classical conditions, as shown in Schemes 20 and 21.

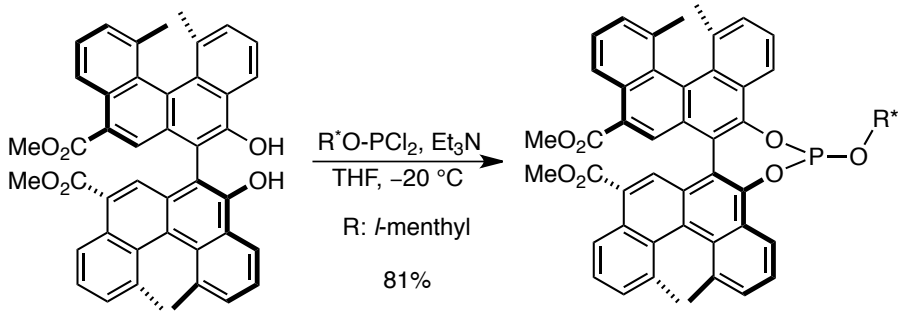


**34** **35**

Scheme 20.

The bis-[4]helicene-derived diol **34**, which displays both helical and axial chirality, was obtained in enantiomerically pure form by separation of its camphanic esters by column chromatography and was converted then into phosphite **35** in 81% yield (Scheme 20).[19] It must be noticed that the [4]helicene unit of **34** displays an only moderate configurational stability, since it epimerizes in refluxing toluene.

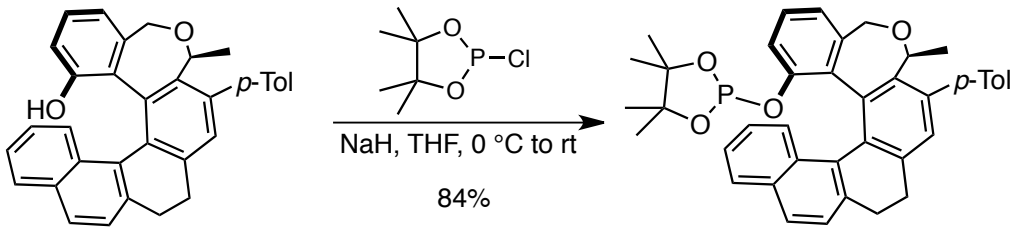


**36** **37**

Scheme 21.

In the similar manner, phosphite **37** was obtained in 84% yield starting from the enantiopure alcohol **36** (Scheme 21).[20b]

### *3.3.3 Helical phospholane derivatives*

In the last years, new typologies of helicene phosphorous derivatives have been reported in literature, and they can be divided in two main groups: *i)* helicenes displaying phosphole substituents phospholane; ii) helicenes with the phospholane unit embed in the helical skeleton.

Concerning the first class, Crassous and co-workers[28] reported different types of *aza*-helicenes with a phospholane unit directly bound on the pyridine ring of the helical scaffold (Figure 15).

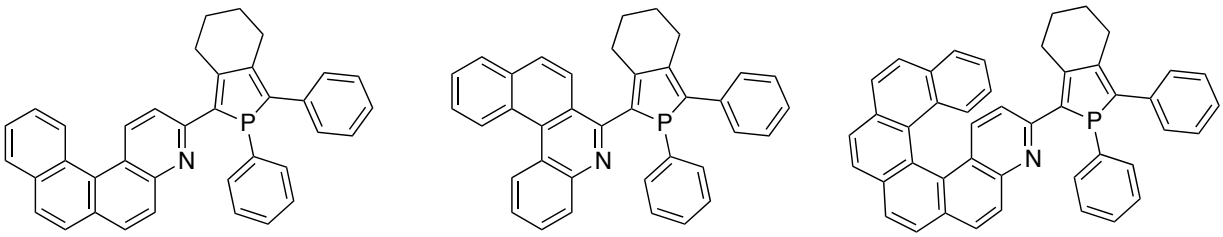


Figure 15.

Compounds of this class have been especially targeted mainly because of their peculiar chiroptical properties that should be easily tunable by coordination of the phosphorus function to transition metals (*e.g.* Pd, Pt, Ru, Cu).

Concerning the second class, first examples of helicenes with phospholane unit embed in the helical skeleton have been reported by Tananka[29] and Nozaki[30], but no application of these phosphahelicenes in catalysis or in other fields, has been reported so far (Figure 16).

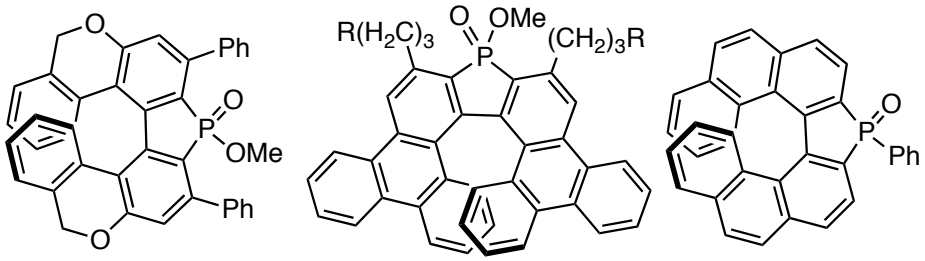


**Tanaka *et al.*** **Nozaki *et al.***

Figure 16.

Next, Marinetti group's[22b,22c, 31] reported different phosphahelicene derivatives, in which the phosphorus center is located at the end of the helical sequence, as sketched in Figure 17.

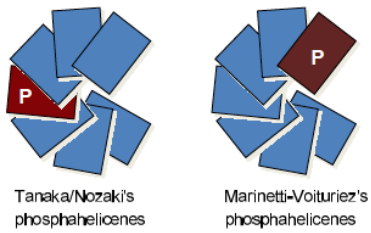


Figure 17.

This new design was motivated by the specific aim of using phosphahelicenes as chiral auxiliaries in asymmetric catalysis. In these compounds, the overlapping of the aromatic rings at the end of the helical sequence will create a three-dimensional, highly asymmetric environment around phosphorus, which could be a key feature for chiral induction (Figure 18).

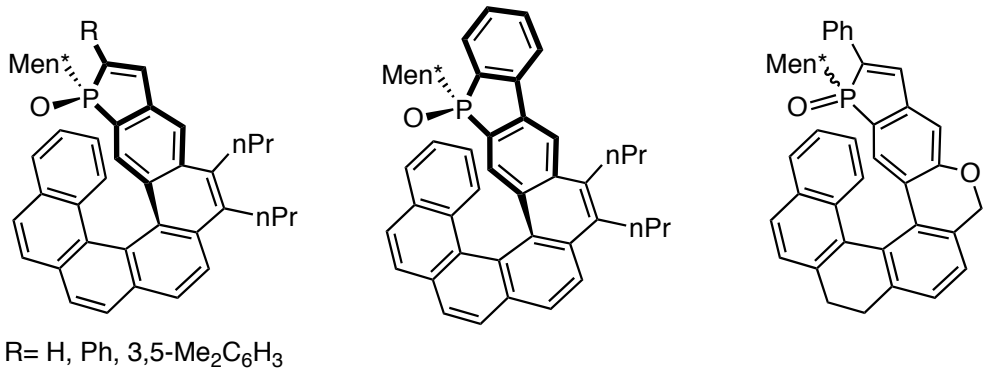


R= H, Ph, 3,5-$Me_2C_6H_3$

***Marinetti et al***

Figure 18.

*3.3.4 Helical phosphanes in palladium (II) promoted allylic alkylations*

One of the first uses of helical phosphines as ligands in enantioselective catalysis has been reported by Reetz et al. in 2000.[17b] Palladium complexes of the [6]helicene derived diphosphine (*P*)-**15b** were formed *in situ* from $[(\eta^3\text{-}C_3H_5)PdCl]_2$, with a phosphine-to-palladium ratio of 2:1. According to $^{31}P$ NMR analysis, the mixture contains several species, which founded the assumption that the diphosphine does not behave as a chelating ligand. Nevertheless, when this catalytic system was used in the kinetic resolution of allylic acetate via enantioselective Tsuji-Trost reaction total conversion was achieved in 4h at room temperature, and very good enantiomeric excess (83-99% *ee*) were obtained (Scheme 22).

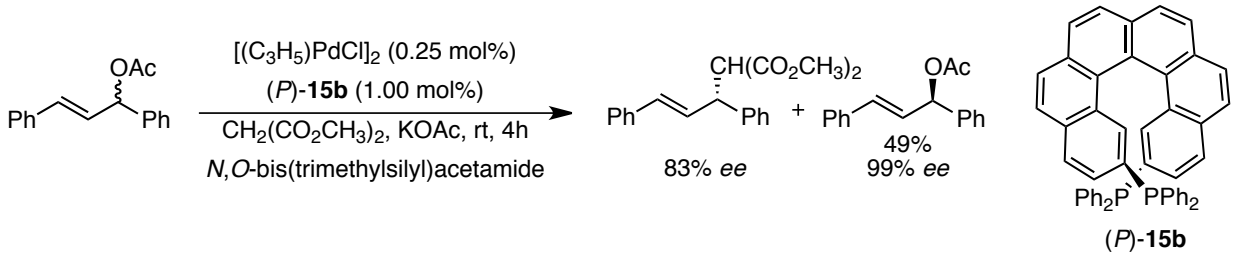


Scheme 22.

*3.3.5 Helicene phosphorous derivatives in rhodium (I) asymmetric catalysis*

Several helicene-like molecules with appended phosphorus functions have been evaluated in olefin hydrogenations as benchmark reactions. In this context, the first example was reported by Reetz in 1997,[17a] showing that the [6]helicene-based diphosphine (*P*)-**15b**, combined with a stoichiometric amount of $(COD)_2RhBF_4$, promotes the hydrogenation of methyl itaconate in 39% *ee* (Scheme 23).

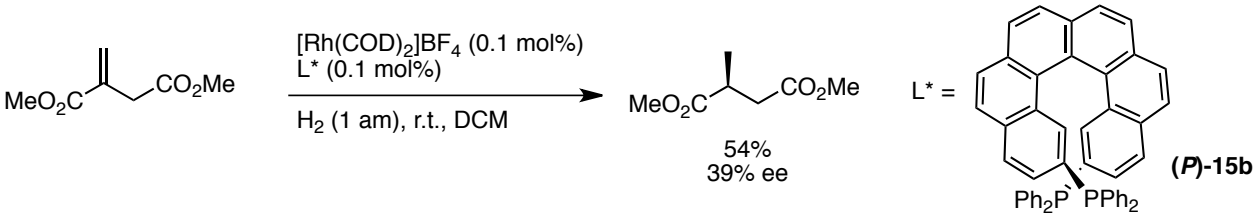


Scheme 23.

Since the chromatographic resolution of the diphosphane **15b** into its enantiomers was difficult because of partial decomposition on the HPLC column, the antipode separation was carried out on (±)-**14b** by chiral HPLC using a preparative column (Chiralcel, 20 μm), obtaining (+)-**14b** and (−)-**14b**

in >96% *ee*. Then, (+)-**14b** was subjected to lithiation/phosphinylation, yielding optically active (+)-**15b** in essentially enantiomerically pure form (>98% *ee*).

Additional hydrogenations of similar substrates, by a rhodium-diphosphine complex, were described by Licandro's group,[21a] in which the catalyst was a preformed cationic rhodium (I) complex **38** of the optically pure thiahelicene-derived diphosphine (*P*)-**29** (Scheme 24).

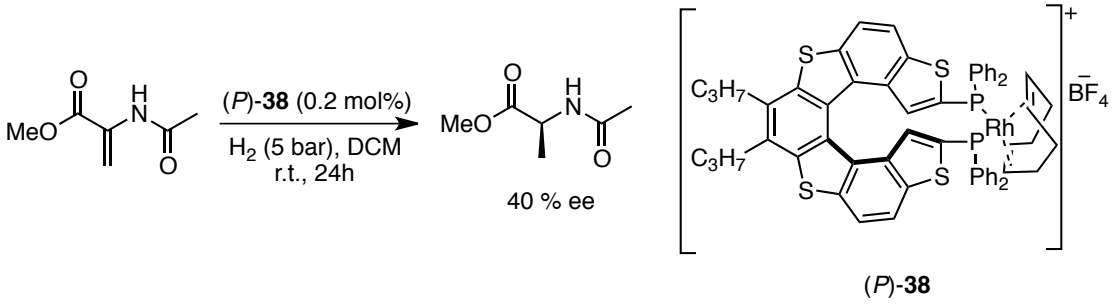


Scheme 24.

In this case, while a lower enantiomeric excess (31% *ee*) was obtained for the hydrogenation of methyl itaconate, the same rhodium catalyst **38** afforded a moderate 40% *ee* in the analogous hydrogenation of 2-acetamidoacrylate. It should be noted that complexes **38** displayed an intrinsic low stability to air, leading to more stable phosphane-phosphane-oxide Rh complexes **39**, whose structure was confirmed by spectroscopic data (Figure 19).

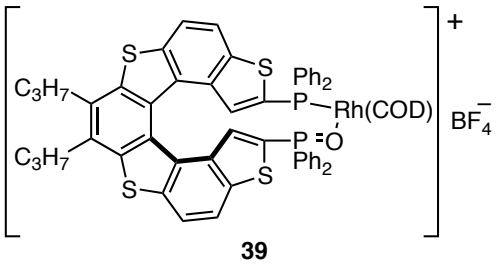


Figure 19.

Further studies from Yamaguchi[19] on the hydrogenation of methyl itaconate were more successful. In particular, rhodium complexes were formed *in situ* from the monodentate phosphite **35** which display both the helical chirality of the [4]helicene unit, the axial chirality of the binaphthyl unit and the central chirality of the menthol derived phosphorus substituent (Scheme 25).

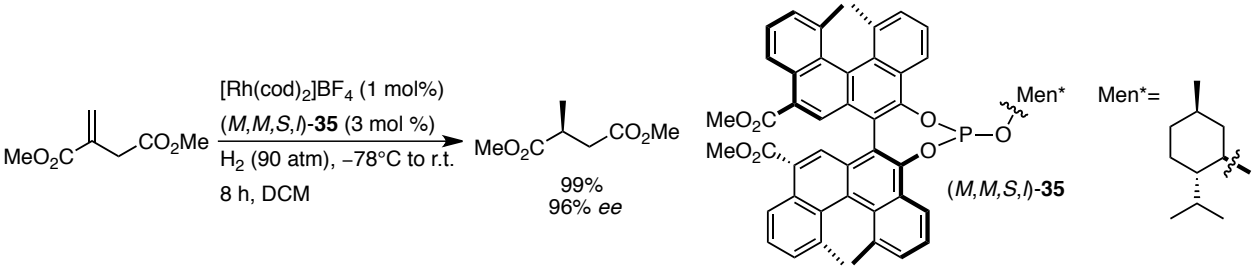


Scheme 25.

Four distinct diastereomers of this ligand were screened, showing that phosphite **35** with (*M*,*M*,*S*,*I*) relative configurations of the stereogenic elements gave the highest *ee* (96% *ee*). Furthermore, matching of the helical and axial chirality seems to be the crucial issue here, while the configuration of the menthyl group plays a minor role in the stereochemical control.

Overall, the rhodium catalysts based on these helical phosphites perform better than helical diphosphine-rhodium complexes in terms of enantioselectivity. They require however harsh

reaction conditions (90 bar), which are likely due to the steric hindrance of the ligand and make these catalysts noncompetitive with other known systems.

Thereafter, in 2011 Starý and co-workers[20b] reported the hydroformylation of styrene using helical phosphites, such as **40**, which display partially saturated helical backbones and cyclic phosphite functions connected to the most hindered C1-position of the helicene. Although the catalytic activity and the branched-to-linear ratios of hydroformylation products were satisfying, the enantiomeric excesses were low, ranging from 0 to 29% *ee*. The highest *ee* value was obtained with a seven-member cyclic phosphite unit derived from (1,1'-biphenyl)-2,2'-diol (Scheme 26).

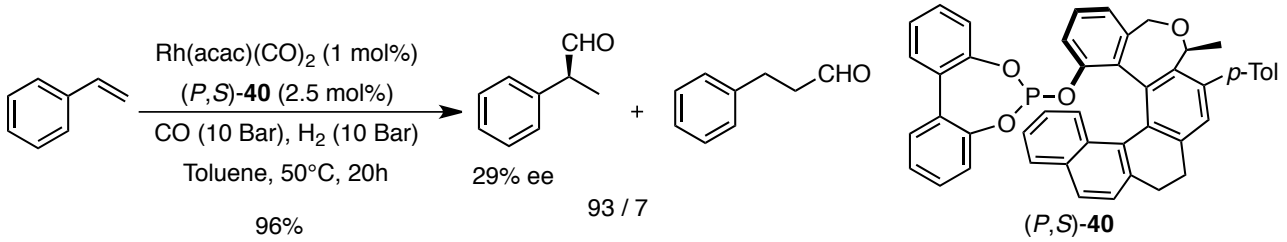


Scheme 26.

*3.3.6 Helical phosphites in iridium promoted allylic aminations*

So far, one of the most successful applications of helicenes with appended phosphorus functions is the iridium-catalyzed amination of allylic carbonates. Starý and co-workers[20b] have screened some phosphites in the amination of cinnamyl carbonate and (pyridinyl)allyl carbonate with primary and secondary amines, including benzylamine, pyrrolidine, morpholine and piperidine. Among these phosphites, compound **37**, which displays a tetramethyl-1,3,2-dioxaphospholane unit, afforded the best results (Scheme 27).

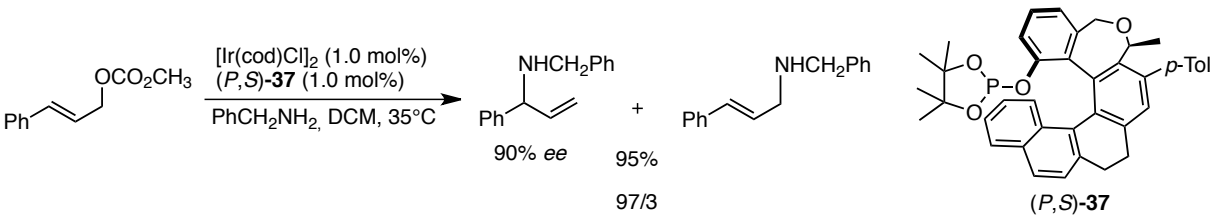


Scheme 27.

The catalyst generated *in situ* from $[Ir(COD)Cl]_2$ and two equivalents of phosphite **37** converted the allylic carbonate into allylic amine in excellent yield (95%), with branched to linear ratios higher than 97:3, and high *ee* (90%).

The allylic aminations above unambiguously demonstrate, for the first time, the high potential of helically chiral phosphorus ligands in asymmetric catalysis.

*3.3.7 Helical phosphanes and phospholanes in gold(I) catalysis*

Gold chemistry is currently one of the most rapidly growing fields of chemistry because of its relevance to a large number of topics, including catalysis,[32] materials science[33] and medicine.[34] In particular, gold(I) complexes incorporating phosphines have been widely developed during the last few years, especially for their use as efficient and selective homogeneous catalysts in organic transformations.[35]

In fact, homogeneous catalysis promoted by Au(I) complexes has emerged as a powerful synthetic tool for organic synthesis, with phosphines and *N*-heterocyclic carbenes[36] as the ligands of choice

for gold(I)-based catalysts. Moreover, asymmetric gold-catalyzed reactions have been applied to a variety of transformations that provide versatile routes leading to the enantioselective formation of new carbon−carbon or carbon−heteroatom bonds.[36a,37] To develop enantioselective catalysts based on phosphorus auxiliaries, different strategies have been successfully implemented so far: the use of bimetallic gold complexes of atropisomeric diphosphines (Figure 20a),[38] the use of tightly associated chiral counterions, mainly chiral phosphoric acid derivatives (Figure 20b),[39] and the use of phosphoramidites with bulky and extended substituents embracing the gold center and its reactive site (Figure 20c).[40,41]

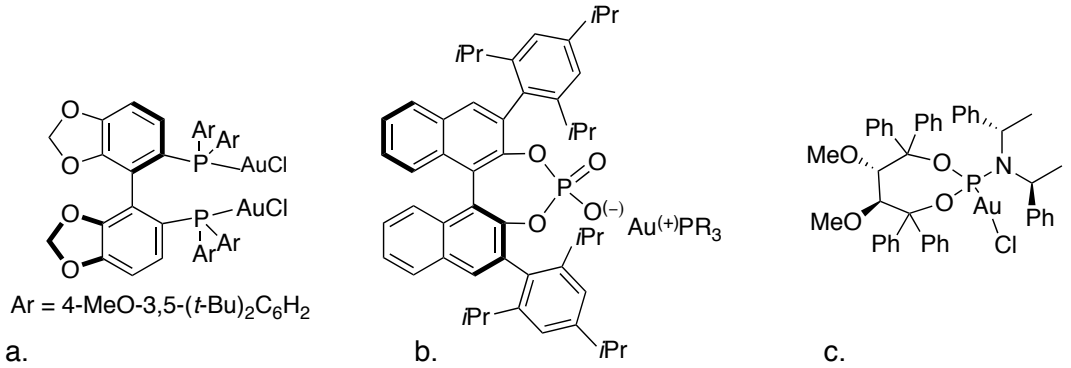


Figure 20.

Despite a large number of gold(I) complexes bearing different mono- or diphosphine ligands have been studied, the first example of gold(I) complexes containing helical-based phosphines have been reported in 2013 by Licandro's group.[21b] In particular, mono and dinuclear tetrathia[7]helicene-based gold(I) complexes **41** and **42** have been synthesized by reaction of the respective phosphine ligands **28** and **29** with Au(tht)Cl in a 1:1 and 1:2 molar ratio, respectively (Scheme 28).

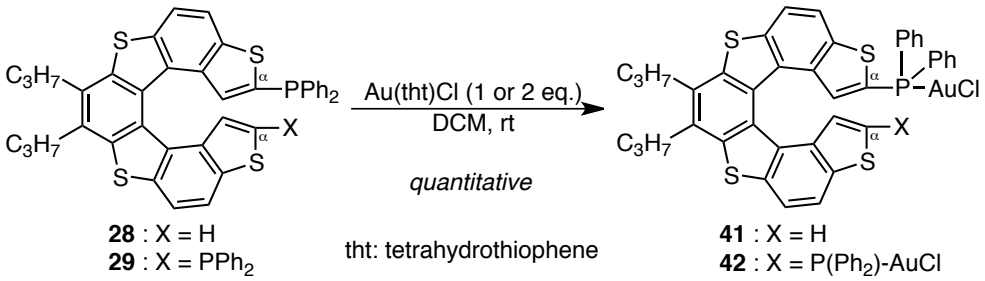


Scheme 28.

These complexes were fully characterized by analytical and spectroscopic techniques as well as quantum chemical calculations, and the molecular structure of **42** has been determined by single-crystal X-ray diffraction, showing a gold-gold interaction of 3.1825 Å.

Preliminary studies on the use of **41** and **42** as catalysts in typical Au(I)-catalyzed cycloisomerizations have demonstrated the high efficiency of these systems in the intramolecular allene hydroarylations and the hydroxycarboxylation of allene-carboxylates. For example, complex **42**, when activated with AgOTf, efficiently catalyzed the hydroxycarboxylation of the allene-carboxylate reported in Scheme 29.

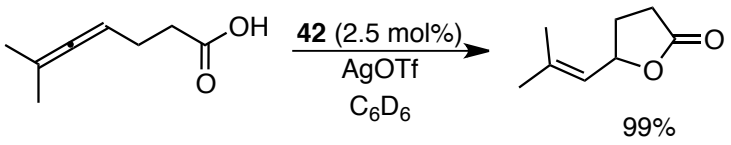


Scheme 29.

However, the asymmetric version of these reactions has not been reported.

Next, Marinetti and co-workers [42] have demonstrated the significant potential of the phosphahelicenes displaying phosphole rings at the end of the helical sequence (see Figure 17) as ligands in enantioselective gold catalysis. Helical phosphanes of this class would not only display peculiar electronic features resulting from extended π conjugation, but also take full advantage of the asymmetric steric environment generated by the helical chirality at the external edge (Figure 21).

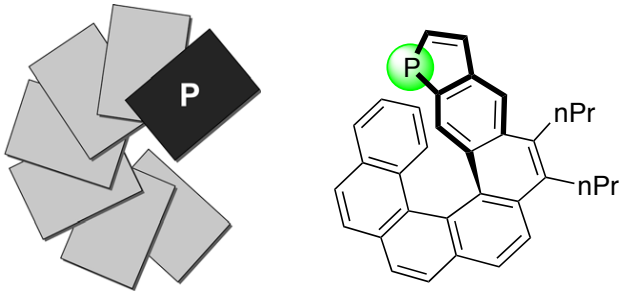


Figure 21.

In particular, various phospha[6]helicene-gold complexes **43**–**47** have been prepared and screened in a model cycloisomerization reaction, namely the rearrangement of *N*-tethered 1,6-enyne **48a** into azabicyclo[4.1.0]heptene **49a** (Figure 22 and Table 1).

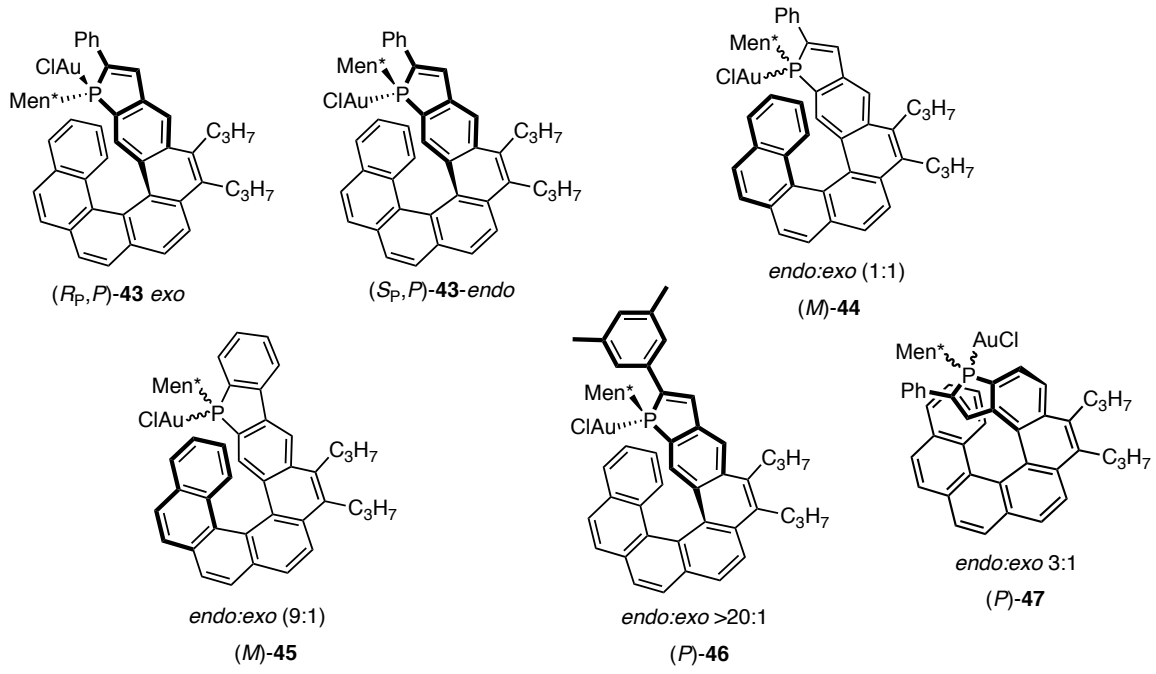


Figure 22.

It should be noted that these reactions are known to be highly challenging, since the linear geometry of Au(I) complexes demands very extended chiral pockets to reach the coordination site opposite to the ligand. Asymmetric variants of this reaction have been reported previously by

using iridium, platinum and rhodium complexes,[43] as well as with gold-phosphoramidite complexes[44] and bimetallic gold complexes of biaryl-type diphosphines.[45]

Table 1.

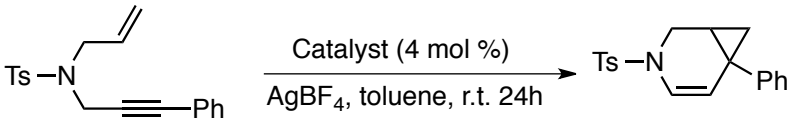


**48a** **49a**

| Entry | Catalyst | *ee* (%) | Conv (%) | Config. |
|---|---|---|---|---|
| 1 |  ($S_P$,*M*)-**45**-*endo* | 7 | 70 | 1S,6R |
| 2 |  ($R_P$,*P*)-**47**-*endo* | 35 | 43 | 1S,6R |
| 3 |  ($R_P$,*M*)-**44**-*endo* | 42 | 90 | 1S,6R |
| 4 | ($S_P$,M)-**44**-*exo* | | (<10) | |
| 5 |  ($R_P$,P)-**43**-*exo* | | (<5) | |
| 6 |  ($S_P$,P)-**43**-*endo* | 81 | >95 | 1R, 6S |
| 7 | ($S_P$,P)-**46**-*endo* | 84 | >95 | 1R, 6S |

Systematic studies demonstrated that phospha[6]helicenes with meta-fused terminal phosphole rings may afford very good catalysts, provided that some structural requirements are fulfilled. These requirements included, notably, an *endo*-position of the gold center, which induces much higher catalytic activity than the *exo*-coordination mode (entries 3 vs 4 and 5 vs 6).

In terms of enantioselectivity, the best results were obtained when the ligands had a terminal phosphole unit (rather than a benzophosphole unit) with aromatic substituents $\alpha$-to phosphorus (rather than unsubstituted phosphole units), as in **43** and **46**. Moreover, the relative configuration of the helical scaffold with respect to the *l*-menthyl group must be taken into account, since the two epimers with opposite helical configurations may give very different enantiomeric excesses (see for instance **44**-*endo* vs **43**-*endo* in entry 3 vs 6). The best catalysts, ClAu[($S_P$,*P*)-**43**-*endo*], and ClAu[($S_P$,*P*)-**46**-*endo*], afforded total conversions and enantiomeric excesses of over 80% (entries 6 and 7). The highly effective enantioselection has been tentatively rationalized based on the geometrical features of ClAu[($S_P$,*P*)-**43**-*endo*]. The phosphorus and gold atoms, which are located on the internal rim of the helical scaffold, benefit indeed from a highly asymmetric environment.

Further studies on the cycloisomerization of the *N*-tethered dienynes have been performed, and the most important results are summarized in Scheme 30.

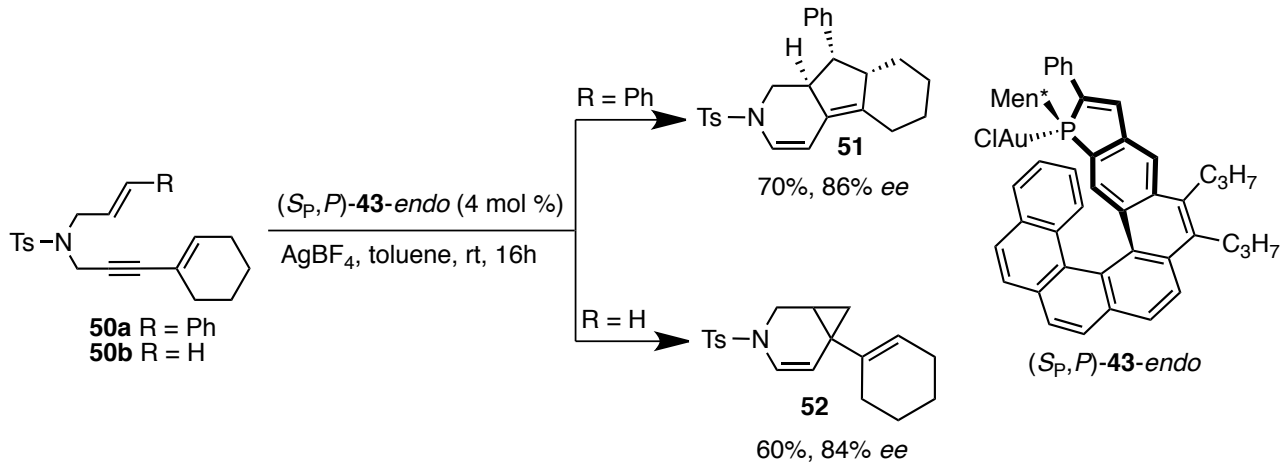


Scheme 30.

In these cases, these complexes represent efficient pre-catalysts only if their geometric features force the gold center to be oriented toward and shielded by the helical moiety. Thus, it was possible to obtain the corresponding cyclized products in excellent *ee* (84–86%).

So far, these are the studies reported in literature on the use of helical phosphorus derivatives in organometallic catalysis, while no example using phosphorous based helicene-based phosphorus derivatives (*e.g.* phosphanes or phosphine oxides) was reported in asymmetric organocatalysis.

**Aims of this PhD thesis**

This Ph.D. thesis aims to provide a meaningful contribution in the development of heterohelicene phosphorus derivatives, especially thiahelicene derivatives, as innovative chiral ligands to use in asymmetric organic and organometallic catalysis. Besides this main objective, other two innovative topics have been preliminary faced, involving the use of thiahelicene derivatives in biological chemistry and in the photovoltaic field.

More in detail, the goals of the present thesis have been:

i. The study of the electronic and chiroptical properties of a new class of tetrathia[7]helicene (7-TH)-based alkyl phosphorus derivatives, including phosphine-borane complexes, phosphanes and phosphine oxides.
ii. The study of 7-TH aryl and alkyl phosphine oxides as chiral organocatalysts in polyhalosilane-mediated reactions.
iii. The study of Au(I) complexes based on chiral phospha-thiahelicene ligands in asymmetric ccycloisomerization of enynes.
iv. The set up of a non-photochemical route to prepare functionalized benzo[1,2-*b*:4,3-*b*']dithiophenes (BdTs).
v. The design and preparation of a nanoconstruct based on PLGA nanoparticles loaded with a luminescent 7-TH derivative for cell uptake and cytotoxicity studies.
vi. The study of a new 7-TH push-pull system, in which the 7-TH skeleton represent a helical π-spacer, for potential applications in DSSCs.

For the sake of clarity, the data concerning the topics covered in this PhD thesis have been organized in seven chapters.

Chapter 1 deals with the synthesis, the structural characterization and the study of the electronic and chiroptical properties of a new class of 7-TH-based alkyl and aryl phosphorus derivatives, including 7-TH phosphine-borane complexes and the corresponding 7-TH aryl and alkyl phosphanes. The first examples on the use of 7-TH phosphanes as organocatalysts in [3+2]-annulation reactions have been also reported.

In the Chapter 2, the synthesis of 7-TH aryl and alkyl phosphine oxides and their application as chiral Lewis base organocatalysts in $SiCl_4$-mediated aldol-type reactions have been discussed.

Chapter 3 deals with the synthesis and the characterization of new chiral phospha-thiahelicene ligands and their corresponding Au(I) complexes. The results concerning the catalytic activity of these Au (I) complexes in several cycloisomerization reactions of enynes have been also described.

A non-photochemical synthetic route to prepare functionalized BdT derivatives have been reported in Chapter 4.

Again, Chapter 5 deals with the synthesis and the characterization of a nanoconstruct based on PLGA nanoparticles loaded with a luminescent 7-TH derivative, together with the study of the cell uptake and cytotoxicity of this nanoconstruct.

In Chapter 6, the results concerning the study of a new 7-TH base push-pull system for potential applications in DSSCs have been described.

Finally, the Experimental Section has been reported in detail in Chapter 7.

# Chapter 1

## 7-TH alkyl and aryl phosphorus derivatives: synthesis, X-ray characterization, chiroptical and electronic properties

Chiral phosphorus-based molecules play a prominent role as catalyst ligands in some of the most important asymmetric processes, in which the choice of the chiral ligand is decisive both for catalytic activity and for achieving a high level of chiral induction. However, whilst axial, central and planar chirality have been largely exploited to build chiral phosphorus ligands and organocatalysts, helical chirality has been rather neglected so far in this field. Some carbohelicenes with appended phosphorus functions have been prepared in either racemic or enantiomerically pure form, but catalytic screenings are limited mainly to Rh- or Ir-catalyzed olefin hydrogenations. Moreover, from literature overview it results that only a few structural variations have been made so far on phosphane containing helicenes. In particular only $PPh_2$ function has been considered for catalytic purposes, and in almost cases the phosphorus functions are located at the 2-position of the carbohelicene scaffolds.[46]

In our laboratories we have been interested in the study and functionalization of tetrathia[7]helicene (7-TH) derivatives for applications in catalysis, and in this context we synthesized 7-TH based mono and diphosphanes,[21a] exploiting the reactivity of the alpha positions of the terminal thiophene rings to introduce the $PPh_2$ moiety (Figure 23).

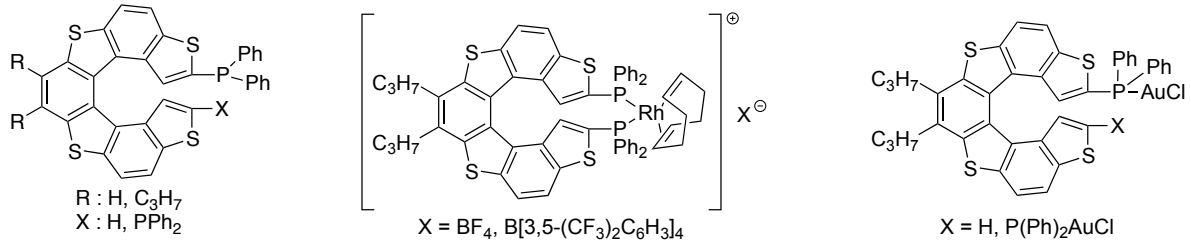


**28-29** **38** **41-42**

Figure 23.

Moreover, 7-TH-based Rh(I)[21a] and Au(I)[21b] complexes **38**, **41** and **42** have been synthesized and preliminary tested in some asymmetric reactions, and they were found to be very efficient catalysts in hydrogenation reactions and cycloisomerizations of unsaturated substrates, respectively, albeit the asymmetric version of these reactions gave moderate *e.e.* (up to 40%). It is easily understood that more extensive investigations and structural variations are needed to fully establish the potential and usefulness of these compounds in both catalysis and other fields.

For these reasons, we focused our attention on the study of a new class of 7-TH-based alkyl phosphorus derivatives to use in asymmetric catalysis. More in detail, this chapter will deal with the synthesis, the characterization and the study of the chiroptical properties of 7-TH-based alkyl phosphane-borane adducts. Next, the study of the electronic properties of the corresponding 7-TH phosphanes will be also described, along with the first application of these phosphanes as organocatalysts in cycloaddition reactions.

### 1.1. Synthesis and characterization of 7-TH-based alkyl phosphine-borane adducts

Based on our previous experience with the preparation of 7-TH diphenyl phosphine-borane adducts,[21a] we attempted the synthesis of a set of 7-TH dialkyl phosphine-borane complexes, exploiting the straightforward route described in Table 2.

Thus, the reaction between the starting helicene **8** with *n*BuLi and the commercially available chlorodialkylphosphines $R_2PCl$ at −78 °C, including $Cy_2PCl$, $nBu_2PCl$, $tBu_2PCl$ and $Et_2PCl$, followed by the *in situ* addition of the complex $BH_3THF$, provided mono and disubstituted 7-TH dialkylphosphine-borane complexes **53a**−**d** and **54a**−**d**, respectively, in moderate to good yields (Entries 1−8, Table 2).

Table 2.

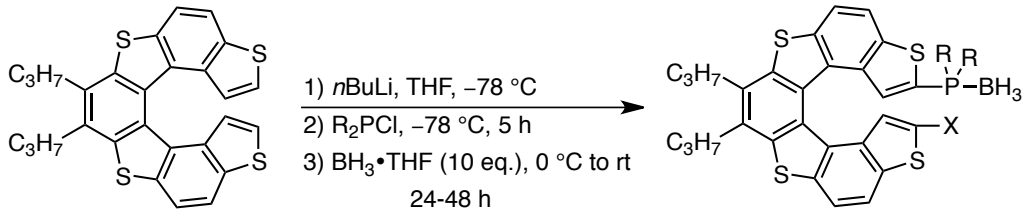


**8**

**53** : X = H
**54** : X = $P(R_2)BH_3$

| Entry | Reagents | | Products | | | |
|---|---|---|---|---|---|---|
| | *n*BuLi/$R_2PCl$ (eq.) | R | **53** | Yield of **53**[a] | **54** | Yield of **54**[a] |
| 1 | 2/2 | Cy | **53a** | 62% | **54a** | - |
| 2 | 4/4 | Cy | **53a** | 20% | **54a** | 70% |
| 3 | 2/2 | *n*Bu | **53b** | 57% | **54b** | - |
| 4 | 4/4 | *n*Bu | **53b** | 13% | **54b** | 61% |
| 5 | 1.5/2 | *t*Bu | **53c** | 49% | **54c** | - |
| 6 | 2/4 | *t*Bu | **53c** | 15% | **54c** | 78% |
| 7 | 1.5/2 | Et | **53d** | 53% | **54d** | - |
| 8 | 2/4 | Et | **53d** | - | **54d** | 76% |

a. Isolated yield.

More in detail, the use of 1.5 or 2 equivalents of *n*BuLi and 2 equivalents of $R_2PCl$ allowed the selective formation of monoadducts **53a**−**d** in 49−62% yield, without traces of the corresponding diborane complexes in the reaction mixtures (Entries 1, 3, 5 and 7, Table 2). In these cases, about 10−40 % of unreacted helicene **8** was also recovered after the chromatography purifications of the crude mixtures. On the other hand, the use of 2 or 4 equivalents of *n*BuLi and 4 equivalents of $R_2PCl$ led to the formation of the disubstituted helicenes **54a**−**d** in 61−78% yield, and no starting helicene **8** was recovered from the reaction mixtures (Entries 2, 4, 6 and 8, Table 2). However, diadducts **54a**−**c** were formed along with 13−20% of the corresponding monoadducts **53a**−**c**, presumably due to the presence of bulky alkyl moieties on the phosphorus atoms. The use of more equivalents (6 or 8 eq.) of base and electrophile did not improve the yield and the selectivity in the formation of **54a**−**c**.

Tetrathiahelicene boranes **53a**−**d** and **54a**−**d** were fully characterized by standard analytical and spectroscopic analysis, whose support the proposed structures, and unambiguously indicate the coordination of $BH_3$ on the phosphorus atoms directly bounded on the alpha positions of the helical scaffold. Indeed, the IR spectra of **53** and **54** exhibited strong absorption bands at 2391−2363 $cm^{-1}$ and at 2354−2331 $cm^{-1}$, which are usual B-H bond stretching frequencies of $BH_3$ in phosphine-borane complexes. Moreover, more diagnostic data derived from their high-resolution ESI mass spectra, which confirm their molecular formula as sodium adduct ions, and $^{31}P$ NMR

spectra of **53a**–**d** and **54a**–**d**, which displayed positive broad signals in the expected range from +13 to +46 ppm (see Table 7).

**1.2 X-ray studies on monoadduct (±)-53c and diadduct (±)-54a**

Single yellow crystals suitable for X-ray diffraction studies of monosubstituted adduct (±)-**53c** and the disubstituted adduct (±)-**54a** were obtained from layered $CH_2Cl_2$/hexane, and their ORTEP diagrams along with the atomic labeling scheme are reported in Figure 24.

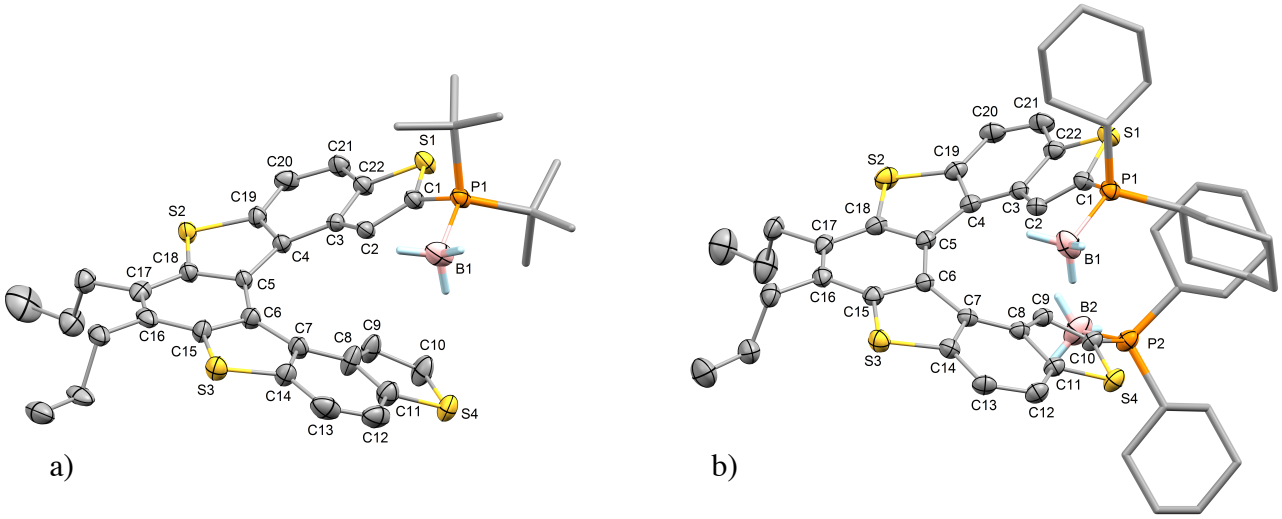


Figure 24. ORTEP diagram of: a) (±)-**53c**; b) (±)-**54a**. Ellipsoids are shown at 30% probability level. Hydrogen atoms and solvent molecules are omitted for clarity.

Complexes **53c** and **54a** crystallized in the monoclinic and triclinic centrosymmetric space groups C2/c and P-1, respectively, so both enantiomers of **53c** and **54a** are present in the crystals, as previously observed for similar 7-TH derivatives.[21a,47] In the crystal structures of both **53c** and **54a** the two *n*-propyl chains, linked to carbon atoms C16 and C17, are disposed on the same side with respect to the mean plane defined by the central benzene moiety. This fact allows the central benzene rings of two adjacent molecules to be stacked parallel, and the distance between their centroids is of 4.109(2) and 4.296(2) Å for **53c** and **54a**, respectively, suggesting that there are no intermolecular interactions (Figure 25).

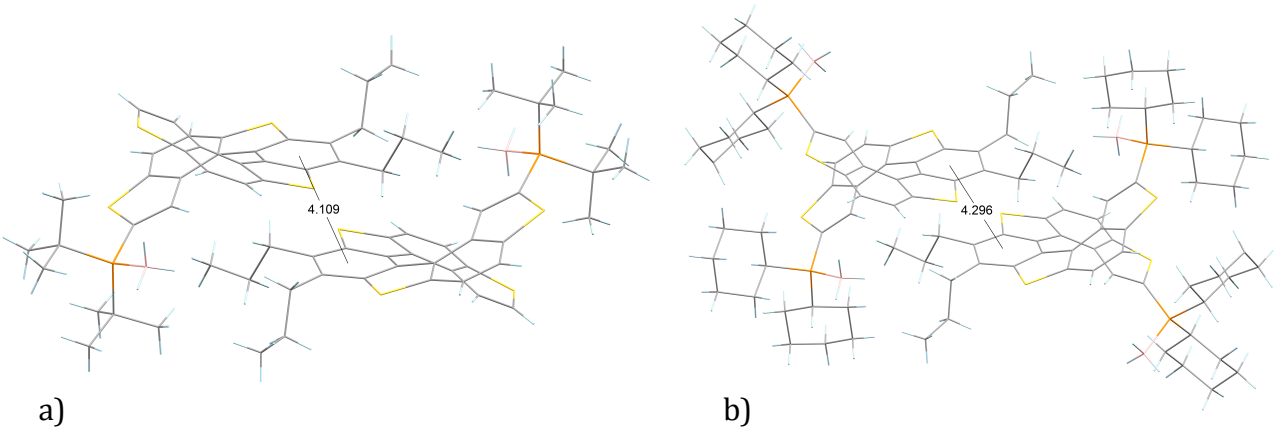


Figure 25. Crystal packing of: a) (±)-**53c**; b) (±)-**54a**.

Moreover, considering the crystal packing of **53c** and **54a**, these crystallized with solvent molecules ($CH_2Cl_2$ and hexane), which are located in the voids left by the packed molecules.

Even if the nature of the phosphine-borane substituents is different in **53c** and **54a**, a general trend for some geometrical parameters can be envisaged. The molecules tend to have shorter outer core bonds and longer inner core bonds with respect to ideal 1.39 Å, as already found in other parent helicenes.[47b] All seven fused rings are deviated from planarity,[48] and the dihedral angles between adjacent rings increased passing from the "external" thiophene rings to the "central" benzene ring of the helicene.
In Table 3 selected bond lengths, distances and angles for **53c** and **54a** are listed, and compared with those of the unsubstituted helicene **8**.

Table 3.

| Lenghts and angles | (±)-**8**[47b] | (±)-**53c** | (±)-**54a** | (+)-**54b** | (–)-**54b** |
|---|---|---|---|---|---|
| C2···C9 [Å] | 3.153(4) | 3.124(3) | 3.325(3) | 3.195(5) | 3.224(4) |
| C1···C10 [Å] | 4.376(5) | 4.411(4) | 4.693(3) | 4.525(4) | 4.525(4) |
| φ [°][a] | 53.3(1) | 55.51(2) | 59.41(4) | 57.65(2) | 57.35(2) |
| P–P [Å] | - | - | 6.932(2) | 6.405(4) | 6.375(2) |
| P–B [Å] | - | 1.940(3) | 1.917(9)<br>1.926(7) | 1.864(1)<br>1.864(2) | 1.928(8)<br>1.913(7) |

a. Dihedral angle between the two terminal thiophene rings of 7-TH skeleton.

While there were no unusual features related to the geometry of the coordination of $BH_3$ to the phosphine, with the P–B bond lengths of 1.940(3) for **53c** and 1.917(9)-1.926(7) Å for **54a**, some more significant distortions were found in the helical skeleton, especially related to the dihedral angle between the two terminal thiophene rings, and the climb of the helix (*e.g.* C2···C9 and C1···C10 distances). In fact, both mono and diborane complexes **53c** and **54a** displayed a total dihedral angle of 55.5° and 59.4°, respectively, which are notably larger than that observed in the unsubstituted helicene **8** (53.3°). Comparable, the C1····C10 distance (4.41 Å for **53c** and 4.69 Å for **54a**) was found to be higher than that of **8** (4.38 Å), with the maximum value for **54a**, bearing two bulky phosphorus moieties. For this latter compound, an intramolecular P–P distance of 6.93 Å was found, which results higher than that obtained by Reetz from the X-ray crystallographic structure of the diphenyl carbo[6]helicene-based diphosphane (6.48 Å).[17a]
Similarly to other conjugated thiahelicenes, these results further confirm that the number and the nature of the substituents strongly influence the distortion from the planarity of the helical skeleton, demonstrating the peculiar flexibility of the helical structures.

**1.3 Resolution of (±)-54b and assignment of the absolute configuration by X-ray analysis**

Exploiting the air-stability and the good solubility in organic solvents of adducts **53** and **54**, we then decided to study the absolute configuration *P* and *M* of these systems by X-ray studies on the two enantiomers of the diborane complex (±)-**54b**, selected as model adduct. Thus, we initially separated the two enantiomers of (±)-**54b** by HPLC on chiral stationary phase, and it turned out that an efficient separation could be achieved with the Chiralpack IA column, using a ternary mobile phase (hexane/$CH_2Cl_2$/2-PrOH) under isocratic conditions.

The enantiopure samples of (+)-**54b** and (−)-**54b** were obtained with *ee* values higher than 98%, and their molar rotation values [$\phi$] were found to be very high ((+)-**54b**: $[\alpha]_D^{22}$ = +1320, $[\phi]_D^{22}$ = +10596 (*c* 0.14, $CHCl_3$); (−)-**54b**: $[\alpha]_D^{22}$ = −1344, $[\phi]_D^{22}$ = −10790 (*c* 0.13, $CHCl_3$)), over three times that of the unsubstituted helicene **8** ((+)-**8**: $[\alpha]_D^{20}$ = +685, $[\phi]_D^{20}$ = +3334 (*c* 0.19, $CHCl_3$)).[47a]
Single yellow crystals suitable for X-ray analysis of both (+)-**54b** and (−)-**54b** were obtained for slow evaporation of the solvents from the corresponding HPLC eluting fractions. The enantiopure molecules crystallize, of course, in chiral space group *P2₁*. In the crystals of (+)-**54b** and (−)-**54b** there are two very similar but crystallographically independent molecules. The absolute configuration of the helicity has been obtained by the refinement of the Flack parameter, which is in agreement with *P*-helicity for (+)-**54b**, and *M*-helicity for (−)-**54b**.
Also in this case, both (+)-**54b** and (−)-**54b** show the two *n*-propyl chains on the same side with respect to the mean plane defined by the central benzene moiety, allowing the central benzene rings of two adjacent molecules to be stacked parallel, and the distance between their centroids is of 4.912 and 4.915 Å for (−)-**54b** and (+)-**54b**, respectively, suggesting that there are no intermolecular interactions (Figure 26).

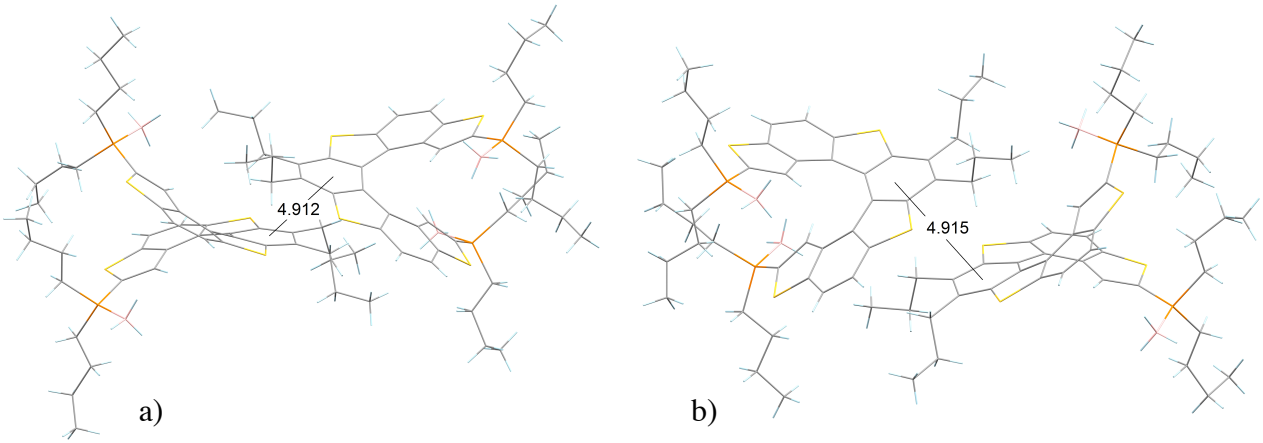


Figure 26. Crystal packing of: a) (−)-**54b;** b) (+)-**54b**

The ORTEP diagrams for (−)-**54b** and (+)-**54b** are reported in Figure 27, and regarding the structural parameters, a trend very similar to that observed in the disubstituted borane complex **54a** is evidenced. Thus, the mean C1···C10 distances are 4.571(5) and 4.525(4) for (+)-**54b** and (−)-**54b**, respectively (Table 3). Again, their total dihedral angle between the two terminal thiophene rings are higher [57.6° for (+)-**54b** and 57.3° for (−)-**54b**] than that of unsubstituted helicene **8**, but shorter than that of **54a** (59.4°), due to the presence on the phosphorus atoms of more bulky cyclohexyl groups in **54a** respect to the *n*butyl moieties in **54b**.

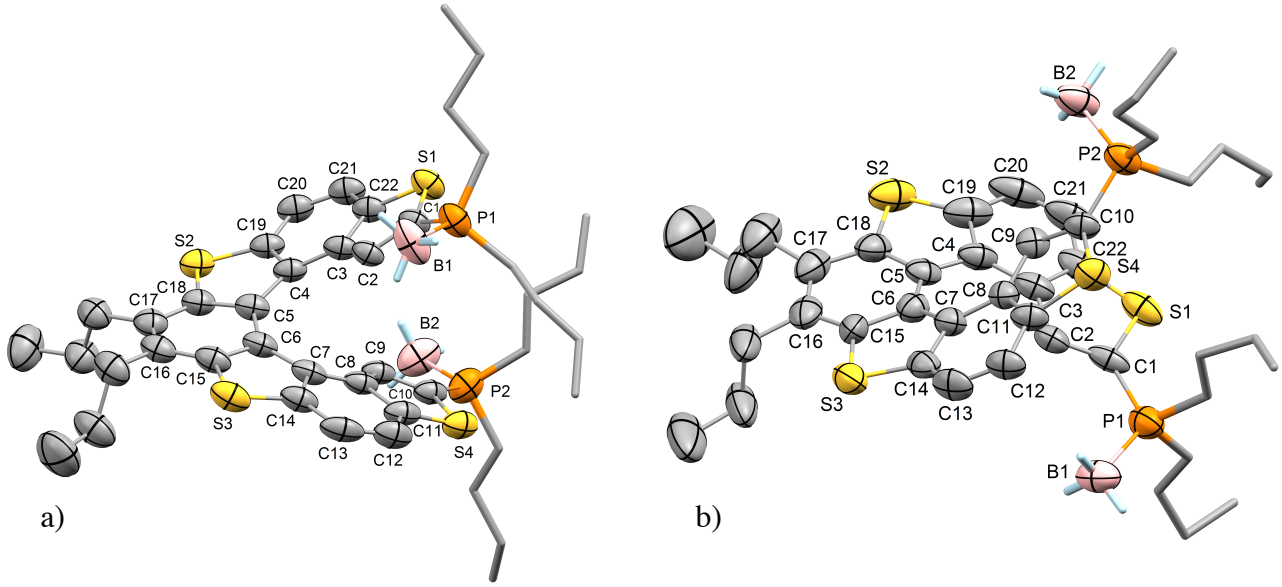


Figure 27. ORTEP diagram of: a) (−)-**54b;** b) (+)-**54b**. Ellipsoids are shown at 30% probability level. Hydrogen atoms and solvent molecules are omitted for clarity.

### 1.4 Chiroptical properties of (−)-54b and (+)-54b by experimental and theoretical calculations

The CD spectra of the enantiopure adducts (+)-**54b** and (−)-**54b** were recorded in diluted $CHCl_3$ solution (C: $10^{-4}$ M, cell length: 0.1 cm, 22 °C), and display a strong positive and negative CD band (β band) around 300-340 nm for (+)-**54b**, and (−)-**54b**, respectively (Figure 28).

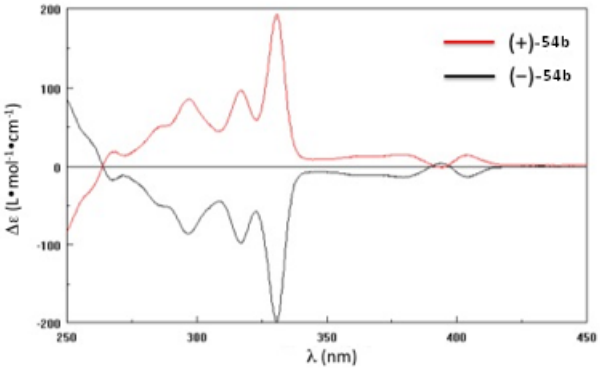


Figure 28. Experimental CD spectra of (+)-**54b** and (−)-**54b**

Since it is commonly accepted that the sign of the most intense CD band (β band) is representative of the absolute configuration of the helicene,[49] with a positive (negative) band corresponding to *P* (*M*) helicity, the *P* helicity can be attributed to the enantiomer (+)-**54b** and *vice versa* for (−)-**54b**, in perfect agreement with the results obtained from X-ray studies.

Next, theoretical investigations on the optical properties of the two enantiomers of **54b** have been performed in collaboration with Prof. Andreas Dreuw of the University of Heidelberg. As first step of this study, the equilibrium ground state structures of (+)-**54b** and (−)-**54b** have been separately optimized at DFT/ωB97XD/cc-pVDZ level of theory. This xc-functional was chosen, because it showed very good agreement with reference methods as well as spectroscopic data for closely related systems. Selected geometrical parameters are compiled in Table 4.

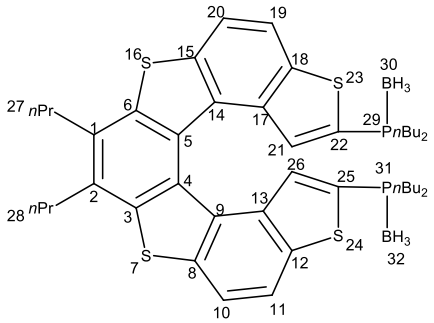


| *Geom. Parameter* | **(±)-54b** |
|---|---|
| d($C_6$-$C_1$-$C_2$-$C_3$) | ±9.6° |
| d($C_{14}$-$C_5$-$C_4$-$C_9$) | ±22.9° |
| d($C_{17}$-$C_{14}$-$C_5$-$C_4$) | ±19.3° |
| d($C_{21}$-$C_{17}$-$C_{14}$-$C_5$) | ±5.4° |
| d($C_5$-$C_4$-$C_9$-$C_3$) | ±18.0° |
| d($C_4$-$C_9$-$C_{13}$-$C_{26}$) | ±5.5° |
| d($C_{20}$-$C_1$-$C_2$-$C_{10}$) | ±25.0° |
| d($C_{22}$-$C_6$-$C_3$-$C_{25}$) | ±42.2° |
| d($S_{23}$-$S_{16}$-$S_7$-$S_{24}$) | ±38.6° |
| r($C_1$-$C_2$) | 1.398 Å |
| r($C_5$-$C_4$) | 1.419 Å |
| r($C_5$-$C_{14}$) | 1.456 Å |
| r($C_{14}$-$C_{17}$) | 1.422 Å |
| r($C_{17}$-$C_{21}$) | 1.439 Å |
| r($C_{20}$-$C_{19}$) | 1.379 Å |
| r($C_{21}$-$C_{26}$) | 3.103 Å |
| r($P_{29}$-$P_{31}$) | 6.051 Å |
| r($B_{30}$-$B_{32}$) | 7.825 Å |
| a($C_{22}$-$C_4$-$C_{25}$) | 52.9° |

**Table 4.** Selected geometrical parameters (d: dihedral angle, r: bond length, a: angle) of (+)-**54b** and (–)-**54b** optimized in the electronic ground state at the theoretical level of DFT/ ω B97XD/cc-pVDZ.

The calculated geometrical parameters of the equilibrium structures agree very favorably with the obtained crystal structures. The bond lengths differ by less than 0.03 Å. Only both layers of the helix approach each other a bit closer in the calculated structures than in the experimental ones as can be seen at the smaller P–P distance or the decreased S23-S16-S7-S24 dihedral angle resulting in a reduced pitch of the helix. This may originate from the applied DFT methodology, which tends to planarize large delocalized π-systems. Also crystal packing effects may play a role for the X-ray structures, which are not included in the calculations.

The four frontier orbitals HOMO-1 (highest occupied molecular orbital) to LUMO+1 (lowest unoccupied molecular orbital) are delocalized over the 7-TH moiety but have no contributions on the side chains (*i.e.* the *n*butyl groups or the boranes) (Figure 29).

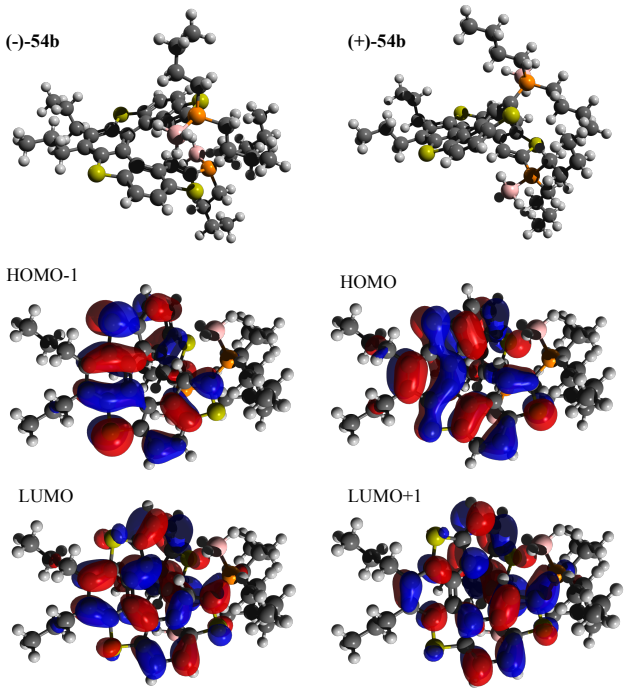


Figure 29. Optimized ground-state equilibrium structures of the enantiomers (-)-**54b** (top left) and (+)-**54b** (top right), and frontier molecular orbitals HOMO-1 to LUMO+1 of (+)-**54b**. The orbitals of (-)-**54b** are identical mirror images.

Turning to the excited-state properties of **54b** the eight energetically lowest excited singlet states were calculated at the optimized ground state equilibrium geometry using RI-CC2/cc-pVDZ (Table 5).[50]

| State | $E_{ex}$ | $f_{osc}$ | $R$ |
|---|---|---|---|
| $S_1$ | 3.41 | 0.16 | -127.80 |
| $S_2$ | 3.46 | 0.17 | 113.06 |
| $S_3$ | 4.11 | 0.23 | -18.10 |
| $S_4$ | 4.12 | 0.07 | 353.94 |
| $S_5$ | 4.31 | 0.06 | -47.53 |
| $S_6$ | 4.46 | 0.01 | 1.86 |
| $S_7$ | 4.54 | 0.11 | 173.63 |
| $S_8$ | 4.55 | 0.02 | 47.52 |

**Table 5.** Excitation energies $E_{ex}$ (eV), oscillator strenghts $f_{osc}$ and rotatory strenths $R$ of the eight lowest excited singlet states of **(+)-54b** at the computed ground-state equilibrium structure at the theoretical level of RI-CC2/cc-pVDZ. Note, that $E_{ex}$ and $f_{osc}$ are identical for **(−)-54b**, only $R$ reverses its sign.

For the comparison of the calculated excitation energies with the experimentally determined absorption spectrum, their values are shifted to lower energies by −0.325 eV accounting for systematic errors in the calculation stemming from the approximate level of computation and the lack of solvation effects. The energy shift has been chosen such that the first excitation energy matches the first absorption band. As can be seen in Figure 30, an overall very good agreement of

the computed excitation energies at the RI-CC2 level of theory and the experimental absorption spectrum is achieved.

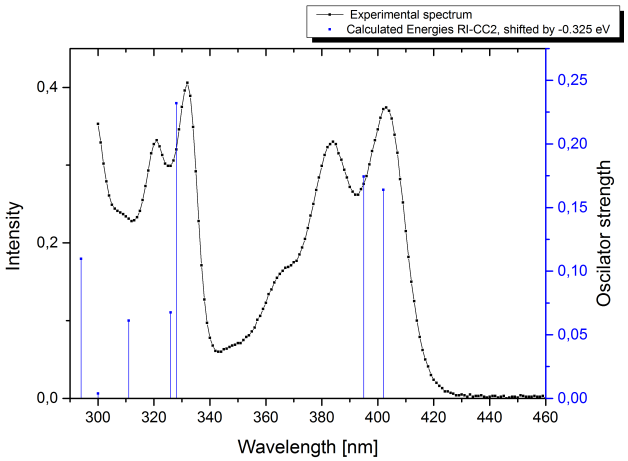


Figure 30. Excitation energies and oscillator strengths of the eight lowest electronically excited states calculated at the RI-CC2/cc-pVDZ level of theory shifted to match the experimental spectrum.

Analyzing the individual excited states in detail, the first electronically excited state ($S_1$) is mainly characterized by a HOMO-1 to LUMO transition (80.3%) and the second excited state ($S_2$) is characterized as HOMO to LUMO transition (89.6%). Both states could both contribute to the first experimental absorption band at 400 nm wavelengths. The third excited state $S_3$, characterized by several lower-contributing orbital transitions (HOMO-2 to LUMO 57.4%, HOMO to LUMO+1 12.3%, HOMO-1 to LUMO 6.0%, HOMO-1 to LUMO+2 4.0%) corresponds most probably to the absorption band at 320 nm wavelengths. However, it remains unclear, whether the second experimental band at 380 nm wavelengths corresponds to the $S_2$ or to vibrational progression of the $S_1$ state. To elaborate this question, vibrationally resolved absorption spectra of the $S_0 \rightarrow S_1$ and the $S_0 \rightarrow S_2$ transitions were calculated at TDDFT/ $\omega$ B97XD/cc-pVDZ level of theory. The calculated vibrationally resolved peaks are analogously shifted to match the excitation energy difference of the states as calculated at the RI-CC2/cc-pVDZ level of theory. Thereby vibrationally resolved absorption spectra are obtained, for which the electronic contributions are calculated at high RI-CC2 level and the vibrational contributions stem from lower-level TDDFT calculations. For comparison with the experimental absorption spectrum, the computed vibrationally resolved spectra of $S_1$ and $S_2$ have been added (Figure 31).

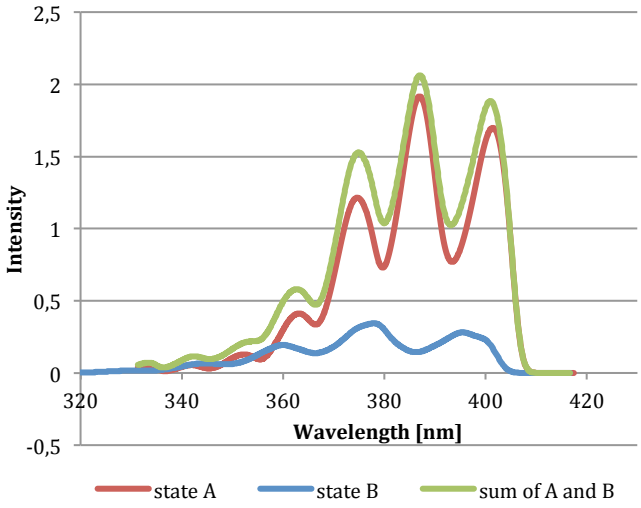


Figure 31. Vibrationally resolved absorption spectra of states $S_1$ and $S_2$ of **54b** and the sum of both spectra contributing both to the first band of the experimental absorption spectrum.

As can be readily seen, the vibrationally resolved spectrum of state $S_1$ exhibits a much weaker intensity than the spectrum of state $S_2$, although both have similar oscillator strengths. Obviously, the band of $S_1$ is much broader than the one of $S_2$ and many vibrational modes contribute to the spectrum. It is clear now that $S_2$ dominates the first band of the spectrum, while $S_1$ contributes only marginally. The vibrational progression of the sum of the $S_0 \rightarrow S_1$ and $S_0 \rightarrow S_2$ transitions (Figure 31) corresponds very nicely to the observed peaks at 405, 385 and 365 nm absorption wavelength in the experimental spectrum. This also nicely explains the mirror-like emission and excitation spectra of several tetrathiahelicenes. Since the $S_2$ state responsible for the first absorption band is located strictly at the central helicene part, which is identical in all 7-TH-analogues, one can expect these compounds to exhibit very similar spectra. The observed negligible variations are then due to electronic and steric effects of side groups or heavy atoms.

Rotatory strengths have been calculated at the RI-CC2/cc-pVDZ level of theory, which are required for the simulation of CD spectra (Figure 32). The first and second excited states show very similar values for the rotatory strength R but with opposite sign. Since they are also very close in energy, they cancel each other almost completely, which can be seen in the experimental CD spectrum. Also taking the computed vibrational broadening of these states into account, this explains for the broad flat region from 420 to 350 nm wavelength in the experimental CD spectrum. $S_3$ shows only a very small rotatory strength although it exhibits the largest oscillator strength. In contrast, $S_4$ has the largest rotatory strength and can thus be assigned to the large band in the experimental spectrum at 330 nm with a vibrational overtone at 315 nm. The next band at 295 nm corresponds most likely to $S_7$. Of course, the simulated CD spectrum of (−)-**54b** is the mirror image of the one of (+)-**54b** inflected at the wavelength axis.

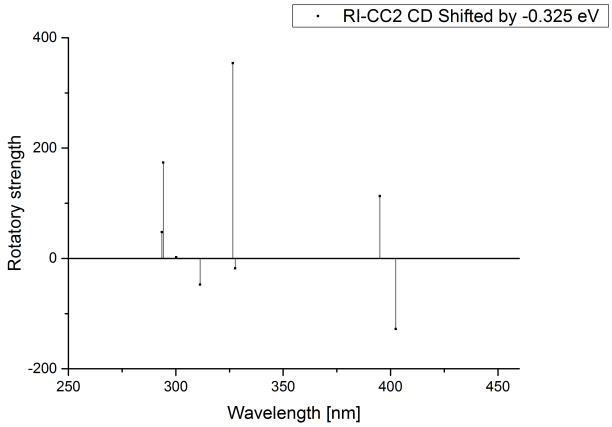


Figure 32. Simulated CD spectrum of (+)-**54b** using the eight energetically lowest electronically excited states at the RI-CC2/cc-pVDZ level of theory.

### 1.5 Synthesis of 7-TH alkyl phosphanes 55 and 56

In order to obtain the free 7-TH alkyl phosphanes from the corresponding 7-TH-based phosphine-borane complexes **53a**–**c** and **54a**–**c** we then decided to investigate the more suitable conditions for the deprotection of adducts **53** and **54**, taking into account the well-known procedure already reported in literature, including the treatment with alcohols or amines.[51]

Initially, we studied the removal of the borane from dialkyl 7-TH phosphane-boranes by means of alcoholysis with EtOH, which was found an efficient and smooth deprotecting agent for the diphenyl 7-TH phosphine-borane adducts **26** and **27**[21a] (Entry 1, Table 6).

Table 6.

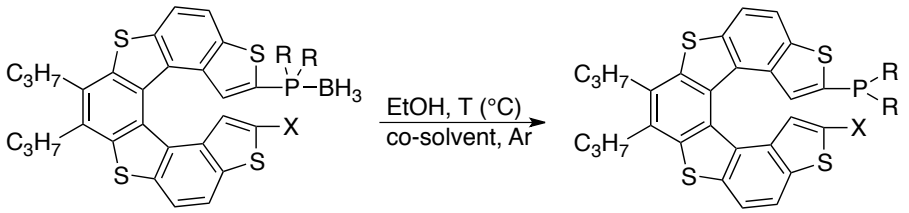


**53a-c** : X = H
**54a-c** : X = $PR_2BH_3$

**55a-c** : X = H
**56a-c** : X = $PR_2$

| Entry | **53**/**54** | R | Co-solvent/T | Time (h) | Conversion (%)[a] |
|---|---|---|---|---|---|
| 1[b] | **26**/**27** | Ph | THF/reflux[c] | 3 | 100 |
| 2 | **53a**/**54a** | Cy | THF/reflux[c] | 96 | 80 |
| 3 | **53a**/**54a** | Cy | Toluene/reflux[c] | 48 | 100 |
| 4 | **53a**/**54a** | Cy | Toluene/140 °C[d] | 1.5 | 100 |
| 5 | **53b**/**54b** | *n*Bu | Toluene/reflux[c] | 48 | <10 |
| 6 | **53b**/**54b** | *n*Bu | Toluene/140 °C[d] | 1.5 | 100 |
| 7 | **53c**/**54c** | *t*Bu | Toluene/reflux[c] | 48 | <10 |
| 8 | **53c**/**54c** | *t*Bu | Toluene/140 °C[d] | 1.5 | 100 |

a. The completion of the reactions was evaluated by TLC analysis. When the substrates were not fully converted, the conversions were estimated on the basis of the $^{31}P$ NMR analysis of the reaction mixtures. b. Literature data.[21a] c. Conventional heating (oil bath). d. Microwave irradiation (300 W, 140 °C).

Unlike **26** and **27**, the deprotection of dicyclohexyl substituted adducts **53a** and **54a** in the presence of EtOH and THF as co-solvent at reflux occurred very slowly (96 h), and the products were contaminated with some phosphine oxides, formed by the oxygen trickling in the reaction vessel for the extended reaction times (Entry 2, Table 6). While the use of toluene as co-solvent gave the complete deprotection of **53a** and **54a** within 48 h under conventional heating (Entry 3, Table 6), dibutyl substituted adducts **53b**–**c** and **54b**–**c** were converted into the corresponding free phosphanes in only 10% after 48 h (Entries 5 and 7, Table 6). On the contrary, all alkyl phosphane-boranes **53a**–**c** and **54a**–**c** were smoothly converted in less than 1.5 h at 140 °C under microwave irradiation (Entries 4, 6 and 8, Table 6). According to the literature,[51] also in this case the rate of the alcoholytic deprotection is strongly influenced by the electronic properties of phosphorus substituents on phosphane-boranes, observing a detrimental effect on the rate of the deprotection when aromatic substituents on phosphorus were replaced with aliphatic ones. However, MW irradiation at a more elevated temperature accelerates significantly the deboronation reaction of **53a**–**c** and **54a**–**c**, as already observed for tertiary phosphane-boranes bearing at least one aromatic substituent.

Alternatively, we also found that aminolysis reaction using diethylamine was a fast and efficient method for the deprotection of both 7-TH dialkyl and diphenyl phosphane-borane adducts **26**, **53**, **27** and **54** (Scheme 31).

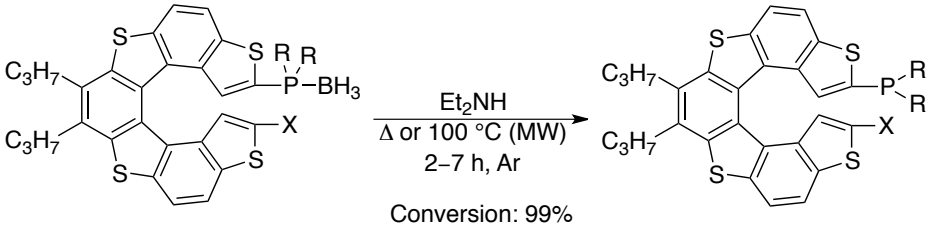


**26, 53a**–**c** : X = H
**27**, **54a**–**c** : X = $PR_2BH_3$

**28, 55a**–**c** : X = H
**29**, **56a**–**c** : X = $PR_2BH_3$

Scheme 31.

Indeed, **26**, **53a**–**c**, **27** and **54a**–**c** were completely converted in the corresponding phosphanes **28**, **55a**–**c**, **29** and **56a**–**c** within 2–7 h by the treatment with $Et_2NH$ at reflux under conventional heating or at 100 °C under MW irradiation. This amine displacement procedure provides complete conversion of **53** and **54** at lower reaction temperatures and shorter reaction times than those required by alcoholysis, and it does not seem to be affected by the electronic nature of the phosphorus substituents.

$^{31}P$ NMR analysis were used to confirm the successful deprotection of **53** and **54**, and the signals related to the free phosphanes **55** and **56** were found to be sharp singlets at more negative values of the chemical shifts (from − 4 to + 30 ppm, see Table 7) than those of the corresponding borane adducts (from + 25 to + 46 ppm, see Table 7), as consequence of the shelding effect due to the removal of $BH_3$. It should be noted that phosphanes **55a**–**c** and **56a**–**c** were found to be highly oxygen-sensitive, thus demonstrating the usefulness of the procedure to prepare them as air-stable borane adducts.

**1.6 Electronic properties of 7-TH aryl and alkyl phosphanes**

The electronic properties of the 7-TH alkyl and aryl phosphanes have been studied by two complementary approaches: *i)* the determination of the first order Se-P coupling constants, $^{1}J_{Se\text{-}P}$, being this constant a fair measure of the basicity of the parent phosphine in phosphine selenides; *ii)* electrochemical studies by means of cyclic voltammetry in collaboration with Prof. P. R. Mussini of the University of Milan.

*1.6.1 Study of the basicity of 7-TH aryl and alkyl phosphanes by the first order Se-P coupling constants of the corresponding phosphine-selenides*

The electron-donating ability of 7-TH phosphines **28**, **55**, **29** and **56** was determined through the first order Se-P coupling constants, $^{1}J_{Se\text{-}P}$, in the $^{77}$Se isotopomer of the corresponding phosphine selenides, being this constant a fair measure of the basicity of the parent phosphine in phosphine selenide compounds, with a larger coupling constant corresponding to a less basic phosphine.[52]

Thus, to estimate the σ-donor ability of phosphorus centers in **28**, **55a**–**c** and **29**, **56a**–**c**, we prepared the corresponding phosphine selenides **57**, **58a**–**c** and **59**, **60a**–**c** in almost quantitative yield, by the simply treatment of phosphine-borane adducts **26**, **53a**–**c** and **27**, **54a**–**c** with $Et_2NH$ at reflux for 8 h, followed by the *in situ* reaction of free phosphines **28**, **55a**–**c** and **29**, **56a**–**c** with elemental selenium in refluxing toluene for 2 h (Scheme 32).

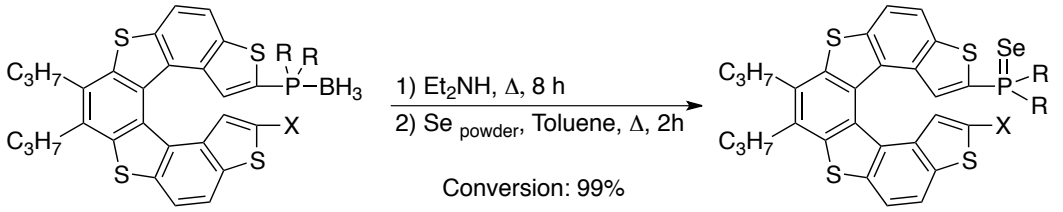


**26, 53a**–**c** : X = H
**27**, **54a**–**c** : X = $PR_2BH_3$

**57** : X = H, R = Ph
**58a** : X = H, R = Cy
**58b** : X = H, R = *n*Bu
**58c** : X = H, R = *t*Bu
**59 :** X = $P(Se)R_2$, R = Ph
**60a :** X = $P(Se)R_2$, R = Cy
**60b**: X = $P(Se)R_2$, R = *n*Bu
**60c** : X = $P(Se)R_2$, R = *t*Bu

Scheme 32.

The coupling constants $^{1}J_{Se\text{-}P}$ of **57**, **58a**–**c** and **59**, **60a**–**c** were then determined from their $^{31}$P NMR spectra performed in $CDCl_3$, and a list of their NMR data is reported in Table 7.

Table 7.

| R | δ (P-$BH_3$) ppm | δ (P:) ppm | δ (P=O) ppm | δ (P=Se) ppm | $^{1}J_{Se\text{-}P}$ [Hz] |
|---|---|---|---|---|---|
| Ph | + 15 | − 15 | + 23 | + 25 | 739 (**57**)<br>741 (**59**) |
| Cy | + 25 | − 4.0 | + 45 | + 48 | 717 (**58a**)<br>713 (**60a**) |
| *n*Bu | + 13 | − 30 | + 39 | + 29 | 712 (**58b**)<br>718 (**60b**) |
| *t*Bu | + 46 | + 30 | + 56 | + 72 | 708 (**58c**)<br>717 (**60c**) |

Dialkyl 7-TH phosphines (**55a**–**c** and **56a**–**c**) and diphenyl 7-TH phosphines (**28** and **29**) differ significantly with regards to their electronic properties, with $\Delta(^1J_{Se\text{-}P})$ values of 20–30 Hz. In particular, **55a**–**c** and **56a**–**c** displayed lower coupling constants ($^1J_{Se\text{-}P}$ = 708–717 Hz) than those of **28** and **29** ($^1J_{Se\text{-}P}$ = 739–740 Hz), which have lower σ-donor ability. As expected, alkyl 7-TH phosphanes resulted then more electron-rich than the aryl ones. However, the σ-basicity within the series of the dialkyl 7-TH phosphines was found to be similar to each other. Moreover, except for **55a** and **56a**, the monophosphanes displayed slightly shorter coupling constants than those of the corresponding diphosphanes, indicating an electron-withdrawing effect of the phosphine substituent on the helical skeleton, as also confirmed by electrochemical studies (see below). Likewise, this behavior has been found, for example, in the ferrocenyl mono and diphosphines **61** and **62**,[52] in which the appearance of the diphenyl-phosphino group in the second ring of ferrocene increases $^1J_{P,Se}$ of the corresponding selenide (Figure 33).

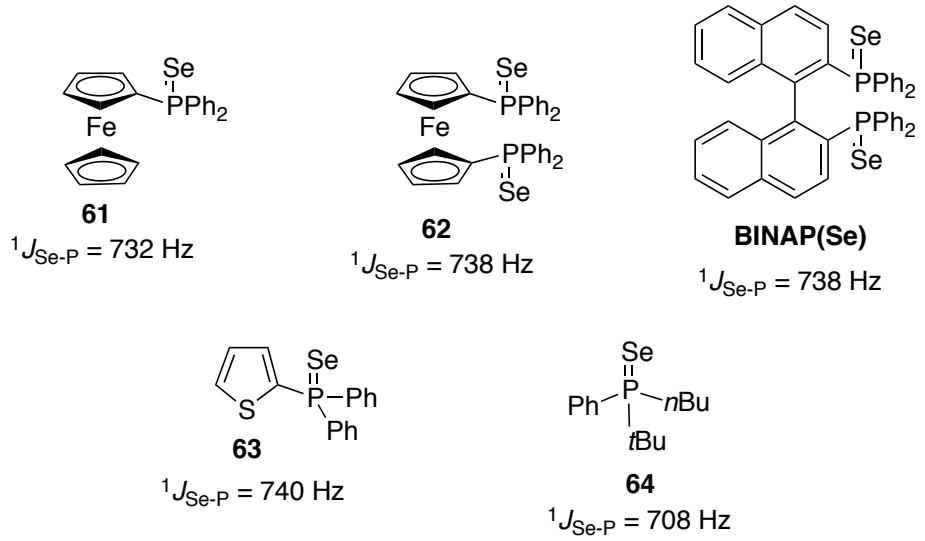


Figure 33.

Finally, from a comparison between the donor ability of these phosphanes with that of other related ligands reported in literature, it can be observed that diphenyl 7-TH phosphanes **57** and **59** displayed σ-donor ability very similar to that of phosphine **63**,[52] containing a thiophene ring in place of the 7-TH moiety, as well as to that of atropisomeric diphosphane **BINAP**[53] (Figure 33). On the other hand, dialkyl 7-TH phosphanes show electron properties similar to those of the dialkyl phenyl phosphanes, such as the phosphine **64**.

*1.6.2 Electrochemical studies by cyclic voltammetry (CV)*

The electrochemical characterization of 7-TH phosphanes **28, 55a–c, 29** and **56a–c** have been performed in terms of localization and features of the redox centers (Figure 34), and compared with those of the corresponding phosphine-borane adducts and phosphine oxides (see Experimental section).

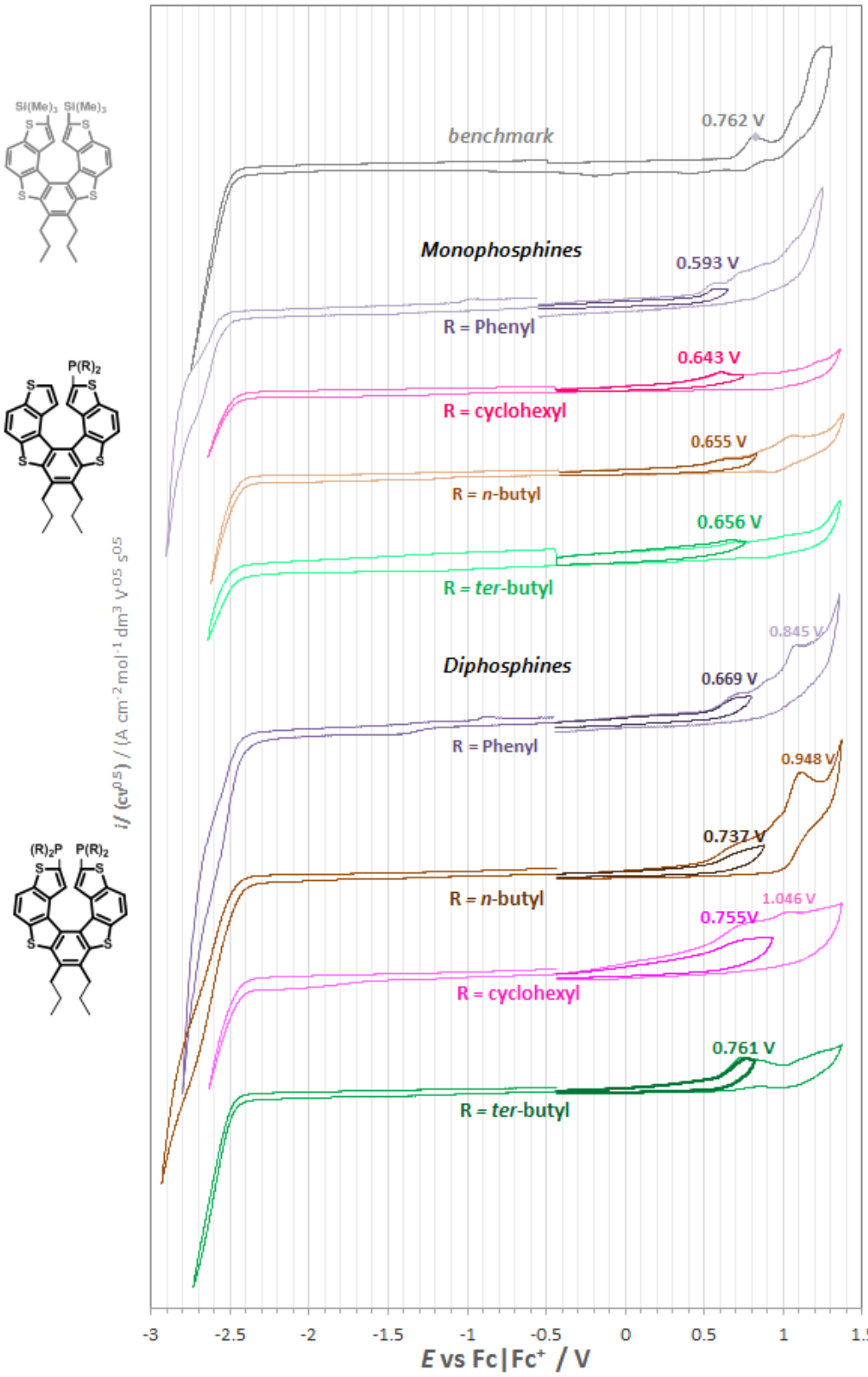


Figure 34. Normalized CV features of the 7-TH mono and diphosphanes **28**, **55a-c**, **29** and **56a-c** recorded on GC in DCM + 0.1 M $TBAPF_6$ at 0.2 V $s^{-1}$ with ohmic drop compensation. The voltammogram of **65** obtained in similar conditions is also reported, for sake of comparison.

As shown in the synopsis in Figure 34, both 7-TH mono and diphosphanes feature a chemically irreversible first oxidation peak, located in most cases at less positive potentials with respect to

the disubstituted helicene **65**, which has been chosen as a benchmark, being a tetrathiahelicene unable to undergo electro-oxidative oligomerization.

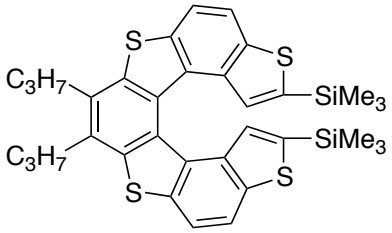


**65**

Figure 35.

In all investigated 7-TH phosphanes, the first oxidation processes are surely localized on the $PR_2$ moiety, on account of the following considerations:

*i)* the inductive effects of alkylphosphane substituents are slightly electron attracting, and therefore would shift the 7-TH oxidation peak to more positive rather than less positive potentials;

*ii)* the phosphane first oxidation peaks are chemically irreversible, while 7-TH systems capped by unreactive terminals, like the benchmark **65**, typically give chemically reversible first oxidation peaks, since oligomerization processes at the terminal thiophene rings are prevented and therefore radical cations delocalized on the 7-TH systems are stable;

*iii)* such peak disappears in the parallel series of 7-TH phosphine oxides and phosphine-borane complexes (see Experimental section), or upon addition of hydrogen peroxide. Moreover, it can be also generated starting from the phosphine oxide, by scanning the electrode potential up to suitably negative potentials.

More in details, considering the 7-TH mono phosphanes **28** and **55a–c**, the diphenyl phosphane **28** results in the easiest oxidation, with the three dialkylphosphanes **55a–c** having their first oxidation peaks shifted to more positive potentials by about 50 mV (with only slight differences among them). Actually, three effects could be considered in discussing these features: a) the higher basicity of the alkyl phopshanes, as previously confirmed by the Se-P coupling constants of the corresponding phosphine-selenides; b) the higher overall conjugation efficiency of the triaryl phosphanes **28** and **29**; c) the higher steric hindrance of the alkyl Cy and *t*Bu substituents with respect to the planar phenyl ones.

While the first effect would favour oxidation resulting in a positive shift of the oxidation potential, the opposite holds for the latter two ones. Their combination might result in the small positive shift of the oxidation potential experimentally observed for alkyl phosphanes with respect to the aryl ones.

The first reduction peak, which should correspond to radical anion formation on the 7-TH backbone, is located close to the negative background; it is fully perceivable only for the aryl phosphanes **28** and **29**, while for the alkyl phosphanes **55** and **56** the background appears to be reached at less negative potentials, so that a comparison between reduction potentials is impossible.

Comparing the diphosphanes **29** and **55a–c** with the monophosphanes **28** and **56a–c**, first oxidation peaks appear to be shifted to more positive potentials by 70−100 mV in all cases. This

feature, that might be associated to higher sterical hindrance and/or higher distorsion and/or to reciprocal interactions between the two $PR_2$ groups, result in a complex multiple oxidation system, which should account for the two equivalent but possibly interacting phosphane oxidation sites now at oxidation potentials comparable to the helicene ones. In any case, considering the first oxidation peak potentials only, a positive shift of 50−70 mV is observed, again, for the alkyl phosphanes **56a–c** with respect to the aryl one, like in the monophosphane series.
Unlike first oxidation peaks, first reduction peaks, mostly located on the helicene backbone, are shifted to less negative potentials for diphosphanes **29** and **56** with respect to the monophosphanes **28** and **55**. This might be partially justified with both the helicene $PR_2$ substituents being slightly electron-attracting groups. In particular, a positive shift of about 0.1 V is observed for the helicene scaffold of **29**, and a reduction peak is this time perceivable also for the *n*butyl derivative **56b** and, at least partially, for the *t*butyl one **56c**.

For comparison, the CV study was also carried out on the corresponding 7-TH-based phosphine-borane complexes **26**, **27**, **53a–c and 54a–c** and 7-TH phosphine-oxides **66**, **67a–c**, **68** and **69a–c**, these latter prepared by oxidation with $H_2O_2$ of the free phosphanes (Scheme 33).

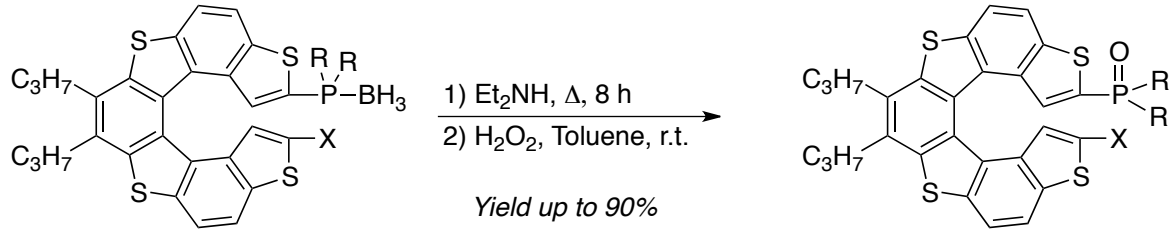


**26, 53a–c** : X = H
**27**, **54a–c** : X = $PR_2BH_3$

**66** : X = H, R = Ph
**67a** : X = H, R = Cy
**67b** : X = H, R = *n*Bu
**67c** : X = H, R = *t*Bu
**68 :** X = $P(O)R_2$, R = Ph
**69a :** X = $P(O)R_2$, R = Cy
**69b**: X = $P(O)R_2$, R = *n*Bu
**69c** : X = $P(O)R_2$, R = *t*Bu

Scheme 33.

As expected, the phosphine-borane complexes did not display the phosphane oxidation peak, but showed an oxidative CV pattern, which closely resembles the benchmark **65**. In particular, a first chemically reversible peak could be observed, corresponding to the formation of a stable radical cation on the 7-TH backbone, followed by a second more complex and chemically irreversible one.
The potential of the reversible peak is nearly coincident with that of the benchmark **65** for the monoadduct **53,** and only slightly shifted in the positive direction for the di adducts **54**.
More evident, and proportional to the number of $PR_2(BH_3)$ moiety, is the positive shift of the reduction peak potentials, which are fully perceivable in all cases, also affording a second reduction peak following the first one. These features are consistent with the electron-attracting effect of the $PR_2(BH_3)$ groups.
Similar results were obtained in the case of the phosphine oxides, for which the electron attracting effect and corresponding positive shift of both oxidation and reduction peaks appears even more pronounced. However, while the shift on the first oxidation peak is low for the mono phosphine

oxides **66** and **67a–c**, a significant shift was perceived for the first oxidation potential in the diphosphine oxides **68** and **69a–c**. Moreover, for the mono and diphosphine oxides **66** and **67a–c** and **68** and **69a–c** two and three reduction peaks could be detected, as consequence of the electron-attracting effect of the $P(O)R_2$ groups. It is worthwhile noticing that the third reduction peak at about −2.7 V corresponds to the reduction of the $P(O)R_2$ group to the corresponding $PR_2$, as evidenced by the appearance of the corresponding oxidation peak.

Finally, a brief study on the electrochemical properties of the 7-TH phosphine selenides **57–60** was carried out, since to the best of our knowledge this is an entirely new class of compounds from the electrochemical point of view. Thus, we have considered two selenides **57** and **58c**, having the aryl and the *t*Butyl substituents of the phosphorus, respectively. The $P(Se)R_2$ groups behave like the corresponding $P(O)R_2$ considering the reduction processes, in spite of Se being less electronegative than O. This might suggest that in both cases the first reduction peak could involve reduction of the P center rather than the helicene conjugated system.

While the selenide effect on the reduction processes is larger than expected, but in the expected direction for an electron-withdrawing group, the effect on the first oxidation is the opposite, since in all cases it take place before the parent helicene one. This suggested us to consider rather than the selenide electronic effects on the adiacent redox sites, the possibility that the selenide group could act itself as the first oxidation site. In fact, it is well-known that phosphine selenides are easily oxidized by hydrogen peroxide,[54] yielding the corresponding phosphine oxides through an intermediate hydroxy species.

**1.7 7-TH mono alkyl phosphanes as Lewis bases in organocatalyzed cycloaddition reactions**

The study of the electronic and electrochemical properties of this new class of 7-TH alkyl phosphanes has demonstrated their greater electron-donating ability than that of the 7-TH phenyl phosphanes, as well as the electrochemical properties of each phosphane are the result of the combination of electronic and steric factors of the substituents on the phosphorus atoms.

Thus, we suppose that the nature of the alkyl or aryl group on the phosphorus of the 7-TH phosphanes could play a key role on their catalytic behaviors, as potential phosphorus ligands in organometallic and organic catalysis. To verify this, we decided to investigate the catalytic activity of the mono dialkyl phosphane **55a** and the mono diphenyl phosphane **28** as Lewis base organocatalysts in two typical phosphine-catalyzed [3+2]-annulation reactions[55] in collaboration with Dr. A. Marinetti of ICSN-CNRS Gif-sur-Yvette, France. In particular, mono dicyclohexyl 7-TH phosphane **55a** efficiently catalyzed the [3+2] cycloaddition reaction between ethyl allenoate **70** and the $\alpha,\alpha$-dicyanoalkene **71** to afford the corresponding functionalized cyclopentene **72** in high conversion (82%). On the contrary, no reaction occurred using the mono diphenyl 7-TH phosphane **28** (Scheme 34).

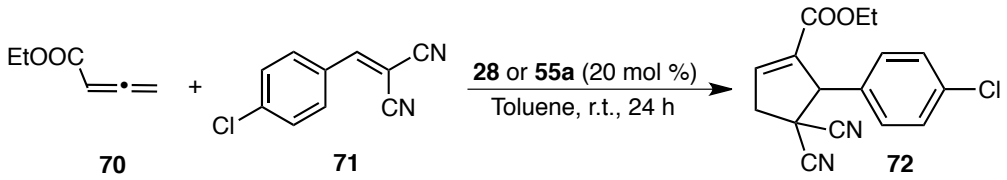


conversion: 82% (for **55a**)
conversion: 0% (for **28**)

Scheme 34.

Likewise, the [3+2] annulations between ethyl 2,3-butadienoate (**70**) and 3-alkylideneindolin-2-one **73** provided the corresponding spirocyclic oxindolic cyclopentane **74** in good conversion (72%) using the alkyl phosphane **55a**, while no cyclized product was obtained with phenyl phosphane **28** (Scheme 35).

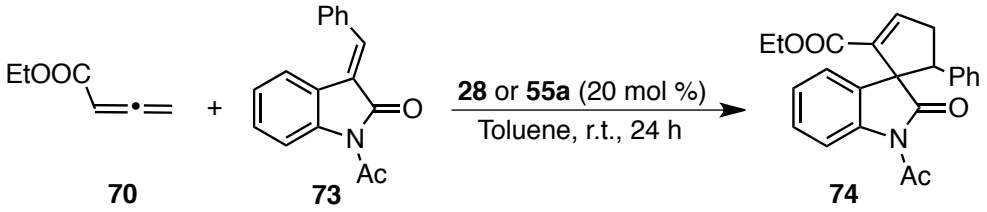


conversion: 72% (for **55a**)
conversion: 0% (for **28**)

Scheme 35.

These examples clearly demonstrate how the electronic and steric nature of the substituents on the phosphorus atoms of these phosphanes strongly influences their efficiency as organocatalysts in specific reactions. It should be also noted that this study represents the first example of using helical phosphanes as organocatalysts.

### 1.8 Conclusions

To conclude, a new set of tetrathia[7]helicene (7-TH) alkyl phosphorus derivatives, including 7-TH mono and diphosphine-borane complexes **53** and **54**, and the corresponding 7-TH mono and diphosphanes **55** and **56** has been synthesized and fully characterized by standard spectroscopic techniques as well as by X-ray analysis. The chiroptical properties of the 7-TH phosphine-borane complex **54b** have been in-depth investigated by experimental CD spectra and theoretical calculations, whose results were in agreement with those obtained by X-ray studies. Next, a systematic study on the electronic properties of the 7-TH phosphanes has been performed by means of cyclic voltammetry experiments and the determination of the first order Se-P coupling constants, $^{1}J_{Se\text{-}P}$, of the corresponding phosphine selenides. Finally, a preliminary study on the catalytic activity of 7-TH aryl and alkyl phosphanes as organocatalysts in typical phosphine-catalyzed [3+2]-annulation reactions has shown that the electronic and steric nature of the substituents on the phosphorus atoms of these phosphanes strongly influences their catalytic behavior.

# Chapter 2

## 7-TH phosphine oxides: synthesis, chiroptical properties and organocatalytic activity

The design and synthesis of new chiral Lewis bases is a field of extraordinary activity, expression of the never ending research towards new catalytic systems of major efficiency and novel synthetic methodologies. Small organic Lewis bases, able to promote a wide variety of synthetic transformations, are protagonists of an incredibly rich chemistry. They include different classes of compounds, such as naturally-occurring alkaloids and amino acids, but also synthetic amine-based catalysts and *N*-oxides. Also, phosphines have witnessed a renewed importance as Lewis basic organic catalysts. However, while *N*-oxides derived from both heteroaromatic systems and aliphatic amines have found widespread application in organocatalysis, phosphine oxides have received little attention so far, despite their easy accessibility from the corresponding phosphines, and their promising results as organocatalysts in polyhalosilane-mediated reactions.[56] Moreover, helical phosphine oxides have been never tested as Lewis base organocatalysts.

Thus, in order to further investigate the potential applications of the 7-TH phosphorus derivatives as chiral ligands in asymmetric catalysis, we decided to study novel 7-TH-based diphosphine oxides as chiral Lewis bases in stereoselective organocatalytic reactions in collaboration with Prof. Maurizio Benaglia of the University of Milan.

This Chapter will deal with the synthesis and the study of the chiroptical properties of three tertiary 7-TH-based diphosphine oxides characterized by substituents on the phosphorus atoms featuring different electronic and steric properties, along with a preliminary investigation on their catalytic activity in $SiCl_4$- and $HSiCl_3$-mediated aldol-type reactions and ketoimines reduction, respectively.

**2.1 Synthesis of tertiary 7-TH-based phosphine oxides and their chiroptical properties**

The introduction of dialkyl or diarylsubstituted phosphinic groups in both the 2- and 13-positions of the helicene (±)-**8**, to prepare phosphine oxides (±)-**68**, (±)-**69a and** (±)-**75**, was easily accomplished by deprotonation of the alpha positions of the terminal thiophene rings of **8** with BuLi, and the reaction with the proper electrophile.

Following this general procedure, phosphine oxide (±)-**68** was prepared by reacting the dianion, generated from **8** with 4 equiv. of *t*BuLi, with 4 equiv. of the commercially available diphenylchlorophosphine oxide $Ph_2POCl$ in THF at – 78 °C (Scheme 36).

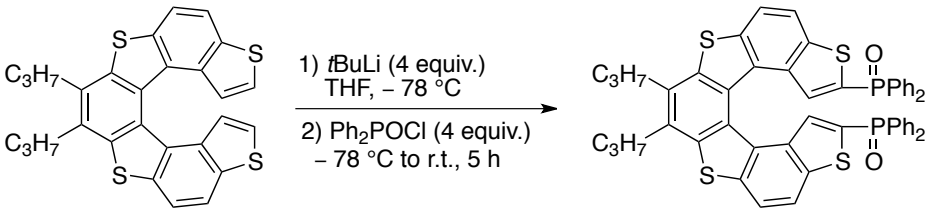


(±)-**8** (±)-**68** 70%

Scheme 36.

After 5 h at room temperature, the reaction mixture did not contain the starting helicene (±)-**8**, and the expected product (±)-**68** was isolated in 70% yield after chromatographic purification.

Since the chlorophosphine oxides $[3,5\text{-}(Me)_2C_6H_3]_2POCl$ and $(C_6H_{11})_2POCl$, necessary to prepare (±)-**75** and (±)-**69a**, respectively, are not commercially available, the first synthetic way explored

was the oxidation, with $H_2O_2$, of phosphines (±)-**76** and (±)-**56a** prepared, in turn, by reacting (±)-**8** with 4 equiv. of *n*BuLi and 4 equiv. of the commercial chlorophosphines $[3,5\text{-}(Me)_2C_6H_3]_2PCl$ and $(C_6H_{11})_2PCl$, respectively, at – 78 °C (Scheme 37).

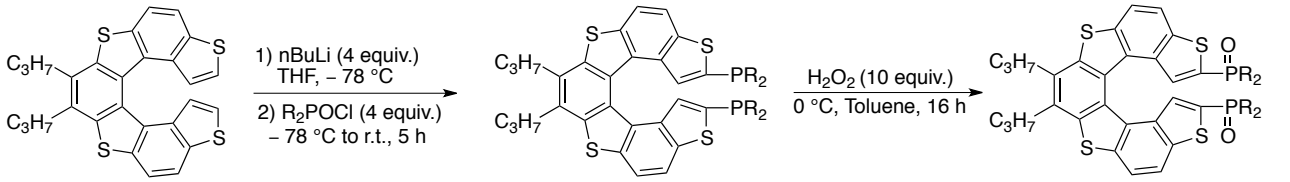


(±)-**8**

(±)-**76**: R = 3,5-$(Me)_2C_6H_3$
(±)-**56a**: R = $C_6H_{11}$

(±)-**75**: R = 3,5-$(Me)_2C_6H_3$ (10%)
(±)-**69a**: R = $C_6H_{11}$ (20%)

Scheme 37.

The crude reaction mixtures so obtained were either directly treated with an aqueous solution of $H_2O_2$ (35 %, 10 equiv.) or quickly purified by column chromatography, and then treated with $H_2O_2$, but in both cases, very complex mixtures were obtained, from which (±)-**75** and (±)-**69a** were isolated in only 10% and 20% yield, respectively (Scheme 37). Thus, to prepare (±)-**75** and (±)-**69a** we then considered the alternative two-step procedure, consisting in the preparation of the phosphines (±)-**76** and (±)-**56a** and their *in situ* transformation into the corresponding stable phosphine-borane complexes (±)-**77** and (±)-**54a** as already reported in Chapter 1 (Scheme 38).

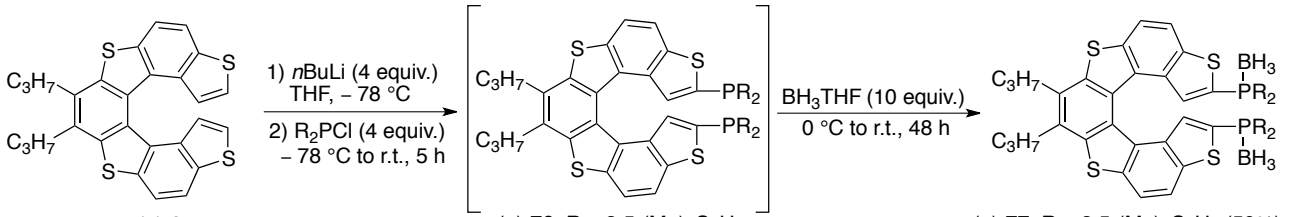


(±)-**8**

(±)-**76**: R = 3,5-$(Me)_2C_6H_3$
(±)-**56a**: R = $C_6H_{11}$

(±)-**77**: R = 3,5-$(Me)_2C_6H_3$ (50%)
(±)-**54a**: R = $C_6H_{11}$ (70%)

Scheme 38.

In particular, the reaction of helicene (±)-**8** with 4 equiv. of *n*BuLi and 4 equiv. of chlorophosphines $[3,5\text{-}(Me)_2C_6H_3]_2PCl$ or $(C_6H_{11})_2PCl$ at – 78 °C, followed by the addition of an excess of $BH_3THF$, provided diborane adducts (±)-**77** and (±)-**54a** in 50% and 70% yield, respectively.

The borane adducts (±)-**77** and (±)-**54a** were then converted into the phosphine oxides (±)-**75** and (±)-**69a** by an one-pot reaction, consisting in the deprotection of (±)-**77** and (±)-**54a** by heating at reflux in a mixture of EtOH and THF under a nitrogen atmosphere, followed by the *in situ* oxidation of the corresponding free phosphanes (±)-**76** and (±)-**56a** with an aqueous solution of $H_2O_2$ (35 %, 10 equiv.) in toluene at room temperature (Scheme 39).

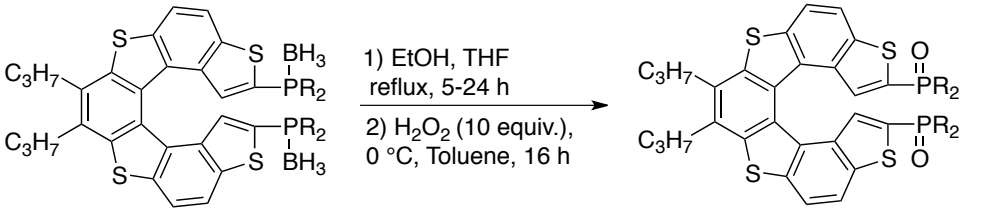


(±)-**77**: R = 3,5-$(Me)_2C_6H_3$
(±)-**54a**: R = $C_6H_{11}$

(±)-**75**: R = 3,5-$(Me)_2C_6H_3$ (60%)
(±)-**69a**: R = $C_6H_{11}$ (90%)

Scheme 39.

The *in situ* oxidation of free phosphanes (±)-**76** and (±)-**56a** derived from adducts (±)-**77** and (±)-**54a** provided phosphine oxides (±)-**75** and (±)-**69a** in good yield (60–90%).

Noteworthy, the above-described two step procedure, thanks to the formation of borane adducts (±)-**77** and (±)-**54a** easy to purify and handle, followed by the removal of the borane moiety and oxidation of the *in situ* generated phosphines (±)-**76** and (±)-**56a** is much more efficient than the procedure described in Scheme 37, and leads to phosphine oxides (±)-**75** and (±)-**69a** in high yields. Therefore, this useful protection-deprotection methodology is an example of participation of a protective group in rendering the experimental procedure easier, and allows to achieve better results.

Both phosphine oxides (±)-**68**, (±)-**75** and (±)-**69a** and borane-phosphine adducts (±)-**77** and (±)-**54a** were isolated as yellow solids after chromatographic purification, and fully characterized by standard analytical and spectroscopic analyses. The most relevant feature of (±)-**77** and (±)-**54a** and phosphine oxides (±)-**68**, (±)-**75** and (±)-**69a** arises from their $^{31}P\{^{1}H\}$ NMR analyses. Whereas the spectra of borane adducts (±)-**77** and (±)-**54a** displayed one broad signal at + 14 and + 26 ppm, respectively, the $^{31}P\{^{1}H\}$ NMR spectra of phosphine oxides (±)-**68**, (±)-**75** and (±)-**69a** showed sharp singlets, ranging from +44 ppm for the dialkyl substituted (±)-**69a** to +23 ppm for the diaryl substituted (±)-**68** and (±)-**75**, which are values consistent with those found in similar tertiary phosphine-borane adducts and tertiary phosphine oxides.

In view of the utilization of enantiopure phosphine oxides **68**, **75** and **69a** in asymmetric organocatalysis, we then focused our attention on their resolution into the corresponding optically pure enantiomers. To achieve this purpose, we first investigated the resolution of diastereomeric salts obtained from the reaction with camphorsulfonic and tartaric acid derivatives, as chiral resolving agents, which were successfully applied to the resolution of BINAP and related $C_2$-symmetric diphosphine oxides.[57] Unfortunately, any attempts of fractional crystallization of diastereomeric salts obtained from **68**, **75** and **69a** with enantiopure dibenzoyl-tartaric acid (DBTA) and di-*p*tolyl-tartaric acid (DPTTA) failed. The alternative resolution method was then accomplished by HPLC on chiral stationary phase. The direct resolution of (±)-**68**, (±)-**75** and (±)-**69a** using a chiral semipreparative column (Chiralpack IA) packed with amylose tris(3,5-dimethylphenylcarbamate) was found to be successful, when an appropriate mixture of solvents was used as the mobile phase (Table 8).

Table 8. Chiral HPLC resolution of phosphine oxides (±)-**68**, (±)-**75** and (±)-**69a**

| Oxide | Eluent | $t_R$ (min) | $[\alpha]_D$ [a)] | Yield | *ee* (%) |
|---|---|---|---|---|---|
| (+)-**68** | Hexane/*i*PrOH/AcOEt (45/40/15) | 16.5 | + 1006[b)] | 98% | 99 |
| (–)-**68** | Hexane/*i*PrOH/AcOEt (45/40/15) | 22.9 | – 1001[b)] | 97% | 98 |
| (+)-**75** | Hexane/*i*PrOH (80/20) | 11.2 | + 1084[c)] | 60% | 96 |
| (–)-**75** | Hexane/*i*PrOH (80/20) | 14.5 | – 1024[c)] | 40% | 90 |
| (–)-**69a** | Hexane/*i*PrOH/AcOEt (70/15/15) | 10.8 | – 1166[d)] | 90% | 98 |
| (+)-**69a** | Hexane/*i*PrOH/AcOEt (70/15/15) | 17.9 | + 1077[d)] | 80% | 92 |

*a*) Measured in $CHCl_3$ at 20 °C. *b*) C = 0.55 g/100 mL. *c*) C = 0.12 g/100 mL. *d*) C = 0.10 g/100 mL.

For the diaryl substituted phosphine oxides **68** and **75** the earlier eluting fractions consisted of the enantiomers exhibiting a positive optical rotation, which were isolated in 60–98% yield (up to 98% *ee*), while for the dialkyl substituted phosphine oxide **69a**, the earlier eluting fractions contained the enantiomer with negative optical rotation that was isolated in 90% yield (98% *ee*). Later eluting fractions gave oxides (–)-**68**, (–)-**75** and (+)-**69a** in 40–97% yield (90–98% *ee*). The specific rotation values obtained for both enantiomers of **68**, **75** and **69a** were found to be great high (up to 1100), in agreement with the known feature of helical structures.

Since neither of the two enantiomers of **68**, **75** and **69a** afforded crystals suitable for the determination of their structure by X-ray diffraction, we could assign the absolute configuration of both antipodes on the basis of circular dichroism (CD) spectra. In particular, the chiroptical properties of phosphine oxide (±)-**68**, which was selected as model 7-TH diphosphine oxide, have been investigated, and the CD spectra of (+)-**68** and (–)-**68** are reported in Figure 36.

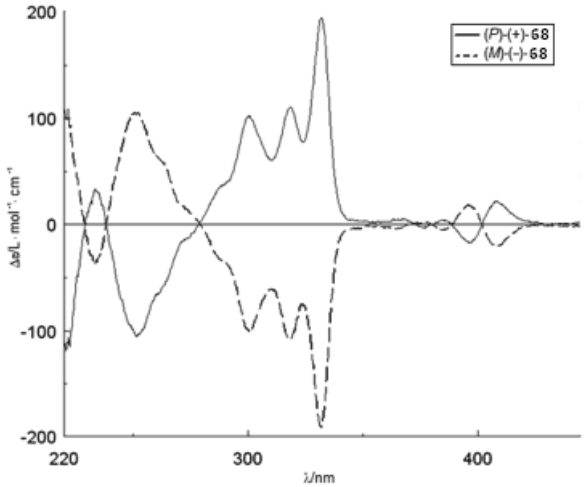


Figure 36.

As expected, the enantiomers (+)-**68** and (**–**)-**68** give mirror image spectra, and possess both spectral envelopes and absorbances analogous to typical conjugated helicenes, including the two intense bands at 250 nm and 335 nm, which are the fingerprint of helicene derivatives.[49] In particular, (+)-**68**, with a positive value of $[\alpha]_D$, displayed two strong bisignate negative and positive Cotton effect (CEs) peaks around 240–280 nm and 280–340 nm, respectively. These CD spectral characteristics are very similar than those obtained for the 7-TH phosphine-borane complex **54b** reported in Chapter 1. Thus, we can assign the absolute *P* configuration for the (+)-**68** and the *M* absolute configuration for (–)-**68**. Likewise, the configuration of (+)-**75**, and (+)-**69a** is *P*, and the absolute configuration of (–)-**75** and (–)-**69a** is *M*.

**2.2 Catalytic studies of 7-TH-based phosphine oxides in polyhalosilane-mediated reactions**

The catalytic behavior of the helical chiral Lewis bases **68**, **75** and **69a** was next investigated in $SiCl_4$-mediated reactions, involving the formation of hypervalent cationic silicon species.[58] The direct addition of the activated thioester **78** to benzaldehyde **79**, in the presence of a stoichiometric amount of tetrachlorosilane was first studied (Table 9).[59]

Table 9. Stereoselective addition of thioester **78** to benzaldehyde **79**.

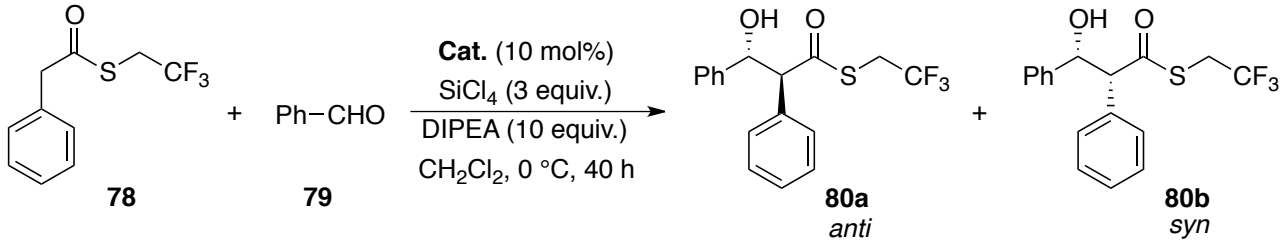


| Entry[a] | **Cat.** | Yield[b] [%] | *Syn*/*anti* ratio[c] | *ee syn*[d] [%] |
|---|---|---|---|---|
| 1 | (±)-**68** | 85 | 92/8 | - |
| 2 | (+)-**68** | 71 | 88/12 | 12 |
| 3[e] | (+)-**68** | No r. | - | - |
| 4 | (±)-**75** | 75 | 87/13 | - |
| 5 | (+)-**75** | 87 | 92/8 | 23 |
| 6 | (+)-**69a** | <5 | - | - |
| 7[f] | (–)-BINAPO | 35 | 97/3 | 81 |

[a] Reaction conditions. **79**: 0.5 mmol, **78**: 1 mmol, dry DCM, 0 °C, 40 h; [b] Isolated yield; [c] Evaluated by $^1$H-NMR analysis on the crude reaction mixture; [d] Evaluated by chiral HPLC analysis on the isolated product; [e] Reaction run at – 40 °C; [f] Literature data.[59] BINAPO [bis-(diphenylphosphanyl)-binaphthyl dioxide].

The condensation of 2 mol equiv. of thioester **78** with 1 mol equiv. of **79** in the presence of 3 mol equiv. of silicon tetrachloride, 10 mol equiv. of DIPEA, and a 10 mol-% amount of the racemic phosphine oxide (±)-**68** in DCM at 0 °C afforded the corresponding β-hydroxytrifluoroethylthioester **80** in 85% yield after 40 hours (entry 1, Table 9). This was isolated almost as single diastereoisomer (*dr* 92/8).

When the enantiomerically pure catalyst (+)-**68** was employed, the product **80** was isolated in good yield (71%), comparable diastereoselectivity (*syn*/*anti* 88/12), and low enantioselectivity (entry 2, Table 9). Unfortunately, at lower reaction temperature (–40 °C), the reaction did not proceed significantly (entry 3, Table 9). While catalyst (+)-**69a** was not able to promote the transformation (entry 6, Table 9), probably for the steric hindrance of the cyclohexyl moieties that prevent the $SiCl_4$ complexation (see theoretical studies below), racemic phosphine oxide (±)-**75**, bearing 3,5-dimethylphenyl rings at the phosphorous atoms, provided the product **80** in 75% yield and good diastereoselectivity (entry 4, Table 9). With enantiopure catalyst (+)-**75**, although only a marginal improvement in the enantioselectivity was observed (entries 2 and 5, 12% *ee* with catalyst (+)-**68** *vs* 23% *ee* obtained with catalyst (+)-**75**), **80** was obtained in high yield and excellent *syn* selectivity (entry 5, Table 9). For comparison, with respect to phosphine oxides (+)-**68** and (+)-**75**, the popular (–)-BINAPO catalyzed the reaction under the same reaction conditions in a significant lower chemical yield, comparable diastereoselectivity *syn*/*anti*, although higher enantioselectivity[59] (compare entries 2 and 5 with entry 7, Table 9).

The chiral phosphine oxides (+)-**68**, (+)-**75** and (+)-**69a** were also tested in other two reactions in the presence of trichlorosilane.[58] The catalytic efficiency of these new organocatalysts were evaluated in the stereoselective reduction of *N*-benzyl imine **81**. By performing the reaction in dry

DCM at 0 °C with catalyst (+)-**68**, the corresponding chiral amine **82** was produced in 43% yield, and 22% enantioselectivity (Scheme 40).

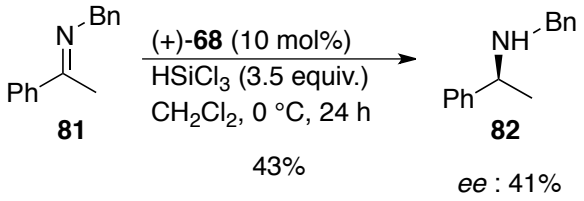


Scheme 40.

Finally, organocatalysts (+)-**68**, (+)-**75** and (+)-**69a** were also employed in the reductive aldol reaction between benzaldehyde **79** and the α,β unsaturated ketone, specifically the *trans* chalcone **83**, in the presence of trichlorosilane (Scheme 41).

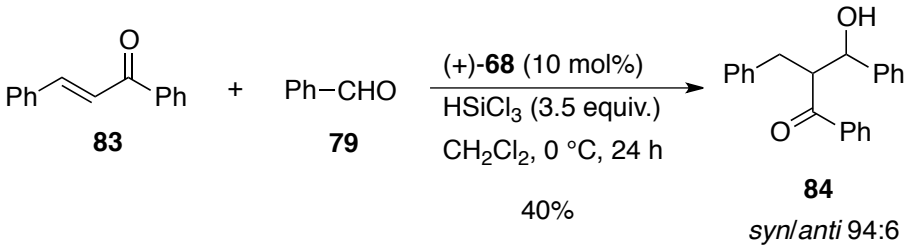


Scheme 41.

Also in this case, best results were obtained using the catalyst (+)-**68**, which gave the product **84** in 40% yield, excellent diastereoselectivity (*syn*/*anti*, 94:6), but low enantioselectivity.

Very preliminary theoretical studies were also performed in order to elucidate the complexation behaviour of the helical 7-TH phosphine oxides. A conformational analysis with Monte Carlo techniques was performed with MMFF force field[60] on the two 7-TH phosphine oxides **68** and **69a**, and on their relative silicon tetrachloride complexes $ASiCl_4$ and $BSiCl_4$, respectively.

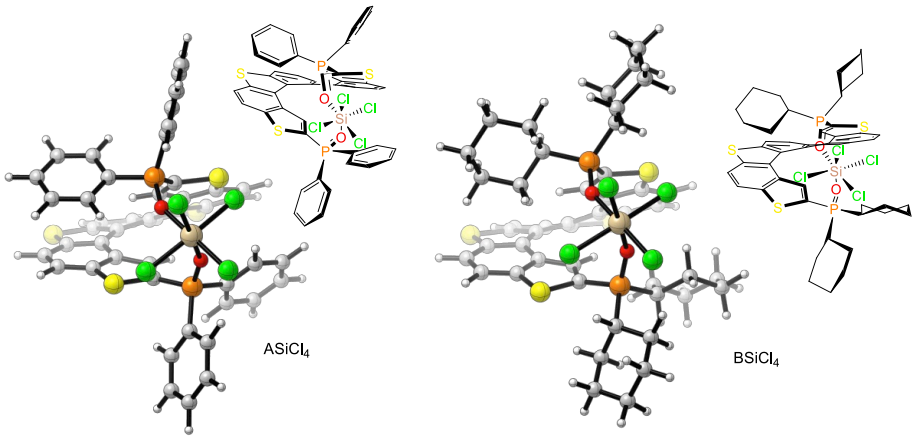


Figure 37.

The global minimum energy structures were, in a second stage, optimized with DFT methods at the B3LYP/6-31G(d,p) level of theory (Figure 37). Finer energy values were obtained performing a single point calculation on these structures at the B3LYP/6-311G(2df,2pd) level.[61] The complexation energy to form the silicon tetrachloride complex of the two chiral bases was

calculated,[a] to give values of 12.8 kcal/mol and 17.7 kcal/mol for **68** and **69a**, respectively. Although **69a** is expected to be a stronger Lewis base than **68**, calculations show a difference in the complexation energy of 4.9 kcal/mol in favour of **68**. This is probably due to the steric hindrance of the four cyclohexyl groups, that frustrates the $SiCl_4$ coordination to the ligand and prevents the formation of the hypervalent silicon specie $BSiCl_4$. In this line, the theoretical calculation may explain the experimentally observed very poor catalytic activity of **69a** in the addition of thioester **78** to benzaldehyde (entry 6, Table 9). While the high diastereoselectivity depends on the mechanism of the aldol reaction, more studies are needed to investigate the mechanism and to attempt a rationalization of the observed enantioselectivity. However, as working hypothesis, a close inspection of the $SiCl_4$ complexes with helical phosphine oxides seems to suggest that low *ee* are probably due to the too large chiral cavity around silicon atom, with the phosphine aryl groups being too far from the catalytic centre to efficiently control the stereochemistry of the reaction.

**2.3 Conclusions**

In summary, the synthesis of new chiral tetrathiahelicene-based tertiary diphosphine oxides (±)-**68**, (±)-**75** and (±)-**69a** was successfully accomplished, by the introduction in both 2 and 13 positions of the helicene (±)-**8** the appropriate phosphinic groups. Phosphine oxides (±)-**68**, (±)-**75** and (±)-**69a** have been completely characterized, resolved into their optical antipodes by chiral HPLC, and the chiroptical properties of both enantiomers of **68** were investigated by CD spectroscopy. The catalytic behavior of the enantiopure diphosphine oxides **68**, **75** and **69a** as Lewis base was preliminary investigated, for the first time, in $SiCl_4$-mediated reactions, and in stereoselective reductions with trichlorosilane. Although the reaction products were obtained with modest enantioselectivity, the 7-TH phosphine oxides **68** and **75** showed to be chemically active organocatalysts, affording the products with good chemical yield, and in some cases excellent diastereoselectivity. Even if further studies are necessary to understand the origins of the stereoselection and to optimize the catalyst performances, the preliminary data described in this work, represent a useful starting point for further development of a totally new and, so far unexplored class of chiral organocatalysts.

[a] The complexation energy of the phosphine oxide **X** was calculated as E[**$XSiCl_4$**]-E[**X**]-E[**$SiCl_4$**] according with the reaction **X + $SiCl_4$** ↔ **$XSiCl_4$**, where E is the calculated B3LYP/6-311G(2df,2pd)//B3LYP/6-31G(d,p) electronic energy.

# Chapter 3

## Chiral phospha-thiahelicenes: synthesis and uses in enantioselective gold catalysis

As reported in the Introduction of this thesis, Marinetti's group has recently developed innovative helical phosphorus ligands, the so-called ***HelPhos*** ligands, in which a trivalent phosphorus function is embedded in the helical structure itself as a phospholane unit (Figure 38).

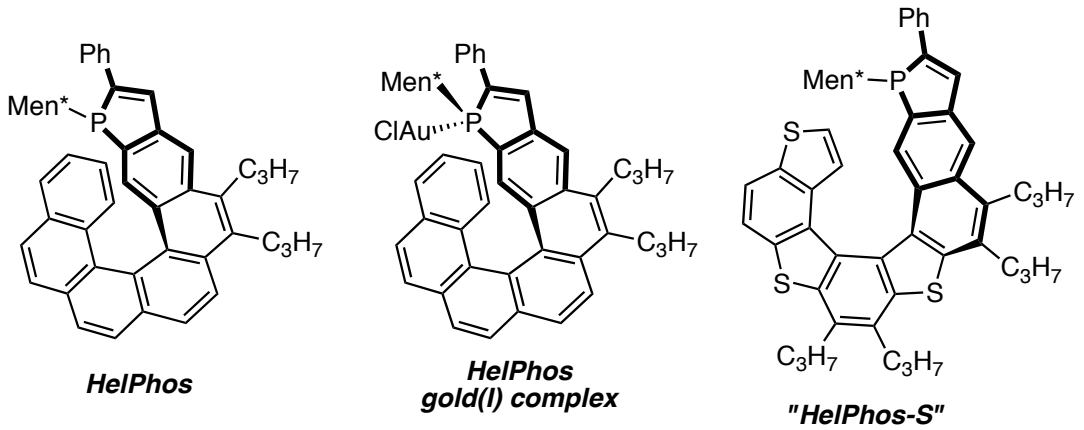


Figure 38.

These systems afforded excellent catalysts for the gold-promoted enantioselective cycloisomerization of *N*-tethered 1,6-enynes into 3-azabicyclo[4.1.0]heptenes (*ee* up to 86%).[42] These promising results are especially rewarding as far as enantioselectivity in gold catalyzed processes remain to date a highly challenging target. In particular, a brief analysis of the structural features of these gold (I) complexes, and comparison of their catalytic behavior with other phosphahelicenes, suggest that a key for high enantioinduction from these ligands specifically relates to the positioning of the phosphorus function in the internal rim of the helical scaffold. Inspired by this work, we then began a collaboration with the Marinetti's group with the aim of preparing thiahelicenes mimics of the ***HelPhos*** ligand, the so-called ***HelPhos-S*** (Figure 38), in order to expand the same design to phosphahelicenes combining phosphole units with different helical scaffolds, and to finely tune their structural features and catalytic behaviors.

This Chapter will deal with the synthesis and characterization of new enantiopure ***HelPhos-S*** ligands and their corresponding gold(I) complexes, which in turn have been tested in some cycloisomerization reactions.

### 3.1 Synthesis of the enantiopure phosphathiahelicene 85

At the onset of this study, we focused our attention on the synthesis of the first ***HelPhos-S*** ligand, the phosphathiahelicene **85**, whose synthesis was planned following a synthetic approach very similar than that employed for the preparation of ***HelPhos*** ligands (Figure 39).

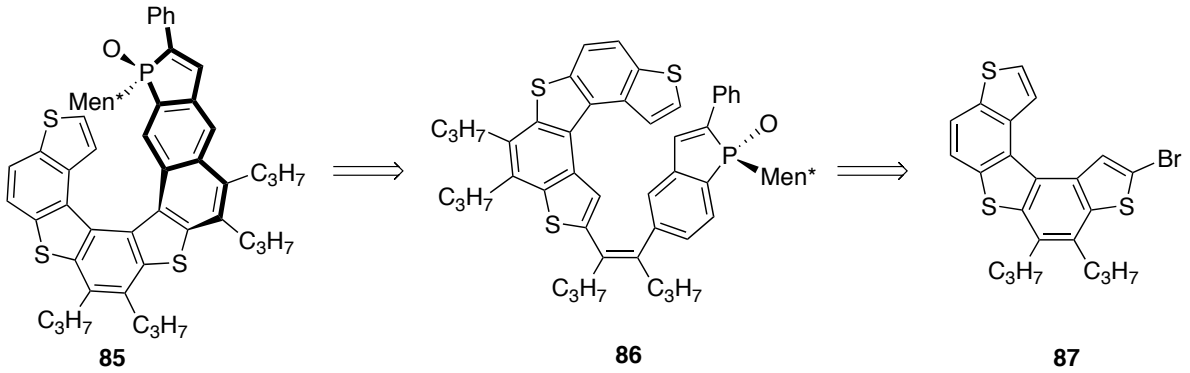


Figure 39.

More in details, the enantiopure phosphathiahelicene **85** could be prepared by a diastereoselective photocyclization of the enantiopure (*Z*)-alkene **86**, which in turn could be prepared by two subsequent Pd-catalyzed Suzuki couplings starting from the bromo-thiahelicene **87**.

*3.1.1 Synthesis of thiahelicene-based bromide **87***

The synthesis of the thiahelicene bromide **87** has been accomplished according to a four-step procedure starting from the benzodi[1,2-*b*:4,3-*b*']thiophene (BDT) **88**.

In particular, BDT **88**[62] was initially converted into the corresponding mono aldehyde **89** by the treatment with 1.05 equivalent of *n*BuLi and 20 equivalent of DMF in THF at −78 °C (Scheme 42).

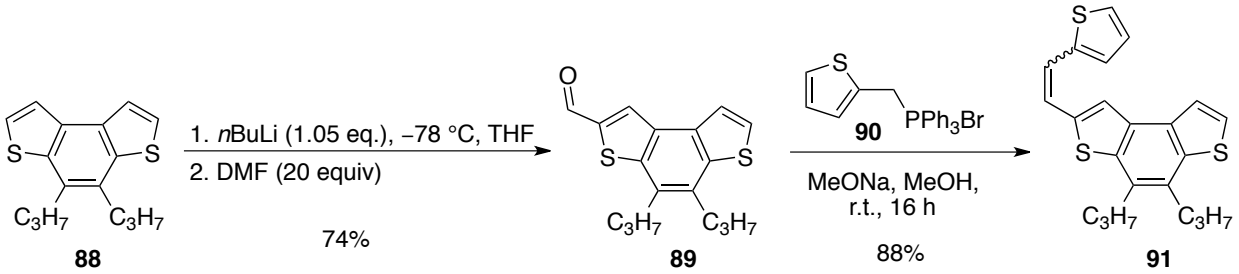


Scheme 42.

Next, the Wittig reaction between the mono aldehyde **89** with the phosphonium salt **90** provided a mixture of (*E*)- and (*Z*)-**91** in overall yield of 88%, which was then converted in the corresponding thia[5]helicene **92** in 74% yield by the photocylclization reaction using 500 Watt medium pressure Hg lamp (Scheme 43).

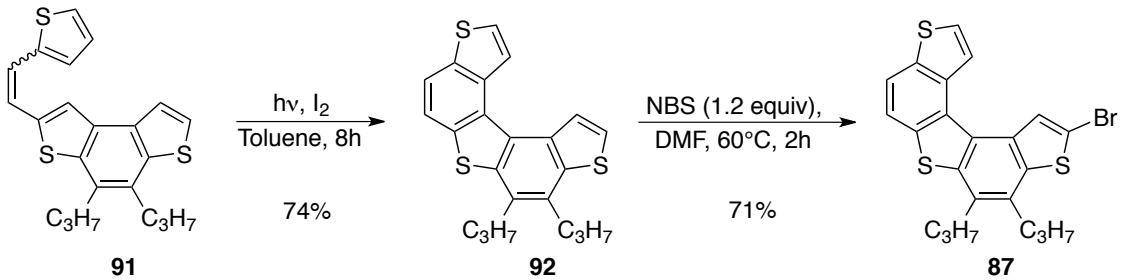


Scheme 43.

Finally, thia[5]helicene **92** was treated with 1.2 equivalents of NBS in DMF at 60 °C to afford the required bromide **87** in 71% yield. It should be noted that this reaction selectively occurs at the

alpha position of the terminal thiophene ring near to the disubstituted benzene ring, as confirmed by $^{1}H$ and $^{13}C$ NMR studies (COSY, HSQC, HMBC experiments).

Next, we devoted to the synthesis of the (*Z*)-alkene **86**, in which are present a [5]-thiahelicene group and a *1H*-phosphindole fragment. The introduction of these moieties was accomplished by two subsequent palladium catalyzed Suzuki couplings between the olefinic bis-boronate **93**[3a] with the [5]-thiahelicene bromide **87** and then with the phosphindole triflate ($R_P$)-**95** (Scheme 44).

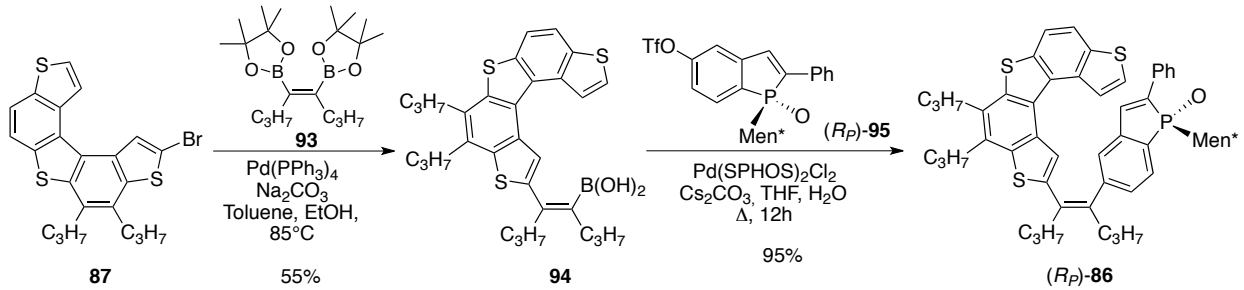


Scheme 44.

The triflate **95** is an optically pure compound, which displays a chiral *l*-menthyl group on phosphorus, and a stereogenic phosphorus with $R_P$ configuration ($[\alpha]_D$ = –150, c 0.2 in $CHCl_3$), whose synthesis has been recently reported in literature.[42]

The intermediate boronic acid **94** was obtained in 55% yield by the coupling between bromide **87** and the olefinic boronate **93** in the presence of $Pd(PPh_3)_4$ as catalyst, $Na_2CO_3$ as base in a mixture of toluene and EtOH at 85 °C. Next, the second coupling between boronic acid **94** and the triflate ($R_P$)-**95** was carried out using $Pd(SPhos)_2Cl_2$ as pre-catalyst, in the presence of $Cs_2CO_3$ as base in a mixture of THF and $H_2O$ at reflux. In this case, the coupling afforded the required olefin ($R_P$)-**86** as a pale yellow solid ($[\alpha]_D$ = −187, c 1 in $CHCl_3$) in almost quantitative yield.

Next, the photocyclization step has been carried out using cyclohexane as solvent, in the presence of iodine and propylene oxide: irradiation of a diluted solution of ($R_P$)-**86** (0.3 mg/mL) for 1.5 h with a 150 Watt Hg-lamp, afforded a mixture of the helical compounds ($R_P$,*P*)-**85** and ($R_P$,*M*)-**96** in 66% overall yield (Scheme 45).

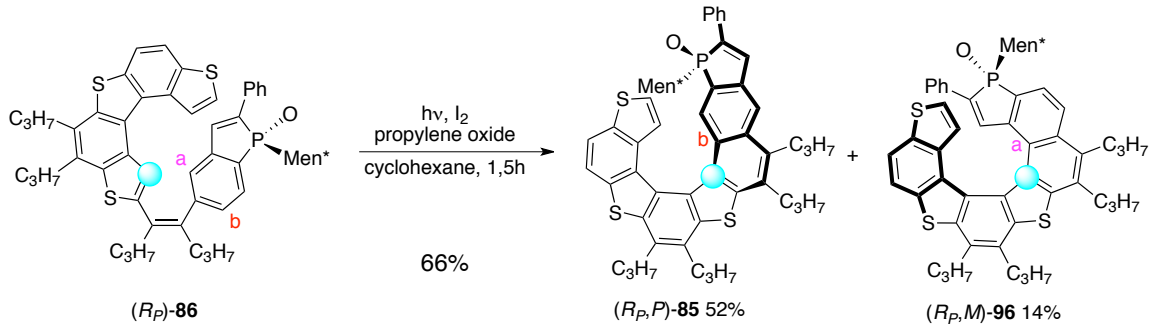


Scheme 45.

Since no suitable crystals for X-ray analysis were obtained, structural assignments have been made by NMR investigations, and the helical configuration has been assigned based on the sign of their optical rotation: $[\alpha]_D$ = +1358 (c 1 in $CHCl_3$) for ($R_P$,*P*)-**85**, and $[\alpha]_D$ = –1366 (c 1 in $CHCl_3$) for ($R_P$,*M*)-**96**.

The photocyclization reaction gives only very small amounts of side products and affords the desired [7]-helicene **85**, as the major product in an 8:2 ratio to **96.** Overall, this reaction is therefore much more efficient that the analogous photochemical generation of phosphahelicenes with all-carbon backbones.[22b-c,42]

Both the [7]-helicene **85** and the [8]-helicene **96** have been isolated as single epimers with defined helical configuration, meaning that the phosphorus configuration dictates the stereochemistry of the helical structures at this photocyclization step.

### 3.2 Synthesis of the enantiopure gold (I) complex ($S_P,P$)-98

Starting from ($R_P,P$)-**85**, the synthesis of the corresponding enantiopure gold (I) complex ($S_P,P$)-**98** has been carried out by a one-pot protocol reported in Scheme 46.

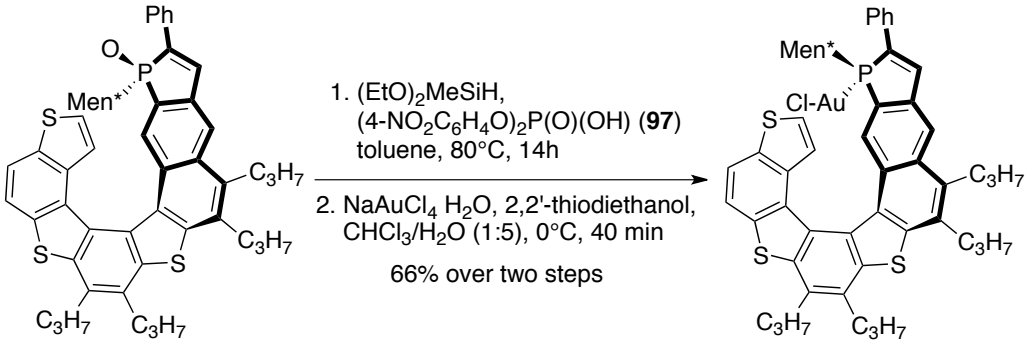


($R_P,P$)-**85** ($S_P,P$)-**98**

Scheme 46.

After reduction of the phosphine oxide ($R_P,P$)-**85** using an efficient and selective reduction system constituted by $(EtO)_2MeSiH$ and phosphonic acid **97**, the *in situ* complexation of the trivalent phosphine so formed has been performed by reaction with a gold (I) specie arising from the *in situ* reduction of $NaAuCl_4$ with 2,2'-thiodiethanol in a mixture of $CHCl_3$ and $H_2O$ at 0 °C. This procedure affords the desired gold complex ($S_P,P$)-**98** as a single diastereomer. Also for this complex, we could not obtain suitable crystals for X-ray analysis, nevertheless, based on NMR data, we assume that the gold atom is oriented toward the helical structure (*endo*-isomer), while the *l*-menthyl group occupies the external face of the phosphahelicene. Thus, the reaction involves overall inversion of the phosphorus configuration, as a result of the well-known configurational lability of the phosphorus in phosphindole-type derivatives.[63]

It is important to note that the same reduction-complexation procedure had been previously applied to the analogous all-carbon ***HelPhos***, but in these cases the reaction displayed much lower diastereoselectivity, giving 1:1 mixtures of the *exo*- and *endo*-isomer of the corresponding gold (I) complexes.[42]

The helical scaffolds of ($S_P,P$)-**98** differs significantly from that of the ***HelPhos-gold complex***, as far as it contains seven *ortho*-condensed aromatic rings, instead of six, and includes five-membered heterocyclic units. These structural and geometrical modifications might result in deep changes in the catalytic behavior of the gold complex ($S_P,P$)-**98**, with respect to ***HelPhos-gold complex***.

### 3.3 First catalytic studies on the enantiopure gold (I) complex ($S_P$,$P$)-98

The catalytic properties of ($S_P$,$P$)-**98** have been investigated in a systematic way, starting from its use as pre-catalyst in enyne cycloisomerization reactions. In this field, a benchmark reaction[64] is the cycloisomerization of the *N*-tethered 1,6-enynes **48** into aza-bicyclo[4.1.0]heptenes **49** shown in Scheme 47. Starting from **48a** (Ar = Ph), the gold complex ($S_P$, $P$)-**98** displayed good catalytic activity at room temperature, after activation with $AgBF_4$. It afforded **49a** in 74% enantiomeric excess. Changing the activating agent from $AgBF_4$ to $AgNTf_2$ did not change the enantioselectivity level (75% *ee*), while other silver salts such as AgOTf and $AgSbF_6$ decreased the enantiomeric excess to 45% and 63%, respectively. Significant enantiomeric excesses were also obtained in the cycloisomerization of enynes with either electron-rich (**48b**) or electron-poor (**48c**) aryl substituents on the alkyne unit (72−68% *ee*, Scheme 47).

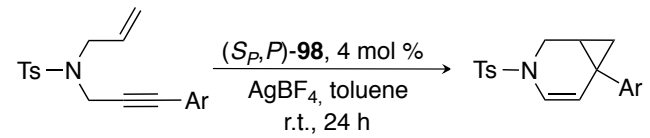


**48a** : Ar = Ph
**48b** : Ar = 4-$MeOC_6H_4$
**48c** : Ar = 4-$NO_2C_6H_4$

**49a** : 74% *ee*
**49b** : 72% *ee*
**49c** : 68% *ee*

Scheme 47.

The promising enantioselectivity levels above encouraged us to extend our investigations to the cycloisomerization of different classes of enynes. At first, dienynes **50**[65] have been considered, which display conjugated enyne moieties (Scheme 48).

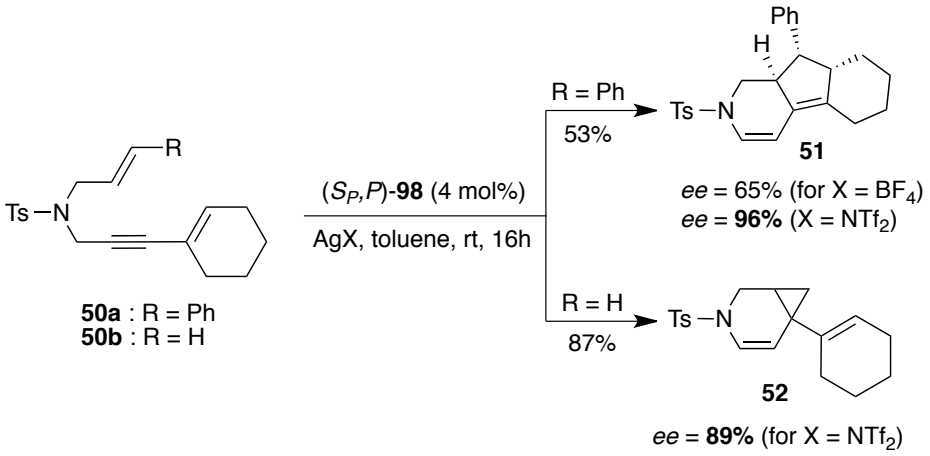


**50a** : R = Ph
**50b** : R = H

Scheme 48.

Depending on the nature of the R substituent, the gold catalyzed cycloisomerization affords either the *aza*-bicyclo[3.1.0]heptene **52** (for R = H) or the tricyclic derivative **51** (for R = Ph). This latter product results from a vinyl-cyclopropane-cyclopentene rearrangement[66] of the intermediate *aza*-bicyclo[3.1.0]heptene. In the cycloisomerization of **50a** (R = Ph), the nature of the silver salt has a remarkable effect on the enantioselectivity level, going from a moderate 65% *ee* for AgX = $AgBF_4$, to an excellent 96% *ee* for AgX = $AgNTf_2$. The same catalytic system (($S_P$,$P$)-**98**/$AgNTf_2$) affords the

aza-bicyclo[3.1.0]heptane **52** in 89% *ee*. Thus, the thia-phospha-helicene-Au(I) catalyst ($S_P$,*P*)-**98** gives the highest enantiomeric excesses attained so far in these cycloisomerization reactions.[b]

Next, the same catalyst has been used in the cycloisomerization of enyne **99**,[67] in which the olefinic function is included into a cyclic structure (Scheme 49).

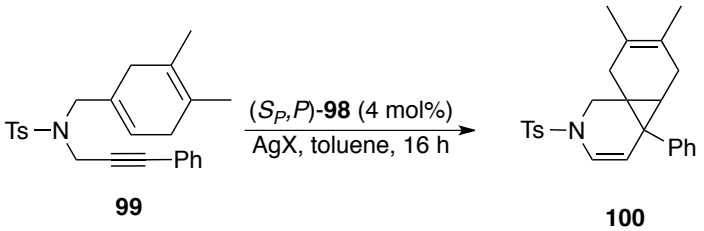


**99** **100**

*ee* = 78% at rt (for X = $BF_4$)
*ee* = 88% at rt (for X = $NTf_2$)
*ee* = **93% *ee*** at = 0 °C (for X = $NTf_2$)
91% yield

Scheme 49.

The reaction affords the expected tricyclic derivative **100** as a single diastereomer, with high enantiomeric excess. Also in this reaction, the enantioselectivity level was found to change significantly by changing the counterion in the cationic gold catalyst. So far, $NTf_2^-$ proved to be the best counterion giving an 88% *ee* for reactions run at room temperature, compared to a 78% *ee* for $BF_4^-$, under the same conditions. The enantiomeric excess could be increased then up to 93% by carrying out the cycloisomerization at 0°C. As far as we know, enantioselective variants of this reaction have been reported before under platinum catalysis (92% *ee*),[43b] and never under gold catalysis.

The excellent enantioselectivity levels obtained above with gold complex ($S_P$,*P*)-**98** encouraged us to extend our investigations to another challenging reaction,[68] such as the cycloisomerization of the enyne **101**, evaluating the influence of some parameters, such as the nature of the silver salt, the solvent and the temperature, on the outcome of this reaction (Table 10).

[b] When applied as catalysts to the same reactions, the **HelPhos-gold complexes** afforded compounds **51** and **52** in up to 85% and 86% *ee*, respectively.

Table 10.

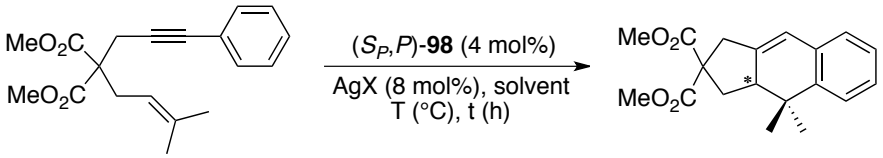


**101** **102**

| Entry | AgX | T (°C) | Solvent | Reaction time (h) | Conversion of **101** (%) | Yield of **102** (%) | *ee* (%) |
|---|---|---|---|---|---|---|---|
| 1 | $AgNTf_2$ | r.t. | Toluene | 24 | 63 | 50 | 73 |
| 2 | $AgBF_4$ | r.t. | Toluene | 16 | 100 | 82 | 59 |
| 3 | $AgSbF_6$ | r.t. | Toluene | 3 | 100 | >80 | 70 |
| 4 | AgOTf | r.t. | Toluene | 16 | <10 | - | - |
| **5** | **$AgSbF_6$** | **−20** | **Toluene** | **5** | **100** | **>90** | **81** |
| 6 | $AgSbF_6$ | −40 | Toluene | 48 | <10 | - | - |
| 7 | $AgSbF_6$ | r.t. | $PhNO_2$ | 16 | 100 | 86 | 48 |
| 8 | $AgSbF_6$ | r.t. | $Et_2O$ | 18 | <10 | - | - |
| 9 | $AgSbF_6$ | r.t. | $CH_3NO_2$ | 24 | 100 | 91 | 47 |

Initially, the influence of the silver salts was evaluated performing the reactions in toluene as solvent at room temperature (Entries 1−4, Table 10). From this first screening we found that the complete conversions of **101** were obtained using $AgBF_4$ and $AgSbF_6$, while lower conversions (<10-63%) were observed with AgOTf and $AgNTf_2$. Concerning the enantioselectivity, $AgSbF_6$ gave better results (70% *ee*) than those obtained with $AgBF_4$ (59% *ee*). Although $AgNTf_2$ provided a bit higher *ee* (73%) than $AgSbF_6$, we decided to carry on the screening using $AgSbF_6$ as salt of choice, for its significant higher efficiency than that obtained with $AgNTf_2$. Thus, to improve the enantiomeric excess in the presence of $AgSbF_6$, the reaction was carried out at lower reaction temperatures (−20 and −40 °C, Entries 5-6, Table 10). Whereas at −40 °C it was observed a conversion of **101** lower than 10%, the reaction run at −20 °C afforded the final product **102** in excellent yield (90%) and high *ee* (81%). On the other hand, the use of different solvents, including $Et_2O$, $PhNO_2$ and $CH_3NO_2$, was detrimental for the enantioselectivity of the reaction (Entries 7-9, Table 10). In summary, this screening shows that both best catalytic activity and enantioselectivity of ($S_P$,*P*)-**98** are obtained using $AgSbF_6$ as silver salt at −20°C in toluene (Entry 6, Table 10).

### 3.4 Further modification of the phosphathiahelicene scaffold

On the base of these very promising results, we have planned the modification of the phosphathiahelicene scaffold by the introduction of different substituents, exploiting the reactivity of the *alpha* position of the terminal thiophene ring, in order to modulated the features of the final gold complex.

Initially, we have functionalized the phospholane ($R_P$,*P*)-**85** by the introduction of the bromine atom in the alpha position of the terminal thiophene ring, using 2 equivalents of NBS at room temperature (Scheme 50).

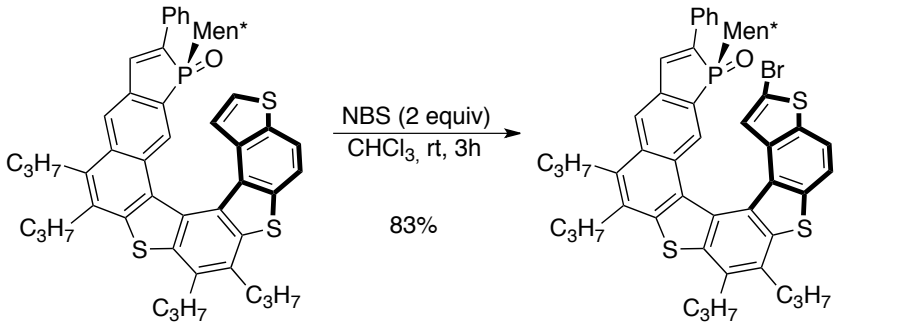


($R_P$,$P$)-**85** ($R_P$,$P$)-**103**

$[\alpha]_D$ = + 1753 ($c$ = 1 in $CHCl_3$)

Scheme 50.

The enantiopure bromide ($R_P$,$P$)-**103** was isolated in 83% yield, and then converted into the phosphathiahelicenes ($R_P$,$P$)-**104a**–**b** by a Suzuki coupling between bromide **103** and the appropriate aryl boronic acids (Scheme 51).

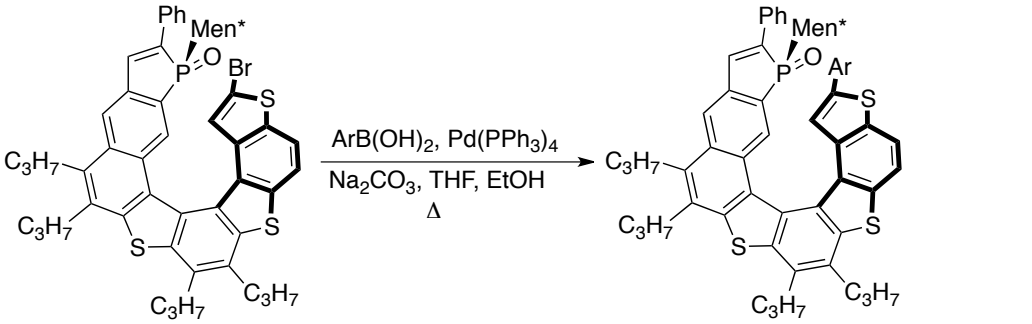


($R_P$,$P$)-**103**

($R_P$,$P$)-**104a** : Ar = $C_6H_5$ 99%

($R_P$,$P$)-**104b** : Ar = 3,5-$(CH_3)_2C_6H_3$ 78%

Scheme 51.

In particular, these coupling reactions were carried out in the presence of $Pd(PPh_3)_4$ as the catalyst, $Na_2CO_3$ as base in a mixture of THF and EtOH at reflux, affording the arylated products **104a**–**b** in very high yields (78–99%).

Next, phosphine-oxides ($R_P$,$P$)-**104a**–**b** were converted into the corresponding gold (I) complexes ($S_P$,$P$)-**105a**–**b** using a procedure very similar than that reported for the synthesis of ($S_P$,$P$)-**98** (Scheme 52).

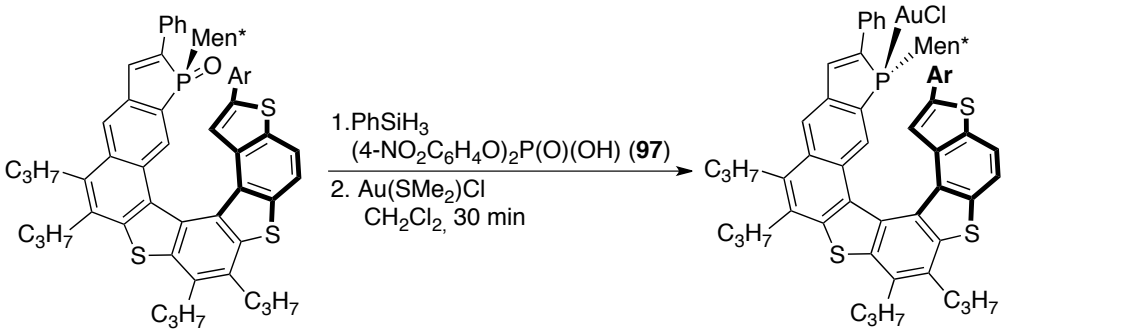


($R_P,P$)-**104a** : Ar = $C_6H_5$

($R_P,P$)-**104b** : Ar = 3,5-$(CH_3)_2C_6H_3$

($S_P,P$)-**105a** : Ar = $C_6H_5$ 76%

($S_P,P$)-**105b** : Ar = 3,5-$(CH_3)_2C_6H_3$ 78%

Scheme 52.

The reduction of phosphine oxides ($R_P,P$)-**104a**–**b** using $PhSiH_3$ in combination with (4-$NO_2C_6H_4O)_2P(O)(OH)$, followed by the *in situ* complexation of the trivalent phosphine so formed by reaction with $Au(SMe_2)Cl$ in $CH_2Cl_2$ afforded the required gold complexes ($S_P,P$)-**105a**–**b** as a single diastereomers in overall yields ranging from 76 to 78%.

To our delight, we have obtained suitable crystals for X-ray analysis of enantiopure complex ($S_P,P$)-**105a**, whose ORTEP view is reported in Figure 40.

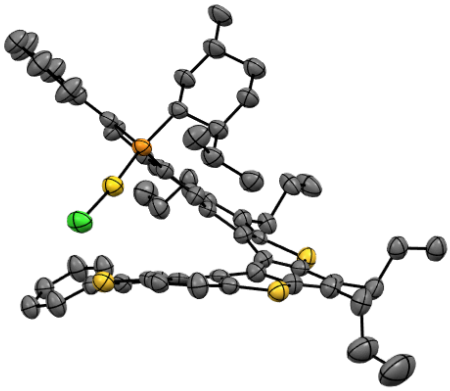

Figure 40.

X-ray data confirm that the gold atom in **105a** is oriented toward the helical structure (*endo*-isomer), while the *l*-menthyl group occupies the external face of the phosphahelicene. Also in this case, the reaction involves the overall inversion of the phosphorus configuration, as a result of the configurational lability of phosphorus in phosphindole-type derivatives.

### 3.5 Further catalytic studies on new gold (I) complexes ($S_P,P$)-105a–b

The catalytic activity of complexes ($S_P,P$)-**105a**–**b** was initially investigated in the challenging cycloisomerization of enyne **101**, and compared with the results previously obtained with complex ($S_P,P$)-**98** (Table 11).

Table 11.

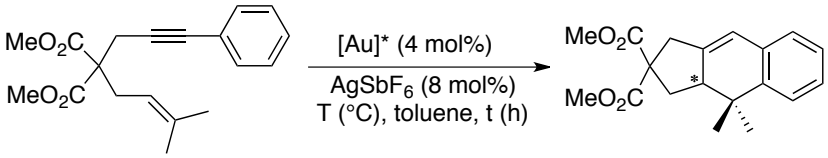


**101** **102**

| Entry | [Au]* | T °C | t (h) | Yield of **102** (%) | *ee* (%) |
|---|---|---|---|---|---|
| 1 | ($S_P$,*P*)-**98** | r.t. | 3 | >80 | 70 |
| 2 | ($S_P$,*P*)-**98** | –20 | 5 | >90 | 81 |
| 3 | ($S_P$,*P*)-**105a** | r.t. | 2 | >90 | 84 |
| 4 | ($S_P$,*P*)-**105a** | 0 | 16 | >90 | 89 |
| 5 | ($S_P$,*P*)-**105a** | –10 | 16 | - | - |
| 6 | ($S_P$,*P*)-**105b** | r.t. | 16 | 80 | 80 |

As reported in Entries 3 and 4 of Table 11, complex ($S_P$,*P*)-**105a**, bearing a phenyl moiety in the alpha position of the terminal thiophene ring, provided the product **102** in excellent yield both at room temperature and at 0 °C, with the best *ee* (89%) achieved at 0° C in 16 h. On the contrary, no reaction occurred at –10 °C after 16 h, showing a less efficiency of this catalyst respect to ($S_P$,*P*)-**98** (compare Entry 2 and Entry 5, Table 11). Finally, the use of the more hindered catalyst ($S_P$,*P*)-**105b** provided the cyclization of **101** in less efficiency (80%) and enantioselectivity (80%) than those obtained with ($S_P$,*P*)-**105a** (compare Entry 6 with Entry 3, Table 11). In summary, these results clearly demonstrate the improvement of the catalytic behaviors of the complexes ($S_P$,*P*)-**105a**–**b** in comparison with those of the parent complex ($S_P$,*P*)-**98** in this reaction. In fact, in this case the introduction of the phenyl ring in the $\alpha$ position of the terminal thiophene ring leads to the best catalyst in terms of efficiency and enantioselectivity (yield=>90%; *ee*=89%), allowing us to achieve the highest enantiomeric excess so far reported in this reaction.[68]

As previously reported for the ***HelPhos***-based gold (I) complexes, the highly effective enantioselection observed with ($S_P$,*P*)-**105a** can be rationalized based on its geometrical features. The phosphorus and gold atoms, which are located on the internal rim of the helical scaffold, benefit indeed from a highly asymmetric environment. According to the X-ray structure reported in Figure 40, the chiral phosphathiahelicene ligand shields three space quadrants around gold. Only the bottom-left quadrant is available to accommodate the most sterically demanding unit of the substrate in the stereodetermining step.

### 3.6 Conclusions

In summary, enantiomerically pure phospha-thiahelicenes **85** and **104a**–**b** can be easily prepared *via* a highly regio- and diastereoselective procedure, involving two subsequent Pd-catalyzed Suzuki coupling and a photochemical step. The corresponding enantiopure gold (I) complexes ($S_P$,*P*)-**98** and ($S_P$,*P*)-**105a**–**b** were then obtained in good yield and complete diastereoselectivity by an one-pot reduction/complexation procedure. Overall, the synthesis of the phospha-thiahelicene ligands **85** and **104a**–**b** and the corresponding gold complexes ($S_P$,*P*)-**98** and ($S_P$,*P*)-**105a**–**b** was found to be more efficient and selective than that used for the synthesis of analogous phospha-carbohelicene ligands and the corresponding gold complexes.

New complex ($S_P,P$)-**98** displays great enantioselectivity levels (up to 96%) in the cycloisomerization of several *N*-tethered enynes, and complex ($S_P,P$)-**105a** allows us to achieve high enantioselectivity levels (up to 89%) in some challenging cycloisomerization reactions. The tridimensional structure of ($S_P,P$)-**105a** has been fully elucidated by X-ray analysis, from which we could confirm the orientation of the gold atom toward the helical structure.

These systems proved to have broad potential in enantioselective gold catalysis, and the very promising results above will also stimulate further developments and applications of these and analogous ligands to new asymmetric organometallic and organocatalytic processes.

# Chapter 4

## A non-photochemical route for the synthesis of benzo[1,2-*b*:4,3-*b'*]dithiophenes: $FeCl_3$-mediated cyclization of dithienyl ethenes

Benzo[1,2-*b*:4,3-*b*']dithiophene (**BDT**, Figure 41) and its derivatives belong to an interesting class of thiophene-containing aromatic π-conjugated systems, which have stimulated a lot of interest thanks to their applications in functional organic materials,[69] and, more recently, as π-spacers in push-pull organic chromophores in photovoltaic field.[70]

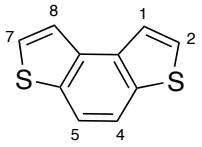


**BDT**

Figure 41.

Moreover, **BDT** represents a key intermediate in the synthesis of inherently chiral helical systems such as tetrathia[7]helicenes (7-TH).[3a]

On the basis of these considerations, **BDT** can be identified as a key starting molecule that, through a judicious functionalization of the α-positions of the thiophene rings, can allow access to more complex and interesting systems. Despite all these potential advantages, convenient synthetic methodologies to prepare BDT are still scarce,[71] and normally involve the oxidative photochemical cyclization of dithienyl ethenes as the key step (Scheme 53).

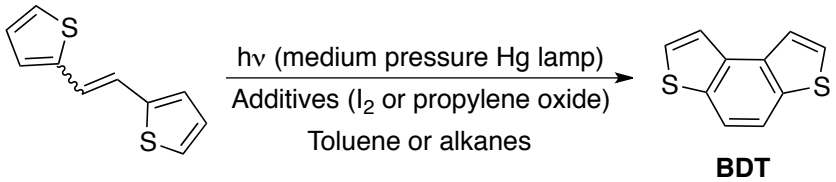


**BDT**

Scheme 53.

However, this reaction requires specific photochemical equipment and highly diluted solutions, takes several hours, and, to a significant extent, can limit the scale-up of the synthesis of BDT.

Within this context, and in view of potential wider and industrial applications, a simple, reliable, reproducible and economic synthesis of BDT which avoids the use of photochemical pathways is highly desirable. We then decided to investigate a new non-photochemical cyclization of dithienyl ethenes, especially by a $FeCl_3$-mediated oxidative intramolecular C-C bond formation between the β-positions of thiophene rings (Scheme 54).

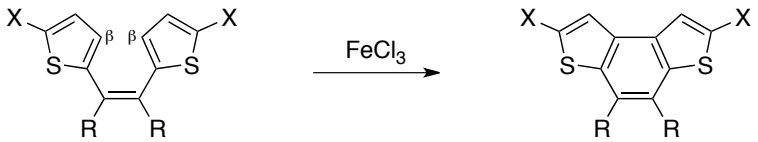


X : FG (*e.g.* halogen, ester, formyl, alkyl)
R : alkyl

Scheme 54.

In fact, iron(III) chloride is an economical and commercially available salt that has found widespread application as a Lewis acid,[72] but also as a mild and selective oxidizing agent, and is therefore particularly useful for C–C coupling reactions involving arenes and heteroarenes.[73] In

this way, while complex polycyclic aromatic compounds, containing the **BDT** framework have been prepared,[74] no synthesis of the simple tricyclic **BDT** scaffold has so far been reported using the $FeCl_3$ mediated oxidative coupling.

This Chapter will deal with the study of the $FeCl_3$-mediated cyclization of α,α'-disubstituted (*Z*)-dithienyl ethenes to synthesize the corresponding benzo[1,2-*b*:4,3-*b*']dithiophenes (**BDTs**), along with the influence of the temperature and the nature of the substituents on the scope and limitations of this methodology. Finally, a preliminary application of this procedure to the synthesis of the tetrathia[7]helicene **8** has been investigated.

### 4.1 Study on the $FeCl_3$-mediated cyclization of α,α'-dibromo (*Z*)-ethene 107b

Initially, we focused our attention on the (*Z*)-dithienyl ethenes bearing two *n*-propyl chains, which would improve the solubility in organic solvents of the prepared compounds. In fact, in our previous experience we observed that the solubility of unsubstituted BDT derivatives was poor, and quickly decreases with the increasing of their molecular weight.

Starting from the commercially available 1-(thiophen-2-yl)butan-1-one (**106**), the alkene (*Z*)-**107a** was then prepared in 74% by a highly steroselective Mc Murry coupling in the presence of $TiCl_4$ and Zn in THF at reflux for 3 h (Scheme 55).

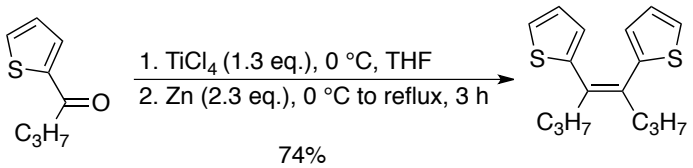


Scheme 55.

Unlike previously reported,[75] it is interesting to underline that, under the McMurry reaction conditions reported in Scheme 55, we isolated **107a** as a 9 : 1 mixture of the *Z* and *E* isomers. This is a fundamental stereochemical prerequisite for the further $FeCl_3$-mediated cyclization, which proceeds only with the *Z* isomer.

As expected, attempts to form the carbon-carbon bond at β-positions of the thiophene rings of **107a** by $FeCl_3$-mediated oxidative cyclization failed, obtaining only unseparable mixtures of polymerization by-products. Also for this substrate, the known higher spin density of the thiophene radical cation at the 2-position favors the formation of polymers[74b] instead of the expected parent benzodithiophene. However, this is not a drawback, since the preliminary substitution of alpha positions of the thiophenes, to prevent the polymerization, allows the direct access of α,α'-disubstituted **BDT** derivatives useful for further elaborations. Thus, we initially focused our attention on the α,α'-dibromo (*Z*)-ethene **107b**, which was synthesized *via* bromination with *N*-bromosuccinimide (NBS) in DMF at 0 °C for 2 h (Scheme 56).

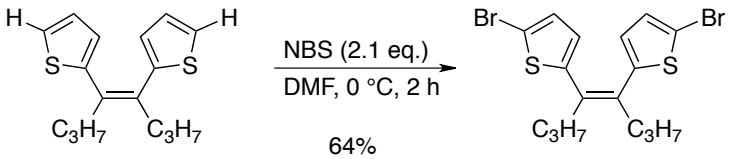


(*Z*)-**107a** (*Z*)-**107b**

Scheme 56.

The use of 2.1 equiv. of NBS at 0 °C allowed the regioselective bromination of the two α-positions of **107a**, providing (*Z*)-**107b** in 64 % yield.

Next, we carried out a brief screening to examine the influence of some parameters, including the amount of anhydrous $FeCl_3$ added, the use of $MeNO_2$ as co-solvent and the temperature, on the outcome of the $FeCl_3$-mediated cyclization reaction of (*Z*)-**107b** (Table 12).

Table 12.

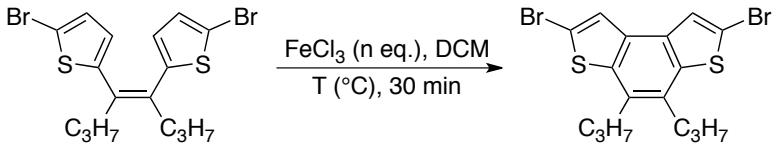


(*Z*)-**107b** **108b**

| Entry[a] | $FeCl_3$ (eq.) | T (°C) | Additives | Yield of **108b** (%)[b] |
|---|---|---|---|---|
| 1 | 4 | r.t. | - | 76 |
| 2 | 12 | r.t. | - | 72 |
| 3 | 0.1 | r.t. | *m*-CPBA (1 eq.) | 13 |
| 4 | 4 | r.t. | $MeNO_2$ | 60 |
| 5 | 4 | 0 | - | **79** |
| 6 | 4 | 40 | - | 57 |
| 7[e] | 4 | 80 | - | 60[f] |

a. Unless otherwise noted, the reactions were run adding $FeCl_3$ (4 equiv.) to a solution of **107b** (0.25 mmol) in $CH_2Cl_2$ (20 mL), and stirred for 30' under a nitrogen atmosphere. b. Isolated yields. c. The reaction was run at 80 °C using DCE as solvent. f. The reaction mixture contained **108b** and **109** in 10:1 molar ratio determined by $^1$H-NMR.

As shown in Table 12, the first experiment was run adding 4 equiv. of $FeCl_3$ to a solution of **107b** in $CH_2Cl_2$ at room temperature (Entry 1, Table 12). After 30' the reaction mixture proved to contain only the expected product **108b**, which was isolated in 76 % yield. Unlike **107a**, the oxidative cyclization of **108b** represents the favor process respect to polymerization or degradation reactions. While an increase of the amount of $FeCl_3$ (12 equiv) under the same reaction conditions gave similar results (Entry 2, Table 12), the use of a catalytic amount of $FeCl_3$ (10 mol%) in combination with a stoichiometric amount of *meta*-chloroperbenzoic acid (*m*-CPBA) as oxidant[76] resulted in a significant decreasing of yield of **108b** (13 %) (Entry 3, Table 12). Although $FeCl_3$-mediated cyclodehydrogenations are often carried out employing nitromethane as co-solvent for $FeCl_3$, in this case its use provided **108b** in lower yield (Entry 4, Table 12).

Concerning the reaction temperature, the cyclization of **107b** carried out at 0 °C afforded **108b** in a bit higher yield (79 %), than that obtained at room temperature (Entry 5 *vs* Entry 1, Table 12). On the contrary, the increase of the temperature (up to 40 or 80 °C) was found to be detrimental

(Entries 6 and 7, Table 12). In fact, the oxidation of **107b** in $CH_2Cl_2$ at 40 °C gave **108b** in only 57 % yield, along with traces of the by-product **109** (Entry 6, Table 12). When the temperature was risen to 80 °C using DCE as solvent, **108b** was obtained in 60 % yield, and the by-product **109** was isolated in 10% yield (Entry 7, Table 12). The structure of the tribromo derivative **109** was assigned on the basis of its spectroscopic and analytical data, and confirmed by the X-ray analysis of the white single crystals grown from layered $CH_2Cl_2$ /$CH_3CN$ (Figure 42).

The ORTEP view of **109** shows that the molecule is essentially planar neglecting the two *n*-propyl chains, which extend on two opposite sites of the mean plane of the benzodithiophene unit (Figure 42b).

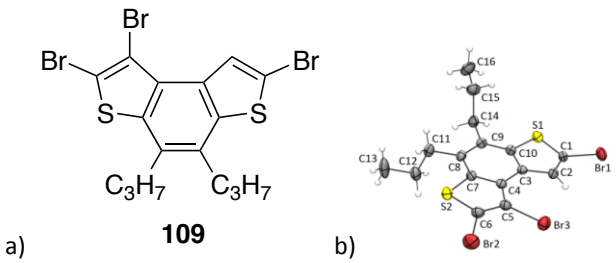


Figure 42. (a) Chemical Structure of **109**. (b) ORTEP view of the crystal structure of **109** (ellipsoids are drawn at their 30% probability level).

The formation of **109** could be rationalized by taking into account that thiophenes brominated in the α-positions readily undergo debromination and/or rearrangement reactions through heating in the presence of catalytic amounts of strong acids.[77] These processes, which generally involve the loss of brominating species, could also occur in the $FeCl_3$-mediated cyclization of **107b** at 80 °C. In fact, the hydrogen chloride generated during the cyclization of **107b** could catalyze the loss, from **108b**, of a ''brominating'' species, which then could be able to brominate **108b** to furnish the tribromide **109**. Moreover, we found that heating **108b** in the presence of 4 equiv. of $FeCl_3$ in DCE at 80 °C or at 110 °C with MW irradiation, resulted in the formation of **109** in 40% yield, besides the recovery of 5% of **108b** (Scheme 57).

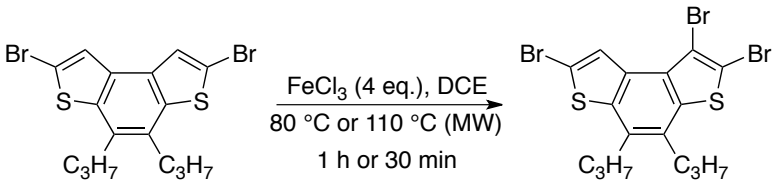


**108b** 40% **109**

Scheme 57.

### 4.2 $FeCl_3$-mediated cyclization of α,α'-disubstituted (*Z*)-ethenes 107: substrate scope

We then explored the substrate scope of this reaction, focusing on the influence of the nature of the substituents in the α-positions of **107a**. For this purpose, we set up the synthesis of a small library of α,α'-disubstituted (*Z*)-dithienyl ethenes **107c**–**f**, which were prepared by deprotonation of the alpha positions of terminal thiophene rings of **107a** with 4 equivalents of *n*BuLi at – 78 °C followed by the reaction with 4 equivalents of the proper electrophiles (Scheme 58).

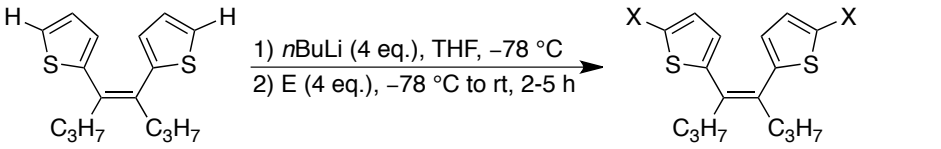


(*Z*)-**107a**

(*Z*)-**107c** : X = I 87%
(*Z*)-**107d** : X = $C_7H_{15}$, 51%
(*Z*)-**107e** : X = COOEt 76%
(*Z*)-**107f** : X = CHO 84%

Scheme 58.

Compounds **107c**–**f**, which were isolated in moderate to good yields (50–87 %), were then tested in the $FeCl_3$-mediated cyclization reaction to give the corresponding BDTs **108c**–**f**. On the basis of the results obtained from the screening on the (*Z*)-dithienyl ethene **107b**, we then investigated the cyclization of **107c**–**f** in the presence of 4 equivalents of $FeCl_3$ in DCM or DCE, evaluating the effect of the temperature on the outcome of these reactions (Table 13).

Table 13.

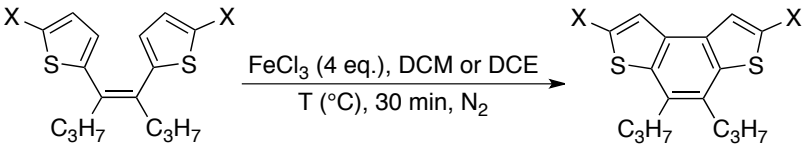


| | (*Z*)-**107c**–**f** | | | **108c**–**f** | | | |
|---|---|---|---|---|---|---|---|
| Entry[a] | Reagents | | Products | Yield (%)[b] | | | |
| | **107** | X | **108** | r.t. | 0 °C | 40 °C | 80 °C |
| 1 | **107b** | Br | **108b** | 76 | 79 | 57 | 60 |
| 2 | **107c** | I | **108c** | 10 | 32 | *dec.* | [c] |
| 3 | **107d** | $C_7H_{15}$ | **108d** | *dec.* | 66 | [c] | [c] |
| 4 | **107e** | COOEt | **108e** | 66 | [c] | 87 | 89 |
| 5 | **107f** | CHO | **108f** | < 10[d] | [c] | < 10[d] | 40 |

a. The reactions were run adding $FeCl_3$ (4 eq.) to a solution of **107** (0.25 mmol) in $CH_2Cl_2$ (20 mL), and stirred for 30' under a nitrogen atmosphere. b. Isolated yield. c. Not performed. d. A *Z*/*E* mixture of **107f** was recovered from the reaction mixture.

In contrast to the bromide **107b** (Entry 1, Table 13), the iodide **107c** gave the cyclized product **108c** in only 10% and 32% yields at room temperature and at 0 °C, respectively (Entry 2, Table 13). Moreover, **107c** decomposed completely and very quickly when the reaction mixture was warmed to 40 °C, with evident loss of iodine presumably due to the carbon–iodine bond lability, which leads to a significant dehalogenation during the oxidation procedure. As consequence of the dehalogenation process, the free $\alpha$-positions of thiophenes in **107c** easily gave uncontrolled polymerization/degradation reactions.

We also found that the substrate **107d**, bearing two alkyl chains in the $\alpha$-positions, underwent fast degradation at room temperature (Entry 3, Table 13). In this case, only a lower reaction temperature (0 °C) allows the cyclization of **107d** instead of its decomposition. Thus, the expected product **108d** could be isolated in 66 % yield, without any significant amount of by-products in the final reaction mixture.

Different results were obtained with (*Z*)-dithienyl ethenes **107e** and **107f**, substituted in the α-positions with the electron-withdrawing groups COOEt and CHO, respectively. In particular, the oxidative coupling of **107e** efficiently occurred at room temperature, 40 °C and 80 °C, providing **108e** in 66%, 87 % and 89% yield, respectively (Entry 4, Table 13). These results indicate that the substrate **107e** is stable under these oxidative conditions, and that its cyclization is favored by heating, affording the highest yield of **108e** at 80 °C.
On the other hand, the more electron-poor substrate **107f** remained practically unreacted, affording only traces of **108f,** both at room temperature and 40 °C (Entry 5, Table 13). In these experiments, we recovered mainly a mixture of (*Z*)- and (*E*)-**107f**. However, increasing the reaction temperature from 40 °C to 80 °C by the use of DCE in place of DCM as solvent, **108e** was isolated in 40 % yield along with *ca.* 10 % of unreacted ethene **107f** (Entry 5, Table 13).
Most likely, the presence of the electron-withdrawing formyl substituents on the thiophene rings of **107f** makes it difficult to generate the supposed radical cation intermediate, and, in this case, the temperature plays a crucial role to promote the intramolecular cyclization.

The complete decomposition of the iodo derivative **107c** at 40°C (Entry 2, Table 13) prompted us to evaluate the possible influence of the order of the reagents addition. In fact, we expected that a faster cyclization of **107c** respect to its decomposition could be achieved by reacting **107c** in the presence of an excess of $FeCl_3$ at 40 °C. Therefore, we added a solution of **107c** to a slurry of $FeCl_3$ (4 eq.) in $CH_2Cl_2$ at reflux (Entry 1, Table 14).

Table 14.

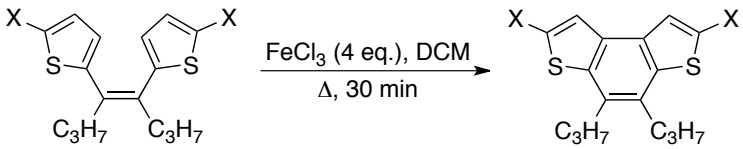


(*Z*)-**107** → **108**

| Entry[a] | Reagent | | Product | | |
|---|---|---|---|---|---|
| | **107** | X | **108** | X | Yield[b] (%) |
| 1 | **107c** | I | **108c** | I | 74 |
| 2 | **107e** | COOEt | **108e** | COOEt | 90 |
| 3 | **107f** | CHO | **108f** | CHO | *Traces* |
| 4 | **107b** | Br | **108b** | Br | 44 |

a. The reactions were run adding a solution of **107** (0.25 mmol) in $CH_2Cl_2$ (5 mL), to a suspension of $FeCl_3$ (4 equiv.) in $CH_2Cl_2$ (20 mL) at 40 °C. b. Isolated yield.

By this way, the cyclized product **108c** was isolated in 74 % yield. For comparison, the same procedure was applied to alkenes **107b**, **107e** and **107f**. For substrates **107e** and **107f**, we did not found any advantages from the inversion of the order of reagents addition (Entries 2 and 3, Table 14). The dibromo alkene **107b** actually gave a mixture of **108b** and **109**, but in this case the amount of **109** (29 % yield) was significantly increased with the contemporary decrease of yields of **108b** (Entry 4, Table 14).

### 4.3 Synthesis of functionalized BDTs bearing free alpha positions

While the synthesis of functionalized benzodithiophene derivatives **108b–f** has important implications for the development of new and more complex molecular architectures, further modifications exploiting the reactivity of the substituents in the α-positions of the thiophene rings appear just as useful. Among these, the possibility of the debromination of **108b** was explored by treating it with *n*BuLi–MeOH at 0 °C (Scheme 59).

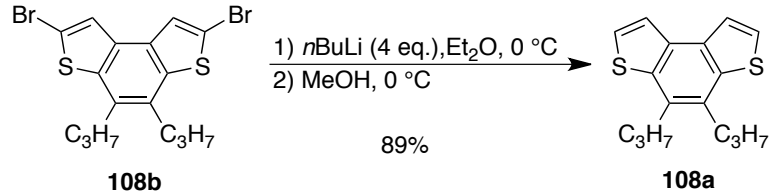


**108b** **108a**

Scheme 59.

From this reaction we isolated, in 89% yield, unsubstituted **108a**, which as already stated above, cannot be obtained by means of the $FeCl_3$-mediated cyclization of **107a**. More interestingly, the analogous regioselective debromination of the two α-positions of **109** also occurred using two equivalents of *n*BuLi–MeOH at –78 °C, providing the β-bromo substituted **110** in 70% yield (Scheme 60).

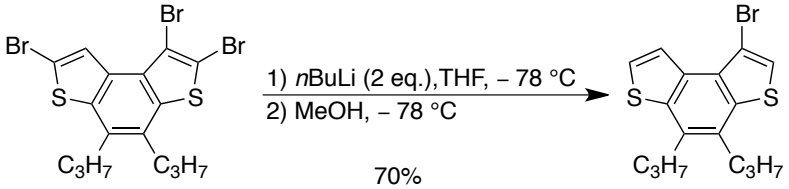


**109** **110**

Scheme 60.

This latter compound represents a potential new key intermediate for the synthesis of an interesting class of chiral atropoisomeric molecules, from which enantiomerically pure thiahelicenes could be prepared.

### 4.4 Synthesis of BDTs functionalized at 4 and 5 positions by $FeCl_3$-mediated cyclization reactions

During our previous researches on BDT derivatives, it came out clearly the rather low solubility of disubstituted BDT and of the more elaborated molecules arised from them. Therefore, we realized the importance of introducing alkyl chains on the BDT moiety. For these reasons, we exploited this methodology towards the synthesis of two α,α'-dibromo substituted BDTs **111** and **112**, bearing two different alkyl chains in the 4 and 5 positions of the BDT scaffold (Figure 43).

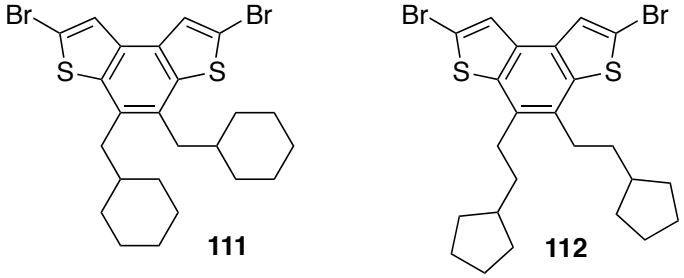


**111** **112**

Figure 43.

In particular, the steroselective McMurry coupling of ketones **113** and **114** provided the corresponding (*Z*)-alkenes **115** and **116** in 85 and 67 % yield, respectively (Scheme 61).

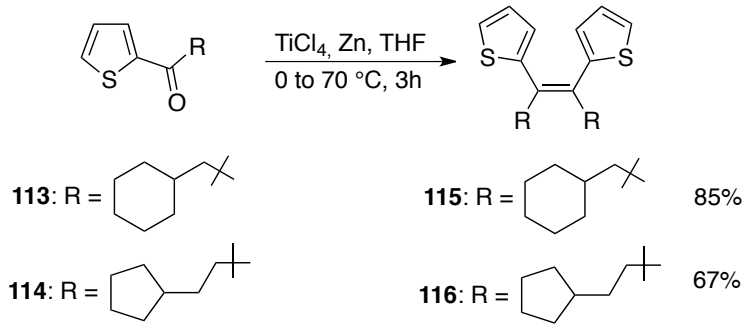


Scheme 61.

Next, the selective α-bromination of (*Z*)-alkenes **115** and **116** with 2.1 equivalents of NBS at 0 °C in DMF afforded the α,α'-disubstituted (*Z*)-alkenes **117** and **118** in 71 and 74 % yield, respectively (Scheme 62).

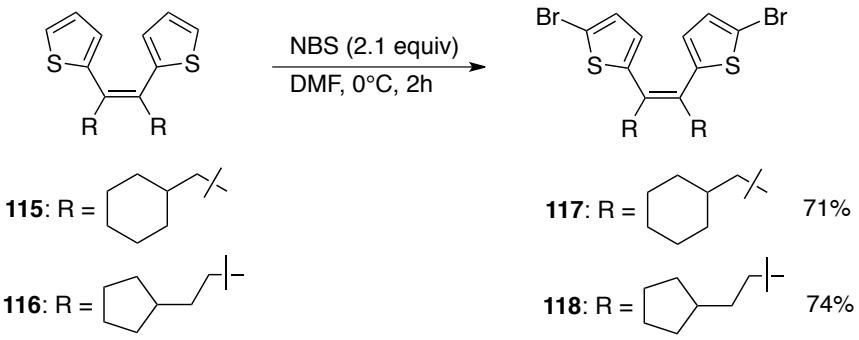


Scheme 62.

Finally, bromides **117** and **118** smoothly cyclized in the presence of 4 equivalents of $FeCl_3$ at room temperature to give benzodithiophenes **111** and **112** in 58 and 70 % yield, respectively (Scheme 63).

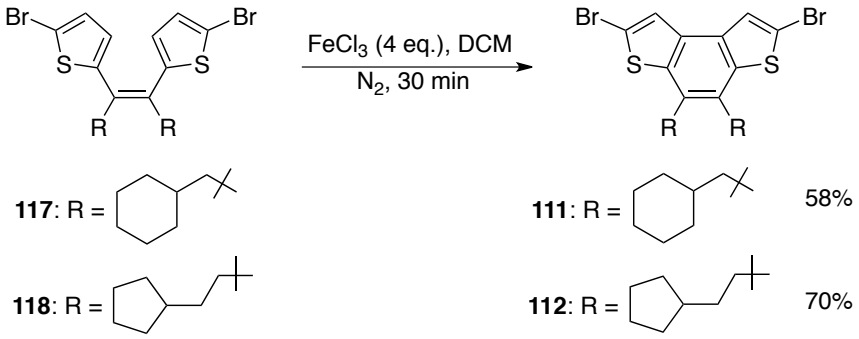


Scheme 63.

**4.5 $FeCl_3$-mediated cyclization of (*Z*)-alkene 119 to give tetrathiahelicene 8**

Within this study, we also explored the possibility of using this procedure for the cyclization of (*Z*)-alkene **119** to afford the tetrathiahelicene **8**. This latter compound is indeed a fundamental precursor for the synthesis of most of the 7-TH phosphorus derivatives prepared in this thesis, and its synthesis involves the photocyclization of (*Z*)-alkene **119**.[3] Thus, in view to prepare **8** on large scale and to overcome the previously drawbacks related to the photocyclization processes, we

decided to investigate the $FeCl_3$-mediated cyclization of (*Z*)-**119** evaluating the influence of the temperature, the amount of $FeCl_3$ and the nature of the solvent, on the efficiency and selectivity of this reaction (Table 15).

Table 15.

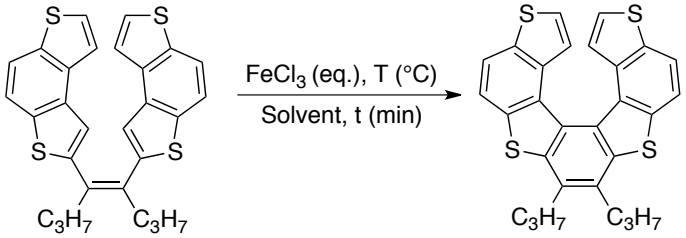


(*Z*)-**119** **8**

| Entry[a] | $FeCl_3$ (eq.) | Solvent | T (°C) | t (min) | Yield (%) |
|---|---|---|---|---|---|
| 1 | 4 | DCM | r.t. | 30 | -[b] |
| 2 | 4 | DCM | 0 | 8 | 50 |
| 3 | 4 | DCM | –20 | 30 | 50 |
| 4 | 2,1 | DCM | 0 | 20 | 60 |
| 5 | 2,1 | DCM | –20 | 30 | 42 |
| 6 | 2,1 | DCM | –20 | 60 | **62** |
| 7 | 2,1 | AcCN | 0 | 60 | 25[c] |
| 8 | 2,1 | DCM/$CH_3NO_2$ | 0 | 60 | 40 |
| 9 | DDQ/ $MeSO_3H$ | DCM | 0 | 60 | -[c] |

[a]The reactions were run adding $FeCl_3$ to a solution of (*Z*)-**119** (0.25 mmol) in the proper solvent (20 mL), and stirred under a nitrogen atmosphere. [b]A complex mixture of byproducts was recovered from the reaction mixture. [c]A by-product resulting from rearrangement mechanism[78] was isolated from the reaction mixture.

As shown in Table 15, the first experiment was run adding 4 equiv. of $FeCl_3$ to a solution of (*Z*)-**119** in $CH_2Cl_2$ at room temperature (Entry 1, Table 15). Unfortunately, after 30' the reaction mixture contained several unseparable polymerization by-products. On the contrary, when the reaction was carried out at lower temperatures (0 or –20 °C), helicene **8** could be isolated in 50% yield (Entries 2 and 3, Table 15). On the other hand, using 2.1 equivalents of $FeCl_3$ at 0 or – 20 °C it was possible to obtain **8** in the highest yields (60-62%) in 20 min or 1 hour, respectively (Entries 4 and 6, Table 15). Finally, any improvements were found in using different solvents (MeCN or $MeNO_2$) and/or organic oxidizing agent such as DDQ (Entries 7-9, Table 15).

From these results, it is clearly evident that the temperature plays a key role in this reaction, obtaining the best efficiency and selectivity in the formation of **8** at low temperatures (0 or – 20 °C). Moreover, these experimental conditions great limit the polymerization side-reactions that typically occur with $FeCl_3$ in the presence of free alpha positions of the thiophene rings. Finally, in this case the (*Z*)-configuration of **119**, that is a fundamental stereochemical prerequisite for the

$FeCl_3$-mediated cyclization, is not a limitation because (*Z*)-**119** can be easily and selectively prepared as (*Z*)-isomer by a McMurry coupling or *via* Suzuki coupling according to the literature.[3]

**4.6 Conclusions**

In summary, a non-photochemical methodology for the synthesis of BDT scaffolds through the $FeCl_3$-mediated oxidative cyclization of 1,2-dithienylethenes **107b–f, 117** and **118** has been set up, demonstrating the feasibility of achieving $\alpha,\alpha'$-disubstituted BDTs without the need to be inserted into more complex polyaromatic systems. Moreover, the presence of two functional groups in the $\alpha,\alpha'$positions of alkenes **107b–f** efficiently prevents polymerization under the oxidative conditions of cyclization, and allows further functionalization of the final BDTs. For these reasons, the establishment of this methodology may promote renewed and increased interest in the [1,2-*b*:4,3-*b*'] BDT scaffold and consequently the development of new applications. Finally, we have also demonstrated that (*Z*)-**119** could be efficiently converted in the corresponding helicene **8** using $FeCl_3$ (2 equivalents) as oxidizing agent at low temperatures (0 or – 20 °C) within one hour, allowing us to avoid the photochemical step. Noteworthy, in this case no protection of the alpha positions of the terminal thiophene rings in (*Z*)-**119** was necessary, and the helicene **8** could be isolated in 60% yield in 1 hour, which is a value comparable with that obtained with the photochemical process in *ca.* 6–8 hours.

# Chapter 5

## Study of a nanostructured PLGA system for cell delivery of a luminescent 7-TH derivative

Among the various applications of helical structures in catalysis and in other very different fields, to date the use of helicene derivatives in biological chemistry are still very rare, but potentially very promising and appealing, in that interesting selectivity in binding to various DNA polymorphs have been reported.[79]In fact, thanks to their peculiar shape, the affinity of helicenes for naturally occurring chiral helical architectures, such as DNA, has led to some studies on their intercalation properties for natural nucleic acids, which is the prerequisite for hidden or suppressed DNA synthesis or inhibition of transcription phenomena, potentially useful in cancer cell treatment.
In 2002, Yamaguchi and co-workers[80] first disclosed the chiral recognition between the small carbohelicenediamine **120** and the right-handed B-DNA structure (Figure 44).

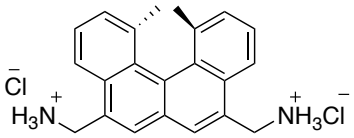


(*P*)-**120**

Figure 44.

The apparent changes in the UV and CD spectra caused by adding calf thymus DNA to the solutions of (*P*)- and (*M*)-**120** suggested that DNA-helicene complexes were formed. According to isothermal titration calorimetry, the binding constant of (*P*)-helicene is slightly larger than that of its enantiomer, whereas the chiral recognition whereby (*P*)-**120** favors right-handed helicity is probably driven by entropy. In 2004, Tanaka's group [81] demonstrated that the (*P*)-2,13-bis(dimethylaminomethyl)-tetrathia[7]helicene **121** had a propensity for a highly enantioselective binding to Z-DNA, effectively converting B- into Z-DNA (Figure 45).

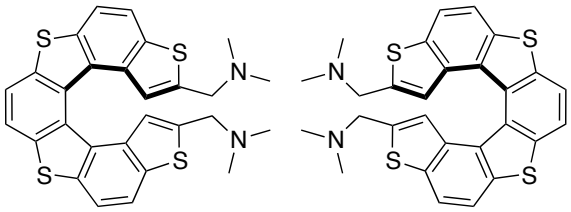

(*M*)-**121** (*P*)-**121**

Figure 45.

However, although (*M*)-**121** exhibited selective binding with Z-DNA, the binding constant of the (*P*)-enantiomer was five times greater. Interestingly, when the amino groups were replaced by hydroxyl groups, the structural selectivity vanished, indicating that the protonated amino substituents were important in binding Z-DNA.
Recently, Latterini and co-workers reported two studies on the DNA-binding properties of *N*-methyl-5-azahelicenium salts **122** (Figure 46), evaluating the counterion effects in the binding between helicenes and DNA using the same organic azahelicenium moiety with different anions,[82] and a first study on the uptake and their localization in eukaryotic cells by fluorescence confocal microscopy.[83]

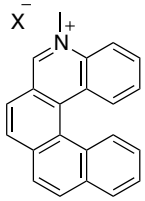

X= $I^-$, $NO_3^-$, $CF_3COO^-$

**122**

Figure 46.

In 2010, Tanaka's group[84] reported an interesting study on the inhibition of telomerase activity by a bridged thiahelicenophane **123** (Figure 47).

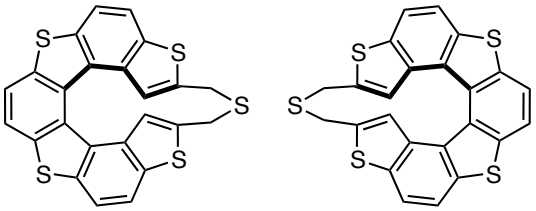

(*M*)-**123** (*P*)-**123**

Figure 47.

In particular, it has been shown that (*M*)-tetrathia[7]helicenophane **123**, with the appropriate dihedral angle and absolute configuration, showed an effective interaction with the substrate, effectively blocking the access of telomerase to telomeres by association with higher order G-quadruplex structures.

On the basis of the above considerations and on their peculiar properties, it is clear that helicenes offer enormous interest in the context of biological activity, and it seems therefore particularly relevant to study their cell uptake, through appropriate drug delivery systems, as well as their cytotoxicity. In fact, the cell uptake is the fundamental prerequisite that a molecule must have for interacting with cell components and therefore exhibiting a biological effect, and in this context, the use of appropriate drug delivery systems are quite often applied.

Thus, we have started a study in collaboration with Dr. Federica Chiellini of the University of Pisa to evaluate the possibility of using poly(lactic-co-glycolic acid) (PLGA) nanoparticles as innovative and useful nanocarriers for tetrathia[7]helicene derivatives. Indeed, owing to the fact that helicenes are known to be very promising DNA intercalators, the tetrathiahelicene has been selected, for this study, as a model therapeutic cytotoxic molecule.

This Chapter will deal with the synthesis and the characterization of a new nanoconstruct based on PLGA nanoparticles loaded with a tetrathiahelicene molecule conjugated to a fluorescent rhodamine probe. The potentiality of the developed nanoconstruct on the ability of internalize the tetrathiahelicene, and deliver it intracellularly safely, has been also discussed by means of cytotoxicity and cell uptake tests on Balb/c 3T3 clone A31 fibroblasts.

### 5.1 Synthesis of fluorescent tetrathia[7]helicene 125

The modified tetrathiahelicene **125**, used as a racemic mixture for this first study, was prepared in 34% yield by reacting the known amino derivative **124**[85] with an equimolar amount of the

commercially available Rhodamine B isothiocyanate mixed isomers (RBITC) in the presence of DIPEA as a base and EtOH at room temperature (Scheme 64).

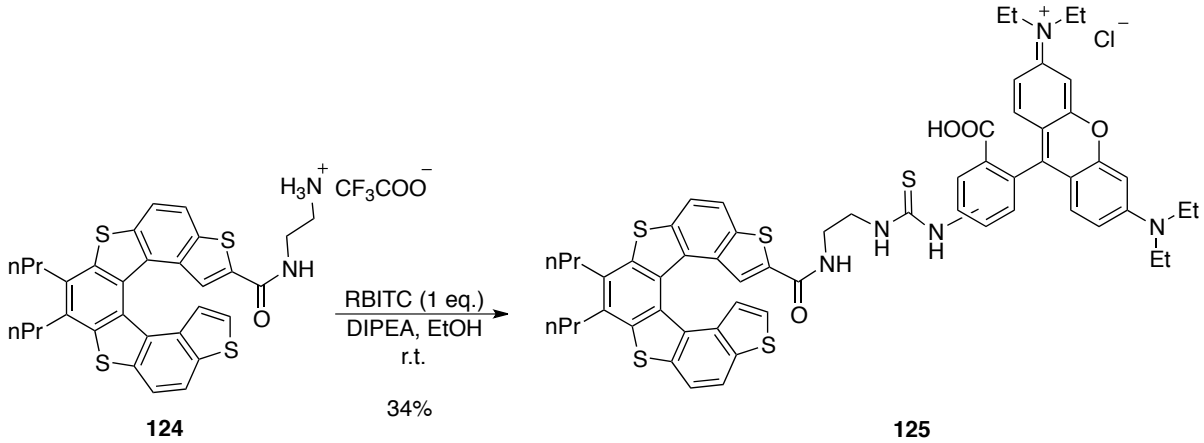


**124** **125**

Scheme 64.

The highly stable thiourea bond thus formed between the helicene and rhodamine assures the rhodamine to remain covalently conjugated to the helicene during biological studies.
In this way, the conjugation of the tetrathiahelicene scaffold to the rhodamine moiety allowed us to use fluorescence techniques to evaluate the encapsulation and the release profile of **125** into PLGA as well as their uptake by cell, exploiting the inherent fluorescent properties of the rhodamine.

### 5.2 Characterization of naked and 125-loaded PLGA nanoparticles (125-NPs)

PLGA based NPs containing **125** (**125-NPs**) were prepared by the nanoprecipitation technique,[86] that has been used extensively to load many different bioactive hydrophobic compounds into nanoparticles.[87] Unloaded **NPs** and **125-NPs** displayed a mean diameter of 112 nm ± 16 nm and 133 nm ± 16 nm, respectively, and no statistically significant difference was observed in the average size of the two **NPs** formulations (Figure 48).

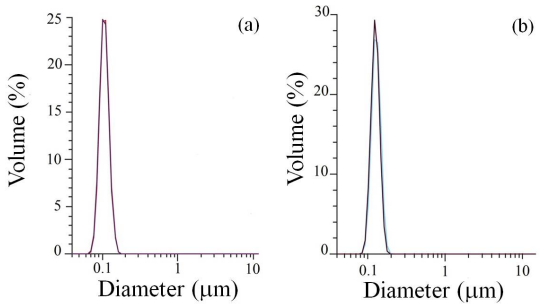


Figure 48. Particle size distribution of: a) blank **NPs**; b) **125**-**NPs**

Moreover, the introduction of **125** did not alter the formation of particles, thus **125** incorporated in **NPs** was used for determination of drug loading and encapsulation efficiency as well as sensitive marker to study cellular uptake by confocal microscopy.
The zeta potential of **125-NPs**, measured using photon correlation spectroscopy, was found to be − 24.27 ± 0.54 mV, that was not significantly different from that of unloaded **NPs** (− 24.50 ± 0.29 mV), suggesting that the loading of **125** did not significantly modify their surface properties. On

the other hand, a high absolute value of zeta potential, such as the value displayed by **125-NPs**, indicates high electric charge on the surface of prepared **NPs**, which can cause strong repellent forces among particles to prevent aggregation of the **NPs**.
Exploiting the inherent fluorescent properties of the rhodamine moiety on **125**, fluorescence techniques were also used to evaluate the amount of **125** encapsulated in **NPs**, and its release profile. A calibration curve of fluorescence values at known concentrations of **125** was set up, allowing the quantification of the encapsulation efficiency of **125** that was resulted in the range of 60% with a loading of 0.3%.

### 5.3 Biological studies on 125-NPs

The potentiality of the developed nanoconstruct on the ability of internalize the tetrathiahelicene and deliver it intracellularly safely, has been investigated by means of cytotoxicity and cell uptake tests on Balb/c 3T3 clone A31 fibroblasts.

#### *5.3.1 In vitro release studies*

As reported in Figure 49, the *in vitro* release profile of **125** from **NPs** was time controlled, with 27% of **125** released in 10 days, and did not display an initial burst step.

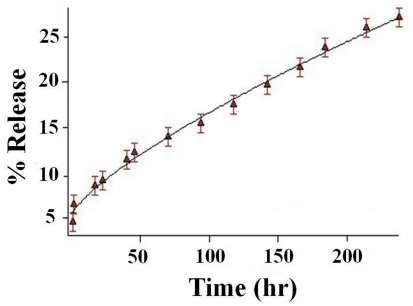


Figure 49.

A slow controlled release of a drug within first hours is an important parameter for *in vitro* studies of **NPs** uptake by cells, and thus the observed slow delivery of **125** from **125-NPs** in physiological conditions makes it a good model for investigations of nanoparticles interactions with cells.

#### *5.3.2 In vitro cytotoxicity activity assay*

To evaluate the cytotoxicity of free **125** and **125-NPs**, *in vitro* experiments were carried out by using the mouse embryo fibroblasts cell line balb/c 3T3 clone A31, and results in terms of cell viability as a function of concentrations of free **125** and **125**-NPs are shown in Figure 50. Cells, were incubated with Dulbecco's Modified Eagle's Medium (DMEM) containing different concentration of free **125** (4−8−15 μg/ml) and **125**-NPs (1.5−3−6 mg/ml) for 24 hours (Figure 50).

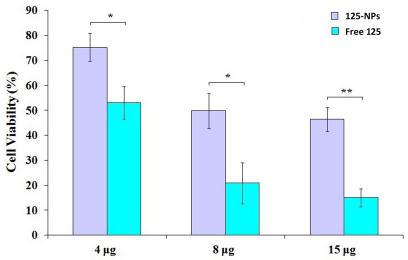


Figure 50.

The amount of free **125** was selected taking into account the same concentration found in the **NPs** formulation. Quantitative evaluation of cell viability was performed by means WST-1 tetrazolium salt using untreated cells as control. It is evident that, at the same concentration, **125-NPs** showed a significant lower cytotoxicity in respect to the free form, likely due to a controlled release of **125** from **NPs** after the internalization within cells.

*5.3.3 Study on the cellular uptake of **125-NPs***

Next, to evaluate the potential ability of **125-NPs** to cross cell membrane, an *in vitro* uptake study was carried out using the Confocal Laser Microscopy (CLSM).[88] Balb/c 3T3 clone A31 fibroblasts were incubated with **125-NPs** as a tracer molecule. The excitation of the rhodamine, with a solid-state laser at 561 nm, allowed us to localize loaded **NPs** in the cellular sample. Confocal microscopic images taken after 1 h of incubation revealed that there was a significant internalization of **NPs** inside the cells cytoplasm (Figure 51).

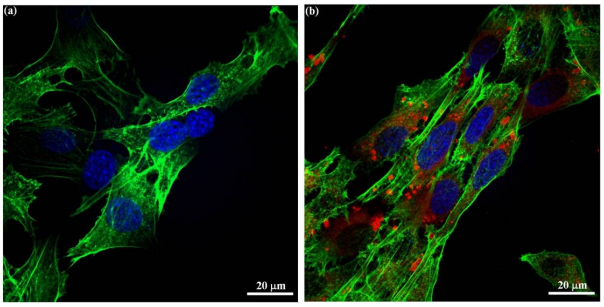


Figure 51. CLSM images of Balb/ 3T3 clone A31 cells a) untreated; b) treated with **125-NPs**

Cell morphology was not affected by incubation with **125-NPs** (Figure 51b), and no evident sign of toxicity was detected in respect to untreated control cells (Figure 51a). Well-oriented actin filaments with thickened longitudinal bundles were observed. Nuclei were healthy and morphologically oval-shaped with a diffused chromatin distribution. These results confirmed the viability of the cells at the experimental concentration of 1 mg/ml of **125-NPs** used throughout our studies. The cellular uptake pathway of **125-NPs** was investigated by treating cells with chemical endocytic inhibitors of: a) clathrin-mediated endocytosis-chlorpromazine;[89] b) caveolae-mediated endocytosis-filipin;[90] c) macropinocytosis-amiloride.[91] Cells were pre incubated with the different inhibitors individually, using concentrations (10 µg/ml of chlorpromazine, 1 µg/ml of filipin, 50 µM of amiloride) that were found non-toxic for the cells. Following the preincubation for 1 hour, the inhibitor solution was removed and replaced with cell culture medium containing **125-NPs** and further incubated for 1 hour.

Finally, samples were treated for confocal microscopy analysis (Figure 52).

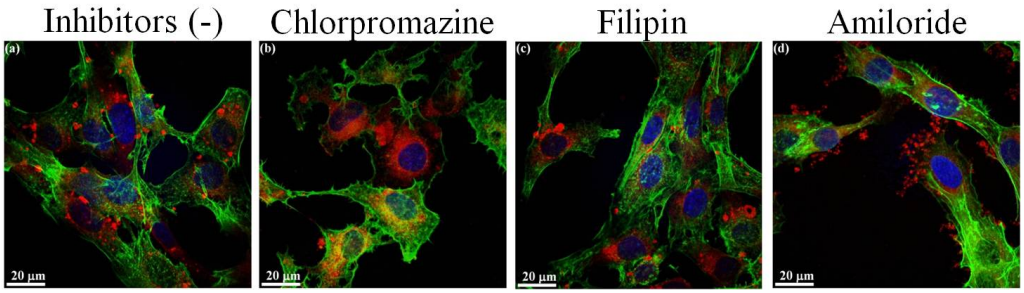


Figure 52. Uptake patterns of **125-NPs** in balb/3T3 cells in: a) absence of inhibitors; or in presence of : b) chlorpromazine, c) filipin, d) amiloride.

Cells incubated with **125-NPs** but not previously treated with inhibitors were used as control. CLSM analysis of cells treated with chlorpromazine (Figure 52b) and filipin (Figure 52c) revealed a strong red fluorescence inside the cells with a similar pattern in respect to control cells (Figure 52a), indicating that the clathrin-mediated and caveolae-mediated endocytosis do not seem to have a key role in the cellular uptake of **125-NPs** under the adopted experimental conditions. Alternatively, when cells were pre-incubated with amiloride, a specific inhibitor of the $Na^+/H^+$ exchange required for macropinocytosis, red fluorescent aggregates were observed outside the cellular membrane with a significant decrease of fluorescence inside cell cytoplasm (Figure 52d).
Taken together these results suggest that the uptake of **125-NPs** into the cells occurs via constitutive macropinocytosis rather then clathrin-dependent or caveolin-dependent mechanisms. These preliminary results are very promising. In fact, **NPs** taken up by clathrin-mediated endocytosis pathway are typically destined for lysosomal degradation, whereas pathways involving caveolae-mediated endocytosis and macropinocytosis are somewhat nonspecific, and neither acidic nor digestive.[92] Therefore the observed macropinocytosis as predominant pathway for the cellular uptake of **125-NPs** could avoid the lysosomal degradation of the internalized **NPs**,[93] thus preserving the bioactivity of the loaded cargo.

### 5.4 Conclusions

In summary, a novel nanoconstruct **125-NPs** obtained by nanoprecipitation of PLGA in the presence of luminescent tetrathiahelicene **125** has been prepared. Characterization, release and preliminary cell uptake studies, as well as toxicity tests performed on **125-NPs** reveal interesting behaviors: *(i)* the particle size distribution was very narrow and no statistically significant difference was observed in the average size between blank **NPs** and **125-NPs**; *(ii)* the *in vitro* release of **125** from **NPs** was time controlled, and did not display an initial burst step; *(iii)* the *in vitro* toxicity resulted to be significantly lower with respect to the free **125**; *(iv)* the preliminary cell uptake study suggests a macropinocytosis pathway of entry into cells.
The outcomes of this study suggests the suitability of the developed nanosystem to act as a vector for the intracellular delivery of hydrophobic small molecules, such as helicenes, thus contributing to their possible future exploitation as novel therapeutics. Moreover, these promising results could bring to a renewed interest for developing the peculiar chiral system of helicenes in biological applications.

# Chapter 6

## 7-TH-based push-pull system for applications in DSSCs: synthesis, optical and electrochemical characterization

Among several new energy technologies, solar cells utilizing the sun as an energy source are the most promising. Traditional solar cells based on silicon have reasonable energy conversion efficiencies of *ca.* 15%. However, they require high-purity silicon and skilled manufacturing techniques, which result in high costs, so their widespread use in our lives has been limited. On the other hand, dye-sensitized solar cells (DSSCs), based on dye sensitizers adsorbed on nanocrystalline $TiO_2$ electrodes, have received considerable attention because of their high incident solar light-to-electricity conversion efficiency, low cost processes, and ease of production.[94]

A DSSC is generally composed of a photo-anode and a photoinert counter electrode (cathode) sandwiching a redox mediator. It consists of five materials: a) a fluorine-doped $SnO_2$ (FTO) glass substrate; b) a nanocrystalline $TiO_2$ thin film as a semiconductor; c) a dye sensitizer; d) an electrolyte (redox mediator); e) a platinum-coated glass substrate.[94]

As described in Figure 53, the generation of photocurrents in the DSSC occurs through the following processes: 1) photoexcitation: the dye sensitizer absorbs a photon (sunlight) to generate the photoexcited state of the dye (S*); 2) injection: the photoexcited dye (S*) injects an electron into the conduction band (CB) of $TiO_2$, and the injected electrons move through the network of interconnected $TiO_2$ nanoparticles to arrive at the transparent conducting oxide (FTO) and then through the external circuit to the counter electrode; 3) reduction: the resultant oxidized dye is subsequently reduced back to its original neutral state by electron donation from the $I^-$ ions in redox mediator; 4) redox mediator: the $I^-$ ion is regenerated by the reduction of triiodide ion $I_3^-$ at the counter electrode through the donation of electrons from the external circuit, and then the circuit is completed. During this electron flow cycle, however, undesirable side processes could occur: 5) recombination or 6) dark current: the electrons injected into the CB of the $TiO_2$ electrode may recombine either with oxidized dye or with $I_3^-$ at the $TiO_2$ surface.

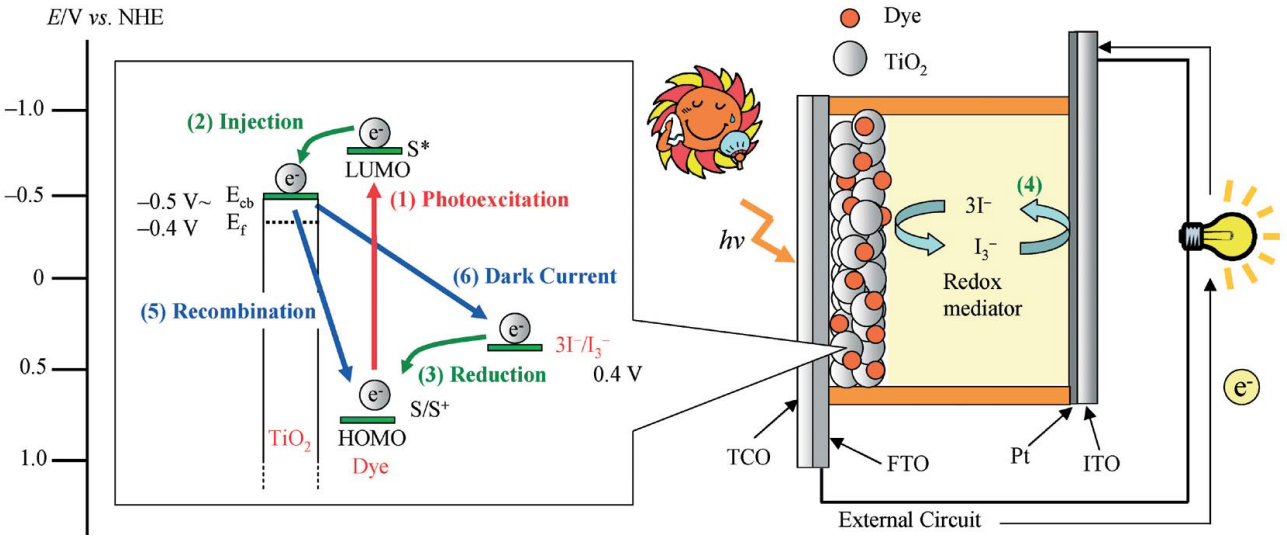


Figure 53.

The first examples of DSSCs, reported by Grätzel and O'Regan, were based on Ru complexes. Because of the high expense of the Ru dyes involved, several environmentally friendly, easily

prepared organic donor (D) acceptor (A) π-conjugated (D-π-A) dyes have been investigated as alternatives. In fact, although the performances of organic-dye-based DSSCs remain inferior to those of DSSCs based on the Ru complexes, the used of organic dyes have been stimulating intensive research efforts because of their advantages as photosensitizers for DSSCs: 1) they can be prepared and purified easily at lower cost; 2) they have higher molar absorption coefficients than the Ru complexes; 3) the wide variety of the structures and their facile modification provides potential for molecular design; 4) there are no concerns about resource limitations. For these reasons, many organic dyes exhibiting relatively high DSSC performances have so far been designed and developed, including dyes-based on coumarins, polyenes, hemicyanines, thiophenes, indolines, heteropolycyclics, xanthenes, perylenes, porphyrins, catechols, polymers, squaraines, cyanines and phthalocyanines.[94]

On the basis of these accumulated knowledge of organic dyes so far synthesized for DSSCs, the most indispensable requirements in the molecular design of organic dyes for DSSCs are:

- the organic dye must have at least one anchoring group (*e.g.* –COOH, $–SO_3H$, $–PO_3H_2$, –OH) for adsorption onto the $TiO_2$ surface;
- to achieve efficient electron injection from the excited dye to the CB of the $TiO_2$, the energy level of the lowest unoccupied molecular orbital (LUMO) of the dye must be higher (more negative) than the conduction band (CB) of the $TiO_2$ electrode;
- to achieve efficient regeneration of the oxidized state by electron transfer from $I_3^-/I^-$ redox couple in the electrolyte, the energy level of the highest occupied molecular orbital (HOMO) of the dye must be lower (more positive) than the $I_3^-/I^-$ redox potential;
- dye aggregation on the $TiO_2$ surface, leading to low conversion efficiency of the DSSC, should be avoided. In fact, donor–acceptor π-conjugated dyes are liable to undergo π-stacked aggregation on the $TiO_2$ surface, which leads to reduction in electron-injection yield from the dyes to the CB of the $TiO_2$ owing to intermolecular energy transfer.

Thus, to obtain further new and efficient organic dye sensitizers for DSSCs, novel molecular designs capable of controlling not only the photophysical and electrochemical properties of the dyes themselves, but also the molecular orientation and arrangement of dyes on the $TiO_2$ surface – such as π-stacked aggregation of dyes and interaction between dye sensitizers and $TiO_2$ surface – are necessary.

While a large number of organic dyes have been developed, and the relationships between their chemical structures and the photovoltaic performances of DSSCs based on these dyes have been examined, curiously the use of helical–based dye for the construction of DSSCs is rare. In this context, the very few examples have been reported by Harima and co-workers,[95] and involve the use of the benzofuro[2,3-*c*]oxazolo[4,5-*a*]carbazole-type scaffolds (Figure 54).

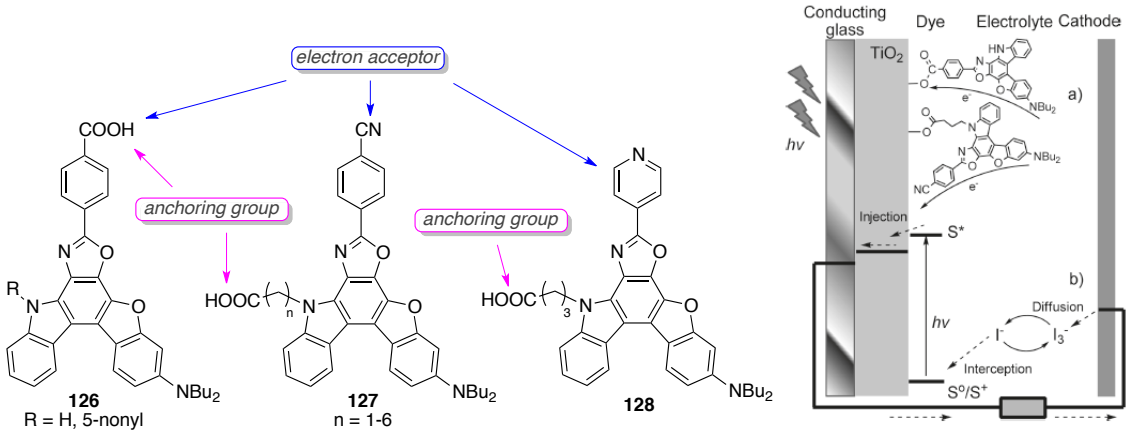


Figure 54.

In particular, a series of benzofuro[2,3-*c*]oxazolo[4,5-*a*]carbazole-type fluorescent dyes using the heterohelicene scaffold as π-spacer has been synthesized with the carboxy groups at different positions of the chromophore skeleton: the –COOH group that acts as anchoring group for attachment to the $TiO_2$ surface and also as the electron acceptor (dyes **126**); the –COOH group that acts as anchoring group and the cyano group or pyridine ring as the electron acceptors (dyes **127** and **128**, respectively). The photovoltaic performances of DSSCs based on these dyes were measured, and provided cell efficiencies η raging from 0.88 to 1.33%.

On the basis of the above considerations, the lack of in-depth and extensive study on the use of helicene scaffolds as π-conjugated spacers in DSSC prompted us to investigate the potential application of thiahelicene derivatives in this field, especially on tetrathiahelicenes, exploiting our wide and longstanding experience in their synthesis and functionalization.

This Chapter will deal with the study of a new tetrathia[7]helicene-based push-pull system, including its synthesis, optical and electrochemical characterization, along with a preliminary investigation on the photovoltaic performances of a DSSCs based on this helical dye.

### 6.1 Design of a new 7-TH-based push-pull system

Initially, we have planned a preliminary investigation of the photovoltaic performance in DSSC of a new helical dye system **129** (Figure 55), in which the thiahelical skeleton represents the π-conjugated-bridge spacer.

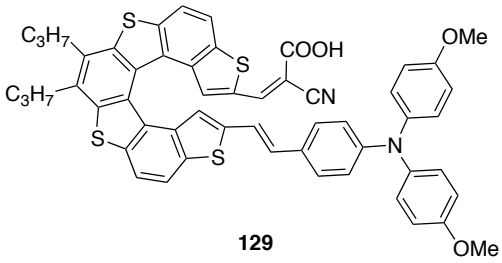


129

Figure 55.

In particular, we have supposed that the target dye **129** could fulfill the requirements as organic dyes for DSSCs, being constituted by:

- the thiahelicene scaffold as π-conjugated system, in which four thiophene rings alternated to three benzene rings form a stable and conjugated helical structure;

- the triarylamine moiety linked to the π-spacer by a double bond as donor group;
- the cyanoacrylic acid group as electron acceptor and anchoring group for attachment to the $TiO_2$ surface.

Moreover, the non-planarity of the helical system along with the presence of the bulky triarylamine donating group should disturbance possible π-π stacking events, suppressing the aggregation of the dye molecules on the $TiO_2$ surface.

### 6.2 Synthesis of the 7-TH-based push-pull 129

Following the synthetic approach previously exploited for the synthesis of benzodithiophene-based dyes,[70b] the helical-based dye **129** was prepared *via* a three-step procedure, involving the synthesis of the dialdehyde **130**, followed by a selective Wittig olefination using the phosphonium salt **131**, and a final Knoevenagel condensation reaction of intermediate **132** with cyanoacetic acid (Scheme 65).

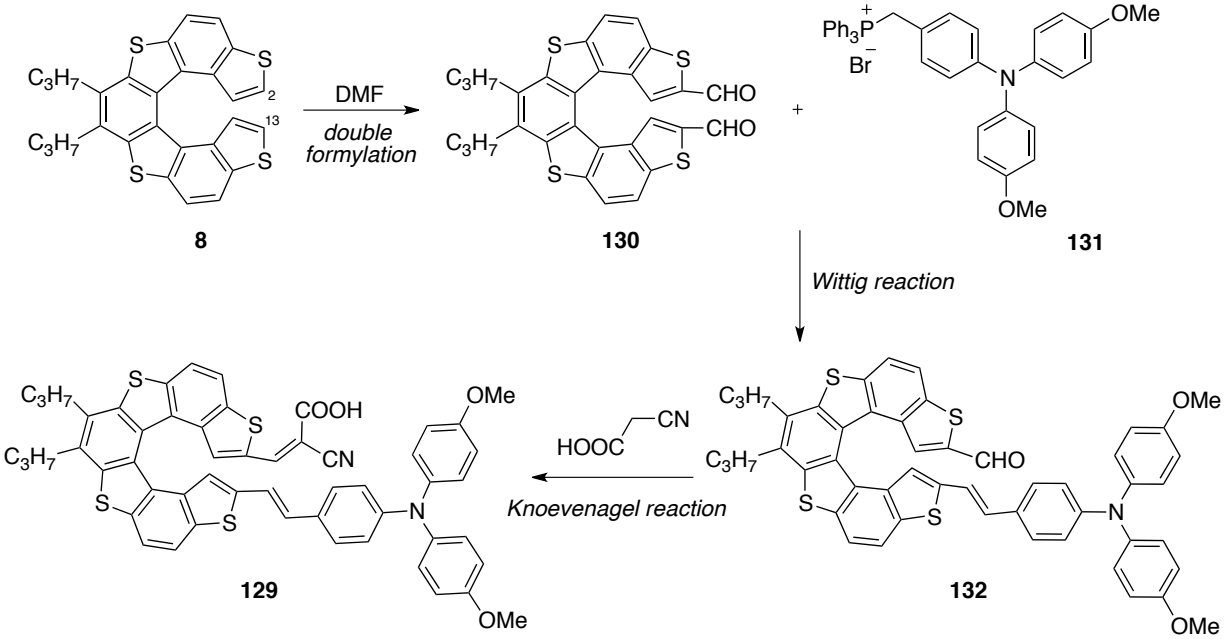


Scheme 65.

Initially, we focused our attention on the synthesis of dialdehyde **130**, which was prepared according to a procedure very similar than that previously set up in our laboratories[3a] (Scheme 66).

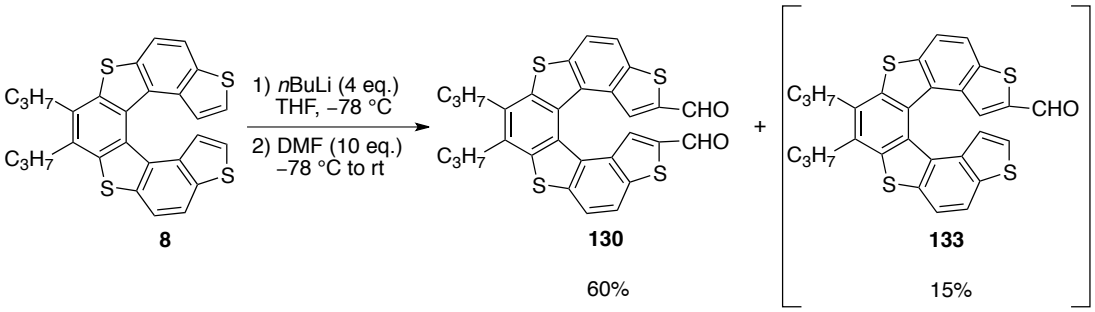


Scheme 66.

In particular, the treatment of the starting helicene **8** with 4 eq. of *n*BuLi at – 78°C, followed by the addition of 10 eq. of dry DMF afforded a final reaction mixture containing some monoaldehyde **133** (*ca.* 15%), and the required dialdehyde **3**, which was isolated in 60% yield.

Next, the introduction of the electron-donor triarylamine group was carried out through a selective Wittig reaction between one formyl group on helicene **130** and the phosphonium salt **131** that has been prepared according to the literature[70b] (Scheme 67).

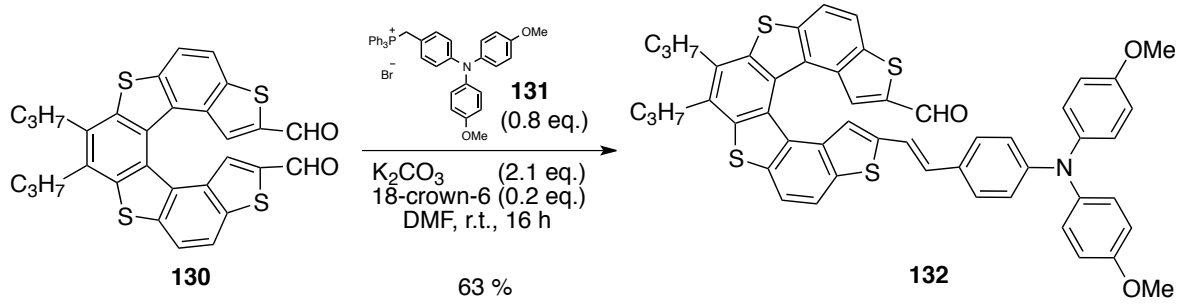


Scheme 67.

In this reaction, the slow addition of a solution of phosphonium salt **131** in DMF to a suspension of the dialdehyde **130**, $K_2CO_3$ as base and a catalytic amount of 18-crown-6 in DMF gave the required compound **132** in 63% yield, along with some unreacted starting material **130**, and about 10% of the corresponding disubstituted derivative. It was found that a slow addition of the phosphonium salt **131** was essential to achieve a good selectivity in the formation of **132**.

Finally, the Knoevenagel condensation reaction of the mono aldehyde **132** with cyanoacetic acid in the presence of 0.5 eq. of piperidine in refluxing mixture of acetonitrile and THF provided the required helical dye **129** in 60% yield (Scheme 68).

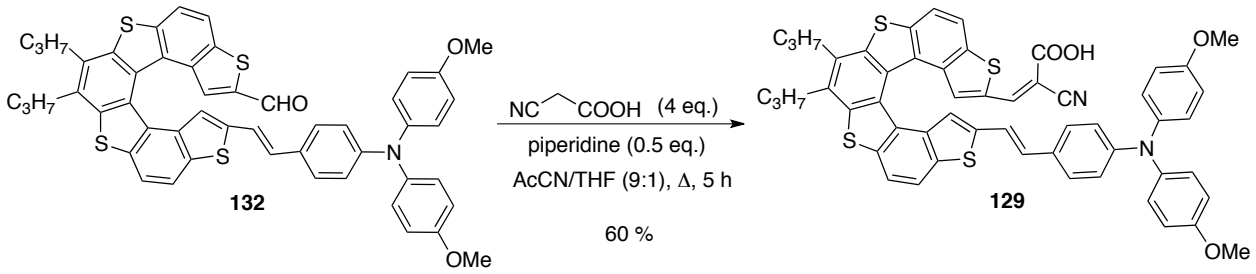


Scheme 68.

The product **129** was fully characterized by means of $^{1}H$, $^{13}C$ NMR and HR-MS (ESI) spectroscopic techniques.

### 6.3 Study of the electrochemical and optical properties of dye 129

The cyclic voltammetry analysis and the Uv-vis adsorption spectra in different solvents were also performed, in order to study its optical and electronic properties of the dye **129**. These studies are a useful tool to verify if **129** could be a good candidate for the construction of a DSSC. In fact, to achieve an efficient electron injection from the excited dye to the CB of the $TiO_2$, the energy level of the lowest unoccupied molecular orbital (LUMO) of the dye must be higher than the conduction band (CB) of the $TiO_2$ electrode (–3.94 eV). On the other hand, to achieve efficient regeneration of the oxidized state by electron transfer from $I_3^-/I^-$ redox couple in the electrolyte, the energy level

of the highest occupied molecular orbital (HOMO) of the dye must be lower than the $I_3^-/I^-$ redox potential (–4.86 eV). Moreover, for a whole comprehension of the electrochemical properties of the push-pull system **129**, we also decided to prepare the 7-TH system bearing only the electron-withdrawing group on the helicene scaffold.

### 6.3.1 *Synthesis of 7-TH-based cyanoacrylic acid **134***

The helicene **134** was obtained in a 42% overall yield, starting from unsubstituted helicene **8**, by a two-step procedure reported in Scheme 69.

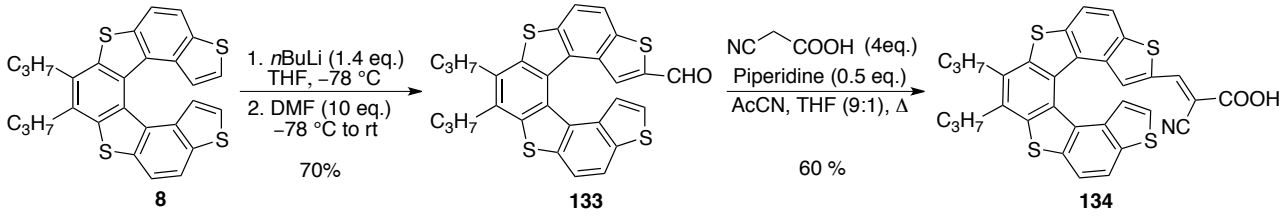


Scheme 69.

More in detail, helicene **8** was treated with 1.4 eq. of *n*BuLi at – 78 °C, and then with a large molar excess of anhydrous DMF, to give the corresponding aldehyde **133** in 70% yield, according to the previous procedure set up in our group.[3] The subsequent Knoevenagel condensation reaction of the mono aldehyde **133** with cyanoacetic acid in the presence of 0.5 eq. of piperidine in a mixture of acetonitrile and THF at reflux for 15 hours gave the target acid **134** in 60% yield (Scheme 69). Compound **134** was found to be poorly soluble in the most common organic solvents, for these reasons this compounds was characterized only by $^1$H-NMR and mass spectroscopy.

### 6.3.2 *Electrochemical characterization of dye **129***

The electrochemical properties of dye **129** were examined in collaboration with Prof. P. R. Mussini of the University of Milan. The electron transfer properties of **129** have been then studied by cyclic voltammetry; and in particular, to understand the localization of first oxidation and first reduction processes (HOMO and LUMO orbitals), the CV behavior of **129** was compared with that of its building blocks, including the 4-methoxy-*N*-(4-methoxyphenyl)-*N*-phenylaniline **135**, the 7-TH cyanoacrylic acid **134**, and the unsubstituted tetrathiahelicene **8** (Figure 56).

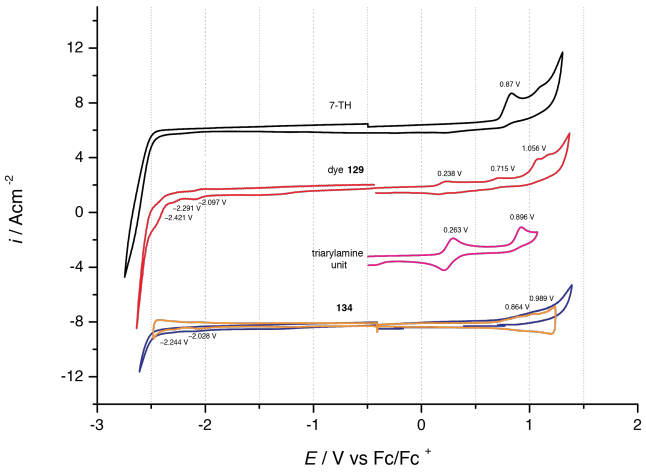


Figure 56. The measurement were run in $CH_2Cl_2$+ 0.1 M $TBAPF_6$ at 0.2 $Vs^{-1}$ scan rate, with ohmic drop compensation.

Based on the CV patterns reported in Figure 56, we can do the following considerations:

- from the comparison between the CV features of **129** and those of the *bis*(4-methoxy)phenylamine, the first two oxidation peaks of **129** (0.238 V and 0.715 V) can be attributed to the triarylamine donor group, indicating that the first and the second oxidation process of **129** could correspond to the oxidation of the triarylamine unit. Thus, the HOMO of **129** should be localized on this molecular terminal;
- the first reduction peak of **129** can be attributed to the cyanoacrylic acid group linked to the 7-TH spacer. Although the comparison between **129** and **134** was difficult due to the low solubility of **134** in the working medium ($CH_2Cl_2$), both reduction and oxidation processes of **134** are perceivable after semi-derivative convolution of the CV curve (yellow line), from which we could confirm that the reduction process and the LUMO in **129** should be localized between the cyanoacrylic acid group and the 7-TH spacer;
- from a comparison between the dye **129**, the compound **134** and the unsubstituted helicene **8**, the oxidation peak at 1.056V and the reduction peak at – 2.42 V of **129** can attribute the to helicene skeleton. In particular, the presence of the cyanoacetic electron-poor group shift the oxidation potentials of helicene scaffold to higher potentials both in **129** (1.056 V) and **134** (0.989 V) than that of unsubstituted 7-TH (0.87 V). As regards the reduction peak of 7-TH scaffold, only in the CV of **129** it was possible to observed it (–2.42V). In fact, thanks to the higher conjugation efficiency of the 7-TH system in **129**, the reduction process is anticipated respect to both **8** and **134**. In fact, in these latter compounds the reduction of the helicene skeleton undergoes after the reduction of the solvent ($CH_2Cl_2$).

6.3.3 *Optical characterization of dye **129***

The Uv-Vis absorption spectra of dye **129** were registered in different organic solvents in the presence of trifluoroacetic acid as solubilizing agent for **129** (Figure 57).

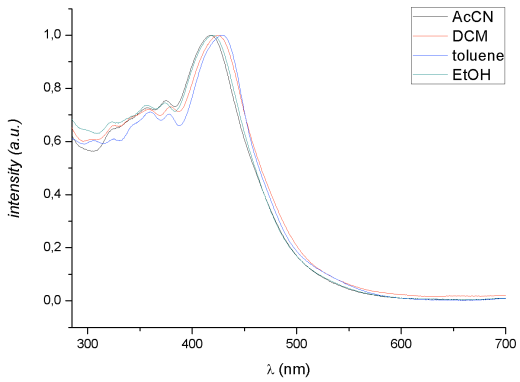


Figure 57.

The maximum absorption of **129** shifts to higher wavelengths going from polar to non-polar solvents (*e.g.* from acetonitrile to toluene), indicating that the excited state has non-polar character, and it is more stabilized in non-polar solvents respect to the polar ones. The non-polar solvents can then promote the electronic transition, which can occur at lower energy (higher

wavelengths). Moreover, from these UV-vis spectra we can also observe that **129** does not show a classical charge transfer transition, typically found in systems bearing both a donor and acceptor unit. In fact, a broad peak located at least at 500 nm is usually found, corresponding to the charge transfer between donor and acceptor units after the light absorption.
The optical energy gap considering the highest absorption wavelength in DCM as solvent and the optical energy gap obtained from the electrochemical measurement along with the HOMO and LUMO level values for dye **129** are listed in Table 16.

Table 16.

| Optical Data[a] | | Electrochemical Data | | |
|---|---|---|---|---|
| $\lambda_{max}$ | Energy Gap | HOMO | LUMO | Energy Gap |
| 426 nm | 2.92 eV | –5.04 eV | –2.70 eV | 2.34 eV |

a. Values in DCM as solvent.

As reported in Table 16 and more clearly shown in Figure 58, the dye **129** satisfies the two most indispensable requirements in the molecular design of organic dyes for DSSCs: the LUMO level of **129** (–2.70 eV) higher than than that of the conduction band of $TiO_2$ (–3.94 eV); the HOMO level of **129** (–5.04 eV) lower than that of the working potential of the redox couple (–4.86 eV), electrolytic mediator.

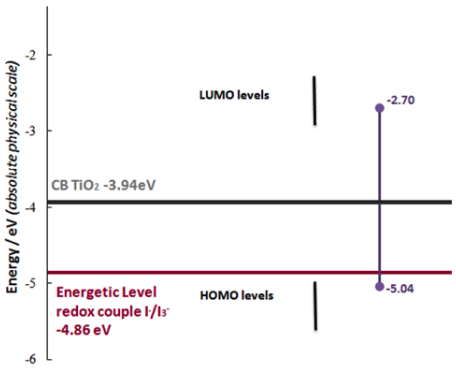


Figure 58.

6.3.4 *Preliminary studies on a DSSC based on dye **129***

The photovoltaic performances of a liquid electrolyte DSSC based on **129** were investigated in collaboration with Prof. Alessandro Abbotto of the University of Milano-Bicocca. The most important parameters obtained in this study have been reported in Table 17, in which the cell efficiency was found to be 2.4%.

Table 17.

| Dye | $\eta$ (%)[a] | *ff* (%)[b] | $V_{oc}$ (mV)[c] | $J_{sc}$ (mA•cm$^{-2}$)[d] |
|---|---|---|---|---|
| **129** | **2.4** | 76 | 669 | 4.7 |

a. Solar energy-to-electricity conversion yield ($\eta$); b. fill factor (*ff*); c. open-circuit voltage ($V_{oc}$); d. short-circuit photocurrent density ($J_{sc}$).

### 6.4 Conclusions

In summary, a new 7-TH based push-pull system **129** has been synthesized and fully characterized by UV-vis absorption spectroscopy and cyclic voltammetry. Its optical and electrochemical properties have then demonstrated that dye **129** displays the requisites, in terms of HOMO and LUMO level values, suitable for application in DSSCs. Thus, a preliminary study on the photovoltaic performances of a DSSC based on **129** has been performed, obtaining a cell efficiency of 2.4%.

# Chapter 7

## Experimental section

**General Methods.**

All reactions were performed under a positive argon atmosphere using standard Schlenk and vacuum-line techniques. All glassware was flame-dried and cooled under vacuum before use. $Ph_2POCl$, $(C_6H_{11})_2PCl$ and $[3,5\text{-}(Me)_2C_6H_3]_2PCl$, $Cy_2PCl$, $n Bu_2PCl$, $t Bu_2PCl$, $Et_2PCl$, Rhodamine B isothiocyanate mixed isomers (RBITC), ketone **106**, dry solvents (MeOH, THF, $CH_2Cl_2$, toluene, and DMF) were purchased from Aldrich. DCE was dried on $CaCl_2$. Solutions of *n*BuLi (1.6 M in hexane) were titrated prior to use. Thin layer chromatography (TLC) was performed on Merck precoated plates (silica gel 60 F254). The products were purified by flash chromatography on silica gel (Merck, Silica gel 60N, 230-400 mesh) or by a CombiFlash Companion TS Chromatography system. Melting points were determined by a Büchi 510 apparatus. $^1H$, $^{13}C\{^1H\}$, $^{31}P\{^1H\}$, COSY, HSQC and HMBC NMR spectra were recorded using a Bruker AMX 300, AV 300, AV 500, Fourier 300. All $^1H$ and $^{13}C\{^1H\}$ NMR spectra are reported in parts per million (ppm), and referenced to the solvent peak. All $^{31}P\{^1H\}$ NMR spectra are reported relative to the external standard $H_3PO_4$. Infrared spectra were recorded with a Perkin–Elmer FT-IR 1725X spectrophotometer. High Resolution mass spectra (EI) were recorded on a Vg Analytical 7070 EQ spectrometer, HRMS (ESI) were recorded with the mass spectrometer Bruker Daltonics ICR-FTMS APEX II or with LCT Waters equipment, MALDI-TOF analysis were executed on a Bruker Omniflex spectrometer. UV spectra were recorded with a Perkin–Elmer Lambda E2 210 spectrophotometer. Optical rotations have been determined on a JASCO P-1010 polarimeter. Data are reported as follows: $[\alpha]_D^{temp}$ (c in g/100 mL, solvent). HPLC was performed at a column temperature of 20°C on a Waters 2695 Separations Module equipped with a diode array UV detector.

An Agilent 1100 series HPLC, equipped with DAD analyzer and the chiral semipreparative column Chiralpack IA (250 × 10 mm), was used to resolve phosphine-borane complex (±)-**54b** and phosphine oxides (±)-**68,** (±)-**69,** (±)-**75**.

**X-ray analysis.**

The intensity data of compounds (±)-**53c**, (±)-**54a**, (+)-**54b**, (–)-**54b**, **109** were collected at room temperature on a Bruker AXS Smart 1000 single crystal diffractometer, equipped with area detector and using a graphite monochromated Mo Kα radiation (λ = 0.71073 Å); the intensity data of compound **105a** was recorded at room temperature on an Enraf–Nonius kappaCCD diffractometer using Mo Kα radiation (λ = 0.71070Å) and equipped with a graphite monochromator.

**Computational Methods.**

For the theoretical investigation of the optical properties of **54b**, time-dependent density functional theory (TD-DFT) and approximate coupled-cluster theory of second-order (CC2) in combination with the basis set cc-pVDZ were employed. In addition, for CC2, the "resolution of the identity" (RI) approximation was applied with the corresponding auxiliary basis set aux-cc-pVDZ. For the underlying ground-state DFT and excited-state TD-DFT calculations, the exchange-correlation (xc)-functional ωB97XD was used. For the RI-CC2 calculations Turbomole 6.3.1 was employed, while for DFT and TD-DFT calculations the Gaussian 09 Rev. A.02 program package was used.

**Electrochemical studies.**

Compounds **26**, **27**, **53**, **54**, **55**, **56**, **28**, **29**, **57**, **59**, **58c**, **60c**, **66**, **68**, **67**, **69**, **129** and **134** were characterized by cyclic voltammetry at potential scan rates typically ranging from 0.05 to 2 $Vs^{-1}$, in a 4 $cm^3$ minicell with 0.5–0.75 mm solutions in $CH_2Cl_2$ with 0.1 M $TBAPF_6$ as the supporting electrolyte, deaerated by $N_2$ purging. The working electrode was a glassy carbon GC disk embedded in Teflon (Amel, 0.071 $cm_2$). The operating reference electrode was aqueous saturated calomel (SCE), but the experimental peak potentials have been normalized *vs* the $Fc^+|Fc$ redox couple having a redox potential of 0.495 V (in $CH_2Cl_2$) vs. the operating SCE reference electrode.
The counter electrode was a platinum disk embedded in glass. The ohmic potential drop was compensated for by the positive feedback technique.

**Liquid Electrolyte Solar Cell Assembly.**

The $TiO_2$ sensitized photoanode and Pt counter electrode were assembled into a sealed sandwich-type cell by a hot-melt ionomer film (Surlyn, 25 µm thickness, Dyesol). Using $TiO_2$ T/SP + R/SP (10 µm + 5 µm) as paste; $2 \cdot 10^{-4}$ M in EtOH (15 mL EtOH, 1 mL di THF) of **129** with 3a,7a-dihydroxy-5b-cholic acid (CDCA) (ratio 1:1) as sensitizing baths and Z960 (1.0 M dimethyl imidazolium iodide, 0.03 M $I_2$, 0.05 M LiI, 0.1 M guanidinium thiocyanate and 0.5 M 4-*t*-butylpyridine in acetonitrile/valeronitrile 85/15) as electrolyte.

Tetrathiahelicene (±)-**8**,[3] alkene (*Z*)-**119**,[3] helicene **124**,[85] monoaldehyde **133**,[3] phosphonium salt **131**,[70b] 7-TH phosphine-borane complexes **26** and **27**,[21a] phosphindole triflate ($R_P$)-**95**,[42] bis-boronate **93**,[3b] were prepared as described in the literature.

**General procedure for the synthesis of phosphane-borane complexes 53a–d and 54a–d**. A solution of *n*BuLi (0.25 or 0.5 mL, 0.40 or 0.80 mmol) was added dropwise to a stirring solution of **8** (100 mg, 0.20 mmol) in dry THF (10 mL) at –78 °C under an argon atmosphere. The solution was stirred for 20 min at –78 °C, and heated to room temperature for 20 min, and then cooled back to 0 °C. To the cooled reaction solution was added the appropriate chlorodialkylphosphine (0.40 or 0.80 mmol) and stirred for 20 min at 0 °C, and for 5 h at r.t. The suspension was cooled back to 0 °C, and treated with a solution of $BH_3$•THF complex (2.0 mL, 2.0 mmol). The yellow suspension was stirred at room temperature for 24–48 h. Upon completion, the reaction mixture was diluted with $CH_2Cl_2$ (10 mL) and slowly added to a saturated aqueous $NH_4Cl$ solution (50 mL). The aqueous phase was extracted with $CH_2Cl_2$ (×3). The organic layer was washed with brine (×3), dried over anhydrous $Na_2SO_4$, filtered and concentrated under reduced pressure. Purification of the residue was accomplished by column chromatography using silica gel with a mixture of hexane and DCM as the eluent.

**Mono adduct 53a**

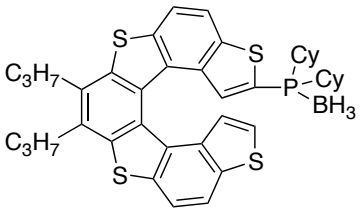


Yield 62 %. M.p. 245 °C; $^1$H NMR (300 MHz, $CDCl_3$): $\delta$= 7.98 (m, 4H), 7.43 (d, $^3J$(H,P)=7.7 Hz, 1H), 6.90 (d, $^3J$(H,H)=5.5 Hz, 1H), 6.79 (d, $^3J$(H,H)=5.5 Hz, 1H), 3.10 (m, 4H), 1.80 (m, 15H), 1.40 (m, 17H) ppm; $^{13}$C NMR (75 MHz, $CDCl_3$): $\delta$= 140.8 (Cq), 140.2 (Cq), 140.0 (Cq), 137.7 (Cq), 136.8 (d, $^2J$(C,P)= 10.6 Hz, CH), 136.7 (Cq), 136.5 (Cq), 135.9 (d, $^3J$(C,P)=11.6 Hz, Cq), 135.6 (Cq), 132.9 (Cq), 132.0 (d, $^1J$(C,P)=56.8 Hz, Cq), 128.7 (Cq), 127.9 (Cq), 126.6 (Cq), 126.0 (Cq), 125.3 (CH), 124.3 (CH), 121.6 (CH), 120.6 (CH), 120.3 (CH), 119.3 (CH), 34.6 ($CH_2$), 34.5 ($CH_2$), 33.3 (d, $J$(C,P)= 29.5 Hz, CH), 32.8 (d, $J$(C,P)= 29.5 Hz, CH), 26.9 ($CH_2$), 26.8 ($CH_2$), 26.7 ($CH_2$), 26.6 ($CH_2$), 26.5 ($CH_2$), 26.4 ($CH_2$), 26.3 26.2 ($CH_2$), 26.1 ($CH_2$), 25.9 ($CH_2$), 23.4 ($2CH_2$), 14.9 ($CH_3$), 14.8 ($CH_3$) ppm; $^{31}$P NMR (121 MHz, $CDCl_3$): $\delta$= 25.6 (br s) ppm;
UV/Vis ($CH_2Cl_2$): λ($\varepsilon$)= 227, 268, 292 (23600), 318 (18300), 326 (16400), 379 (17800), 397 nm (19400 $mol^{-1}dm^3cm^{-1}$); IR (neat): $\tilde{\nu}$=2370 (B[bond]H), 2332 $cm^{-1}$ (B[bond]H); HRMS (ESI) *m*/*z*: $[M+Na]^+$ calcd. for $C_{40}H_{46}S_4PBNa$ 719.2205; found 719.2210.

**Mono adduct 53b**

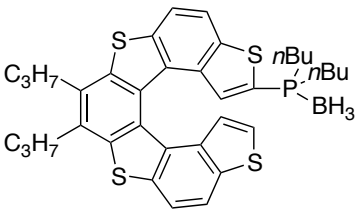


Yield 57 %. M.p. 199 °C; $^1$H NMR (300 MHz, $CDCl_3$): $\delta$ = 8.00 (m, 4H), 7.23 (d, $^3J$(H,P)=7.3 Hz, 1H), 6.91 (d, $^3J$(H,H)=5.6 Hz, H), 6.75 (d, $^3J$(H,H)=5.6 Hz, 1H), 3.11 (m, 4H), 1.87 (m, 4H), 1.47 (m, 4H), 1.25 (m, 6H), 1.17 (m, 8H), 0.85 (m, 6H) ppm. $^{13}$C NMR (75 MHz, $CDCl_3$): $\delta$ = 140.7 (Cq), 140.2 (Cq), 137.2 (Cq), 136.6 (Cq), 136.1 (d, $^3J$(C,P)=10.5 Hz, Cq), 135.9 (Cq), 135.8 (Cq), 133.7 (d, $^2J$(C,P)=7.6 Hz, CH), 132.9 (Cq), 132.4 (Cq), 132.0 (Cq), 131.5 (Cq), 129.5 (d, $J$(C,P)= 48 Hz, Cq), 128.4 (Cq), 128.0 (CH), 125.4 (CH), 124.3 (CH), 121.4 (CH), 119.2 (CH), 34.5 ($2CH_2$), 26.0 (d, $J$(C,P)=36.0 Hz, $CH_2$), 25.8 (d, $J$(C,P)= 36 Hz, $CH_2$), 25.0 ($2CH_2$), 24.1 (d, $^2J$(C,P)=14 Hz, $CH_2$), 24.0 (d, $^2J$(C,P)=13.7 Hz, $CH_2$), 23.4 ($2CH_2$), 14.7 ($2CH_3$) 13.6 ($CH_3$), 13.5 ($CH_3$) ppm; $^{31}$P NMR (121 MHz, $CDCl_3$)$\delta$ = 13.4 (br, s) ppm;

UV/Vis ($CH_2Cl_2$): λ ($\varepsilon$)= 228, 243, 292 (28900), 318 (23500), 326 (20800), 378 (23000), 398 nm (25800 $mol^{-1}dm^3cm^{-1}$); IR (neat): $\tilde{\nu}$= 2386 (B[bond]H), 2340 $cm^{-1}$ (B[bond]H); HRMS (ESI) *m/z* : $[M+Na]^+$ calcd. for $C_{36}H_{42}S_4PBNa$ 667.1892; found 667.1892.

**Mono adduct 53c**

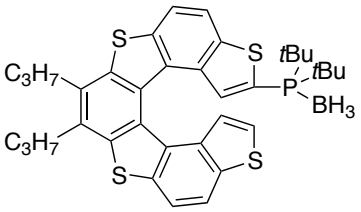

Yield 49 %. M.p. 172 °C; $^1$H NMR (300 MHz, $CDCl_3$): $\delta$ = 8.00 (m, 4H), 7.66 (d, $^3J$(H,P)=7.2 Hz, 1H), 6.93 (d, $^3J$(H,H)=5.6 Hz, 1H), 6.86 (d, $^3J$(H,H)=5.6 Hz, 1H), 3.11 (m, 4H), 1.87 (m, 4H), 1.17 (m, 24H) ppm; $^{13}$C NMR (75 MHz, $CDCl_3$): $\delta$ = 140.8 (Cq), 140.1 (Cq), 139.8 (Cq), 137.9 (Cq), 137.2 (d, $^2J$(C,P)=7.5 Hz, CH), 136.6 (Cq), 136.2 (Cq), 135.6 (d, $^3J$(C,P)=10.5 Hz, Cq), 135.5 (Cq), 132.7 (Cq), 131.8 (Cq), 131.7 (d, $^1J$(C,P)=48.7 Hz, Cq), 128.5 (Cq), 127.7 (Cq), 126.5 (Cq), 126.2 (Cq), 124.9 (CH), 124.6 (CH), 121.3 (CH), 120.5 (CH), 119.9 (CH), 119.2 (CH), 34.4 ($2CH_2$), 33.3 (d, $^1J$(C,P)= 27.0 Hz, $CH_2$), 32.9 (d, $^1J$(C,P)= 27.0 Hz, $CH_2$), 28.5 ($3CH_3$), 28.3 ($3CH_3$), 23.3 ($2CH_2$), 14.7 ($2CH_3$) ppm; $^{31}$P NMR (121 MHz, $CDCl_3$) $\delta$ = 45.76 (br s) ppm; UV/Vis ($CH_2Cl_2$): λ ($\varepsilon$)= 228, 292 (20900), 318 (16000), 327 (15100), 378 (16200), 397 nm (17800 $mol^{-1}dm^3cm^{-1}$); IR (neat): $\tilde{\nu}$= 2384 (B[bond]H), 2354 $cm^{-1}$ (B[bond]H); HRMS (ESI) *m/z*: $[M+Na]^+$ calcd. for $C_{36}H_{42}S_4PBNa$ 667.1892; found 667.1898.

**Mono adduct 53d**

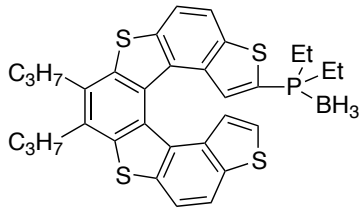

Yield 53 %. M.p. 170 °C; $^1$H NMR (300 MHz, $CDCl_3$): $\delta$ = 8.03 (m, 4H), 7.26 (d, $^3J$(H,P)= 7.3 Hz, 1H), 6.91 (d, $^3J$(H,H)= 5.4 Hz, 1H), 7.49 (d, $^3J$(H,H)= 5.4 Hz, 1H), 3.14 (m, 4H), 1.90 (m, 4H), 1.67 (m, 4H), 1.18 (m, 6H), 0.91 ppm (m, 6H); $^{13}$C NMR (75 MHz, $CDCl_3$): $\delta$ = 140.6 (Cq), 140.0 (Cq), 137.1 (Cq), 136.5 (Cq), 136.0 (Cq), 135.9 (Cq), 135.5 (Cq), 133.9 (d, $^2J$(C,P)= 7.9 Hz, CH), 132.7 (Cq), 132.2 (Cq), 131.8 (Cq), 131.3 (Cq), 128.6 (d, $J$(C,P)= 48.6 Hz, Cq), 128.2 (Cq), 127.8 (Cq), 125.3 (CH), 124.2 (CH), 121.1 (CH), 120.4 (CH), 120.3 (CH), 119.1 (CH), 34.4 ($CH_2$), 23.6 ($CH_2$), 19.6 (d, $J$(C,P)= 31.6 Hz, $CH_2$), 19.1 (d, $J$(C,P)= 32.0 Hz, $CH_2$), 14.7 ($CH_3$), 7.0 ppm ($CH_3$); $^{31}$P NMR (121 MHz, $CDCl_3$): $\delta$ = 18.55 ppm (br,s); UV/Vis ($CH_2Cl_2$): λ($\varepsilon$)= 228, 235, 291 (30300), 318 (24400), 327 (21800), 378 (23400), 397 nm (25600 $mol^{-1}dm^3cm^{-1}$); IR (neat): $\tilde{\nu}$= 2364 (B[bond]H), 2331 $cm^{-1}$ (B[bond]H); HRMS (ESI): *m/z* calcd. for $C_{32}H_{34}S_4PB+Na^+$ 611.12662 [*M*+Na]$^+$; found 611.12645.

**Di adduct 54a**

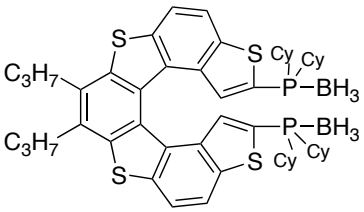

Yield 70 %. M.p. 263 °C; $^1$H NMR (300 MHz, $CDCl_3$): $\delta$= 8.05 (d, $^3J$(H,H)= 8.7 Hz, 2H), 8.00 (d, $^3J$(H,H)= 8.7 Hz, 2H), 7.29 (d, $^3J$(H,P)= 7.1 Hz, 2H), 3.12 (m, 4H), 1.88 (m, 4H), 1.65 (m, 20H), 1.27 (m, 6H), 1.18 (t, $^3J$(H,H)= 7.3 Hz, 6H), 1.07 (m, 16H), 0.89 (m, 2H) ppm; $^{31}$P NMR (121 MHz, $CDCl_3$): $\delta$= 25.7 (br s) ppm; $^{13}$C NMR (75 MHz, $CDCl_3$): $\delta$= 141.6 (Cq), 140.1 (Cq), 136.7 (Cq), 135.6 (Cq), 134.7 (d, $^2J$(C,P)= 7.5 Hz, CH), 132.7 (Cq), 131.6 (Cq), 127.9 (Cq),126.55 (d, $J$(C,P)= 42 Hz, Cq), 121.0 (CH) 120.5 (CH), 34.4 ($CH_2$), 32.6 (d, $J$(C,P)= 34.2 Hz, CH), 32.2 (d, $J$(C,P)= 34.3 Hz, CH), 26.8 ($CH_2$), 26.7 ($CH_2$), 26.6 ($CH_2$), 26.4 ($CH_2$), 26.2 ($CH_2$), 26.1 ($CH_2$), 26.0 ($CH_2$), 25.7 ($CH_2$), 23.3 ($CH_2$), 14.7 ($CH_3$) ppm; UV/Vis ($CH_2Cl_2$): λ ($\varepsilon$)= 250,

296 (31700), 322 (23800), 333 (32600), 383 (23800), 402 nm (26600 $mol^{-1}dm^3cm^{-1}$); IR (neat): $\tilde{\nu}$= 2363 (B[bond]H), 2342 $cm^{-1}$ (B[bond]H); HRMS (ESI): *m/z* calcd. for $C_{52}H_{70}S_4P_2B_2$+$Na^+$ 929.39139 $[M+Na]^+$; found 929.39234.

**Di adduct 54b**

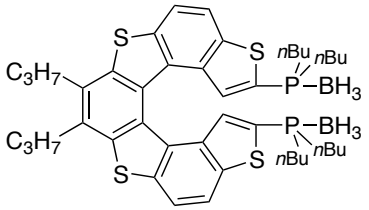

Yield 61 %. M.p. 215 °C; $^1$H NMR (300 MHz, $CDCl_3$): $\delta$ = 8.05 (m, 4H), 7.18 (d, $^3J$(H,P)=7.3 Hz, 2H), 3.13 (m, 4H), 1.88 (m, 4H), 1.44 (m, 2H), 1.32 (m, 6H), 1.17 (m, 22H), 0.85 (m, 12H) ppm; $^{13}$C NMR (75 MHz, $CDCl_3$): $\delta$ = 141.1 (Cq, Ar), 140.3 (Cq, Ar), 136.9 (Cq, Ar), 135.5 (d, $^3J$(C,P)=10.4 Hz; Cq), 133.5 (d, $^2J$(C,P)=7.9 Hz; CH), 132.9 (Cq), 131.6 (Cq), 130.1 (d, $^1J$(C,P)=48.8 Hz; Cq), 127.9 (Cq), 120.9 (CH), 120.8 (CH), 34.3 ($CH_2$), 26.9 (d, $^1J$(C,P)=30.8 Hz; $CH_2$), 25.2 (d, $^1J$(C,P)=30.8 Hz; $CH_2$), 24.9 (d, $^3J$(C,P)=6.8 Hz; $2CH_2$), 24.2 (d, $^2J$(C,P)=13.7 Hz; $CH_2$), 24.1 (d, $^2J$(C,P)=13.7 Hz; $CH_2$), 23.4 ($CH_2$), 14.8 ($CH_3$) 13.7 ($CH_3$), 13.6 ($CH_3$) ppm; $^{31}$P NMR (121 MHz, $CDCl_3$) $\delta$ = 13.35 (br s) ppm; UV/Vis ($CH_2Cl_2$): λ ($\varepsilon$)= 227, 249, 292 (29600), 321 (23100), 332 (28200), 384 (22900), 404 nm (25700 $mol^{-1}dm^3cm^{-1}$); IR (neat): $\tilde{\nu}$= 2389 (B[bond]H), 2343 $cm^{-1}$ (B[bond]H); HRMS (ESI) *m/z* : $[M+Na]^+$ calcd. for $C_{44}H_{62}S_4P_2B_2Na$ 825.3287; found 825.3310.

**Di adduct 54c**

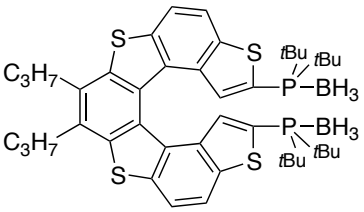

Yield 78 %. M.p. 296 °C; $^1$H NMR (300 MHz, $CDCl_3$): $\delta$ = 8.05 (d, $^3J$(H,H)=8.7 Hz, 2H), 7.99 (d, $^3J$(H,H)= 8.7 Hz, 2H), 7.65 (d, $^3J$(H,P)=6.8 Hz, 2H), 3.11 (m, 4H), 1.87 (m, 4H), 1.17 (m, 6H), 1.02 (m, 36H) ppm;$^{13}$C NMR (121 MHz, $CDCl_3$): $\delta$ = 142.1 (Cq), 140.4 (Cq), 137.0 (Cq), 136.0 (d, $^2J$(C,P)= 6.4 Hz; CH), 135.5 (d, $^2J$(C,P)= 10.5 Hz; Cq), 132.5 (Cq), 132.0 (Cq), 128.0 (Cq), 127.0 (d, $^1J$(C,P)= 38.3 Hz; Cq), 121.0 (CH), 120.7 (CH), 34.5 ($CH_2$), 33.1 (d, $^1J$(C,P)= 26.3 Hz; Cq), 32.8 (d, $^1J$(C,P)= 26.3 Hz; Cq), 28.6 ($3CH_3$), 28.4 ($3CH_3$), 23.5 ($CH_2$), 14.9 ($CH_3$) ppm; $^{31}$P NMR (121 MHz, $CDCl_3$) $\delta$ = 45.95 (br s) ppm; UV/Vis ($CH_2Cl_2$): λ($\varepsilon$)= 259, 295 (34700), 321 (26000), 333 (36900), 384 (26600), 403 nm (29400 $mol^{-1}dm^3cm^{-1}$); IR (neat): $\tilde{\nu}$= 2391 (B[bond]H), 2352 $cm^{-1}$ (B[bond]H); HRMS (ESI) *m/z*: calcd. for $[M+Na]^+$ $C_{44}H_{62}S_4P_2B_2Na$ 825.3288; found 825.3296.

**Di adduct 54d**

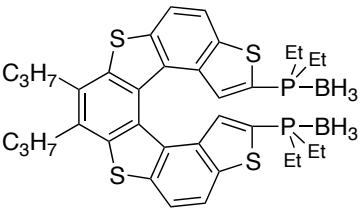

Yield 76 %; M.p. 168 °C; $^1$H NMR (300 MHz, $CDCl_3$): $\delta$ = 8.06 (d, $^3J$(H,H)= 8.7 Hz, 2H), 8.02 (d, $^3J$(H,H)= 8.7 Hz, 2H), 7.22 (d, $^3J$(H,P)= 7.4 Hz, 2H), 3.11 (m, 4H), 1.87 (m, 4H), 1.50 (m, 4H), 1.15 (t, $^3J$(H,H)= 7.3 Hz, 6H), 0.87 (m, 6H) ppm; $^{13}$C NMR (75 MHz, $CDCl_3$): $\delta$ =140.7 (Cq), 139.7 (Cq), 136.3 (Cq), 135.0 (Cq), 134.9 (Cq), 131.4 (d, $^2J$(C,P)= 7.5 Hz, CH), 132.3 (Cq), 130.0 (Cq), 128.5 (d, $^2J$(C,P)= 47 Hz, Cq), 127.2 (Cq), 120.3 (CH), 120.2 (CH), 33.8 ($CH_2$), 22.8 ($CH_2$), 25.5 (d, *J*(C,P)= 37 Hz, $CH_2$), 24. (d, *J*(C,P)= 37 Hz, $CH_2$), 14.7 ($CH_3$) 13.5 ($CH_3$), 13.4 ($CH_3$) ppm; $^{31}$P NMR (121 MHz, $CDCl_3$): $\delta$ = 18.51 (br s) ppm; UV/Vis ($CH_2Cl_2$): λ ($\varepsilon$)= 249, 292 (27700), 320 (21000), 332 (27400), 384 (21300), 403 nm (24300 $mol^{-1}dm^3cm^{-1}$); IR (neat):

$\tilde{\nu}$= 2365 (B[bond]H), 2335 $cm^{-1}$ (B[bond]H); HRMS (ESI): *m/z* calcd. for $C_{36}H_{46}S_4P_2B_2$+$Na^+$ 713.20359 [*M*+Na]$^+$; found 713.20469.

**Di adduct 77**

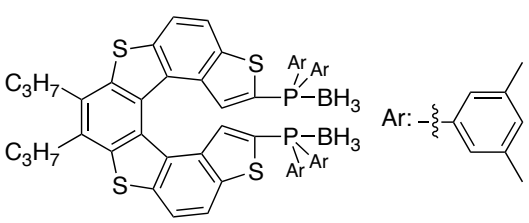


Yield: 50 % Mp 250 °C (dec.). $^1$H NMR (300 MHz, $CDCl_3$): $\delta$ = 7.90 (d, *J*(H,H)= 8.6 Hz, 2 H), 7.79 (d, *J*(H,H) = 8.6 Hz, 2 H), 7.18 (d, *J*(H,H) = 7.8 Hz, 2 H), 6.95 (m, 12 H), 3.10 (m, 4 H), 2.23 (s, 12 H), 2.15 (s, 12 H), 1.86 (m, 4 H), 1.16 (t, *J*(H,H) = 7.3 Hz, 6 H). $^{13}$C NMR (75 MHz, $CDCl_3$): $\delta$ = 142.3 (d, *J*(C,P)= 3.3 Hz, Cq), 140.0 (Cq), 138.3 (d, *J*(C,P) = 11.1 Hz, 2 Cq), 137.9 (d, *J*(C,P) = 11.1 Hz, 2 Cq), 136.2 (Cq), 135.4 (d, *J*(C,P) = 11.4 Hz, Cq), 134.6 (d, *J*(C,P) = 9.7 Hz, CH), 133.3 (d, *J*(C,P) = 2.2 Hz, CH), 133.2 (d, *J*(C,P) = 2.2 Hz, CH), 132.5 (Cq), 131.4 (Cq), 130.5 (d, *J*(C,P) = 10.2 Hz, 2 CH), 130.15 (d, *J*(C,P) = 56.3 Hz, Cq), 130.13 (d, *J*(C,P) = 10.2 Hz, 2 CH), 129.5 (d, *J*(C,P) = 59.5 Hz, Cq), 128.6 (d, *J*(C,P) = 58.1 Hz, Cq), 128.1 (Cq), 121.3 (CH), 120.0 (CH), 34.5 ($CH_2$), 25.3 ($CH_2$), 21.5 (2 $CH_3$), 14.9 ($CH_3$) ppm. $^{31}$P NMR (121 MHz, $CDCl_3$): $\delta$ = 14.7 (br s) ppm. HRMS (ESI): calcd. for $C_{60}H_{62}P_2B_2S_4Na$ 1017.3318, found 1017.3324.

**General procedure for the synthesis of phosphine selenides**

A solution of phosphine-borane complex (0.05 mmol) in $Et_2NH$ was stirred and heated to reflux under an argon atmosphere, and the progress of the reaction was monitored by $^{31}$P NMR analysis. After 4-8 h, the yellow solution was cooled to room temperature, and the solvents together with diethylamine borane adduct as byproduct were removed under reduced pressure at 50 °C for 2 h. The resulting yellow solid was dissolved in degassed toluene (10 mL), and to this solution was added selenium powder (0.50 mmol, 10 equiv.). The mixture was stirred at reflux for 2 h, then the solvent was removed under reduce pressure, and the residue was purified by column chromatography using silica gel with a mixture of hexane and DCM as the eluent.

**Mono selenide 57**

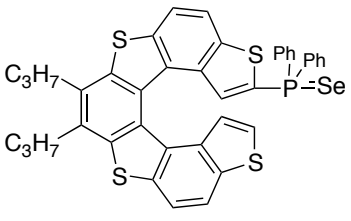


Yield: >90%; $R_f$=0.48 (Hexane/$CH_2Cl_2$ 1:1) $^1$H NMR (300 MHz, $CDCl_3$): $\delta$=7.96 (m, 4H), 7.35 (m, 10H), 7.13 (d, $^3J$(H,P)=9.4 Hz, 1H), 7.05 (d, $^3J$(H,H)=5,6 Hz, 1H), 6.82 (d, $^3J$(H,H)=5.6 Hz, 1H), 3.08 (m, 4H), 1.83 (m, 4H), 1.15 (m, 6H) ppm; $^{13}$C NMR (75 MHz, $CDCl_3$): $\delta$= 142.2 (d, $^4J$(C,P)=5.9 Hz; Cq), 140.2 (Cq), 137.4 (Cq), 137.0 (Cq), 136.7 (Cq), 136.4 (Cq), 135.5 (d, $^3J$(C,P)=13.5 Hz; Cq), 135.3 (Cq), 135.1 (Cq), 135.0 (d, $^2J$(C,P)=9.2 Hz; CH), 134.3 (Cq), 132.9 (d, $^1J$(C,P)=61.1 Hz; Cq), 132.8 (Cq), 132.3 (d, $^3J$(C,P)=10.8 Hz; 2CH),132.2 (d, $^1J$(C,P)=46.5 Hz; Cq), 132.1 (d, $^3J$(C,P)=10.8 Hz; 2CH), 131.6 (d, $^4J$(C,P)=2.2 Hz; CH), 131.5 (d, $^4J$(C,P)=2.2 Hz; CH), 131.3 (Cq), 130.9 (d, $^1J$(C,P)=46.5 Hz; Cq), 128.5 (d, $^2J$(C,P)=13.1 Hz; 2CH), 128.3 (d, $^4J$(C,P)=13.1Hz; 2CH), 127.7 (Cq), 125.4 (CH), 124.8 (CH), 121.4 (CH), 121.1 (CH), 120.7 (CH), 119.0 (CH), 34.5 ($CH_2$), 34.5 ($CH_2$), 23.4 (2$CH_2$), 14.9 ($CH_3$), 14.8 ppm ($CH_3$).$^{31}$P NMR (121 MHz, $CDCl_3$): $\delta$=25.01 (s), 25.01 ppm (d, $^1J$(P,Se)=739.0 Hz); MALDI-TOF (*m/z*): 670.5 [*M-Se*$^+$], 749.7 [*M*$^+$]; MS-ESI (*m/z*): 751.0 [*M*$^+$];

**Mono selenide 58a**

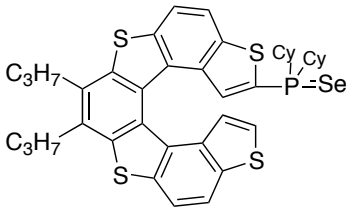

Yield: >90%; $R_f$=0.44 (Hexane/$CH_2Cl_2$ 1:1); $^1$H NMR (300 MHz, $CDCl_3$): δ=8.01 (m, 4H), 7.58 (d, $^3$J(H,P)=8.7 Hz, 1H), 6.92 (d, $^3$J(H,H)=5,6 Hz, 1H), 6.83 (d, $^3$J(H,H)=5.6 Hz, 1H), 3.12 (m, 4H), 1.71 (m, 16H), 1.13 (m, 16H) ppm; $^{13}$C NMR (75 MHz, $CDCl_3$): δ= 141.3 (Cq), 140.3 (Cq), 140.2 (Cq), 137.8 (Cq), 136.8 (d, $^2$J(C,P)=8.3 Hz; CH), 136.7 (Cq), 136.6 (Cq), 135.7 (d, $^3$J(C,P)=7.7 Hz; Cq), 132.9 (Cq), 132.2 (Cq), 132.0 (d, $^1$J(C,P)=63.9 Hz; Cq), 129.7 (Cq), 128.6 (Cq), 128.4 (Cq), 128.0 (Cq), 125.3 (CH), 124.5 (CH), 121.6 (CH), 120.8 (CH), 120.4 (CH), 119.2 (CH), 38.7 (d, $^1$J(C,P)=44.1 Hz; CH), 38.5 (d, $^1$J(C,P)=44.1 Hz; CH), 34.5 ($CH_2$), 34.4 ($CH_2$), 26.5 ($2CH_2$), 26.4 ($2CH_2$), 26.3 ($2CH_2$), 26.2 ($2CH_2$), 26.1 ($2CH_2$), 23.4 ($2CH_2$), 14.9 ($CH_3$), 14.8 ($CH_3$) ppm. $^{31}$P NMR (121 MHz, $CDCl_3$): *δ*=48.54 (s), 48.54 (d, $^1$*J*(P,Se)=717.1 Hz) ppm; MALDI-TOF (*m/z*): 683 [*M-Se*$^+$], 763.2 [*M*$^+$]; MS-ESI (*m/z*): 763.4 [*M*$^+$].

**Mono selenide 58b**

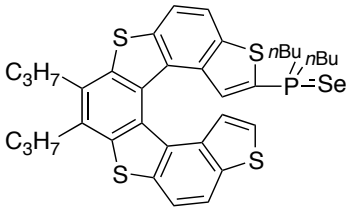

Yield: >90%; $R_f$=0.25 (Hexane/$CH_2Cl_2$ 1:1); $^1$H NMR (300 MHz, $CDCl_3$): *δ*=8.01 (m, 4H), 7.22 (m, 1H), 6.95 (m, 1H), 6.79 (m, 1H), 3.12 (m, 4H), 1.87 (m, 4H), 1.71 (m, 4H), 1,41 (m, 4H), 1.16 (m, 10H), 0.91 (m, 3H), 0.77 (m, 3H) ppm; $^{13}$C NMR (75 MHz, $CDCl_3$): *δ*= 140.9 (d, $^4$*J*(C,P)=4.6 Hz; Cq), 140.3 (Cq), 140.2 (Cq), 137.1 (Cq), 136.7 (Cq), 136.5 (Cq), 136.0 (d, $^3$*J*(C,P)=12.5 Hz; Cq), 135.8 (Cq), 132.3 (d, $^1$*J*(C,P)=68.4 Hz; Cq), 132.9 (Cq), 132.5 (Cq), 132.2 (Cq), 132.1 (d, $^2$*J*(C,P)=8.3 Hz; CH), 131.5 (Cq), 128.3 (Cq), 127.9 (Cq), 125.5 (CH), 124.5 (CH), 121.2 (CH), 120.8 (CH), 120.6 (CH), 119.2 (CH), 34.5 ($2CH_2$), 34.0 (d, $^1$*J*(C,P)=47 Hz; $CH_2$), 33.3 (d, $^1$*J*(C,P)=47 Hz; $CH_2$), 25.1 (d, $^2$*J*(C,P)=17.6 Hz; $2CH_2$), 23.8 ($CH_2$), 23.7 ($CH_2$), 23.4 ($2CH_2$), 14.8 ($2CH_3$), 13.9 ($CH_3$), 13.6 ($CH_3$) ppm. $^{31}$P NMR (121 MHz, $CDCl_3$): *δ*=28.57 (s), 28.57 (d, $^1$*J*(P,Se)=711.7 Hz) ppm; MALDI-TOF (*m/z*): 630.3 [*M-Se*$^+$], 710.6 [*M*$^+$]; MS-ESI (*m/z*): 711.4 [*M*$^+$];

**Mono selenide 58c**

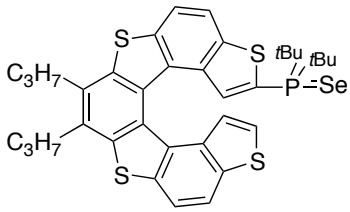

Yield: >90%; $R_f$=0.4 (Hexane/$CH_2Cl_2$ 1:1); $^1$H NMR (300 MHz, $CDCl_3$): *δ*=8.03 (m, 4H), 7.65 (d, $^3$*J*(H,P)=7.0 Hz, 1H), 6.98 (d, $^3$*J*(H,H)=5,6 Hz, 1H), 6.91 (d, $^3$*J*(H,H)=5.6 Hz, 1H), 3.11 (m, 4H), 1.86 (m, 4H), 1.17 (m, 6H), 1.06 (m, 18H) ppm; $^{13}$C NMR (75 MHz, $CDCl_3$): *δ*= 141.3 (d, $^4$*J*(C,P)=3.7 Hz; Cq),140.3 (Cq), 140.2 (Cq), 138.1 (Cq), 137.0 (d, $^3$*J*(C,P)=12.4 Hz; Cq), 136.8 (Cq), 136.5 (Cq), 135.7 (Cq), 134.3 (d, $^2$*J*(C,P)=5.6 Hz; CH), 132.9 (Cq), 132.4 (Cq), 132.2 (Cq), 131.7 (Cq), 131.5 (d, $^1$*J*(C,P)=54 Hz; Cq), 128.5 (Cq), 127.9 (Cq), 125.3 (CH), 125.1 (CH), 121.3 (CH), 120.6 (CH), 120.3 (CH), 119.3 (CH), 38.4 (d, $^1$*J*(C,P)=33.8 Hz; Cq), 38.3 (d, $^1$*J*(C,P)=33.8 Hz; Cq), 34.5 ($CH_2$), 34.4 ($CH_2$), 28.2 ($3CH_3$), 28.1 ($3CH_3$), 23.4 ($2CH_2$), 14.9 ($CH_3$), 14.8 ($CH_3$) ppm. $^{31}$P NMR (121 MHz, $CDCl_3$): *δ*=72.53 (s), 72.53 (d, $^1$*J*(P,Se)=707.7 Hz) ppm; MALDI-TOF (*m/z*): 631.0 [*M-Se*$^+$], 711.2 [*M*$^+$]; MS-ESI (*m/z*): 711.4 [*M*$^+$];

**Di selenide 59**

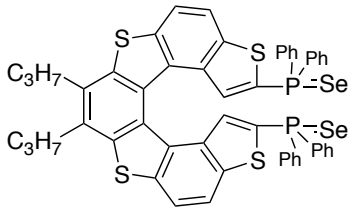

Yield: >90%; $R_f$=0.6 (Hexane/$CH_2Cl_2$ 1:1); $^1$H NMR (300 MHz, $CDCl_3$): $\delta$=7,91 (d, $^3J$(H,H)=8.6 Hz, 2H), 7.82 (d, $^3J$(H,H)=8.6 Hz, 2H), 7.37 (m, 20H), 7.16 (d, $^3J$(H,P)=9.5 Hz, 2H), 3.07 (m, 4H), 1.80 (m, 4H), 1.14 (m, 6H) ppm; $^{13}$C NMR (75 MHz, $CDCl_3$): $\delta$=142.8 (d, $^4J$(C,P)=5.1 Hz; Cq), 140.4 (Cq), 136.8 (Cq), 135.1 (d, $^3J$(C,P)=13.8 Hz; Cq), 134.8 (Cq), 134.7 (d, $^2J$(C,P)=9.3 Hz; Cq), 132.9 (d, $^1J$(C,P)=33.0 Hz; Cq), 132.8 (Cq), 132.2 (d, $^2J$(C,P)=11.0 Hz; 2CH), 132.1 (Cq), 131.8 (d, $^2J$(C,P)=11.0 Hz; 2CH), 131.7 (d, $^4J$(C,P)=4.9 Hz; 2CH), 131.1 (d, $^1J$(C,P)=59.0 Hz; Cq), 128.7 (d, $^3J$(C,P)=9.0 Hz; 2CH), 128.6 (d, $^3J$(C,P)=9.0 Hz; 2CH), 127.7 (Cq), 121.5 (CH), 120.1 (CH), 34.4 ($CH_2$), 23.4 ($CH_2$), 14.8 ($CH_3$) ppm; $^{31}$P NMR (121 MHz, $CDCl_3$): $\delta$=25.22 (s), 25.22 (d, $^1J$(P,Se)=741.3 Hz) ppm; MALDI-TOF (*m/z*): 855.5 [*M-2Se*$^+$], 935.8 [*M-Se*$^+$], 1015 [*M*$^+$].

**Di selenide 60a**

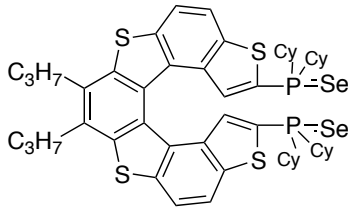

Yield: >90%; $R_f$=0.2 (Hexane/$CH_2Cl_2$ 1:1); $^1$H NMR (300 MHz, $CDCl_3$): $\delta$=8.04 (d, $^3J$(H,H)=8.6 Hz, 2H), 8.00 (d, $^3J$(H,H)=8.6 Hz, 2H), 7.36 (d, $^3J$(H,P)=8.0 Hz, 2H), 3.11 (m, 4H), 1.79 (m, 18H), 1.12 (m, 36H) ppm; $^{13}$C NMR (75 MHz, $CDCl_3$): $\delta$= 142.2 (d, $^4J$(C,P)=4.1 Hz; Cq), 140.3 (Cq), 137.0 (Cq), 135.8 (d, $^3J$(C,P)=12.0 Hz; Cq), 133.7 (d, $^2J$(C,P)=8.0 Hz; CH), 132.8 (Cq), 132.0 (Cq), 130.1 (d, $^1J$(C,P)=58.9 Hz; Cq), 128.0 (Cq), 121.4 (CH), 120.8 (CH), 38.9 (d, *J*(C,P)=43.7 Hz; CH), 37.3 (d, *J*(C,P)=43.7 Hz; CH), 34.5 ($CH_2$), 26.5 ($2CH_2$), 26.3 ($2CH_2$), 26.1 ($2CH_2$), 25.8 ($2CH_2$), 25.7 ($2CH_2$), 23.4 ($CH_2$), 14.9 ($CH_3$) ppm. $^{31}$P NMR (121 MHz, $CDCl_3$): $\delta$=48.71 (s), 48.71 (d, $^1J$(P,Se)=713.6 Hz) ppm; MALDI-TOF (*m/z*): 880.1 [*M-2Se*$^+$], 959.5 [*M-Se*$^+$], 1039.2 [*M*$^+$]; MS-ESI (*m/z*): 1061.5 [*M+Na*$^+$].

**Di selenide 60b**

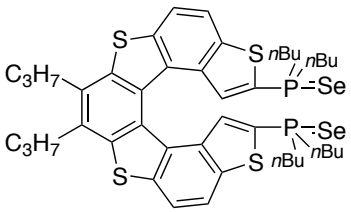

Yield: >90%; $R_f$=0.16 (Hexane/$CH_2Cl_2$ 1:1); $^1$H NMR (300 MHz, $CDCl_3$): $\delta$=8.06 (d, $^3J$(H,H)=8.1 Hz, 2H), 7.99 (d, $^3J$(H,H)=8.1 Hz, 2H), 7.20 (d, $^3J$(H,P)=9.0 Hz, 2H), 3.13 (m, 4H), 1.89 (m, 4H), 1.72 (m, 4H), 1.26 (m, 26H) 0.84 (m, 12H) ppm; $^{13}$C NMR (75 MHz, $CDCl_3$): $\delta$= 141.4 (d, $^4J$(C,P)=4.4 Hz; Cq), 140.5 (Cq), 137.0 (Cq), 135.5 (d, $^3J$(C,P)=13.5 Hz; Cq), 133.6 (d, $^1J$(C,P)=68.5 Hz; Cq), 133.0 (Cq), 132.6 (d, $^2J$(C,P)=8.7 Hz; CH), 131.8 (Cq), 127.7 (Cq), 121.0 (2CH), 34.5 ($CH_2$), 34.4 (d, $^1J$(C,P)=47 Hz; $CH_2$), 34.3 (d, $^1J$(C,P)=47 Hz; $CH_2$), 25.2 (d, $^3J$(C,P)=8.8 Hz; $2CH_2$), 23.8 (d, $^2J$(C,P)=13.4 Hz; $CH_2$), 23.6 (d, $^2J$(C,P)=13.4 Hz; $CH_2$), 23.4 ($CH_2$), 14.8 ($CH_3$), 13.9 ($CH_3$), 13.7 ($CH_3$) ppm; $^{31}$P NMR (121 MHz, $CDCl_3$): $\delta$=28.72 (s), 28.72 (d, $^1J$(P,Se)=717.8 Hz) ppm;MALDI-TOF (*m/z*): 775.5 [*M-2Se*$^+$], 855.6 [*M-Se*$^+$], 934.8 [*M*$^+$];

**Di selenide 60c**

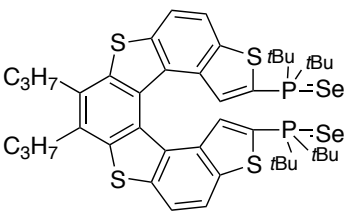

Yield: >90%; $R_f$=0.15 (Hexane/$CH_2Cl_2$ 1:1); $^1$H NMR (300 MHz, $CDCl_3$): $\delta$=8.02 (d, $^3J$(H,H)=8.6 Hz, 2H), 7.95 (d, $^3J$(H,H)=8.6 Hz, 2H) 7.65 (d, $^3J$(H,P)=6.7 Hz, 2H), 3.09 (m, 4H), 1.87 (m, 4H), 1.17 (m, 6H), 1.03 (m, 36H) ppm; $^{13}$C NMR (75 MHz, $CDCl_3$): $\delta$= 142.3 (d, $^4J$(C,P)=4.1 Hz; Cq), 140.5 (Cq), 137.0 (Cq), 136.5 (d, $^3J$(C,P)=11.5 Hz; Cq), 133.0 (d,

$^{2}J$(C,P)=6.1 Hz; CH), 132.8 (Cq), 132.2 (Cq), 132.1 (Cq), 127.9 (Cq), 120.9 (CH), 129.7 (CH), 38.4 (d, $^{1}J$(C,P)=34.2 Hz; Cq), 38.2 (d, $^{1}J$(C,P)=34.2 Hz; Cq), 34.5 ($CH_2$), 28.5 ($3CH_3$), 28.0 ($3CH_3$), 23.4 ($CH_2$), 14.9 ($CH_3$) ppm; $^{31}$P NMR (121 MHz, $CDCl_3$): $\delta$=72.33 (s), 72.33 (d, $^{1}J$(P,Se)=716.7 Hz) ppm; MALDI-TOF (*m/z*): 775.3 [*M-Se*$^{+}$], 855.1 [*M-Se*$^{+}$], 933.6 [*M*$^{+}$]; MS-ESI (*m/z*): 957.3 [*M+Na*$^{+}$].

**General procedure for the synthesis of phosphine oxides.**

A solution of phosphine-borane complex (0.05 mmol) in $Et_2NH$ was stirred and heated to reflux under an argon atmosphere, and the progress of the reaction was monitored by $^{31}$P NMR analysis. After 4-8 h, the yellow solution was cooled to room temperature, and the solvents together with diethylamine borane adduct as byproduct were removed under reduced pressure at 50 °C for 2 h. The yellow solid so obtained was dissolved in degassed toluene (10 mL), and to this solution was added dropwise an aqueous solution of $H_2O_2$ (35% w/w, 0.5 mmol, 10 equiv.) at 0 °C under an argon atmosphere. The mixture was stirred overnight at room temperature, then diluted with $H_2O$ (15 mL). The aqueous phase was extracted with toluene (3 × 20 mL), and the combined organic layers were dried over $Na_2SO_4$, concentrated on vacuum. The residue was purified by column chromatography on silica gel (with a gradient from hexane/AcOEt, 1:9 to 0:10).

**Mono phosphine oxide 66**

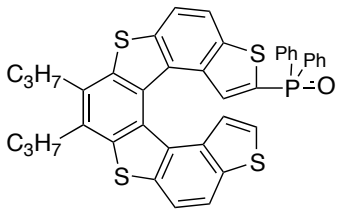


Yield: >90%; $R_f$=0.4 (AcOEt); $^{1}$H NMR (300 MHz, $CDCl_3$): $\delta$=7.93 (m, 4H), 7.42 (m, 5H), 7.23 (m, 5H), 7.03 (m, 2H), 6.81 (d, $^{3}J$(H,H)=5,6 Hz, 1H), 3.08 (m, 4H), 1.83 (m, 4H), 1.14 (m, 6H) ppm; $^{13}$C NMR (75 MHz, $CDCl_3$): $\delta$= 141.6 (d, $^{4}J$(C,P)=5.5 Hz; Cq), 140.2 (Cq), 137.0 (Cq), 136.7 (Cq), 136.5 (Cq),135.6 (d, $^{3}J$(C,P)=13.3 Hz; Cq), 135.4 (Cq), 134.5 (d, $^{2}J$(C,P)=10.5 Hz; CH), 134.2 (Cq), 133.0 (Cq), 132.9 (Cq), 132.8 (Cq), 132.5 (Cq), 132.3 (Cq), 132.2 (d, $^{4}J$(C,P)=2.2 Hz; 2CH), 131.9 (d, $^{3}J$(C,P)=10.5 Hz; 2CH), 131.4 (d, $^{3}J$(C,P)=10.5 Hz; 2CH), 131.3 (Cq), 130.8 (Cq), 128.6 (d, $^{2}J$(C,P)=10.8 Hz; 2CH), 128.4 (d, $^{2}J$(C,P)=10.8 Hz; 2CH), 128.3 (Cq), 127.7 (Cq), 125.4 (CH), 124.9 (CH), 121.3 (CH), 121.1 (CH), 120.8 (CH), 119.0 (CH), 34.4 ($2CH_2$), 23.4 ($2CH_2$), 14.9 ($2CH_3$) ppm; $^{31}$P NMR (121 MHz, $CDCl_3$): $\delta$=23.82 (s) ppm; MALDI-TOF (*m/z*): 687.1 [*M*$^{+}$]; MS-ESI (*m/z*): 687.2 [*M*$^{+}$].

**Mono phosphine oxide 67a**

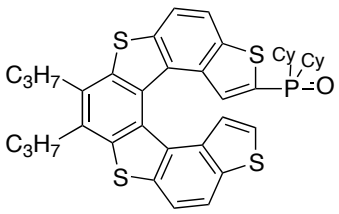


Yield: >90%; $R_f$=0.4 (AcOEt); $^{1}$H NMR (300 MHz, $CDCl_3$): $\delta$=7.99 (m, 4H), 7.34 (d, $^{3}J$(H,P)=7.2 Hz, 1H), 6.94 (d, $^{3}J$(H,H)=5,6 Hz, 1H), 6.87 (d, $^{3}J$(H,H)=5.6 Hz, 1H), 3.12 (m, 4H), 1.89−0.88 (m, 32H) ppm; $^{13}$C NMR (75 MHz, $CDCl_3$): $\delta$= 140.7 (d, $^{4}J$(C,P)=4.5 Hz; Cq),140.3 (Cq), 140.2 (Cq), 137.1 (Cq), 136.8 (Cq), 136.6 (Cq), 136.2 (d, $^{3}J$(C,P)=2.5 Hz; Cq), 135.8 (Cq), 132.9 (Cq), 132.8 (Cq), 132.6 (d, $^{2}J$(C,P)=6.7 Hz; CH), 132.3 (Cq), 131.7 (Cq), 131.0 (d, $^{1}J$(C,P)=85.4 Hz; Cq), 128.5 (Cq), 128.0 (Cq), 125.4 (CH), 124.6 (CH), 121.2 (CH), 120.6 (CH), 119.3 (CH), 36.9 (d, $^{1}J$(C,P)=68.4 Hz; CH), 36.8 (d, $^{1}J$(C,P)=68.4 Hz; CH), 34.5 ($2CH_2$), 26.7 ($CH_2$), 26.6 ($CH_2$), 26.4 ($CH_2$), 26.3 ($CH_2$), 25.9 ($CH_2$), 25.8 ($CH_2$), 25.7 ($CH_2$), 25.0 ($CH_2$), 24.8 ($CH_2$), 24.7 ($CH_2$), 23.4 ($2CH_2$), 14.8 ($2CH_3$) ppm. $^{31}$P NMR (121 MHz, $CDCl_3$): $\delta$=45.40 (s) ppm; MALDI-TOF (*m/z*): 699.6 [*M*$^{+}$]; MS-ESI (*m/z*): 699.2 [*M*$^{+}$];

**Mono phosphine oxide 67b**

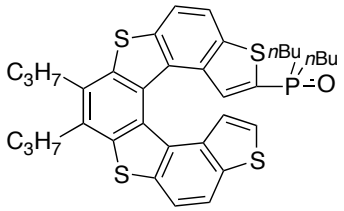

Yield: >90%; $R_f$=0.4 (AcOEt);$^1$H NMR (300 MHz, $CDCl_3$): $\delta$=8.02 (m, 4H), 7.11 (d, $^3J$(H,P)=7.4 Hz, 1H), 6.93 (d, $^3J$(H,H)=5,4 Hz, 1H), 6.78 (d, $^3J$(H,H)=5.4 Hz, 1H), 3.11 (m, 4H), 1.87 (m, 4H), 1.40 (m, 8H), 1.16 (m, 10H), 0.93 (m, 3H) 0.73 (m, 3H) ppm; $^{13}$C NMR (75 MHz, $CDCl_3$): $\delta$= 140.3 (Cq), 140.2 (Cq), 136.9 (Cq), 136.7 (Cq), 136.0 (d, $^3J$(C,P)=13.4 Hz; Cq), 135.9 (Cq), 132.9 (Cq), 132.6 (Cq), 132.1 (Cq), 132.0 (d, $^1J$(C,P)=64.7 Hz; Cq), 131.5 (Cq), 130.9 (d, $^2J$(C,P)=9.6 Hz; CH), 128.2 (Cq), 128.0 (Cq), 125.5 (CH), 124.6 (CH), 121.0 (CH), 120.7 (CH), 120.6 (CH), 119.3 (CH), 34.5 ($2CH_2$), 30.7 (d, $^1J$(C,P)=65.0 Hz; $CH_2$), 30.3 (d, $^1J$(C,P)=65.0 Hz; $CH_2$), 24.0 (d, $^2J$(C,P)=13.0 Hz; $CH_2$), 23.6 (d, $^2J$(C,P)=15.0 Hz; $CH_2$), 23.5 ($CH_2$), 23.4 ($2CH_2$), 14,8 ($2CH_3$), 13.9 ($CH_3$), 13.5 ($CH_3$) ppm; $^{31}$P NMR (121 MHz, $CDCl_3$): $\delta$=39.87 (s) ppm; MALDI-TOF (*m/z*): 646.2 [$M^+$]; MS-ESI (*m/z*): 647.7 [$M^+$], 669.7 [$M$+$Na^+$];

**Mono phosphine oxide 67c**

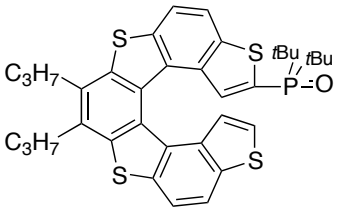

Yield: >90%; $R_f$=0.4 (AcOEt); $^1$H NMR (300 MHz, $CDCl_3$): $\delta$=7.98 (m, 4H), 7.37 (d, $^3J$(H,P)=5.7 Hz, 1H), 6.98 (d, $^3J$(H,H)=5,6 Hz, 1H), 6.90 (d, $^3J$(H,H)=5.6 Hz, 1H), 3.11 (m, 4H), 1.86 (m, 4H), 1.15 (m, 6H), 0.92 (m, 18H) ppm; $^{13}$C NMR (75 MHz, $CDCl_3$): $\delta$= 140.5 (Cq), 140.1 (Cq), 137.7 (Cq), 136.7 (d, $^3J$(C,P)=10.4 Hz; Cq), 136.4 (Cq), 135.6 (Cq), 132.8 (Cq), 132.3 (Cq), 132.3 (Cq), 131.8 (d, $^1J$(C,P)=52.0 Hz; Cq), 131.7 (d, $^2J$(C,P)=5.7 Hz; CH), 128.5 (Cq), 128.0 (Cq), 125.2 (CH), 125.1 (CH), 121.0 (CH), 120.6 (CH), 120.3 (CH), 119.4 (CH), 36.0 (d, $^1J$(C,P)=62.1 Hz; Cq), 35.9 (d, $^1J$(C,P)=62.1 Hz; Cq), 34.5 ($CH_2$), 34.4 ($CH_2$), 26.5 ($6CH_3$), 23.4 ($2CH_2$), 14.8 ($2CH_3$) ppm; $^{31}$P NMR (121 MHz, $CDCl_3$): $\delta$=56.15 (s) ppm; MALDI-TOF (*m/z*): 646.6 [$M^+$]; MS-ESI (*m/z*): 647.5 [$M^+$].

**Di phosphine oxide 69a**

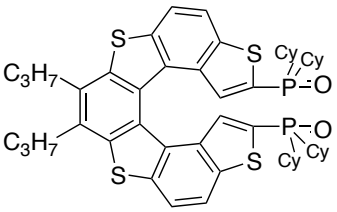

Yield: >90%; Mp 140–141 °C. $^1$H NMR (300 MHz, $CDCl_3$): $\delta$ = 8.01 (m, 4 H), 7.21 (d, *J*(H,P)= 6.6 Hz, 2 H), 3.11 (m, 4 H), 1.90 (m, 4 H), 1.59 (m, 20 H), 1.08 (m, 30 H) ppm. $^{13}$C NMR (75 MHz, $CDCl_3$): $\delta$ = 141.2 (d, *J*(C,P) = 3.8 Hz, Cq), 140.4 (Cq), 137.0 (Cq), 136.0 (d, *J*(C,P) = 12.0 Hz, Cq), 132.8 (Cq), 132.1 (Cq), 132.0 (d, *J*(C,P) = 83.7 Hz, Cq), 131.6 (d, *J*(C,P) = 7.3 Hz, CH), 128.0 (Cq), 121.0 (CH), 120.8 (CH), 37.1 (d, *J*(C,P) = 31.6 Hz, CH), 36.2 (d, *J*(C,P) = 31.4 Hz, CH), 34.7 ($CH_2$), 26.7 ($CH_2$), 26.6 ($CH_2$), 26.5 ($CH_2$), 26.4 ($CH_2$), 26.3 ($CH_2$), 25.8 ($CH_2$), 25.3 ($CH_2$), 24.8 ($CH_2$), 24.73 ($CH_2$), 24.70 ($CH_2$), 24.6 ($CH_2$), 23.5 ($CH_2$), 14.8 ($CH_3$) ppm. $^{31}$P NMR (121 MHz, $CDCl_3$): $\delta$ = 44.5 (s) ppm. HRMS (ESI): calcd. for $C_{52}H_{64}S_4P_2O_2Na$ 933.3156, found 933.3158.

Compounds (*P*)-(+)-**69a** and (*M*)-(–)-**69a** were obtained in 80 and 90% yield, respectively, with a mixture of hexane/*i*PrOH/AcOEt (70:15:15) as eluent under isocratic conditions (3 mL/min flow rate): $t_R$ = 10.8 min, $[\alpha]_D$ = – 1166 (c = 0.10, $CHCl_3$) [for (*M*)-(–)-**69a**]; $t_R$ = 17.9 min, $[\alpha]_D$ = + 1077 (c = 0.10, $CHCl_3$) [for (*P*)-(+)-**69a**].

**Di phosphine oxide 69b**

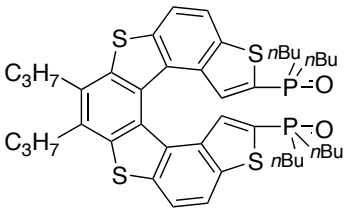

Yield: >90%; $R_f$=0.4 (AcOEt/MeOH 9:1) $^1$H NMR (300 MHz, $CDCl_3$): $\delta$=8.04 (m, 4H), 7.09 (d, $^3J$(H,P)=6.1 Hz, 2H), 3.13 (m, 4H), 1.88 (m, 4H), 1.25 (m, 30H), 0.93 (m, 6H), 0.75 (m, 6H) ppm; $^{13}$C NMR (75 MHz, $CDCl_3$): $\delta$=140.6 (Cq), 140.4 (Cq), 137.1 (Cq), 135.8 (d, $^3J$(C,P)=12.8 Hz; Cq), 134.7 (d, $^1J$(C,P)=91.5 Hz; Cq), 133.1 (Cq), 131.8 (Cq), 130.8 (d, $^2J$(C,P)=9.6 Hz; CH), 127.8 (Cq), 121.0 (CH), 120.8 (CH), 34.5 ($CH_2$), 30.9 (d, $^1J$(C,P)=71.0 Hz; $CH_2$), 30.5 (d, $^1J$(C,P)=71.0 Hz; $CH_2$), 24.3 (d, $^2J$(C,P)=15.0 Hz; $CH_2$), 24.0 (d, $^2J$(C,P)=15.0 Hz; $CH_2$), 23.6 ($CH_2$), 23.5 ($CH_2$), 23.4 ($CH_2$), 14,8 ($CH_3$), 13.8 ($CH_3$), 13.5 ($CH_3$) ppm. $^{31}$P NMR (121 MHz, $CDCl_3$): $\delta$=38.33 (s) ppm; MALDI-TOF (*m/z*): 807.9 [$M^+$], 830.2 [$M$+$Na^+$]; MS-ESI (*m/z*): 807.8 [$M^+$], 829.5 [$M$+$Na^+$];

**Di phosphine oxide 69c**

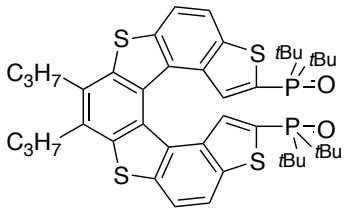

Yield: >90%; $R_f$=0.3 (AcOEt/MeOH 9:1); $^1$H NMR (300 MHz, $CDCl_3$): $\delta$=8.01 (d, $^3J$(H,H)=8.6 Hz, 2H), 7.96 (d, $^3J$(H,H)=8.6 Hz, 2H) 7.39 (d, $^3J$(H,P)=5.9 Hz, 2H), 3.11 (m, 4H), 1.85 (m, 4H), 1.16 (m, 6H), 0.92 (m, 36H) ppm; $^{13}$C NMR (75 MHz, $CDCl_3$): $\delta$= 141.6 (d, $^4J$(C,P)=3.3 Hz; Cq), 140.4 (Cq), 136.9 (Cq), 136.0 (d, $^3J$(C,P)=11.2 Hz; Cq), 133.0 (d, $^1J$(C,P)=74.7 Hz; Cq), 132.8 (Cq), 132.1 (Cq), 131.7 (d, $^2J$(C,P)=6.5 Hz; CH), 128.0 (Cq), 120.8 (CH), 120.7 (CH), 36.0 (d, $^1J$(C,P)=62.0 Hz; Cq), 35.9 (d, $^1J$(C,P)=62.0 Hz; Cq), 34.5 ($CH_2$), 26.7 (d, $^2J$(C,P)=22.9 Hz; 6$CH_3$), 23.5 ($CH_2$), 14.9 ($CH_3$) ppm; $^{31}$P NMR (121 MHz, $CDCl_3$): $\delta$=56.5 (s) ppm; MALDI-TOF (*m/z*): 807.1 [$M^+$], 830.1 [$M$+$Na^+$]; MS-ESI (*m/z*): 807.7 [$M^+$], 829.8 [$M$+$Na^+$].

**Di phosphine oxide 75**

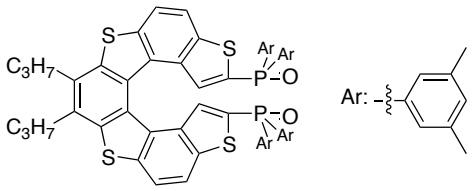

Yield: 60%; Mp 132–135 °C (hexane). $^1$H NMR (300 MHz, $CDCl_3$): $\delta$ = 7.85 (d, *J* = 8.6 Hz, 2 H), 7.68 (d, *J* = 8.6 Hz, 2 H), 6.98 (m, 14 H), 3.10 (m, 4 H), 2.27 (s, 12 H), 2.22 (s, 12 H), 1.86 (m, 4 H), 1.17 (t, *J* = 7.3 Hz, 6 H) ppm. $^{13}$C NMR (75 MHz, $CDCl_3$): $\delta$ = 141.6 (d, *J*(C,P) = 5.1 Hz, Cq), 140.2 (Cq), 138.1 (d, *J*(C,P) = 13.4 Hz, 2 Cq), 138.0 (d, *J*(C,P) = 13.3 Hz, 2 Cq), 136.3 (Cq), 134.9 (d, *J*(C,P) = 13.7 Hz, Cq), 134.2 (CH), 133.9 (CH), 133.7 (d, *J*(C,P) = 10.4 Hz, CH), 133.1 (d, *J*(C,P) = 53.2 Hz, Cq), 132.7 (Cq), 132.4 (d, *J*(C,P) = 52.5 Hz, Cq), 131.5 (Cq), 131.3 (d, *J*(C,P) = 104,2 Hz, Cq), 129.3 (d, *J*(C,P) = 10.4 Hz, 2 CH), 129.0 (d, *J*(C,P) = 10.4 Hz, 2 CH), 128.0 (Cq), 121.2 (CH), 120.1 (CH), 34.5 ($CH_2$), 23.4 ($CH_2$), 21.5 ($CH_3$), 21.4 ($CH_3$), 14.8 ($CH_3$) ppm. $^{31}$P NMR (121 MHz, $CDCl_3$): $\delta$ = 23.3 (s) ppm. HRMS (ESI): calcd. for $C_{60}H_{56}S_4P_2O_2Na$ 1021.2531, found 1021.2530.

Compounds (*P*)-(+)-**75** and (*M*)-(–)-**75** were obtained in 60 and 40% yield, respectively, with a mixture of hexane/*i*PrOH (80:20) as eluent under isocratic conditions (3 mL/min flow rate): $t_R$ = 11.2 min, $[\alpha]_D$ = + 1084 (c = 0.12, $CHCl_3$) [for (*P*)-(+)-**2b**]; $t_R$ = 14.5 min, $[\alpha]_D$ = – 1024 (c = 0.12, $CHCl_3$) [for (*M*)-(–)-**2b**].

**Synthesis of di phosphine oxide 68**

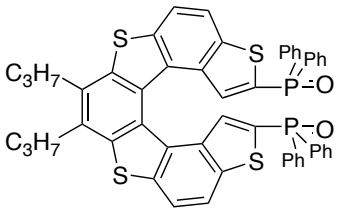

A solution of *t*BuLi (1.7 M in pentane, 1.40 mL, 0.820 mmol, 4 equiv.) was added dropwise to a stirring solution of helicene (±)-**8** (0.205 mmol, 0.100 g) in dry THF (10 mL) at – 78 °C under a nitrogen atmosphere. The solution was stirred for 40 min at – 78 °C. The resulting yellow suspension was treated with $Ph_2POCl$ (0.156 mL, 0.820 mmol, 4 equiv.) at – 78 °C, and the progress of the reaction was monitored by TLC (hexane/AcOEt, 90:10). After 5 h at – 78 °C, the yellow solution was warmed to room temperature, and THF was removed under reduced pressure. The crude material was taken up with a 5 % aqueous solution of $NaHCO_3$ (20 mL), and the aqueous phase was extracted with $CH_2Cl_2$ (3 × 15 mL). The organic fractions were washed with water (2 × 20 mL), dried over $Na_2SO_4$, and evaporated under vacuum. The crude product was purified by column chromatography on silica gel (AcOEt) to give (±)-**68** (0.127 g, 70%) as a pale yellow solid. Mp 140–143 °C (hexane/ $CH_2Cl_2$). $^1$H NMR (300 MHz, $CDCl_3$): $\delta$ = 7.86 (m, 4 H), 7.37 (m, 20 H), 6.98 (d, *J*(H,P) = 9.0 Hz, 2 H), 3.07 (m, 4 H), 1.83 (m, 4 H), 1.14 (t, *J* = 6.0 Hz, 6 H) ppm. $^{13}$C NMR (75 MHz, $CDCl_3$): $\delta$ = 141.6 (Cq), 140.3 (Cq), 136.6 (Cq), 134.9 (d, *J*(C,P) = 17 Hz, Cq), 133.8 (d, *J*(C,P) = 11.2 Hz, CH), 132.7 (2 Cq), 132.3 (CH), 131.9 (CH), 131.6 (d, *J*(C,P) = 10.5 Hz, 2 CH), 131.5 (Cq), 131.2 (d, *J*(C,P) = 10.5 Hz, 2 CH), 128.4 (d, *J*(C,P) = 12.0 Hz, 2 CH), 128.8 (d, *J*(C,P) = 13.0 Hz, 2 CH), 127.6 (Cq), 121.3 (CH), 120.9 (CH), 34.3 ($CH_2$), 23.2 ($CH_2$), 14.7 ($CH_3$) ppm. $^{31}$P NMR (121 MHz, $CDCl_3$): $\delta$ = 23.5 (s) ppm. HRMS (ESI): calcd. for $C_{52}H_{46}P_2O_2S_4Na$ 909.1279, found 909.1264.

Compounds (*P*)-(+)-**68** and (*M*)-(–)-**68** were obtained in 98 and 97% yield, respectively, with a mixture of hexane/*i*PrOH/AcOEt (45:40:15) as eluent under isocratic conditions (3 mL/min flow rate): $t_R$ = 16.5 min, $[\alpha]_D$ = + 1006 (c = 0.55, $CHCl_3$) [for (*P*)-(+)-**68**]; $t_R$ = 22.9 min, $[\alpha]_D$ = – 1001 (c = 0.55, $CHCl_3$) [for (*M*)-(–)-**68**].

*The general procedure of organocatalyzed reaction reported in Schemes 34–35 were performed according to the literature.* [55]

*The general procedure of organocatalyzed reaction reported in Table 9 and Schemes 40–41 were performed according to the literature.* [58,59]

**Synthesis of aldehyde 89**

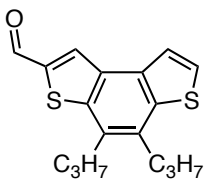

A solution of *n*BuLi (1.55 M in hexane, 2.11 mL, 3.28 mmol, 1 equiv.) was added dropwise to a stirring solution of **88** (900 mg, 3.28 mmol) in dry THF (30 mL) at –78 °C under an argon atmosphere. The solution was stirred for 30 min at –78 °C and 30 min at room temperature. The resulting yellow suspension was treated with DMF (5 mL, 20 equiv.) at 0 °C, and after 10 minutes the yellow solution was warmed to room temperature. The progress of the reaction was monitored by TLC (hexane/ AcOEt, 9:1). After 1 h, the suspension was diluted with a saturated aqueous solution of $NH_4Cl$ (30 mL), taken up with $CH_2Cl_2$ (10 mL), and the aqueous phase was extracted into $CH_2Cl_2$ (3 x 15 mL). The organic phase was dried with $Na_2SO_4$, concentrated under reduced pressure and the residue was

purified by flash chromatography on silica gel (hexane/ AcOEt, 9:1) to give **89** as a orange solid (731 mg, 74%); R*f* 0.3 (Ep 9 : EtOAc 1); M.p.: 116 °C; $^{1}$H NMR (300 MHz, $CDCl_3$) δ 10.10 (s, 1H), 8.32 (s, 1H), 7.71 (d, *J* = 5.4 Hz, 1H), 7.58 (d, *J* = 5.4 Hz, 1H), 3.02-2.94 (m, 4H), 1.85-1.73 (m, 4H), 1.11 ppm (m, 6H); $^{13}$C NMR (75 Hz, $CDCl_3$) δ 184.2 (CH), 143.0 (C), 141.6 (C), 139.6 (C), 134.6 (C), 134.1 (C), 132.4 (CH), 132.0 (C), 130.4 (C), 126.7 (CH), 122.2 (CH), 34.6 ($CH_2$), 34.1 ($CH_2$), 23.1 ($CH_2$), 22.9 ($CH_2$), 14.7 ($CH_3$), 14.6 ppm ($CH_3$); HRMS (EI) calcd. for $C_{17}H_{18}S_2O$: 302.0799, found: 302.0791;

**Synthesis of alkene 91**

The aldehyde **89** (2.35 mmol, 1034 mg) and the phosphonium salt **90** (2.35 mmol, 714 mg) were added to a solution of Na (2.35 mmol, 54 mg) in MeOH (40 mL). The reaction mixture was then stirred for 18 h at room temperature, then, quenched with a saturated aqueous $NH_4Cl$ solution, and the acqueous phase was extracted with EtOAc. The combined organic phases were washed with water and brine, dried over $MgSO_4$, and concentrated *in vacuo*. The residue was then purified by flash chromatography on silica gel with a heptane-EtOAc gradient (0% to 100% EtOAc) to afford the desired product **91** as a pale yellowish powder (800 mg, 88%). R*f* 0.8 (heptane 9 : DCM 1); M.p.: 115 °C; $^{1}$H NMR (300 MHz, $CDCl_3$) δ 7.62 (d, *J* = 5.4 Hz, 1H), 7.56 (s, 1H), 7.47 (d, *J* = 5.4 Hz, 1H), 7.22 (m, 3H), 7.10 (d, *J* = 3.4 Hz, 1H), 7.08 - 6.98 (m, 1H), 3.08 - 2.80 (m, 4H), 1.90 - 1.75 (m, 4H), 1.35 - 0.95 ppm (m, 6H).$^{13}$C NMR (75 Hz, $CDCl_3$) δ 142.4 (C), 141.2 (C), 139 (C), 137.7 (C), 133.3 (C), 132.5 (C), 131.0 (C), 130.0 (C), 127.8 (CH), 126.4 (CH), 125.2 (CH), 124.7 (CH), 123.0 (CH), 122.4 (CH), 122.2 (CH), 121.8 (CH), 34.5 ($CH_2$), 34.3 ($CH_2$), 23.2 ($CH_2$), 23.1 ($CH_2$), 14.7 ($2CH_3$) ppm. HRMS (EI) calcd. for $C_{22}H_{22}S_3$: 382.0883, found: 382.0879

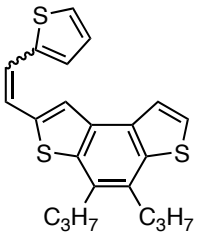


**Synthesis of helicene 92**

Iodine (0.1 mmol, 40 mg) was added to a solution of alkene **91** (2.01 mmol, 770 mg) in toluene (3,2 L), and the mixture was irradiated with a 500 W medium pressure Hg lamp in presence of air. The crude mixture was monitored by $^{1}$H NMR. After 9 h the solvent was removed, and the crude was purified by column chromatography on silica gel with heptane to afford the desired product **92** as white powder (570 mg, 74 %). $^{1}$H NMR (300 MHz, $CDCl_3$) δ 8.33 (m, 2H), 7.98 (d, *J* = 5.4 Hz, 1H), 7.87 (d, J = 5.4 Hz, H), 7.68 (d, *J* = 5.4 Hz, 1H), 7.61 (d, *J* = 5.4 Hz, 1H), 3.11-3.03 (m, 4H), 1.90-1.78 (m, 4H), 1.14 ppm (m, 6H); $^{13}$C NMR (75 Hz, $CDCl_3$) δ $^{13}$C NMR (75 MHz, $CDCl_3$) δ 139.7 (C), 138.6 (C), 137.5 (C), 135.6 (C), 133.9 (C), 132.2 (2C), 130.6 (C), 129.7 (C), 128.1 (C), 125.2 (CH), 124.6 (CH), 124.1 (CH), 124.1 (CH), 120.0 (CH), 118.4 (CH), 34.03 ($CH_2$), 33.98 ($CH_2$), 22.66 ($2CH_2$), 14.21 ppm ($2CH_3$). HRMS (EI) calcd. for $C_{22}H_{20}S_3$: 380.0727, found: 380.0724

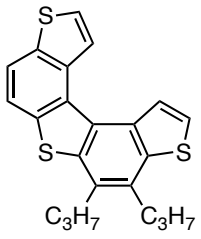

**Synthesis of bromide 87**

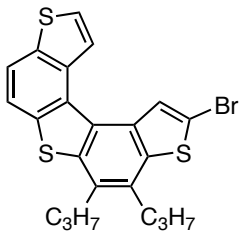

NBS (1.1 mmol, 231 mg) was added to a solution of helicene **92** (1.18 mmol, 450 mg) in DMF (20 mL), and the reaction mixture was stirred for 1.5 h at 60 °C. The reaction mixture was quenched with a saturated aqueous $NH_4Cl$ solution, and the acqueous phase was extracted with EtOAc. The combined organic phases were washed with water and brine, dried over $MgSO_4$, and concentrated *in vacuo*. The residue was then purified by flash chromatography on silica gel with a heptane to afford the desired product **87** as a pale yellowish powder (387 mg, 71%). $^1$H NMR (300 MHz, $CDCl_3$) δ 8.24 (s, 1H), 8.18 (d, *J* = 5.4 Hz, 1H), 7.93 (d, *J* = 8.4 Hz, 1H), 7.79 (d, *J* = 8.7 Hz, H), 7.68 (d, *J* = 5.4 Hz, 1H), 3.02-2.94 (m, 4H), 1.85 - 1.75 (m, 4H), 1.16 ppm (m, 6H); $^{13}$C NMR (75 Hz, $CDCl_3$) δ 140.7 (C), 138.9 (C), 137.5 (C), 135.6 (C), 133.6 (C), 132.0 (C), 131.2 (2C), 130.0 (2C), 127.4 (CH), 125.7 (CH), 123.6 (CH), 120.2 (CH), 118.2 (CH), 113.0 (C), 33.9 ($2CH_2$), 22.6 ($2CH_2$), 14.7 ppm ($2CH_3$); HRMS (EI) calcd. for $C_{22}H_{19}S_3Br$: 457.9832, found: 457.9827;

**Synthesis of boronic acid 94**

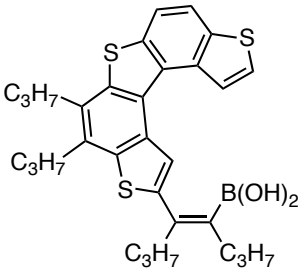

To a solution of **93** (1.304 mmol, 574 mg) in 6 mL of toluene were added **87** (0.652 mmol, 300 mg), $Pd(PPh_3)_4$ (0.033 mmol, 38 mg), 5,3 mL of a solution of $Na_2CO_3$ 2M in water and 3 mL of EtOH. The reaction mixture was stirred for 1.5h at 85°C. The crude mixture was extracted with EtOAc, washed with water and brine, dried over $MgSO_4$ and concentrated *in vacuo*. The residue was purified by flash chromatography on silica gel with an heptane/ethyl acetate gradient (0% to 10% EtOAc) to afford the desired compound **94** as a pale yellow solid (210 mg, 55% ). R*f* 0.2 (heptane 9 : EtOAc 1); $^1$H NMR (300 MHz, $CDCl_3$) δ 8.30 (d, *J* = 5.6 Hz, 1H), 8.07 (s, 1H), 7.95 (d, *J* = 8.5 Hz, 1H), 7.84 (d, *J* = 8.5 Hz, 1H), 7.65 (d, *J* = 5.6 Hz, 1H), 3.10 - 2.96 (m, 4H), 2.61 - 2.50 (m, 2H), 2.45 - 2.32 (m, 2H), 1.90 - 1.77 (m, 4H), 1.60 - 1.36 (m, 4H), 1.20 - 1.10 (t, *J* = 7.3 Hz, 6H), 1.02 (t, *J* = 7.3 Hz, 3H), 0.92 ppm (t, *J* = 7.4 Hz, 3H); $^{13}$C NMR (75 Hz, $CDCl_3$) δ 145.6 (C), 138.9 (C), 138.3 (C), 137.9 (C), 136.1 (C), 134.4 (C), 134.3 (C), 133.6 (C), 132.4 (C), 131.1 (C), 130.5 (C), 130.0 (C), 138.2 (C), 125.5 (CH), 124.5 (CH), 120.4 (CH), 120.2 (CH), 118.9 (CH), 34.5 ($2CH_2$), 34.4 ($2CH_2$), 23.1 ($3CH_2$), 22.9 ($CH_2$), 14.7 ($3CH_3$), 14.4 ppm ($CH_3$); HRMS (ESI) calcd. for $C_{30}H_{35}S_3BO_2$ $[M+H]^+$: 534.1892, found: 534.1873

**Synthesis of alkene 86**

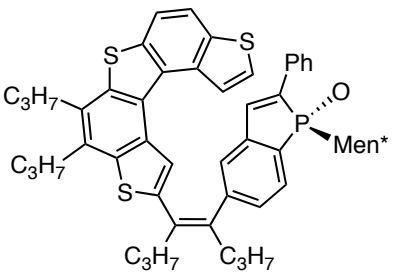

To boronic acid **94** (0.46 mmol, 236 mg) and ($R_P$)-**95** (0.60 mmol, 320 mg) in 8 mL of THF were added $Cs_2CO_3$ (1.32 mmol, 450 mg), $PdCl_2(SPhos)_2$ (0.06 mmol, 46 mg) and 0.8 mL of degassed water. The reaction mixture was then stirred for 18h at 85°C before cooling to room temperature. The reaction mixture was extracted with EtOAc, the extract washed with water and brine, dried over $MgSO_4$ and concentrated *in vacuo*. The residue was then purified by flash chromatography on silica gel with a heptane-EtOAc gradient (0% to 100% EtOAc) to afford the desired product **86** as a pale yellowish powder (400 mg, 95%). R*f* 0.8 (heptane

8 : EtOAc 2); $^{1}$H NMR (300 MHz, $CDCl_3$) δ 7.89 (d, *J* = 8.5 Hz, 1H), 7.78 (s, 1H), 7.77 (d, *J* = 8.4 Hz, 1H), 7.69 (d, J = 7.2 Hz, 2H), 7.65 (d, J = 7.8 Hz, 1H), 7.61 (d, J = 5.4 Hz, 1H), 7.57 (d, J = 5.4 Hz, 1H), 7.40-7.25 (m, 4H), 7.25-7.15 (m, 1H), 7.15 (d, $J_{H\text{-}P}$ = 24.0 Hz, 1H), 2.99-2.92 (m, 4H), 2.69-2.48 (m, 4H), 2.37-2.09 (m, 1H), 1.82-1.71 (m, 4H), 1.53-1.44 (m, 4H), 1.43-1.31 (m, 4H), 1.11-1.08 (m, 6H), 0.99-0.91 (m, 8H), 0.75-1.55 (m, 3H), 0.43 (d, *J* = 6.6 Hz, 3H), 0.28 (d, *J* = 6.8 Hz, 3H), 0.23 ppm (d, *J* = 6.7 Hz, 3H); $^{13}$C NMR (75 Hz, $CDCl_3$) δ 148.4 (C), 143.9 (C), 141.9 (d, *J* = 25.5 Hz, C), 141.3 (C), 139.9 (C), 139.5 (d, *J* = 84.1 Hz, C), 138.8 (C), 137.9 (C), 137.2 (d, *J* = 17.9 Hz, CH), 135.9 (C), 134.8 (d, *J* = 10.5 Hz, C), 134.2 (C), 132.9 (C), 132.5 (C), 132.2 (C), 130.9 (C), 129.8 (C), 129.5 (d, *J* = 10.5 Hz, CH), 128.7 (2CH), 128.5 (CH), 128.4 (CH), 128.0 (C), 126.5 (CH), 126.4 (CH), 125.8 (d, *J* = 8.8 Hz, CH), 125.5 (CH), 125.2 (CH), 124.7 (CH), 120.3 (CH), 118.8 (CH), 43.2 (CH), 40.2 (d, *J* = 63.4 Hz, CH), 37.2 ($CH_2$), 36.8 ($CH_2$), 35.0 ($CH_2$), 34.4 ($2CH_2$), 33.9 ($CH_2$), 32.6 (d, *J* = 13.8 Hz, CH), 28.0 (CH), 24.6 (d, *J* = 13.3 Hz, $CH_2$), 23.2 ($CH_2$), 23.1 ($CH_2$), 21.9 ($CH_2$), 21.67 ($CH_3$), 21.3 ($CH_2$), 20.7 ($CH_3$), 15.6 ($CH_3$), 14.8 ($CH_3$), 14.7 ($CH_3$), 14.0 ppm ($2CH_3$); $^{31}$P (121 MHz, $CDCl_3$) δ 55.7 ppm; HRMS (ESI) calcd. for $C_{54}H_{62}S_3OP$ $[M+H]^+$: 853.3700, found: 853.3723; $[\alpha]_D^{25}$= -187 (c = 1, $CHCl_3$); IR: 2957, 2928, 2869, 1601, 1455, 1388, 1375, 1315, 1202, 1179, 1162, 1094, 900, 829, 786, 762, 697.

**Synthesis of phosphathiahelicene 85.** To a solution of alkene **86** (0.01 mmol, 80 mg) in THF (5 mL), iodine (0.2 mmol, 80 mg), propylene oxide (10 mmol, 0.7 mL) and cyclohexane (350 mL) were added. The mixture was irradiated for 90 min (Heraeus TQ, 150 Watt). After removal of the solvent, the crude mixture was monitored by $^{1}$H NMR and separated then by column chromatography on silica gel with a heptane/ethyl acetate gradient (100% ep to 80% ep in 20 min). Three fractions were collected which contain (*R*$_P$,*P*)-**85** (40 mg, 52% yield), and (*R*$_P$,*M*)-**96** (18 mg, 14% yield, $R_f$ = 0.2) respectively.

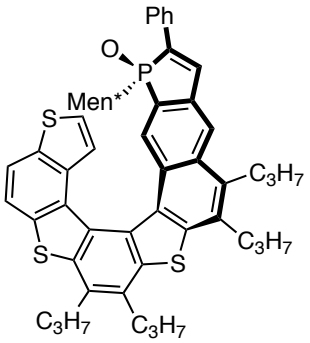


(*R*$_P$,*P*)-**85** $R_f$ = 0.4 in 10% EtOAc / Heptane; $^{1}$H NMR (300 MHz, $CDCl_3$) δ 8.15 (d, *J* = 10.3 Hz, 1H), 7.96 (d, *J* = 8.5 Hz, 1H), 7.91 (d, *J* = 8.2 Hz, 1H), 7.90 (s, 1H), 7.70 (d, J = 7.0 Hz, 2H), 7.40-7.25 (m, 4H), 6.82 (d, *J* = 5.6 Hz, 1H), 6.68 (d, br, 1H), 3.25-3.06 (m, 8H), 2.00-1.82 (m, 8H), 1.60-1.51 (m, 2H), 1.26-1.16 (m, 16H), 0.9-0.45 ppm (m, 13H); $^{13}$C NMR (75 Hz, $CDCl_3$) δ 140.2 (d, *J* = 11.0 Hz, C), 138.9 (C), 138.1 (d, *J* = 15.0 Hz, C), 135.2 (C), 135.1 (C), 134.3 (C), 132.3 (C), 132.1 (C), 131.9 (C), 128.7 (2CH), 128.5 (C), 128.4 (CH), 127.3 (d, *J* =12.8 Hz, C), 126.5 (CH), 126.4 (CH), 125.2 (CH), 123.9 (CH), 120.3 (d, *J* = 11.0 Hz, CH), 119.3 (CH), 42.4 (CH), 37.4 (d, *J* = 61.0 Hz, CH), 35.0 ($CH_2$), 34.2 ($CH_2$), 33.9 ($CH_2$), 33.6 ($CH_2$), 32.2 (d, *J* = 17.1 Hz, CH), 31.0 ($CH_2$), 29.7 ($CH_2$), 27.1 (CH), 24.9 (d, *J* = 13.5 Hz, $CH_2$), 24.6 ($CH_2$), 23.5 ($CH_2$), 23.4 ($CH_2$), 23.2 ($CH_2$), 22.9 ($CH_3$), 21.4 ($CH_3$), 15.7 ($CH_3$), 14.8 ($CH_3$), 14.7 ($CH_3$), 14.6 ppm ($CH_3$); $^{31}$P (121 MHz, $CDCl_3$) δ 58.7 ppm; HRMS (ESI) calcd. for $C_{54}H_{60}S_3OP$ $[M+ H]^+$: 851.3544, found: 851.3563; $[\alpha]_D^{25}$= +1358 (c = 1, $CHCl_3$); IR: 2957, 2927, 2869, 1548, 1455, 1368, 1318, 1260, 1199, 1161, 1092, 1031, 948, 902, 854, 829, 785, 751, 697, 664.

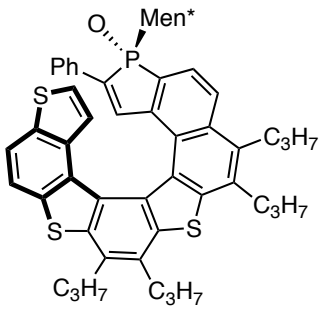


($R_P$,$M$)-**96**: $R_f$ = 0.2 in 10% EtOAc / Heptane; $^1$H NMR (300 MHz, $CDCl_3$) δ 8.17 (d, *J* = 8.5 Hz, 1H), 8.03 (d, *J* = 9.8 Hz, 1H), 7.92 (d, *J* = 5.7 Hz, 1H) 7.90 (s, 1H), 7.77 (d, *J* = 7.1 Hz, 3H), 7.44 (s, 1H), 7.36-7.27 (m, 3H), 6.78 (d, *J* = 5.5 Hz, 1H), 6.51 (d, *J* = 5.5 Hz, 1H), 3.31-3.03 (m, 8H), 2.00-1.82 (m, 8H), 1.41-1.10 (m, 16H), 0.9-0.75 (m, 6H), 0.59 (d, *J* = 6.3 Hz, 3H) 0.38 (d, *J* = 6.7 Hz, 3H), 0.07 (d, *J* = 6.7 Hz, 3H); $^{13}$C NMR (75 Hz, $CDCl_3$) δ 140.2 (C), 139.9 (C), 139.8 (d, *J* = 86.0 Hz, C), 138.8 (C), 138.1 (C), 137.4 (C), 137.1 (d, *J* = 16.6 Hz, CH), 137.0 (C), 135.2 (d, *J* = 12.0 Hz, C), 135.1 (C), 134.8 (C), 134.3 (C), 132.2 (C), 131.9 (C), 131.8 (C), 131.7 (C), 131.2 (C), 129.2 (C), 129.1 (C), 128.7 (C) 128.5 (2CH), 128.4 (CH), 128.0 (CH), 126.5 (CH), 126.4 (CH), 124.6 (CH), 124.5 (CH), 122.0 (CH), 119.7 (d, *J* = 8.3 Hz, CH), 118.2 (CH), 43.2 (CH), 40.51 (d, *J* = 63.0 Hz, CH), 35.5 ($CH_2$), 35.0 ($CH_2$), 34.5 ($CH_2$), 34.3 ($CH_2$), 34.2 ($CH_2$), 32.9 (d, *J* = 13.1 Hz, CH), 31.0 ($CH_2$), 28.1 (CH), 24.6 ($CH_2$), 24.4 (d, *J* = 13.5.0 Hz, $CH_2$), 23.4 ($2CH_2$), 23.3 ($CH_2$) 22.1 ($CH_3$), 21.1 ($CH_3$), 15.6 ($CH_3$), 14.9 ($CH_3$), 14.7 ppm ($3CH_3$); $^{31}$P (121 MHz, $CDCl_3$) δ 51.5 ppm; HRMS (ESI) calcd. for $C_{54}H_{60}S_3OP$ $[M]^+$: 851.3544, found: 851.3568; $[\alpha]_D^{25}$= -1366 (c = 1, $CHCl_3$)

**Synthesis of the gold complex ($S_P$,$P$)-98**

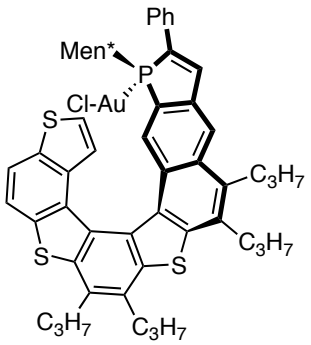


To ($R_P$,$P$)-**85** (0.047 mmol, 40 mg) in 5 mL of degazed anhydrous toluene was added bis(4-nitrophenyl) hydrogen phosphate **97** (0.007 mmol, 2.4 mg), diethoxy(methyl)silane (0.188 mmol, 0.021 mL). The mixture was stirred overnight at 90°C, before being extract twice with degazed $CHCl_3$, The organic phase was dried with $MgSO_4$ and evaporated under argon. The crude phosphane, checked by $^{31}$P-NMR (δ=–0.35 ppm in $CDCl_3$), was used for the next step without further purification. Thioethanol (0.141 mmoli, 0.014 mL) was added a 0°C to a solution of $NaAuCl_4(H_2O)_2$ (0.056 mmoli, 22.5 mg) in 5 mL of degazed water. The mixture turned from yellow to colorless. A solution of the phosphine in 2 mL of degazed $CHCl_3$ was added to this mixture which was stirred then for 10 minutes at 0°C and 20 minutes at room temperature. The reaction mixture was extracted with AcOEt, washed with water, dried on $MgSO_4$ and concentrated *in vacuo.* The residue was purified by flash chromatography on silica gel (gradient heptane 100 to heptane 80/ AcOEt 20 in 20 min) to obtain ($S_P$,$P$)-**98** (20 mg, 40% yield). $R_f$ = 0.5 in 10% EtOAc / Heptane; $^1$H NMR (300 MHz, $CDCl_3$) δ 8.52 (d, *J* = 8.6 Hz, 1H), 8.23 (d, *J* = 8.6 Hz, 1H), 8.01 (d, *J* = 8.6 Hz, 1H), 7.81 (m, 3H), 7.70 (d, J = 26.2 Hz, H), 7.55-7.30 (m, 3H), 6.69 (d, *J* = 5.5 Hz, 1H), 6.23 (d, *J* = 5.5 Hz, 1H), 3.40-2.9 (m, 8H), 2.14-1.71 (m, 8H), 1.43-1.04 (m, 16H), 1.02-0.77 (m, 9H), 0.34 ppm (t, *J* = 7.2 Hz, 6H); $^{13}$C NMR (75 Hz, $CDCl_3$) δ 141.5 (d, *J* = 15.6 Hz, C), 139.9 (C), 138.6 (C), 138.0 (C), 137.1 (d, *J* = 8.69 Hz, CH), 135.8 (C), 135.0 (C), 134.9 (C), 134.3 (C), 132.5 (C), 131.8 (C), 131.5 (C), 130.8 (C), 130.4 (C), 130.2 (d, *J* = 12.5 Hz, CH), 129.2 (2CH), 128.9 (CH), 128.4 (CH), 126.8 (CH), 126.6 (CH), 124.9 (CH), 124.5 (CH), 124.4 (CH), 122.3 (C), 120.7 (d, *J* = 6.0 Hz, CH), 117.4 (CH), 43.3 (CH), 39.6 (d, *J* = 29.1 Hz, CH), 35.5 ($CH_2$), 34.4 ($CH_2$), 33.4 ($CH_2$), 32.8 (d, *J* = 10.1 Hz, CH), 31.1 ($CH_2$), 29.7 (CH), 29.5 (CH), 24.7 ($CH_2$), 23.8 ($CH_2$), 23.5 ($CH_2$), 23.4 ($CH_2$), 21.9 ($CH_3$), 20.3 ($CH_3$), 16.5 ($CH_3$), 14.9 ($CH_3$), 14.8 ($CH_3$), 14.7 ($CH_3$), 14.6 ppm ($CH_3$); $^{31}$P (121 MHz, $CDCl_3$) δ 25 ppm; $[\alpha]_D^{25}$= +1080 (c

= 1, $CHCl_3$), IR: 2956, 2926, 2868, 1730, 1547, 1457, 1387, 1368, 1317, 1214, 1197, 1181, 1160, 1091, 1032, 897, 829, 788, 756, 708, 687.

**Synthesis of bromide ($R_P$,*P*)-103**

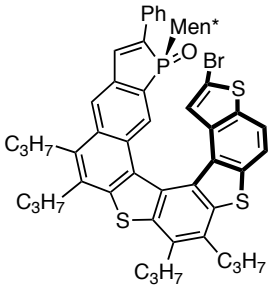


NBS (2.1 mmol, 21 mg) was added to a solution of ($R_P$,*P*)-**85** (0.058 mmol, 50 mg) in $CHCl_3$ (4 mL), and the reaction mixture was then stirred for 2 h at room temperature. The reaction mixture was quenched with a saturated aqueous $NH_4Cl$ solution, and the acqueous phase was extracted with EtOAc. The combined organic phases were washed with water and brine, dried over $MgSO_4$, and concentrated *in vacuo*. The residue was then purified by flash chromatography on silica gel with a heptane to afford the desired product ($R_P$,*P*)-**103** as a pale yellowish powder (45 mg, 83%). $^1$H NMR (300 MHz, $CDCl_3$) δ 8.07 (d, *J* = 9.7 Hz, 1H), 7.96 (m, 2H), 7.73 (d, J = 8.2 Hz, 2H), 7.42-7.29 (m, 4H), 6.62 (brs, 1H), 3.33-3.07 (m, 8H), 1.96- 1.83 (m, 8H), 1.66-1.53 (m, 2H), 1.34-1.14 (m, 16H), 0.87-0.45 (m, 13H); $^{13}$C NMR (75 MHz, $CDCl_3$) δ 140.5 (d, i = 21.7 Hz, C), 139.1 (C), 138.4 (CH), 138.2 (CH), 137.7 (d, *J* = 19.0 Hz, C), 136.8 (C), 135.9 (C), 135.0 (C), 134.4 (C), 132.6 (C), 132.5 (C), 131.5 (C), 131.0 (C), 128.8 (2CH), 128.7 (CH), 128.4 (C), 128.1 (C), 127.2 (d, *J* =6.1 Hz, C), 126.5 (d, *J* = 4.8 Hz, CH), 120.9 (bs, CH), 119.6 (CH), 119.1 (bs, CH), 113.2 (Cq), 42.6 (CH), 37.8 (d, *J* = 64.5 Hz, CH), 35.6 (CH2), 34.4 (2CH2), 34.2 (CH2), 33.9 (CH2), 32.6 (d, *J* = 5.2 Hz, CH), 30.8 (CH2), 27.2 (CH), 27.2 (CH3), 25.1 (CH2), 25.0 (CH2), 24.9 (CH2), 23.6 (2CH2), 23.3 (CH2), 23.1 (CH3), 21.5 (CH3), 15.8 (CH3), 14.8 (2CH3), 14.7 (2CH3), 14.78 ppm (2CH3); $^{31}$P (121 MHz, $CDCl_3$) δ 58.9 ppm.

**Synthesis of ($R_P$,*P*)-104a**

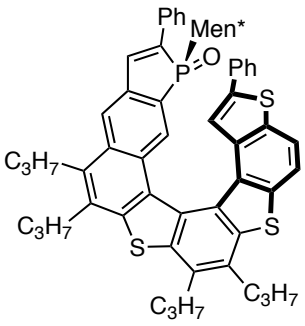


To a solution of phenylboronic acid (0.096 mmol, 12 mg) in 3 mL of THF were added ($R_P$,*P*)-**103** (0.096 mmol, 45 mg), $Pd(PPh_3)_4$ (0.0024 mmol, 3 mg), 3 mL of a solution of $Na_2CO_3$ 0.45 M in water and 1.5 mL of EtOH. The reaction mixture was stirred for 2h at 85°C. The crude mixture was extracted with EtOAc, washed with water and brine, dried over MgSO4 and concentrated *in vacuo*. The residue was purified by flash chromatography on silica gel with an heptane/ethyl acetate gradient (0% to 10% EtOAc) to afford the desired compound ($R_P$,*P*)-**104a** as a pale yellow solid (45 mg, 99% ). $^1$H NMR (300 MHz, $CDCl_3$) δ 8.23 (d, *J* = 10.0 Hz, 1H), 7.93 (d, *J* = 8.5 Hz, 1H), 7.86 (brs, 1H), 7.80 (d, *J* = 8.5 Hz, 1H), 7.69 (d, *J* = 7.4 Hz, 2H), 7.33-7.27 (m, 4H), 7.15 (m, 4H), 6.91 (brs, 1H), 6.86 (d, *J* = 6.3 Hz, 2H), 3.27-3.10 (m, 8H), 2.03-1.85 (m, 8H), 1.56 (m, 6H), 1.36-1.12 (m, 16H), 0.90-0.45 (m, 13H); $^{13}$C NMR (75 MHz, $CDCl_3$) δ 141.8 (C), 140.5 (C), 139.0 (C), 138.3 (CH), 138.2 (CH), 138.0 (CH), 137.9(C), 135.6 (d, *J* =10.9 Hz, C), 135.4 (C), 134.5 (C), 134.0 (C), 132.6 (C), 132.3 (C), 131.9 (C), 130.2 (C), 130.0 (C), 129.6 (C), 128.8 (2CH), 128.7 (2CH), 128.5 (CH), 127.8 (CH), 127.5 (d, J =11.2 Hz, CH), 126.6 (d, J = 4.3 Hz, CH), 126.0 (2CH), 121.7 (CH), 120.5 (bs, CH), 120.1 (bs, CH), 119.4 (CH), 43.5 (CH), 39.6 (d, *J* = 28.5 Hz, CH), 35.7 (CH2), 34.6 (CH2), 34.0 (CH2), 33.9 (CH2), 33.6 (CH2), 33.0 (CH2), 32.9 (CH2), 31.3 (CH2), 29.9 (CH), 29.7, 29.5, 26.5 (d, *J* = 7.5 Hz,), 25.2, 24.7 (d, J = 11.3 Hz, CH2), 23.6 (CH2), 23.57 (CH2), 23.5 (CH2), 22.8 (CH2), 22.0 (CH3), 20.4 (CH3), 16.7 (CH3), 15.1 (CH3), 14.9 (CH3), 14.8 (CH3) ppm; $^{31}$P (121 MHz, $CDCl_3$) δ 58.9 ppm.

**Synthesis of gold complex ($S_P$,$P$)-105a**

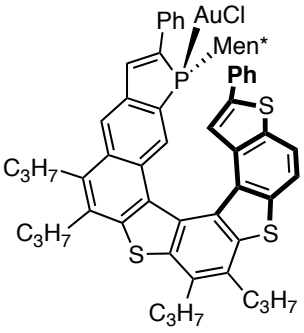


To ($R_P$,$P$)-**104a** (0.04 mmol, 40 mg) in 1 mL of degazed anhydrous toluene was added bis(4-nitrophenyl) hydrogen phosphate **97** (0.006 mmol, 2.2 mg), phenylsilane (0.129 mmol, 0.016 mL). The mixture was stirred 2h at 100°C, before being extract twice with degazed $CH_2Cl_2$, The organic phase was dried with $MgSO_4$ and evaporated under argon. The crude phosphine checked by $^{31}$P-NMR (δ=–0.35 ppm in $CDCl_3$), was used for the next step without further purification. To a solution of the phosphine in 2 mL of degazed $CH_2Cl_2$ was added $AuSMe_2Cl$ (0.04mmoli, 12mg) and the mixture was stirred for 20 minutes at room temperature. The reaction mixture was extracted with AcOEt, washed with water, dried on $MgSO_4$ and concentrated *in vacuo.* The residue was purified by flash chromatography on silica gel (gradient heptane 100 to heptane 80/ AcOEt 20 in 20 min) to obtain ($S_P$,$P$)-**105a** (35 mg, 76% yield). $R_f$ = 0.5 in 10% EtOAc / Heptane; $^1$H NMR (500 MHz, $CDCl_3$) δ 8.47 (d, *J* = 8.5 Hz, 1H), 8.07 (d, *J* = 8.5 Hz, 1H), 7.98 (d, *J* = 8.5 Hz, 1H), 7.88 (d, *J* = 9.5 Hz, 1H), 7.81 (d, *J* = 7.7 Hz, 2H), 7.57 (d, *J* = 26.3 Hz, 1H), 7.41 (m, 2H), 7.32 (m, 1H), 7.12 (m, 3H), 6.83 (d, *J* = 7.2 Hz, 2H), 6.45 (s, 1H), 3.35-3.11 (m, 8H), 2.07-1.84 (m, 8H), 1.65 (m, 2H), 1.45-1.08 (m, 14H), 0.96-0.66 (m, 7H), 0.35 (m, 6H), 0.21 (m, 1H), –0.33 ppm (m, 1H); $^{13}$C NMR (75 Hz, $CDCl_3$) δ 142.7 (C), 141.8 (d, *J* = 15.6 Hz, C), 140.7 (C), 140.2 (C), 138.9 (C), 138.2 (d, *J* = 26.2 Hz, C), 137.7 (C), 137.2 (d, *J* = 8.8 Hz, CH), 136.2 (C), 135.9 (C), 135.2 (C), 134.7 (C), 134.2 (C), 133.7 (d, *J* = 12.5 Hz, C), 132.7 (C), 132.0 (C), 131.8 (C), 131.0 (C), 130.5 (C), 129.9 (d, *J* = 12.8 Hz, CH), 129.3 (2CH), 129.0 (CH), 128.5 (CH), 128.4 (2CH), 128.2 (C), 127.5 (CH), 126.9 (CH), 126.8 (CH), 126.3 (2CH), 124.6 (CH), 123.5 (d, *J* = 61.0 Hz, C), 121.5 (CH), 120.7 (d, *J* = 6.2 Hz, CH), 117.6 (CH), 43.5 (CH), 39.6 (d, *J* = 29.0 Hz, CH), 35.7 ($CH_2$), 34.6 ($CH_2$), 33.9 ($CH_2$), 32.9 (d, *J* = 11.1 Hz, CH), 31.3 ($CH_2$), 29.9 (CH), 29.7 (CH), 25.2 ($CH_2$), 24.7 (d, *J* = 11.4 Hz, $CH_2$), 23.6 ($CH_2$), 23.65 ($CH_2$), 23.5 ($CH_2$), 22.0 ($CH_3$), 20.5 ($CH_3$), 16.7 ($CH_3$), 15.2 ($CH_3$), 15.0 ($CH_3$), 14.8 ppm ($CH_3$); $^{31}$P (121 MHz, $CDCl_3$) δ 25 ppm; $[\alpha]_D^{25}$= +1756 (c = 1, $CHCl_3$).

*Typical procedure for the gold-catalyzed cycloisomerization reactions.* [63,64,67]

The enyne substrate (0.1 mmol) and AgX (8 mol %) were added to a solution of the gold(I)complex (4 mol %) in toluene under argon. The mixture was stirred at the proper temperature, and the reaction was monitored by $^1$H NMR. The solvent was removed under reduced pressure, and the final product was purified by flash chromatography. Enantiomeric excesses have been measured by chiral HPLC.

**Synthesis of (*Z*)-2,2'-(Oct-4-ene-4,5-diyl)dithiophene (*Z*)-107a**

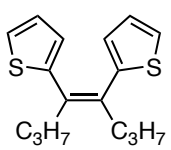


To a solution of ketone **106** (24 mmol, 3.701 g) in dry THF (110 mL) at – 20 °C, $TiCl_4$ (5.4 mL, 28.7 mmol, 1.2 equiv) was added dropwise in 10 min. After 30 min at – 20 °C, Zn powder (3.90 g, 60 mmol, 2.5 equiv) was added in 3 portions in 10 min, and then the mixture was refluxed for 3 h. After this time, the mixture was cooled to room temperature, and ice-water (40 mL) along with an aqueous solution of HCl (1N, 40 mL) was added under vigorously stirring. THF was removed under reduced pressure, and the crude

material was taken up with $CH_2Cl_2$ (50 mL). The aqueous phase was extracted into $CH_2Cl_2$ (4 × 20 mL), and the combined organic layers were dried on $Na_2SO_4$, concentrated under reduced pressure. The crude product was purified by column chromatography on silica gel (hexane) to give (*Z*)-**107a** (2.45 g, 8.87 mmol, 74%) as yellow oil.
$^1$H NMR (300 MHz, $CDCl_3$): $\delta$ 7.18 (m, 2 H), 6.90 (m, 2 H), 6.78 (m, 2 H), 2.60 (m, 4 H), 1.53 (m, 4 H), 1.02 (m, 6 H) ppm. $^{13}$C NMR (75 MHz, $CDCl_3$): $\delta$ 145.1, 133.0, 126.6, 126.4, 125.0, 37.7, 21.9, 14.2 ppm. MS-EI: *m/z* (%) 276 (65, $[M]^+$), 247 (60), 97 (100). HRMS-EI: *m/z* calcd for $C_{16}H_{20}S_2$ 276.0939, found 276.0948.

**Synthesis of (*Z*)-5,5'-(Oct-4-ene-4,5-diyl)bis(2-bromothiophene) (*Z*)-107b**

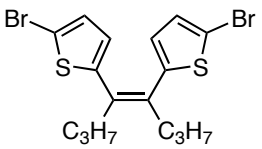


To a solution of (*Z*)-**107a** (0.200 g, 0.723 mmol) in dry DMF (2 mL) was added *N*-bromosuccinimide (0.270 g, 1.52 mmol, 2.1 equiv) at 0 °C. The mixture was stirred in the dark at 0 °C and the progress of the reaction was monitored by TLC (hexane). After 2 h, the mixture was quenched with water (10 mL), and the aqueous phase was extracted into $CH_2Cl_2$ (3 × 10 mL). The organic phase was washed with water, and dried with $Na_2SO_4$. The solvent was removed at reduced pressure, and the residue was purified by chromatography on silica gel (hexane) to give (*Z*)-**107b** (0.201 g; 0.463 mmol, 64%) as pale yellow oil. $^1$H NMR (300 MHz, $CDCl_3$): $\delta$ 6.82 (d, *J* = 3.7 Hz, 2 H), 6.50 (d, *J* = 3.7 Hz, 2 H), 2.44 (m, 4 H), 1.44 (m, 4 H), 0.93 (t, *J* = 7.3 Hz, 6 H) ppm. $^{13}$C NMR (75 MHz, $CDCl_3$): $\delta$ 145.9, 133.0, 129.4, 127.1, 111.8, 37.2, 21.7, 14.0 ppm. MS-EI: *m/z* (%) 434 (100, $[M]^+$), 326 (52), 297 (18), 216 (20). HRMS-EI: *m/z* calcd for $C_{16}H_{18}Br_2S_2$ 431.9217, found 431.9224.

**Synthesis of (*Z*)-5,5'-(Oct-4-ene-4,5-diyl)bis(2-iodothiophene) (*Z*)-107c**

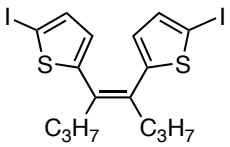


To a solution of (*Z*)-**107a** (0.200 g, 0.723 mmol) in dry THF (5 mL) at – 78 °C was added dropwise a solution of *n*BuLi (1.6 M in hexane, 1.81 mL, 2.89 mmol, 4 equiv). The solution was stirred for 10 min at – 78 °C and 30 min at room temperature. The resulting yellow suspension was cooled to – 78 °C and a solution of $I_2$ (0.734 g, 2.89 mmol, 4 equiv) in dry THF (8 mL) was added dropwise. The mixture was stirred for 30 min at – 78 °C, and then warmed to room temperature. A saturated aqueous solution of $Na_2S_2O_3$ (20 mL) was added to quench the reaction, and the aqueous phase was extracted with $CH_2Cl_2$ (3 × 20 mL). The combined organic layers were washed with water, dried with $Na_2SO_4$, and concentrated under reduced pressure. The residue was purified by chromatography on silica gel (hexane) to give (*Z*)-**107c** (0.332 g, 0.628 mmol, 87%) as a yellow oil.
$^1$H NMR (300 MHz, $CDCl_3$): $\delta$ 7.00 (d, *J* = 3.7 Hz, 2 H), 6.40 (d, *J* = 3.7 Hz, 2 H), 2.44 (m, 4 H), 1.43 (m, 4 H), 0.93 (t, *J* = 7.3 Hz, 6 H) ppm. $^{13}$C NMR (75 MHz, $CDCl_3$): $\delta$ 150.8, 136.6, 133.2, 128.5, 73.1, 37.5, 21.8, 14.1 ppm. MS-EI: *m/z* (%) 528 (100, $[M]^+$), 402 (68), 372 (75), 246 (48), 203 (45), 171 (58). HRMS-EI: *m/z* calcd for $C_{16}H_{18}I_2S_2$ 527.8939, found 527.8927.

**Synthesis of (*Z*)-5,5'-(Oct-4-ene-4,5-diyl)bis(2-heptylthiophene) (*Z*)-107d**

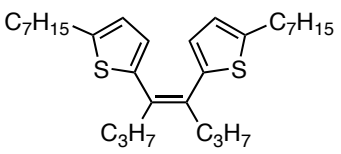

To a solution of (*Z*)-**107a** (0.200 g, 0.723 mmol) in dry THF (5 mL) at −78 °C was added dropwise a solution of *n*BuLi (1.6 M in hexane, 1.81 mL, 2.89 mmol, 4 equiv). The solution was stirred for 10 min at – 78 °C and 30 min at room temperature. The resulting yellow suspension was cooled to – 78 °C and treated with 1-bromoheptane (0.454 mL, 2.89 mmol, 4 equiv). The mixture was stirred for 30 min at – 78 °C, and then warmed to room temperature. After 4 h, the reaction was quenched with water (20 mL), and the aqueous phase was extracted with $CH_2Cl_2$ (3 × 20 mL). The combined organic layers were washed with water, dried with $Na_2SO_4$, and concentrated under reduced pressure. The residue was purified by column chromatography on silica gel (hexane) to afford (*Z*)-**107d** (0.175 g, 0.370 mmol, 51%) as yellow oil. $^1$H NMR (300 MHz, $CDCl_3$): $\delta$ 6.51 (m, 4 H), 2.69 (m, 4 H), 2.46 (m, 4 H), 1.43 (m, 24 H), 0.91 (m, 12 H) ppm. $^{13}$C NMR (75 MHz, $CDCl_3$): $\delta$ 145.5, 142.7, 132.6, 126.2, 123.4, 37.5, 32.1, 32.0, 31.8, 30.2, 29.9, 29.8, 29.5, 29.2, 29.1, 22.9, 22.1, 14.2 ppm. MS-EI: *m/z* (%) 472 (100, $[M]^+$), 443 (15). HRMS-EI: *m/z* calcd for $C_{30}H_{48}S_2$ 472.3197, found 472.3160.

**Synthesis of (*Z*)-Diethyl 5,5'-(oct-4-ene-4,5-diyl)bis(thiophene-2-carboxylate) (*Z*)-107e**

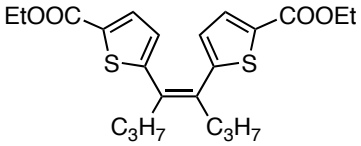

To a solution of (*Z*)-**107a** (0.200 g, 0.723 mmol) in dry THF (5 mL) at – 78 °C was added dropwise a solution of *n*BuLi (1.6 M in hexane, 1.81 mL, 2.89 mmol, 4 equiv). The solution was stirred for 10 min at – 78 °C and 30 min at room temperature. The resulting yellow suspension was cooled to – 78 °C, and treated with ethyl chloroformate (0.276 mL, 2.89 mmol, 4 equiv). The mixture was stirred for 30 min at – 78 °C and then warmed to room temperature. After 5 h, the reaction was quenched with water (20 mL), and the aqueous phase was extracted with $CH_2Cl_2$ (3 × 20 mL). The combined organic layers were washed with water, dried with $Na_2SO_4$, and concentrated under reduced pressure. The residue was purified by column chromatography on silica gel (hexane:AcOEt, gradient 100:0 to 90:10) to afford (*Z*)-**107e** (0.230 g, 0.547 mmol, 76%) as a pale orange oil. $^1$H NMR (300 MHz, $CDCl_3$): $\delta$ 7.50 (d, *J* = 3.7 Hz, 2 H), 6.62 (d, *J* = 3.7 Hz, 2 H), 4.30 (q, *J* = 7.1 Hz, 4 H), 2.50 (m, 4 H), 1.43 (m, 4 H), 1.34 (t, *J* = 7.1 Hz, 6 H), 0.94 (t, *J* = 7.3 Hz, 6 H) ppm. $^{13}$C NMR (75 MHz, $CDCl_3$): $\delta$ 162.2, 151.8, 134.3 (2 C), 133.0, 127.7, 61.0, 37.6, 21.6, 14.3, 13.9 ppm. IR (*neat*): 1707 (stretching C=O) cm$^{-1}$. MS-EI: *m/z* (%) 420 (100, $[M]^+$), 391 (21), 375 (10), 318 (18).HRMS-EI: *m/z* calcd for $C_{22}H_{28}O_4S_2$ 420.1429, found 420.1427.

**Synthesis of (*Z*)-5,5'-(Oct-4-ene-4,5-diyl)bis(thiophene-2-carbaldehyde) (*Z*)-107f**

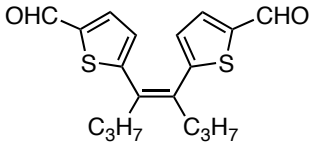

To a solution of (*Z*)-**107a** (0.200 g, 0.723 mmol) in dry THF (5 mL) at – 78 °C was added dropwise a solution of *n*BuLi (1.6 M in hexane, 1.81 mL, 2.89 mmol, 4 equiv). The solution was stirred for 10 min at – 78 °C and 30 min at room temperature. The resulting yellow suspension was cooled to – 78 °C, and treated with DMF (0.223 mL, 2.89 mmol, 4 equiv). The mixture was stirred for 30 min at – 78 °C, and then warmed to room temperature. After 5 h, the reaction was

quenched with water (20 mL), and the aqueous phase was extracted with $CH_2Cl_2$ (3 × 20 mL). The combined organic layers were washed with water, dried with $Na_2SO_4$, and concentrated under reduced pressure. The residue was purified by column chromatography on silica gel (hexane:AcOEt, gradient 100:0 to 80:20) to afford (*Z*)-**107f** (0.220 g, 0.662 mmol, 84%) as an orange oil. $^1$H NMR (300 MHz, $CDCl_3$): $\delta$ 9.78 (s, 2 H), 7.49 (d, *J* = 3.0 Hz, 2 H), 6.76 (d, *J* = 3.0 Hz, 2 H), 2.55 (m, 4 H), 1.44 (m, 4 H), 0.95 (t, *J* = 7.3 Hz, 6 H) ppm. $^{13}$C NMR (75 MHz, $CDCl_3$): $\delta$ 182.8, 154.8, 143.2, 136.3, 135.1, 128.5, 37.7, 21.7, 14.0 ppm. IR (*neat*): 1665 (stretching C=O) cm$^{-1}$. MS-EI: *m/z* (%) 332 (85, $[M]^+$), 303 (20), 275 (33), 134 (100). HRMS-EI: *m/z* calcd for $C_{18}H_{20}O_2S_2$ 332.0905, found 332.0921.

**General Procedure for the $FeCl_3$-mediated Cyclization of Alkenes 108b–f**.

To a solution of the alkene (*Z*)-**107b–f** (0.25 mmol) in dry $CH_2Cl_2$ (20 mL), constantly sparged with nitrogen at the proper temperature (0, 25, 40 or 80 °C), $FeCl_3$ (1 mmol, 4 eq.) was added. The resulting mixture was stirred under a nitrogen purge for 30 min, and then treated with methanol (*ca*. 50 mL) for 1h. The solvents were removed under reduced pressure, and the residue was purified by flash chromatography on silica gel.

**Synthesis of 2,7-Dibromo-4,5-dipropylbenzo[1,2-*b*:4,3-*b*′]dithiophene 108b**

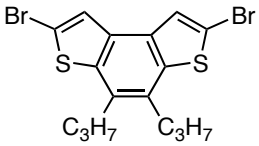


Following the general procedure of the Table 12 entry 5, (*Z*)-**107b** (0.108 g, 0.250 mmol) was reacted with $FeCl_3$ (0.162 g, 1 mmol, 4 eq) at 0 °C for 30 min. After the treatment with MeOH, the solvents were removed under vacuum, and the residue was purified by column chromatography on silica gel (hexane) to afford **108b** (85 mg, 0.197 mmol, 79%) as a colourless solid. Mp 94-95 °C (hexane). $^1$H NMR (300 MHz, $CDCl_3$): $\delta$ 7.54 (s, 2 H), 2.85 (t, *J* = 8.0 Hz, 4 H), 1.74 (m, 4 H), 1.07 (t, *J* = 7.3 Hz, 6 H) ppm. $^{13}$C NMR (75 MHz, $CDCl_3$): $\delta$ 140.2, 131.8, 130.0, 125.2, 114.3, 34.4, 23.1, 14.7 ppm. MS-EI: *m/z* (%) 432 (100, $[M]^+$), 403 (65), 375 (25), 322 (42). HRMS-EI: *m/z* calcd for $C_{16}H_{16}Br_2S_2$ 429.9060, found 429.9072.

**Synthesis of 2,7-Diiodo-4,5-dipropylbenzo[1,2-*b*:4,3-*b*′]dithiophene 108c**

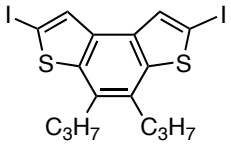


To a suspension of $FeCl_3$ (0.162 g, 1 mmol, 4 eq) in $CH_2Cl_2$ (20 mL) at 40 °C, a solution of the alkene (*Z*)-**107c** (0.132 g, 0.250 mmol) in $CH_2Cl_2$ (5 mL) was added dropwise under a nitrogen purge. The resulting mixture was stirred for 30 min, and then treated with methanol (ca. 50 mL) for 1h. The solvents were removed under reduced pressure, and the residue was purified by flash chromatography on silica gel (hexane) to afford **108c** (97 mg, 0.185 mmol, 74%) as a colourless solid.

Mp 117-118 °C (hexane). $^1$H NMR (300 MHz, $CDCl_3$): $\delta$ 7.77 (s, 2 H), 2.87 (m, 4 H), 1.72 (m, 4 H), 1.06 (t, *J* = 7.3 Hz, 6 H) ppm. $^{13}$C NMR (75 MHz, $CDCl_3$): $\delta$ 143.8, 132.6, 132.3, 129.8, 76.6, 34.4, 23.1, 14.7 ppm. MS-EI: *m/z* (%) 526 (100, $[M]^+$), 497 (60), 469 (21), 370 (50), 227 (37). HRMS-EI: *m/z* calcd for $C_{16}H_{16}I_2S_2$ 525.8783, found 525.8773.

**Synthesis of 2,7-Diheptyl-4,5-dipropylbenzo[1,2-*b*:4,3-*b*′]dithiophene 108d**

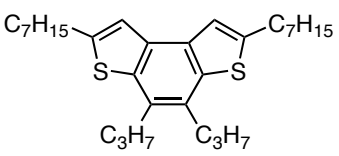

Following the general procedure of the Table 13, (*Z*)-**107d** (0.118 g, 0.250 mmol) was reacted with $FeCl_3$ (0.162 g, 1 mmol, 4 eq) at 0 °C for 30 min. After the treatment with MeOH, the solvents were removed under vacuum, and the residue was purified by column chromatography on silica gel (hexane) to afford **108d** (77 mg, 0.165 mmol, 66%) as a pale yellow oil. $^1$H NMR (300 MHz, $CH_2Cl_2$): $\delta$ 7.28 (s, 2 H), 2.92 (m, 8 H), 1.75 (m, 8 H), 1.35 (m, 16 H), 1.06 (t, *J* = 7.3 Hz, 6 H), 0.92 (m, 6 H) ppm. $^{13}$C NMR (75 MHz, $CDCl_3$): $\delta$ 145.4, 137.7, 132.7, 129.2, 119.2, 34.5, 32.1, 31.9, 31.6, 31.1, 29.9, 29.8, 29.5, 29.3, 29.2, 23.3, 22.85, 22.81, 14.8, 14.3, 14.2 ppm. MS-EI: *m/z* (%) 470 (100, $[M]^+$), 441 (12), 385 (20). HRMS-EI: *m/z* calcd for $C_{30}H_{46}S_2$ 470.3041, found 470.3027.

**Synthesis of diethyl 4,5-dipropylbenzo[1,2-*b*:4,3-*b'*]dithiophene-2,7-dicarboxylate 108e**

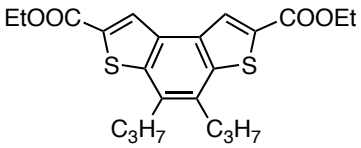

Following the general procedure of the Table 13, (*Z*)-**107e** (0.105 g, 0.250 mmol) was reacted with $FeCl_3$ (0.162 g, 1 mmol, 4 eq) at 80 °C for 30 min. After the treatment with MeOH, the solvents were removed under vacuum, and the residue was purified by column chromatography on silica gel (hexane/AcOEt, 9:1) to afford **108e** (94 mg, 0.225 mmol, 89%) as a pale yellow solid. Mp 179-180 °C (hexane/$CH_2Cl_2$). $^1$H NMR (300 MHz, $CDCl_3$): $\delta$ 8.39 (s, 2 H), 4.44 (q, *J* = 7.1 Hz, 4 H), 2.98 (m, 4 H), 1.79 (m, 4 H), 1.45 (t, *J* = 7.1 Hz, 6 H), 1.11 (t, *J* = 7.3 Hz, 6 H) ppm. $^{13}$C NMR (75 MHz, $CDCl_3$): $\delta$ 162.9, 142.6, 133.3, 133.2, 133.1, 128.5, 61.8, 34.4, 23.1, 14.8, 14.5 ppm. IR (*neat*): 1719 (stretching C=O) cm$^{-1}$. MS-EI: *m/z* (%) 418 (100, $[M]^+$), 389 (22), 361 (15). HRMS-EI: *m/z* calcd for $C_{22}H_{26}O_4S_2$ 418.1272, found 418.1280.

**Synthesis of 4,5-Dipropylbenzo[1,2-*b*:4,3-*b*′]dithiophene-2,7-dicarbaldehyde 108f**

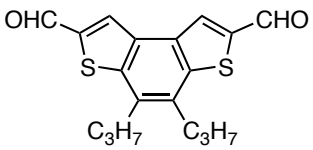

Following the general procedure of the Table 13, (*Z*)-**107f** (0.105 g, 0.250 mmol) was reacted with $FeCl_3$ (0.162 g, 1 mmol, 4 eq) at 80 °C for 30 min. After the treatment with MeOH, the solvents were removed under vacuum, and the residue was purified by column chromatography on silica gel (hexane/AcOEt, 8:2) to afford **108f** (94 mg, 0.225 mmol, 40%) as a yellow solid. Mp 145-147 °C (hexane/$CH_2Cl_2$). $^1$H NMR (300 MHz, $CDCl_3$): $\delta$ 10.2 (s, 2 H), 8.37 (s, 2 H), 3.00 (m, 4 H), 1.79 (m, 4 H), 1.11 (t, *J* = 7.3 Hz, 6 H) ppm. $^{13}$C NMR (75 MHz, $CDCl_3$): $\delta$ 184.2, 143.9, 143.0, 135.1, 133.4, 131.5, 34.5, 23.1, 14.7 ppm. IR (*neat*): 1672 (stretching C=O) cm$^{-1}$. MS-EI: *m/z* (%) 330 (100, $[M]^+$), 301 (83), 273 (36). HRMS-EI: *m/z* calcd for $C_{18}H_{18}O_2S_2$ 330.0714, found 330.0724.

**Synthesis of 1,2,7-Tribromo-4,5-dipropylbenzo[1,2-*b*:4,3-*b*′]dithiophene 109**.

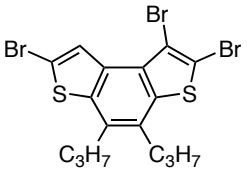

To a solution of **108b** (50 mg, 0.115 mmol) in dry DCE (20 mL) at 80 °C, $FeCl_3$ (0.46 mmol, 4 eq) was added. The resulting mixture was stirred under nitrogen purge for 30', and then treated with methanol (ca. 50 mL). The solvents were removed under reduced pressure, and the residue was

purified by flash chromatography on silica gel (hexane) to afford **109** (23 mg, 0.046 mmol, 40%) as a colourless solid. Mp 128-129 °C (MeCN/DCM). $^{1}$H NMR (300 MHz, $CDCl_3$): $\delta$ 8.60 (s, 1 H), 2.87 (m, 4 H), 1.72 (m, 4 H), 1.07 (m, 6 H) ppm. $^{13}$C NMR (75 MHz, $CDCl_3$): $\delta$ 142.0, 138.6, 131.5, 131.0, 129.9, 128.8, 124.9, 114.0, 113.6, 110.5, 34.3, 33.7, 23.1, 23.0, 14.7 (2 C) ppm. MS -EI: *m/z* (%) 511 (100, $[M]^+$), 480 (55), 454 (35), 402 (65). HRMS-EI: *m/z* calcd for $C_{16}H_{15}Br_3S_2$ 507.8165, found 507.8164.

**Synthesis of 4,5-Dipropylbenzo[1,2-*b*:4,3-*b*′]dithiophene 108a**

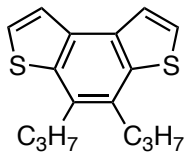


A solution of *n*BuLi (1.6 M in hexane, 0.181 mL, 0.290 mmol, 2 eq) was added dropwise to a stirring solution of **108b** (40 mg, 0.145 mmol) in dry THF (5 mL) at 0 °C under a nitrogen atmosphere. The resulting mixture was stirred for 10 min at 0 °C and then warmed to room temperature. After 2 h at room temperature, the solution was cooled at 0 °C and treated with MeOH (0.5 mL). After 10 min at 0 °C, the mixture was warmed at room temperature, and slowly added to a saturated aqueous solution of $NH_4Cl$ (10 mL). The aqueous phase was extracted with $CH_2Cl_2$ (3 × 10 mL), and the organic phases were dried with $Na_2SO_4$, and concentrated under reduced pressure. The crude product was purified by chromatography on silica gel (hexane) to give **108a** (35.3 mg, 0.129 mmol, 89%) as a colorless solid. Mp 65-66 °C (pentane). $^{1}$H NMR (300 MHz, $CDCl_3$): $\delta$ 7.68 (d, *J* = 5.4 Hz, 2 H), 7.48 (d, *J* = 5.4 Hz, 2 H), 3.01 (m, 4 H), 1.80 (m, 4 H), 1.11 (t, *J* = 7.3 Hz, 6 H) ppm. $^{13}$C NMR (75 MHz, $CDCl_3$): $\delta$ 138.9, 132.9, 130.3, 125.0, 122.5, 34.5, 23.3, 14.8 ppm. MS-EI: *m/z* (%) 274 (90, $[M]^+$), 245 (100), 229 (17). HRMS-EI: *m/z* calcd for $C_{16}H_{18}S_2$ 274.0850, found 274.0832. All spectroscopical data were in agreement with those previously reported.[62]

**Synthesis of 1-Bromo-4,5-dipropylbenzo[1,2-*b*:4,3-*b*′]dithiophene 110**.

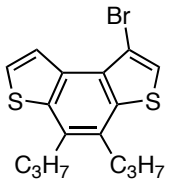


A solution of *n*BuLi (1.5 M in hexane, 0.430 mL, 0.646 mmol, 2.2 eq) was added dropwise to a stirring solution of **109** (150 mg, 0.294 mmol) in dry THF (10 mL) at – 78 °C under a nitrogen atmosphere. The resulting mixture was stirred for 10 min at – 78 °C, and then warmed to room temperature. After 40 min at room temperature, the solution was cooled at – 78 °C, and treated with MeOH (1.5 mL). After 30 min at – 78 °C, the mixture was warmed at room temperature, and slowly added to a saturated aqueous solution of $NH_4Cl$ (10 mL). The aqueous phase was extracted with $CH_2Cl_2$ (3 × 10 mL), and the organic phases were dried with $Na_2SO_4$, and concentrated under reduced pressure. The crude product was purified by chromatography on silica gel (hexane) to give **110** (71 mg, 0.213 mmol, 70%) as a colourless solid. Mp 72-73 °C (hexane). $^{1}$H NMR (300 MHz, $CDCl_3$): $\delta$ 8.67 (d, *J* = 5.6 Hz, 1 H), 7.53 (d, *J* = 5.6 Hz, 1 H), 7.46 (s, 1 H), 2.99 (m, 4 H), 1.78 (m, 4 H), 1.10 (m, 6 H) ppm. $^{13}$C NMR (75 MHz, $CDCl_3$): $\delta$ 140.7, 138.5, 132.2, 131.6, 130.2, 129.7, 124.8, 122.8, 122.3, 106.6, 34.6, 33.6, 23.3, 23.2, 14.79, 14.77 ppm. MS-EI: *m/z* (%) 352 (100, $[M]^+$), 323 (53), 295 (20), 244 (75), 227 (24). HRMS-EI: *m/z* calcd for $C_{16}H_{17}S_2Br$ 351.9955, found 352.0005.

**Synthesis of (*Z*)-2,2'-(1,4-dicyclohexylbut-2-ene-2,3-diyl)dithiophene (*Z*)-115**

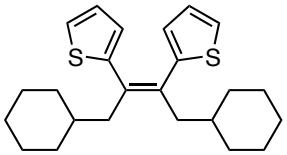

To a solution of **113** (24 mmol) in dry THF (110 mL) at – 20 °C, $TiCl_4$ (28.7 mmol, 1.2 equiv) was added dropwise in 10 min. After 30 min at – 20 °C, Zn powder (60 mmol, 2.5 equiv) was added in 3 portions in 10 min, and then the mixture was refluxed for 3 h. After this time, the mixture was cooled to room temperature, and ice-water (40 mL) along with an aqueous solution of HCl (1N, 40 mL) was added under vigorously stirring. THF was removed under reduced pressure, and the crude material was taken up with $CH_2Cl_2$ (50 mL). The aqueous phase was extracted into $CH_2Cl_2$ (4 × 20 mL), and the combined organic layers were dried on $Na_2SO_4$, concentrated under reduced pressure. The crude product was purified by column chromatography on silica gel (hexane) to give (*Z*)-**115.**

Y: 63% m.p. 90 °C. $^1$H NMR (300 MHz, $CDCl_3$): 7.13 (m, 2H) 6.84 (m, 2H), 6.68 (m, 2H), 2.48 (d, *J* = 7.1 Hz, 4H), 1.65 (m, 12H), 1.30 (m, 2H), 1.14 (m, 4H), 0.97 (m, 4H) ppm. $^{13}$C NMR (75 MHz, $CDCl_3$): 145.5, 132.6, 126.4, 126.2, 124.6, 43.5, 36.7, 33.2, 26.5, 26.4 ppm. MS (EI): *m/z* (%) = 384 (100, $[M]^+$), 301 (83), 219 (17). HRMS (EI): calcd. for $C_{24}H_{32}S_2$ $[M]^+$ 384.19454; found 384.1945.

**Synthesis of (*Z*)-5,5'-(1,4-dicyclohexylbut-2-ene-2,3-diyl)bis(2-bromothiophene) (*Z*)-117**

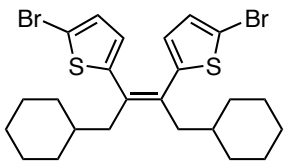

To a solution of (*Z*)-**115** (0.723 mmol) in dry DMF (2 mL) was added *N*-bromosuccinimide (0.270 g, 1.52 mmol, 2.1 equiv) at 0 °C. The mixture was stirred in the dark at 0 °C and the progress of the reaction was monitored by TLC (hexane). After 2 h, the mixture was quenched with water (10 mL), and the aqueous phase was extracted into $CH_2Cl_2$ (3 × 10 mL). The organic phase was washed with water, and dried with $Na_2SO_4$. The solvent was removed at reduced pressure, and the residue was purified by chromatography on silica gel (hexane) to give (*Z*)-**117**.

Y: 71% m.p. 128 °C. $^1$H NMR (300 MHz, $CDCl_3$): 6.81 (d, *J* = 3.8 Hz, 2H) 6.46 (d, *J* = 3.8 Hz, 2H), 2.48 (d, *J* = 7.1 Hz, 4H), 1.65 (m, 12H), 1.33 (m, 2H), 1.13 (m, 4H), 0.94 (m, 4H) ppm. $^{13}$C NMR (75 MHz, $CDCl_3$): 146.6, 132.8, 129.4, 127.0, 111.5, 43.1, 36.7, 33.2,26.45, 26.3ppm. MS (EI): *m/z* (%) = 540 (100, $[M]^+$). HRMS (EI): calcd. for $C_{24}H_{30}Br_2S_2$ $[M]^+$ 540.0156; found 540.014.

**Synthesis of 2,7-dibromo-4,5-bis(cyclohexylmethyl)benzo[1,2-*b*:4,3-*b*']dithiophene 111**

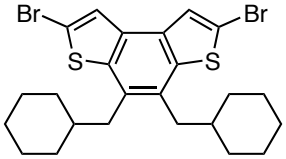

Following the general procedure of the Table 13, (*Z*)-**117** (0.250 mmol) was reacted with $FeCl_3$ (0.162 g, 1 mmol, 4 eq) at 0 °C for 30 min. After the treatment with MeOH, the solvents were removed under vacuum, and the residue was purified by column chromatography on silica gel (hexane) to afford **111**

Y: 58% m.p. 193 °C. $^1$H NMR (300 MHz, $CDCl_3$): 7.56 (s, 2H), 2.83 (d, *J* = 7.1 Hz, 4H), 1.70 (m, 12H), 1.17 (m, 10H) ppm. $^{13}$C NMR (75 MHz, $CDCl_3$): 140.6, 131.5, 129.5,124.9, 114.2, 40.1, 38.8, 33.8, 26.4, ppm. MS (EI): *m/z* (%) = 540 (75, $[M]^+$), 462 (8), 375 (100), 297 (13). HRMS (EI): calcd. for $C_{24}H_{28}Br_2S_2$ $[M]^+$ 537.9999; found 538.0112.

**Synthesis of (*Z*)-2,2'-(1,6-dicyclopentylhex-3-ene-3,4-dyl)dithiophene (*Z*)-116**

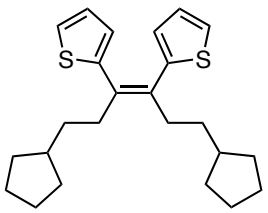

To a solution of **114** (24 mmol) in dry THF (110 mL) at – 20 °C, $TiCl_4$ (5.4 mL, 28.7 mmol, 1.2 equiv) was added dropwise in 10 min. After 30 min at – 20 °C, Zn powder (3.90 g, 60 mmol, 2.5 equiv) was added in 3 portions in 10 min, and then the mixture was refluxed for 3 h. After this time, the mixture was cooled to room temperature, and ice-water (40 mL) along with an aqueous solution of HCl (1N, 40 mL) was added under vigorously stirring. THF was removed under reduced pressure, and the crude material was taken up with $CH_2Cl_2$ (50 mL). The aqueous phase was extracted into $CH_2Cl_2$ (4 × 20 mL), and the combined organic layers were dried on $Na_2SO_4$, concentrated under reduced pressure. The crude product was purified by column chromatography on silica gel (hexane) to give (*Z*)-**116.**

Y: 67%. $^1$H NMR (300 MHz, $CDCl_3$): 7.13 (m, 2H) 6.84 (m, 2H), 6.70 (m, 2H), 2.52 (m, 4H), 1.77 (m, 8H), 1.51 (m, 12H), 1.12 (m, 2H) ppm. $^{13}$C NMR (75 MHz, $CDCl_3$): 144.7, 132.3, 125.9, 125.8, 124.3, 39.8, 34.7, 34.6, 32.2, 24.7 ppm. MS (EI): *m/z* (%) = 384 (100, $[M]^+$), 301 (30). HRMS (EI): calcd. for $C_{24}H_{32}S_2$ $[M]^+$ 384.19454; found 384.1923.

**Synthesis of (*Z*)-5,5'-(1,6-dicyclopentylhex-3-ene-3,4-dyl)bis(2-bromothiophene) (*Z*)-118**

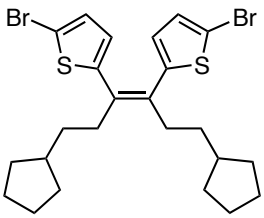

To a solution of (*Z*)-**116** (0.723 mmol) in dry DMF (2 mL) was added *N*-bromosuccinimide (1.52 mmol, 2.1 equiv) at 0 °C. The mixture was stirred in the dark at 0 °C and the progress of the reaction was monitored by TLC (hexane). After 2 h, the mixture was quenched with water (10 mL), and the aqueous phase was extracted into $CH_2Cl_2$ (3 × 10 mL). The organic phase was washed with water, and dried with $Na_2SO_4$. The solvent was removed at reduced pressure, and the residue was purified by chromatography on silica gel (hexane) to give (*Z*)-**118** Y: 74%. $^1$H NMR (300 MHz, $CDCl_3$): 6.82 (d, *J* = 3.8 Hz, 2H), 6.50 (d, *J* = 3.8 Hz, 2H), 2.44 (m, 4H), 1.77 (m, 6H), 1.59 (m, 6H), 1.42 (m, 6H), 1.10 (m, 4H), $^{13}$C NMR (75 MHz, $CDCl_3$): 146.6, 132.4, 128.9, 126.5, 111.3, 39.7, 34.5, 34.1, 32.1, 24.7 ppm. MS (EI): *m/z* (%) = 542 (100, $[M]^+$), 464 (13), 380(17). HRMS (EI): calcd. for $C_{24}H_{30}Br_2S_2$ $[M]^+$ 540.0156; found 540.0139.

**Synthesis of 2,7-dibromo-4,5-bis(2-cyclopentylethyl)benzo[1,2-*b*:4,3-*b*']dithiophene 112**

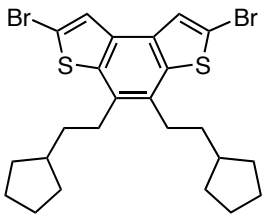

Following the general procedure of the Table 13, (*Z*)-**118** (0.250 mmol) was reacted with $FeCl_3$ (1 mmol, 4 eq) at 0 °C for 30 min. After the treatment with MeOH, the solvents were removed under vacuum, and the residue was purified by column chromatography on silica gel (hexane) to afford **112**

Y: 70% m.p. 110 °C. $^1$H NMR (300 MHz, $CDCl_3$): 7.52 (s, 2H) 2.85 (m, 4H), 1.68 (m, 4H), 1.63 (m, 6H), 1.28 (m, 6H), 0.9 (m, 6H) ppm. $^{13}$C NMR (75 MHz, $CDCl_3$): 139.4, 131.5, 129.5, 124.5, 113.5, 40.1, 35.5, 32.1, 31.0, 24.7 ppm. MS (EI): *m/z* (%) = 540 (100, $[M]^+$), 462 (8), 375 (80). HRMS (EI): calcd. for $C_{24}H_{28}Br_2S_2$ $[M]^+$ 537.9999; found 537.9965.

**Synthesis of helicene 8 by $FeCl_3$-mediated cyclization of (*Z*)-119**

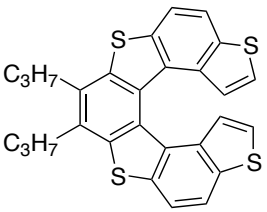

$FeCl_3$ (0.6 mmol, 4 eq) was added to a solution of (*Z*)-**119** (0.150 mmol) in $CH_2Cl_2$ (30 mL) at –20 °C and the reaction mixture was stirred for 60 min. After the treatment with MeOH, the solvents were removed under vacuum, and the residue was purified by column chromatography on silica gel (hexane) to afford **8** in 62% yield. All spectroscopical data were in agreement with those previously reported.[3]

**Synthesis of tetrathiahelicene derivative 125**.

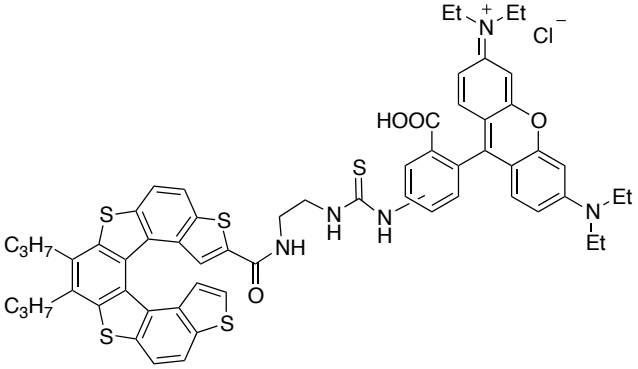

To a solution of helicene **124** (60.3 mg, 0.088 mmol) in EtOH (1.4 mL) was added DIPEA (0.15 mL, 0.088 mmol) at room temperature. After 30 min, to this solution was added a solution of **RBITC** (47.1 mg, 0.088 mmol) in EtOH (1.4 mL) at room temperature, and the mixture was stirred overnight in the dark. Then, the solvent was removed under reduced pressure, and the crude residue was washed with methanol (5 × 2 mL), affording the required product **125** (33.3 mg, 34%) as a violet solid. M.p. 218−220 °C. $^1$H-NMR (500 MHz; DMSO-$d_6$): $\delta$ 10.02 (br s, 1 H) 6.47−10.8 (m, 16 H arom + 3 H, NH), 3.39−3.69 (m, 16 H), 1.02−1.49 (m, 22 H) ppm. $^{13}$C-NMR (75 MHz; DMSO-$d_6$): $\delta$ 180.87, 180.34, 168.02, 161.56, 154.94, 141.15, 140.98, 139.28, 139.18, 138.98, 137.62, 137.33, 136.84, 136.52, 135.67, 135.60, 134.80, 134.55, 132.38, 132.31, 131.97, 131.86, 130.95, 130.29, 128.87, 127.94, 127.47, 126.98, 126.11, 125.82, 125.49, 123.77, 121.45, 120.94, 120.74, 119.12, 115.08, 103.05, 99.25, 96.77, 69.77, 54.85, 53.43, 44.01, 43.78, 41.68, 38.21, 36.41, 33.70, 31.23, 28.94, 28.64, 28.15, 24.45, 22.83, 22.03, 20.35, 14.34, 12.55, 12.31 ppm. HRMS-ESI$^+$: *m/z* calculated for $C_{60}H_{58}N_5O_4S_5^+$: 1072.30869, found: 1072.30925 ($M^+$).

**Synthesis of di-aldehyde 130**

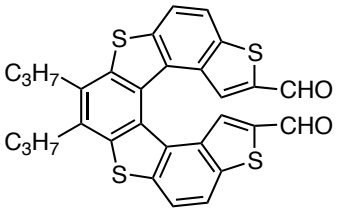

*n*BuLi (1.56 M in hexane; 150 mL, 0.234 mmol) was added to a solution of **6** (0.082 g, 0.168 mmol) at –78 °C in THF (10 mL). The solution was stirred 10 min at –78 °C and 20 min at room temperature. The resulting yellow solution was cooled at –78 °C and DMF (300 mL, 3.89 mmol) was added dropwise. The mixture was stirred for 40 min at room temperature. The solution was quenched with aqueous solution of $NH_4Cl$ (8 mL) and exatrated with $CH_2Cl_2$ (3 × 8 mL). The collected organic phase was dried with $Na_2SO_4$, and filtered. After evaporation of the solvent, the crude product was purified by silica gel column chromatography (hexane/AcOEt, 9:1) to afford **130** (95 mg, 63%) as orange

solid.The spectral properties of this compound were in agreement with those previously reported.[3]

**Synthesis of intermediate 132**.

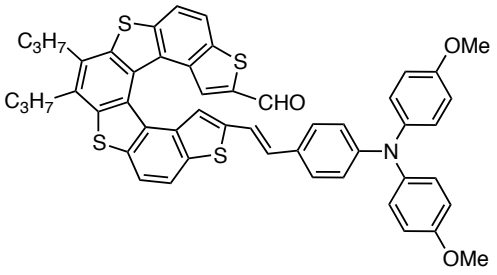

A solution of phosphonium salt **131** (120 mg, 0.18 mmol) in DMF (4 mL) was slowly added to a slurry of dialdehyde **130** (117 mg, 0.21 mmol), 18-crown-6 ether (9 mg), and anhydrous $K_2CO_3$ (50 mg, 2.1 mmol) in DMF (4 mL). The resulting orange solution was stirred overnight at room temperature. The solution was then poured into water (10 mL) and extracted with dichloromethane (4×10 mL). The organic phase was washed with water (20 mL), dried with $Na_2SO_4$, and filtered. After evaporation of the solvent, the crude dark-orange product was purified by silica gel column chromatography (hexane/AcOEt, 9:1) to afford **132** (95 mg, 63%) as a red solid.
$^1$H NMR (300 MHz, $CDCl_3$): δ = 9.23 (s, 1H), 8.06-5.88 (m, 20H), 3.80 (s, 6H), 3.16 (m, 4H), 1.89 (m, 4H), 1.18 ppm (m, 3H). $^{13}$C NMR (75 MHz, $CDCl_3$): δ 184.2, 156.2, 156.0, 148.8, 148.3, 142.8, 140.8, 140.4, 140.3, 136.7, 136.5, 136.0, 135.8, 135.6, 134.9, 133.2, 132.6, 132.5, 131.6, 130.9, 130.3, 129.7, 128.5, 128.2, 127.6, 126.9, 126.8, 122.9, 121.0, 120.8, 120.1, 120.0, 118.9, 118.6, 116.9, 115.2, 114.8, 55.6, 34.6, 23.4, 12.9 ppm. HRMS (ESI): calcd. for $C_{51}H_{41}NO_3S_4$ 843.1969; found 843.2075. UV/Vis ($CH_3CN$): $\lambda_{max}$ = 252, 297, 362, 425 nm.

**Synthesis of dye 129**

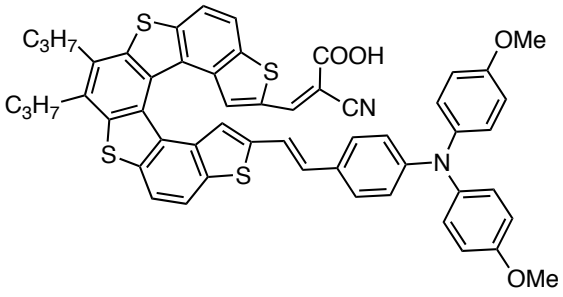

Cyanoacetic acid (18.0 mg, 0.21 mmol) and piperidine (2 mg, 0.5 mmol) were added to a solution of **132** (41 mg, 0.05 mmol) in THF (1 mL) and $CH_3CN$ (10 mL). The reaction mixture was stirred for 5 h at 80 °C. The solvent was then evaporated, and the residue was taken up with a mixture HCl 0.1M (6 mL) and hexane (4 mL), filtered and washed with AcCN to afford **129** (27 mg, 60%) as a red solid. $^1$H NMR (300 MHz, $CD_3COCD_3$): δ = 8.26–7.77 (m, 6H), 7.27–6.40 (m, 15H), 3.79 (s, 6H), 3.11 (m, 4H), 1.87 (m, 4H), 1.18 ppm (m, 3H). $^{13}$C NMR (75 MHz, $CD_3SOCD_3$): δ 163.8, 157.5, 154.5, 149.9, 147.1, 143.3, 141.3, 141.2, 141.0, 140.8, 137.7, 137.4, 137.3, 136.7, 136.5, 135.2, 134.7, 134.0, 133.9, 133.2, 132.3, 131.4, 130.9, 129.3, 129.1, 128.9, 128.4, 127.9, 124.0, 123.7, 121.9, 120.2, 120.2, 119.7, 119.2, 117.1, 116.5, 116.0, 115.7, 55.8, 35.0, 24.1, 14.9 ppm. HRMS (ESI): calcd. for $C_{54}H_{42}N_2O_4S_4$ 910.2027; found 910.2064.

**Synthesis of 7-TH derivative 134**

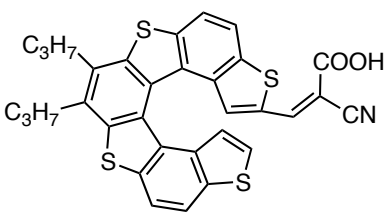

Cyanoacetic acid (18.0 mg, 0.21 mmol) and piperidine (2 mg, 0.5 mmol) were added to a solution of mono aldehyde **133** (41 mg, 0.05 mmol) in THF (1 mL) and $CH_3CN$ (10 mL). The reaction mixture was stirred for 5 h at 80 °C. The solvent was then evaporated and

the residue was taken up with a mixture HCl 0.1M (6 mL) and hexane (4 mL), filtered and washed with AcCN to afford **134** (27 mg, 60%) as a red solid. $^{1}$H NMR (300 MHz, $(CD_3)_2CO$): δ = 8.66–5.91 (m, 8H), 3.79 (s, 6H), 2.50 (m, 4H), 1.21 (m, 4H), 0.60 ppm (m, 3H). HRMS (ESI): calcd. for $C_{31}H_{23}NS_4$ [M–$CO_2$] 537.0713; found 537.0405.

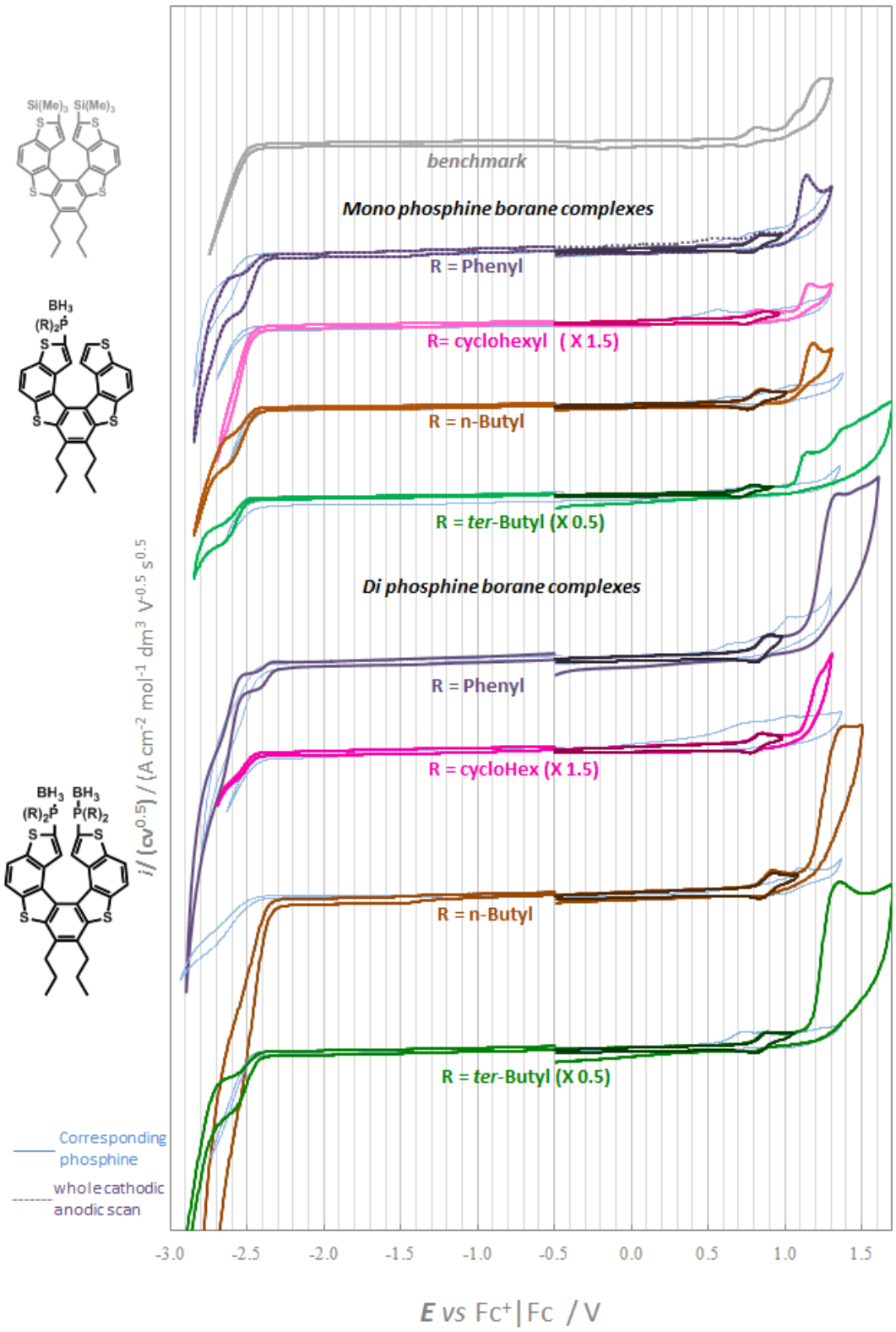


Normalized CV features of the borane complexes **26**, **27**, **53a-c**, **54a-c** recorded on GC in $CH_2Cl_2$ + 0.1 M $TBAPF_6$, at 0.2 V $s^{-1}$, with ohmic drop compensation. The voltammogram of the corresponding phosphine and of **65** obtained in similar conditions is also reported, for sake of comparison.

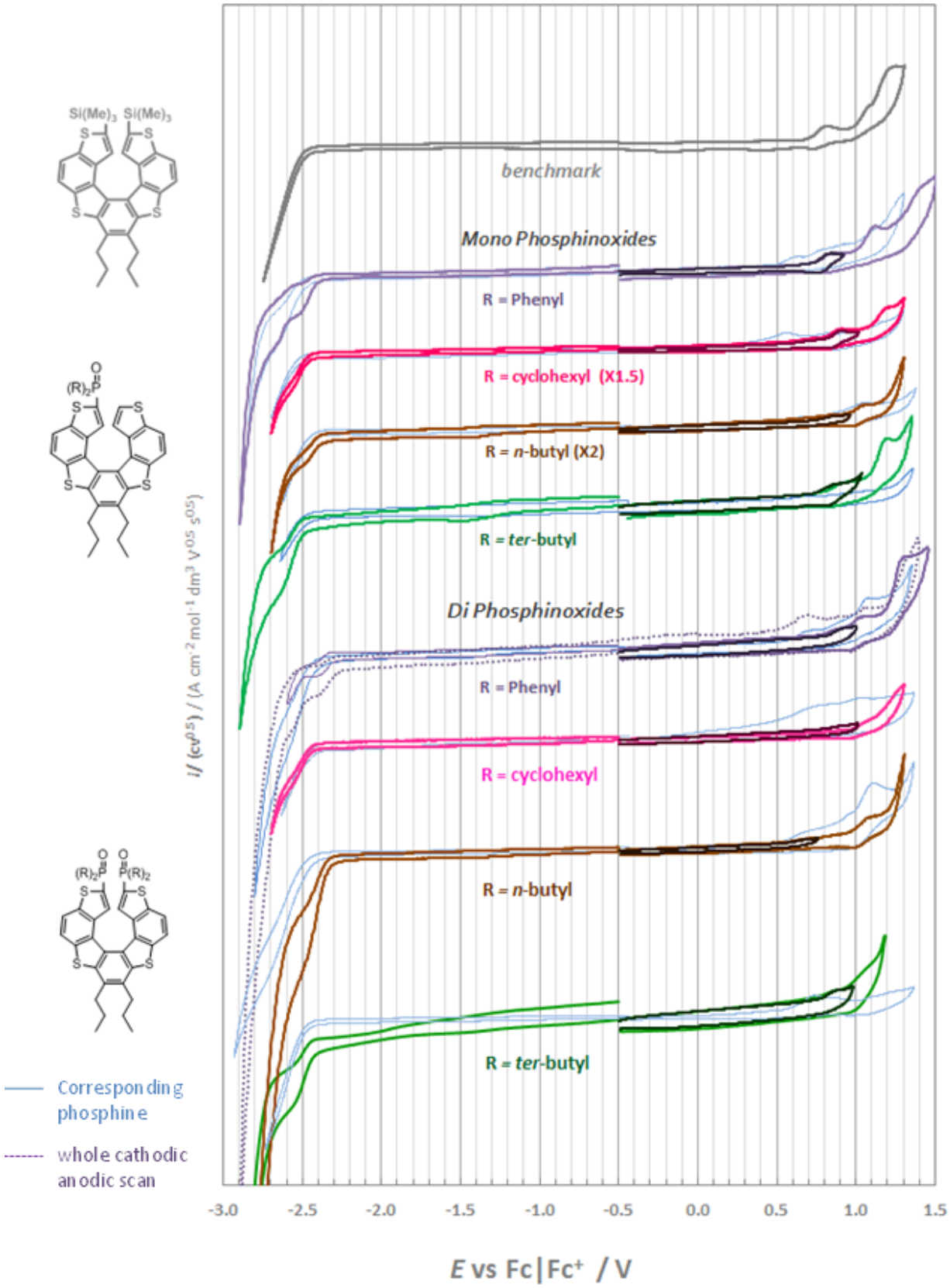


Normalized CV features of the **66**, **68**, **67a-c**, **69a-c** (contrasted with the corresponding phosphanes reported in light blue) recorded on GC in DCM + 0.1 M $TBAPF_6$, at 0.2 V $s^{-1}$, with ohmic drop compensation. The voltammogram of the corresponding phosphine and of **65** obtained in similar conditions is also reported, for sake of comparison.

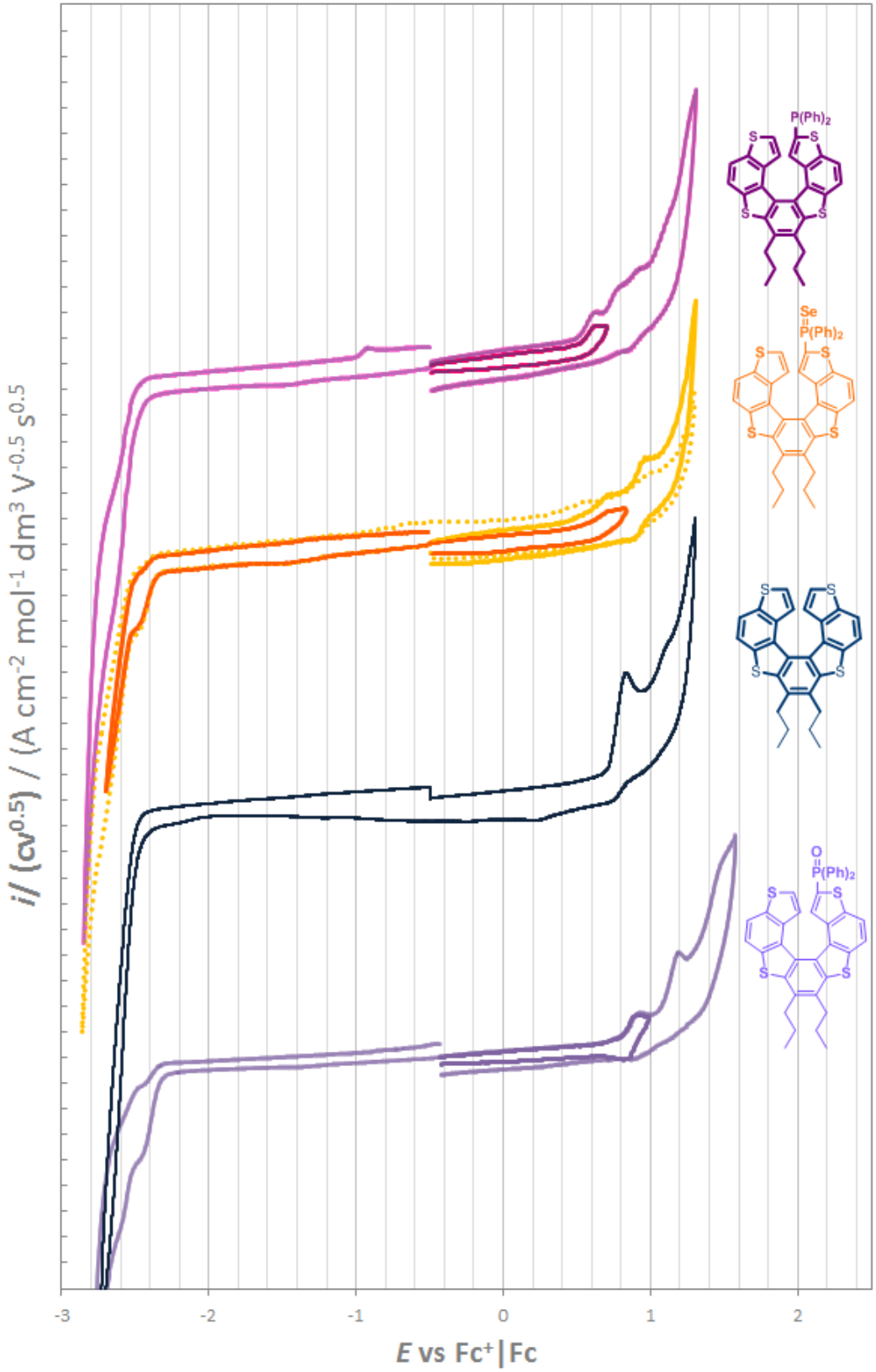


Normalized CV features of the **28**, **57**, **8**, **66** recorded on GC in DCM + 0.1 M TBAP, at 0.2 V $s^{-1}$, with ohmic drop compensation.

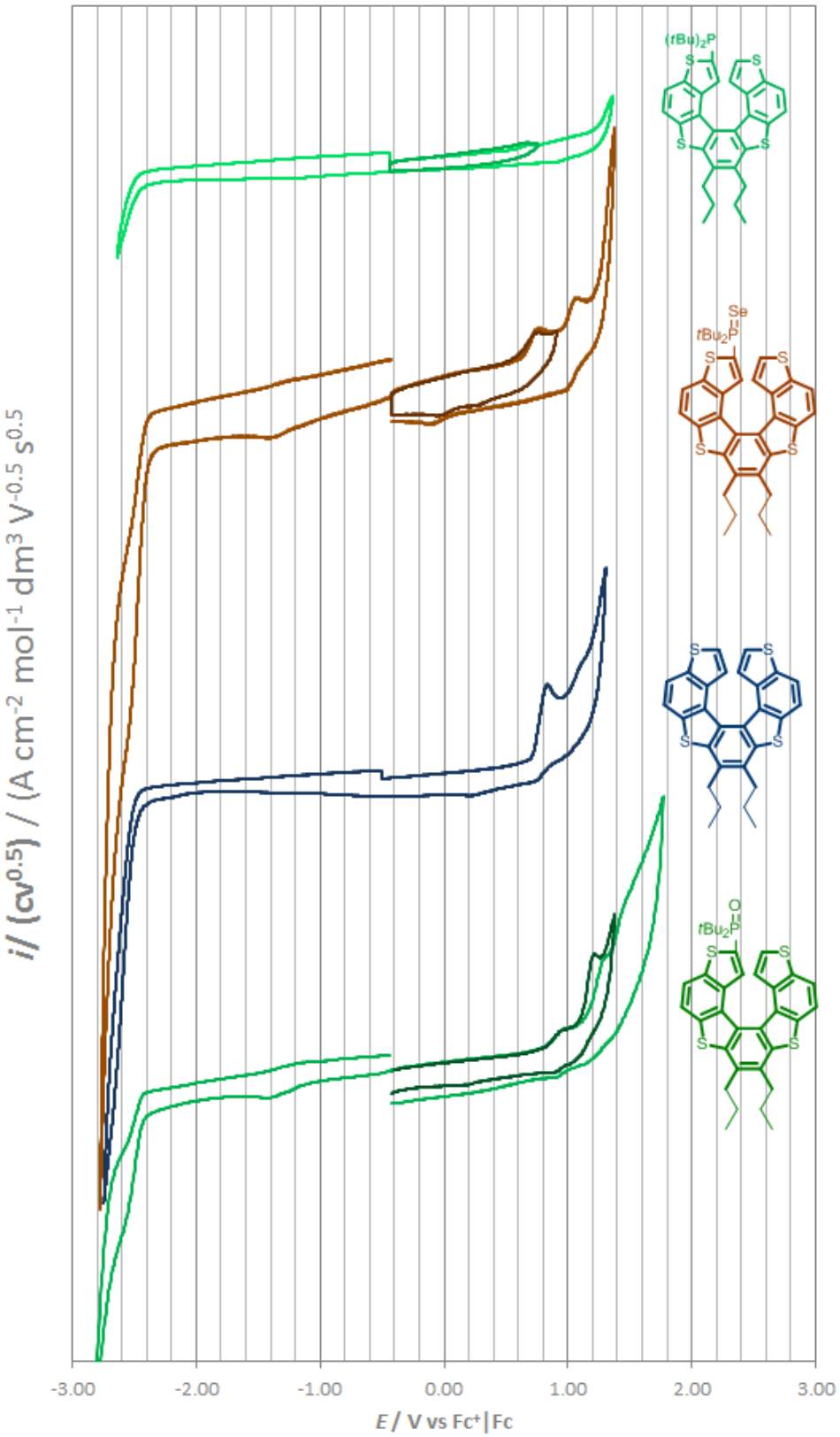


Normalized CV features of the **55c**, **58c**, **8**, **67c** recorded on GC in DCM + 0.1 M $TBAPF_6$, at 0.2 V $s^{-1}$, with ohmic drop compensation**.**

## References


[1] General review: a) Shen, Y.; Chen, C.-F. *Chem. Rev.* **2012**, *112*, 1463-1535; b) Hoffmann N. *Journal of Photochemistry and Photobiology C: Photochemistry Reviews* **2014**, *19,* 1–19 Review on carbohelicenes: a) Urbano, A. *Angew. Chem., Int. Ed.* **2003**, *42*, 3986; b) Gingras, M. *Chem. Soc. Rev.* **2012**, *42*, 968-1006; Gingras, M.; Felix, G.; Peresutti, R. *Chem. Soc. Rev.* **2012**, *42*, 1007-1050; Gingras, M. *Chem. Soc. Rev.* **2012**, *42*, 1051-1095; Review on thiahelicenes: Collins, S. K.; Vachon, M. P. *Org. Biomol. Chem.* **2006**, *4*, 2518-2524

[2] a) Caronna, T.; Catellani, M.; Luzzati, S.; Malpezzi, L.; Meille, S. V.; Mele, A.; Richter C.; Sinisi, R.; *Chem. Mater.*, **2001**, *13,* 3906-3914; b) Champagne, B.; Andrè, J. M.; Botek, E.; Licandro, E.; Maiorana, S.; Bossi, A.; Clays, K.; Persoons, A. *ChemPhysChem*, **2004**, *5*, 1438–1442; c) Bossi, A.; Licandro, E.; Maiorana, S.; Rigamonti, C.; Righetto, S.; Stephenson, G. R.; Spassova, M.; Botek, E.; Champagne, B. *J. Phys. Chem. C* **2008**, *112*, 7900–7907; d) Facchetti, A.; Schiavo, M.; Bossi, A.; Maiorana, S.; Licandro, E.; Todescato, F.; Toffanin, S.; Muccini, M.; Graiff, C.; Tiripicchio, A. *Organic Electronics* **2009**, *10*, 1511–1520.

[3] a) Licandro, E.; Rigamonti, C.; Ticozzelli, M. T.; Monteforte, M.; Baldoli, C.; Giannini, C.; Maiorana S. *Synthesis,* **2006**, *21*, 3670-3678; b) Baldoli, C.; Bossi, A.; Giannini, C.; Licandro, E.; Maiorana, S.; Perdicchia D.; Schiavo, M.; *Synlett*, **2005**, *7*, 1137-1141.

[4] Tanaka, K.; Suzuki H.; Osuga, H.; *J. Org. Chem*., **1997**, *62*, 4465-4470; *Tetrahedron Lett.*, **1997**, *38*, 457-460

[5] Ben Hassine, B.; Gorsane, M.; Pecter, J.; Martin, R. H. *Bull. Soc. Chim. Belg.*, **1985**, *94*, 597-603; 759-769; 801-808.

[6] Ben Hassine, B.; Gorsane, M.; Geerts-Evrard, F.; Pecher, J.; Martin, R. H.; Castelet, D. *Bull. Soc. Chim. Belg.* **1986**, *95*, 557-566.

[7] Ben Hassine, B.; Gorsane, M.; Geertz-Evrand, F.; Pecter, J.; Martin, R.H.; Castelet, D. *Bull. Soc. Chim. Belg.* **1986**, *95*, 556-557.

[8] Reetz, M.T.; Sostmann, S. *Tetrahedron* **2001**, *57*, 2515-2520.

[9] Okubo, H.; Yamaguchi, M.; Kabuto, C.; *J. Org. Chem.* **1998**, *63*, 9500-9509.

[10] Dreher, S. D.; Katz, T. J.; Lam, K. C.; Rheingold, A. L. *J. Org. Chem.* **2000**, *65*, 815-822.

[11] a) Sato, I.; Yamashima, R.; Kadowaki, K.; Yamamoto, J.; Shibata, T.; Soai, K. *Angew. Chem., Int. Ed.* **2001**, *40*, 1096-1098; b) Kawasaki, T.; Suzuki, K.; Licandro, E.; Bossi, A.; Maiorana, S.; Soai, K. *Tetrahedron: Asym.* **2006**, *17*, 2050-2053.

[12] Takenaka, N.; Sarangthem, R. S.; Captain, B. *Angew. Chem. Int. Ed*. **2008**, *47*, 9708-9710.

[13] Chen, J.; Captain, B.; Takenaka, N. *Org. Lett.* **2011**, *13*, 1654-1657.

[14] Samal, M.; Mísek, J.; Stará, I. G.; Starý, I. *Collect. Czech. Chem. Commun.* **2009**, *74*, 1151-1159.

[15] a) Carbery, D. R.; Crittall, M. R.; Rzepa, H. S. *Org. Lett.* **2011**, *13*, 1250-1253; b) Crittall, M. R.; Fairhurst, N. W. G.; Carbery, D. R. *Chem. Commun.* **2012**, *48*, 11181-11183.

[16] Takenaka, N.; Chen, J. S.; Captain, B.; Sarangthem, R. S.; Chandrakumar, A. *J. Am. Chem. Soc.* **2010**, *132*, 4536-4537.

[17] a) Reetz, M. T.; Beuttenmuller, E. W.; Goddard, R. *Tetrahedron Lett.* **1997**, *38*, 3211-3214; b) Reetz, M. T.; Sostmann, S. *J. Organomet. Chem.* **2000**, *603*, 105-109.

[18] a) Weix, D. J., Dreher, S. D., Katz, T. J *J. Am. Chem. Soc.* **2000**, *122*, 10027-10032; b) Wang, D. Z.; Katz, T. J. *J. Org. Chem.* **2005**, *70*, 8497-8502.

[19] Nakano, D.; Yamaguchi, M. *Tetrahedron Lett.* **2003**, *44*, 4969-4971.

[20] a) Teply, F.; Stará, I.G.; Starý, I.; Kollarovic, A.; Saman, D.; Vyskocil, S.; Fiedler, P. *J. Org. Chem.* **2003**, *68*, 5193-5197; b) Krausova, Z.; Sehnal, P.; Bondzic, B.P.; Chercheja, S.; Eilbracht, P.; Stará, I.G.; Saman, D.; Starý, I. *Eur. J. Org. Chem.* **2011**, 3849-3857.

[21] a) Monteforte, M.; Cauteruccio, S.; Maiorana, S.; Benincori, T.; Forni, A.; Raimondi, L.; Graiff, C.; Tiripicchio, A.; Stephenson, G. R.; Licandro, E. *Eur. J. Org. Chem.* **2011**, 5649-5658; b) Cauteruccio, S.; Loos, A.; Bossi, A.; Jaimes, M. C. B.; Dova, D.; Licandro, E.; Hashmi, A. S. K. *Inorg. Chem*. **2013**, *52*, 7995-8004.

[22] a) El Abed, R.; Aloui, F.; Genet, J.P.; Ben Hassine, B.; Marinetti, A. *J. Organomet. Chem.* **2007**, *692*, 1156-1160; b) Yavari, K.; Moussa, S.; Ben Hassine, B.; Retailleau, P.; Voituriez, A.; Marinetti, A. *Angew. Chem. Int. Ed.* **2012**, *51*, 6748; c) Yavari, K.; Retailleau, P.; Voituriez, A.; Marinetti, A. *Chem. Eur. J.* **2013**, *19*, 9939.

[23] Terfort, A.; Görls, H.; Brunner, H. *Synthesis* **1997**, 79-86.

[24] Paruch, K.; Vyklický, L.; Wang, D.Z.; Katz, T. J.; Incarvito, C.; Zakharov, L.; Rheingold A. L. *J. Org. Chem.* **2003**, *68*, 8539-8544.

[25] Ž.dný, J.; Velýšek, P.; Jakubec, M.; Sýkora, J.; C.rkva V.; Storch, J. *Tetrahedron*, **2013**, *69*, 6213-6218.

[26] Aloui, F.; El Abed, R.; Marinetti, A.; Hassine, B. *Tetrahedron Letters* **2007,** *48*, 2017–2020.

[27] a) Aloui, F.; Moussa, S.; Hassine, B. *Tetrahedron Letters* **2011,** *52*, 572–575; b) Aloui, F.; Moussa, S.; Hassine, B. *Synthetic Communications* **2013**, *43*, 268-276.

[28] a) Graule, S.; Rudolph, M.; Vanthuyne, N.; Autschbach, J.; Roussel, C.; Crassous, J.; Réau, R. *J. Am. Chem. Soc.* **2009**, *131*, 3183-3185; b) Shen, W.; Graule, S.; Crassous, J.; Lescop, C.; Gornitzka H.; Reau R. *Chem. Commun.*, **2008**, 850–852.

[29] a) Fukawa, N.; Osaka, T.; Noguchi, K.; Tanaka, K. *Org. Lett.* **2010**, *12*, 1324-1327; b) Sawada, Y.; Furumi, S.; Takai, A.; Takeuchi, M.; Noguchi, K.; Tanaka, K. *J. Am. Chem. Soc.* **2012**, *134*, 4080-4083.

[30] Nakano, K.; Oyama, H.; Nishimura, Y.; Nakasako, S.; Nozaki, K. *Angew. Chem. Int. Ed.* **2012**, *51*, 695-699.

[31] Aillard, P.; Retailleau, P.; Voituriez, A.; Marinetti, A. *Chem. Commun.* **2014**, *50*, 2199-2201.

[32] Hashmi, A. S. K.; Toste, D. F., Ed. *Modern Gold Catalyzed Synthesis*; Wiley-VCH: Weinheim, Germany, 2012.

[33] Schmidbaur, H., Ed. *Gold: Progress in Chemistry, Biochemistry and Technology*; John Wiley & Sons: Chichester, U.K., 1999.

[34] a) Berners-Price, S. J.; Filipovska, A. *Metallomics* **2011**, *3*, 863-873. b) Shaw, C. F. *Chem. Rev*. **1999**, *99*, 2589-2600.

[35] a) Gómez-Suárez, A.; Nolan, S. P. *Angew. Chem. Int. Ed.* **2012**, *51*, 8156-8159. b) Hashmi, A. S. K. *Angew. Chem. Int. Ed.* **2010**, *49*, 5232-5241. c) Gorin, D. J.; Sherry, B. D.; Toste, F. D. *Chem. Rev*. **2008**, *108*, 3351-3378. d) Arcadi, A. *Chem. Rev.* **2008**, *108*, 3266-3325. e) Li, Z.; Brouwer, C.; He, C. *Chem. Rev*. **2008**, *108*, 3239-3265. f) Hashmi, A. S. K. *Chem. Rev*. **2007**, *107*, 3180-3211. g) Gorin, D.

J.; Toste, F. D. *Nature* **2007**, *446*, 395-403. h) Hashmi, A. S. K.; Hutchings, G. J. *Angew. Chem. Int. Ed.* **2006**, *45*, 7896-7936.

[36] a) Wang, F. J.; Liu, L. J.; Wang, W. F.; Li, S. K.; Shi, M. *Coord. Chem. Rev.* **2012**, *256*, 804−853. b) Nolan, S. P. *Acc. Chem. Res.* **2011**, *44*, 91-100. c) Marion, N.; Nolan, S. P. *Chem. Soc. Rev.* **2008**, *37*, 1776-1785. c) Hashmi, A. S. K.; Lothschütz, C.; Böhling, C.; Hengst, T.; Hubbert, C.; Rominger, F. *Adv. Synth. Catal.* **2010**, *352*, 3001-3012. d) Hashmi, A. S. K.; Riedel, D.; Rudolph, M.; Rominger, F.; Oeser, T. *Chem. Eur. J.* **2012**, *18*, 3827-3830.

[37] a) Pradal, A.; Toullec, P. Y.; Michelet, V. *Synthesis* **2011**, 1501−1514. b) Sengupta, S.; Shi, X. D. *ChemCatChem* **2010**, *2*, 609−619. c) Widenhoefer, R. A. *Chem.-Eur. J.* **2008**, *14*, 5382−5391. d) Ito, Y.; Sawamura, M.; Hayashi, T. *J. Am. Chem. Soc.* **1986**, *108*, 6405−6406.

[38] Johansson, M. J.; Gorin, D. J.; Staben, S. T.; Toste, F. D. *J. Am. Chem. Soc.* **2005**, *127*, 18002-18003.

[39] Hamilton, G. L.; Kang, A. J.; Nba, M.; Toste, F. D.; *Science* **2007**, *317*, 496–499.

[40] a) Alonso, I.; Trillo, B.; Lopez, F.; Montserrat, S.; Ujaque, G.; Castedo, L.; Lledos, A.; Mascarenas, J. L. *J. Am. Chem. Soc.* **2009**, *131*, 13020–13030; b) Gonzalez, A. Z.; Toste, F. D. *Org. Lett.* **2010**, *12*, 200–203; c) Teller, H.; Flugge, S. Goddard, S. R.; Furstner, A. *Angew. Chem. Int. Ed.* **2010**, *49*, 1949–1953; d) Teller, H.; Corbet, M.; Mantilli, L.; Gopakumar, G.; Goddard, R.; Thiel, W.; Furstner, A. *J. Am. Chem. Soc*. **2012**, *134*, 15331–15342.

[41] Alternatively, N-heterocyclic carbenes (NHCs) and acyclic diaminocarbenes (ADCs) have been successfully used as chiral ligands in enantioselective gold catalysis: a) Wang, Y. -M.; Kuzniewski, C.; Rauniyar, N.; Hoong, V. C.; Toste, F. D. *J. Am. Chem. Soc.* **2011**, *133*, 12972–12975; b) Francos, J.; Grande-Carmona, F., Faustino, H.; Iglesias-Siguenza, J.; Diez, E.; Alonso, I.; Fernandez, R.; Lassaletta, J. M.; Lopez, F.; Mascarenas, J. L. *J. Am. Chem. Soc.* **2012**, *134*, 14322–14325; c) Handa, S.; Slaughter, L. M.; *Angew. Chem. Int. Ed.* **2012**, *51*, 2912–2915.

[42] K. Yavari, P. Aillard, Y. Zhang, F. Nuter, P. Retailleau, A. Voituriez, A. Marinetti, *Angew. Chem. Int. Ed.* **2014**, *53*, 861-865.

[43] a) Shibata, T.; Kobayashi, Y.; Maekawa, S.; Toshida N.; Takagi, K. *Tetrahedron*, **2005**, *61*, 9018-9024. b) Brissy, D.; Skander, M.; Jullien, H.; Retaillea, P.; Marinetti, A. *Org. Lett.,* **2009**, *11*, 2137-2139. c) Nishimura, T.; Kawamoto, T.; Nagaosa, M.; Kumamoto H.; Hayashi, T. *Angew. Chem. Int. Ed*., **2010**, *49*, 1638-1641.

[44] Teller, H.; Corbet, M.; Mantilli, L.; Gopakumar, G.; Goddard, R.; Thiel, W.; Fürstner, A. *J. Am. Chem. Soc.,* **2012**, *134*, 15331-15342.

[45] Pradal, A.; Chao, C.-M.; Toullec P. Y.; Michelet, V. *Beilstein J. Org. Chem*., **2011**, *7*, 1021-1029.

[46] Aillard, P.; Voituriez, A.; Marinetti, A. *Dalton Trans.*, **2014**, *43*, 15263-15278.

[47] a) Bossi, A.; Maiorana, S.; Graiff, C.; Tiripicchio, A.; Licandro, E. *Eur. J. Org. Chem*. **2007**, 4499–4509; b) Bossi, A.; Falciola, L.; Graiff, C.; Maiorana, S.; Rigamonti, C.; Tiripicchio, A.; Licandro, E. Mussini, P.R. *Electrochimica Acta* **2009**, *54,* 5083–5097.

[48] Nakagawa, H.; Obata, A.; Yamada, K.-I.; Kawazura, H. *J. Chem. Soc. Perkin Trans. 2* **1985**, 1899-1903.

[49] a) Groen, M. B.; Wynberg, H. *J. Am. Chem. Soc.* **1971**, *93*, 2968–2974; b) Rajca, A.; Pink, M.; Xiao, S.; Miyasaka, M.; Rajca, S.; Das, K.; Plessel, K. *J. Org. Chem.* **2009**, *74*, 7504–7513.

[50] Friese D. H.; Hättig C. *Phys. Chem.Chem.Phys*., **2014**, *16*, 5942-5951.

[51] Van Overschelde, M.; Vervecken, E.; Modha, S. G.; Cogen, S.; Van der Eycken, E.; Van der Eycken, J. *Tetrahedron*, **2009**, *65*, 6410–6415.

[52] Chevykalova, M. N.; Manzhukova, L. F.; Artemova, N. V.; Luzikov, Yu. N.; Nifant´ev, I. E.; Nifant´ev E. E. *Russian Chemical Bulletin, International Edition*,**2003**, *52*, 78-84.

[53] Severine, J.; De Paule, S.; Ratovelomanana-Vidal, D.; Genet, V.; Champion, J. -P. Nicolas; Philippe, D.; Angew. Chem. Int.Ed., **2004** , *43*, 320-325.

[54] Wojciech, S. J.; Okruszek, A.; Michalski, J.; *J. Org. Chem.*, **1976**, *41*, 233-238.

[55] a) Xiao, H.; Chai, Z.; Zheng, C. -W.; Yang, Y. -Q.; Liu, W.; Zhang, J. -K.; Zhao G. *Angew. Chem. Int. Ed.* **2010**, *49*, 4467-4470 b) Schuler, M.; Voituriez, A.; Marinetti A.; *Tetrahedron: Asymmetry*, **2010**, *21*, 1569-1573 c) Voituriez, A.; Pinto, N.; Neel, M.; Retailleau, P.; Marinetti, A.; *Chem. Eur. J.*, **2010**, *16*, 12541-12544.

[56] Benaglia, M.; Rossi, S. *Org. Biomol. Chem.* **2010**, *8*, 3824–3830.

[57] a) Takaya, H.; Mashima, K.; Koyano, K. *J. Org. Chem.* **1986**, *51*, 629–635; b) Benincori, T.; Brenna, E.; Sannicolò, F.; Trimarco, L.; Antognazza, P.; Cesarotti, E.; Demartin, F.; Pilati, T. *J. Org. Chem.* **1996**, *61*, 6244–6251; c) Duprat de Paule, S.; Jeulin, S.; Ratovelomanana–Vidal, V.; Genêt, J.; Champion, –P. N.; Dellis, P. *Tetrahedron Lett.* **2003**, *44*, 823–826.

[58] a) Benaglia, M.; Guizzetti, S.; Pignataro, L. *Coord. Chem. Rev.* **2008**, *252*, 492–508; b) Guizzetti, S.; Benaglia, M. *Eur. J. Org. Chem.,* **2010**, 5529–5541; c) Jones, S.; Warner, C. J. A. *Org. Biomol. Chem.* **2012**, *10,* 2189–2200.

[59] Rossi, S.; Benaglia, M.; Cozzi, F.; Genoni, A.; Benincori, T. *Adv. Synth. Catal.* **2011**, *353*, 848–854.

[60] Leach, A. R. in Molecular Modelling – principles and applications, **2001**, Prentice Hall.

[61] Gaussian 09, Revision **A.1**, Gaussian, Inc., Wallingford CT, 2009.

[62] Fusco, R.; Biagini, P.; Maiorana, S.; Licandro, E. WO-2013/098726 (A1).

[63] Egan, W.; Tang, R.; Zon, G.; Mislow, K. *J. Am. Chem. Soc.* **1971**, *93*, 6205-6216.

[64] Examples of enantioselective variants **with platinum catalysts**: a) Brissy, D.; Skander, M.; Retailleau, P.; Frison, G.; Marinetti, A. *Organometallics* **2009**, *28*, 140-151; b) ref 43b; c) Jullien, H.; Brissy, D.; Sylvain, R.; Retailleau, P.; Naubron, J.-V.; Gladiali, S.; Marinetti, A. *Adv. Synth. Catal.* **2011**, *353*, 1109-1124; **with rhodium catalysts**: d) ref 43c; e) Nishimura, T.; Maeda, Y.; Hayashi, T.; *Org. Lett.* **2011**, *13*, 3674-3677; f) Nishimura, T.; Takiguchi, Y.; Maeda, Y.; Hayashi, T. *Adv. Synth. Catal.* **2013**, *355*, 1374-1382; **with gold catalysts**: g) Chao, C.-M.; Beltrami, D.; Toullec, P. Y.; Michelet, V. *Chem. Commun.* **2009**, 6988-6990; h) Pradal, A.; Chao, C.-M.; Toullec, P. Y.; Michelet, V. *Beilstein J. Org. Chem.* **2011**, *7*, 1021-1029; i) Deschamps, N. M.; Elitzin, V. I.; Liu, B.; Mitchell, M. B. M.; Sharp, J.; Tabet, E. A. *J. Org. Chem.* **2011**, *76*, 712-715; j) Teller, H.; Fürstner, A. *Chem. Eur. J.* **2011**, *17*, 7764-7767; k) ref 44; **with iridium catalysts**: l) ref 43a; m) Barbazanges, M.; Augé, M.; Moussa, J.; Amouri, H.; Aubert, C.; Desmarets, C.; Fensterbank, L.; Gandon, V.; Malacria, M.; Ollivier, C. *Chem. Eur. J.* **2011**, *17*, 13789-13794.

[65] Kim, S. Y.; Park, Y.; Son, S.; Chung, Y. K. *Adv. Synth. Catal.* **2012**, *354*, 179-186.

[66] Hudlicky, T.; Reed, J. W. *Angew. Chem. Int. Ed.* **2010**, *49*, 4864-4876.

[67] a) Lee, S. I.; Kim, S. M.; Choi, M. R.; Kim, S. Y.; Chung, Y. K.; Han, W. -S.; Kang, S. O. *J. Org. Chem.* **2006**, *71*, 9366-9372; b) Sim, S. O.; Lee, S. I.; Park, J. H.; Chung, Y. K. *Adv. Synth. Catal.* **2010**, *352*, 317-322.

[68] Delpont, N.; Escofet, I.; Pérez-Galán, P.; Spiegl, D.; Raducan, M.; Bour, C.; Sinisia R.; Echavarren A.M. *Catal. Sci. Technol.*, **2013**, *3*, 3007-3012.

[69] a) Roncali, J. *Chem*. *Rev.*, **1997**, *97*, 173-206. b) Skotheim, T. A.; Reynolds, J. R. Eds. *Conjugated Polymers: Theory, Synthesis, Properties, and Characterization (Handbook of Conducting Polymers)*, 3rd ed.; CRC Press LLC.:Boca Raton, FL, **2007**. c) Roncali, J. *Acc. Chem. Res.* **2009**, *42*, 1719-1730.

[70]a) Gao, P.; Tsao, H. N.; Grätzel, M.; Nazeeruddin, M. K. *Org. Lett.*, **2012**, *14*, 4330-4333. b) Longhi, E.; Bossi, A.; Di Carlo, G.; Maiorana, S.; De Angelis, F.; Salvatori, P.; Petrozza, A.; Binda, M.; Roiati, V.; Mussini, P. R.; Baldoli, C.; Licandro, E. *Eur. J. Org. Chem.*, **2013**, 84-94.

[71] a) Rajca, A.; Pink, M.; Xiao, S.; Miyasaka, M.; Rajca, S.; Das, K.; K. Plessel, *J. Org. Chem.*, **2009**, *74*, 7504-7513. b) Shimozu, M.; Nagao, I.; Tomioka, Y.; Hiyama, T. *Angew. Chem., Int. Ed.*, **2008**, *47*, 8096-8099. c) Xia, Y.; Qu, P.; Liu, Z.; Ge, R.; Xiao, Q.; Zhang, Y.; Wang, J. *Angew. Chem., Int. Ed.*, **2013**, *52*, 2543-2546. d) Wang, Z.; Shi, J.; Tian, X.; Xu, L.; Li, C; Wang, H.; *Journal of Heterocyclic Chemistry* **2013**, *50*, 1021-1024. e) Stephenson G. R.; Cauteruccio, S.; Doulcet J.; *Synlett*, **2014**, *25*, 0701–0707.

[72] Bolm, C.; Legros, J.; Le Paih, J.; Zani, L. *Chem. Rev.*, **2004**, *104*, 6217-6254.

[73] For recent reviews, see: a) Sarhan, A. A. O.; Bolm, C. *Chem. Soc. Rev.*, **2009**, *38*, 2730-2744. b) Cao, Y.; Wang, X. -Y.; Wang, J. -Y.; Pei, J. *Synlett*, **2014**, *25*, 313-323.

[74] a) Larsen, J.; Bechgaard, K. *J. Org. Chem.*, **1996**, *61*, 1151-1152; b) Tovar, J. D.; Rose, A.; Swager, T. M. *J. Am. Chem. Soc.*, **2002**, *124*, 7762-7769; c) Pei, J.; Zhang, W. Y.; Mao, J.; Zhou, X. H. *Tetrahedron Letters*, **2006**, *47*, 1551-1554; d) Liu, W. J.; Zhou, Y.; Ma, Y.; Cao, Y.; Wang, J.; Pei, J. *Org. Lett.*, **2007**, *9*, 4187-4190; e) Zhou, Y.; Liu, W. Y.; Ma, Y.; Wang, H.; Qi, L.; Cao, Y.; Wang, J.; Pei, J. *J. Am. Chem. Soc.*, **2007**, *129*, 12386-12387; f) Brusso, J. L.; Hirst, O. D.; Dadvand, A.; Ganesan, S.; Cicoira, F.; Robertson, C. M.; Oakley, R. T.; Rosei, F.; Perepichka, D. F. *Chem. Mater.*, **2008**, *20*, 2484-2494; g) Yan, Q.; Zhou, Y.; Ni, B. –B.; Ma, Y.; Wang, J.; Pei, J.; Cao, Y. *J. Org. Chem.*, **2008**, *73*, 5328-5339; h) Luo, J.; Zhao, B.; Shao, J.; Lim, K. A.; Chan, H. S. O.; Chi, C. *J. Mater. Chem.*, **2009**, *19*, 8327-8334; i) Luo, J.; Zhao, B.; Chan, H. S. O.; Chi, C. *J. Mater. Chem*., **2010**, *20*, 1932-1941; j) Ye, Q.; Chang, J.; Huang, K. W.; Chi, C. *Org. Lett.*, **2011**, *13*, 5960-5963; k) He, F.; Wang, W.; Chen, W.; Xu, T.; Darling, S. B.; Strzalka, J.; Liu, Y.; Yu, L. *J. Am. Chem. Soc.*, **2011**, *133*, 3284-3287; l) Zöphel, L.; Enkelmann, V.; Rieger, R.; Müllen, K. *Org. Lett.*, **2011**, *13*, 4506-4509; m) Ye, Q.; Chang, J.; Huang, K. –H.; Dai, G.; Zhang, J.; Chen, Z. –K.; Wu, Chi, J. C. *Org. Lett.*, **2012**, *14*, 2786-2789; n) Wang, J.; Xu, H.; Li, B.; Cao, X. –P.; Zhang, H. –L. *Tetrahedron*, **2012**, *68*, 1192-1197; o) Geng, W.; Wang, H.; Wang, Z.; Zhang, S.; Zhang, W. -X.; Xi, Z. *Tetrahedron*, **2012**, *68*, 5283-5289.

[75] The *E* isomer was obtained as the only compound in different reaction conditions. Huang, H.; Chen, Z.; Ortiz, R. P.; Newman, C.; Usta, H.; Lou, S.; Youn, J.; Noh, Y.-Y.; Baeg, K.-J.; Chen, L. X.; Facchetti, A.; Marks, T. *J. Am. Chem. Soc.*, **2012**, *134*, 10966-10973.

[76] Wang, K.; Lu, M.; Yu, A.; Zhu, X.; Wang, Q. *J. Org. Chem*., **2009**, *74*, 935-938.

[77] Kellogg, R. M.; Schaap, A. P.; Harper, E. T.; Wynberg, H. *J. Org. Chem.*, **1968**, *33*, 2902-2909.

[78] Maiorana, S.; Papagni, A.; Licandro, E.; Annunziata, R.; Paravidino, P.; Perdicchia, D.; Giannini, C.; Bencini, M.; Clays, K.; Persoons A. *Tetrahedron* **2003**, *59*, 6481–6488.

[79] Amemiya, R.; Yamaguchi, M. *Org. Biomol. Chem.* **2008**, *6*, 26-35.

[80] Honzawa, S.; Okubo, H.; Anzai, S.; Yamaguchi, M.; Tsumoto, K.; Kumagai, I. *Bioorg. Med. Chem*. **2002**, *10*, 3213-3218.

[81] Xu, Y.; Zhang, Y. X.; Sugiyama, H.; Umano, T.; Osuga, H.; Tanaka, K. *J. Am. Chem. Soc.* **2004**, *126*, 6566-6567.

[82] Latterini, L.; Passeri, R.; Aloisi, G. G.; Elisei, F.; Caronna, T.; Fontana F.; Natali Sora, I. *J. Photochem. Photobiol. Sci.* **2009**, *8*, 1574-1582.

[83] Latterini, L.; Galletti, E.; Passeri, R.; Barbafina, A.; Urbanelli, L.; Emiliani, C.; Elisei, F.; Fontana, F.; Mele, A.; Caronna, T. *J. Photochem. Photobiol. A Chem.* **2011**, *222*, 307-313.

[84] Shinohara, K.; Sannohe, Y.; Kaieda, S.; Tanaka, K.; Osuga, H.; Tahara, H.; Xu, Y.; Kawase, T.; Bando, T.; Sugiyama, H. *J. Am. Chem. Soc.* **2010**, *132*, 3778-3782.

[85] Rigamonti, C.; Ticozzelli, M. T.; Bossi, A.; Licandro, E.; Giannini, C.; Maiorana, S. *Heterocycles*, 2008, **76**, 1439-1470.

[86] Fessi, H.; Puisieux, F.; Devissaguet, J. P.; Ammoury, N.; Benita, S. *Int. J. Pharm.*, **1989**, *55*, R1-R4.

[87] Chiellini, F.; Piras, A. M.; Errico, C.; Chiellini, E. *Nanomedicine* **2008**, *3*, 367-393.

[88] Chiellini, F.; Dinucci, D.; Bartoli, C.; Piras, A. M.; Chiellini, E. *J. Bioact. Compat. Pol.* **2007**, *22*, 667–685.

[89] Chiu, Y. L.; Ho, Y. C.; Chen, Y. M.; Peng, S. F.; Ke, C. J.; Chen, K. J.; Mi, F. L.; Sung, H. W. *J. Control. Release* **2010**, *146*, 152-159.

[90] Payne, C. K.; Jones, S. A.; Chen, C.; Zhuang, X. *Traffic* **2007**, *8*, 389-401.

[91] Koivusalo, M.; Welch, C.; Hayashi, H.; Scott, C. C.; Kim, M.; Alexander, T.; Touret, N.; Hahn, K. M.; Grinstein, S. *J. Cell. Biol.* **2010**, *188*, 547-563.

[92] Conner, S. D.; Schmid, S. L. *Nature*, **2003**, *422*, 37-44.

[93] Nam, H. Y.; Kwon, S. M.; Chung, H.; Lee, S. Y.; Kwon, S. H.; Jeon, H.; Kim, Y.; Park, J. H.; Kim, J.; Her, S.; Oh, Y. K.; Kwon, I. C.; Kim, K.; Jeong, S. Y. *J. Control. Release* **2009**, *135*, 259-267.

[94] Ooyama, Y.; Harima, Y.; *Eur. J. Org. Chem.* **2009**, 2903.

[95] a) Ooyama, Y.; Ishii, A.; Kagawa, Y.; Imae, I.; Harima, Y. *New J. Chem.* **2007**, *31*, 2076-2082; b) Ooyama, Y.; Shimada, Y.; Kagawa, Y.; Imae, I.; Harima, Y. *Org. Biomol. Chem.* **2007**, *5*, 2046-2054. c) Ooyama, Y.; Shimada, Y.; Kagawa, Y.; Yamada, Y.; Imae, I.; Komaguchi, K.; Harima, Y. *Tetrahedron Lett.* **2007**, *48*, 9167-9170; d) Ooyama, Y.; Harima, Y. Eur. J. Org. Chem. **2009**, 2903. d) Ooyama, Y.; Shimada, Y.; Ishii, A.; Ito, G.; Kagawa, Y.; Imae, I.; Komaguchi, K.; Harima, Y. *J. Photochem. Photobiol. A* **2009**, *203*, 177-185; e) Ooyama, Y.; Inoue, S.; Asada, R.; Ito, G.; Kushimoto, K.; Komaguchi, K.; Imae, I.; Harima, Y. *Eur. J. Org. Chem.* **2010**, 92-100.